isvr Institute of Sound and Vibration Research

Blast Induced Shock Waves in Structure
Part 1 – Theoretical Aspects

M. Schaedlich, N.S. Ferguson and S.J.C. Dyne

ISVR Technical Memorandum No 936

June 2005

University of Southampton

SCIENTIFIC PUBLICATIONS BY THE ISVR

Technical Reports are published to promote timely dissemination of research results by ISVR personnel. This medium permits more detailed presentation than is usually acceptable for scientific journals. Responsibility for both the content and any opinions expressed rests entirely with the author(s).

Technical Memoranda are produced to enable the early or preliminary release of information by ISVR personnel where such release is deemed to the appropriate. Information contained in these memoranda may be incomplete, or form part of a continuing programme; this should be borne in mind when using or quoting from these documents.

Contract Reports are produced to record the results of scientific work carried out for sponsors, under contract. The ISVR treats these reports as confidential to sponsors and does not make them available for general circulation. Individual sponsors may, however, authorize subsequent release of the material.

UNIVERSITY OF SOUTHAMPTON

INSTITUTE OF SOUND AND VIBRATION RESEARCH

DYNAMICS GROUP

Blast Induced Shock Waves in Structures
Part I – Theoretical Aspects

by

M. Schaedlich, N.S. Ferguson and S.J.C. Dyne

ISVR Technical Memorandum No: 936

June 2005

Authorised for issue by
Professor M.J. Brennan
Group Chairman

Contents

List of Figures

List of Tables

Notation

This section is intended to give a short overview over the variables used in this report. A general definition made is that small **bold** Latin and Greek letters stand for vectors whereas capital **bold** letters stand for matrices.

Parameters and Variables

A		cross sectional area	m^2
D	$= \frac{Eh^3}{12(1-\nu^2)}$	plate bending stiffness	$\mathsf{N}\cdot\mathsf{m}$
E		modulus of elasticity	$\mathsf{N}\cdot\mathsf{m}^{-2}$
I		second moment of area	m^4
c		damping coefficient	$\mathsf{N}\cdot\mathsf{s}\cdot\mathsf{m}^{-1}$
$f_1(u)$, $f_2(u)$		nonlinear restoring forces	N
f_n		natural frequency	Hz
f_{NL}		nonlinear oscillation frequency	Hz
f_p		excitation force frequency	Hz
m		system mass	kg
$p(t), P(t)$		general force (per unit)	$\mathsf{N}\cdot(\mathsf{unit})^{-1}$
p_0		positive overpressure magnitude	$\mathsf{N}\cdot\mathsf{m}^{-2}$
$p_I(t)$, $p_{II}(t)$		time history of pressure profile I/II	$\mathsf{N}\cdot\mathsf{m}^{-2}$
$p_{0\Delta}$, $p_{1\Delta}$		magnitudes of approximate profile	$\mathsf{N}\cdot\mathsf{m}^{-2}$
t_a		blast wave positive pressure rising time	s
t_d		blast wave total positive pressure time	s
t_{A2}		time of maximum negative overpressure	s

t_E			total forcing time of approximate profile	s
t_{Ex}			time points at which u_{Ex} occurs	s
$u(t)$			displacement function	m
$\dot{u}(t)$, $v(t)$	=	$\frac{du(t)}{dt}$	velocity	$m \cdot s^{-1}$
$\ddot{u}(t)$, $a(t)$	=	$\frac{d^2u(t)}{dt^2}$	acceleration	$m \cdot s^{-2}$
u_0, $\dot{u}_0$			differential equation initial conditions	$m, m \cdot s^{-1}$
u_{Ex}			extreme (minimum/maximum) solutions of $u(t)$	m
α			blast wave decaying parameter	–
ζ	=	$\frac{c}{2\sqrt{km}}$	viscous damping ratio	
ω_n, ω_{jk}	=	$2\pi f_n$	circular natural frequencies	$rad \cdot s^{-1}$
ω_f	=	$2\pi f_p$	excitation frequency	$rad \cdot s^{-1}$
ρ	=	$\omega_n t_d$	normalised circular natural frequency	rad
η	=	$f_n t_d$	normalised natural frequency	–

Special Symbols and Transformations

$\mathbb{i}$	=	$\sqrt{-1}$	imaginary unit
$\mathbb{e}$			exponential function
$(.)_{,x}$	=	$\frac{\partial(.)}{\partial x}$	differentiation with respect to x
$(.)_{,t}$	=	$\frac{\partial(.)}{\partial t}$	differentiation with respect to t
Δ	=	$\left(\frac{\partial^2}{\partial x^2} + \frac{\partial^2}{\partial y^2}\right)$	Laplacian operator
a	:=	b	a is defined by b
a	$\stackrel{!}{=}$	b	values for a are restricted so that the condition relating them to b is fulfilled
$\Re\{\ \}$			real part
$\Im\{\ \}$			imaginary part
$\delta(t-t_0)$	=	$\begin{cases} 0, & t < t_0, \\ \infty, & t \geq t_0. \end{cases}$	Dirac-delta distribution

$\mathbb{H}(t-t_0)$	=	$\begin{cases} 0, & (t-t_0)<0, \\ 1, & (t-t_0)\geq 0. \end{cases}$	Heaviside function
$f(t)*g(t)$	=	$\int_0^t f(\tau)g(t-\tau)\,\mathrm{d}\tau$	Convolution of two functions
$\mathfrak{F}\{f(t);\omega\}$	=	$\int_{-\infty}^{\infty} f(t)\,\mathrm{e}^{-\mathrm{i}\omega t}\,\mathrm{d}t$	Fourier transform
$\mathfrak{F}^{-1}\{\tilde{f}(\omega);t\}$	=	$\frac{1}{2\pi}\int_{-\infty}^{\infty} \tilde{f}(\omega)\,\mathrm{e}^{\mathrm{i}\omega t}\,\mathrm{d}\omega$	Inverse Fourier transform
$\mathfrak{L}\{f(t);s\}$	=	$\int_0^{\infty} f(t)\,\mathrm{e}^{-st}\,\mathrm{d}t$	Laplace transform
$\mathfrak{L}^{-1}\{\bar{f}(s);t\}$	=	$\frac{1}{2\pi\mathrm{i}}\int_{\gamma-\mathrm{i}\infty}^{\gamma+\mathrm{i}\infty} \bar{f}(s)\,\mathrm{e}^{st}\,\mathrm{d}s$	Inverse Laplace transform

Special Functions

$\mathcal{E}(...,...)$	elliptic integral of second kind
$\mathcal{F}(...,...)$	elliptic integral of first kind
${}_2\mathcal{F}_1$	Gauss' hypergeometric function
${}_v\mathcal{F}_w$	generalised hypergeometric function
Γ	Gamma function
$\Pi(...,...,...)$	elliptic integral of third kind
$\mathrm{sign}(...)$	signum function

Number Sets

$\mathbb{N}$	set of natural numbers
$\mathbb{Z}$	set of integer numbers
$\mathbb{R}$	set of real numbers
$\mathbb{C}$	set of complex numbers

Introduction

The dynamic loading of structures from detonating explosions is the result of an instantaneous pressure increase in the surrounding medium, typically either air or water, associated with an impinging shock front acting as primary load. Immediately following are transient blast winds exciting the structure as secondary loading after the shock front has passed.

There is significant complexity in the excitation force, which varies considerably with every detonation depending on innumerable uncertainties of the explosive charge itself, the surrounding medium, the structure and many other not less important factors, predicting the dynamic response of structures to this type of forcing function is therefore a rather complex area of research within the field of structural dynamics. The structural response itself involves numerous aspects of nonlinear system behaviour including large deformation, multi-modal response and in most cases a significant amount of material nonlinearities. The latter one is generally regarded as the most difficult in terms of modelling. This might be a decisive reason why past research in the field is mainly concerned with overall damage assessment of the structure subjected to diverse types of blast wave excitation rather than exploring the theoretical aspects of the structural deformation process.

In the case of experimental investigations a reasonable amount of work has been done by exposing numerous real-sized and model-scaled structures to explosive charges of different type, e.g. high explosives (TNT, Octol, etc.), liquid and gaseous fuels. A comprehensive but by no means complete list is given in [1]. Unfortunately, the majority of these experiments have been carried out by placing explosive charges directly upon or very close to the structure. This makes it very complicated if not impossible to establish any relationship between the spatial shock wave profile originating from the explosion and its deformable effects on the structure. However, considering a standardised, empirical blast wave profile as given in KINNEY *et al* [2] analytical solutions of the time-displacement history for the linear, undamped single-degree-of-freedom (SDOF) system can be obtained. The work presented here introduces a second shock wave profile based on the one in [2], which takes the very small but finite positive overpressure rising time into account. For both empirical blast wave models analytical solutions for the special case of *linear* conservative mass-spring systems can be found. Using the Laplace integral transform the ordinary second order differential equation of motion of the linear oscillator is reformulated in the complex domain. Multiplication with the transformed blast wave profile function gives the SDOF system response in the frequency domain. A subsequent inverse transform of

the entire product yields the solution of the problem in the original time domain.

This inverse Fourier transformation of the linear SDOF equation of motion leads to complex analytical though explicit expressions for displacement and velocity. Despite the fact that for linear systems with any combination of the four classification terms *conservative* or *non-conservative* and *autonomous* or *non-autonomous* analytical solutions exist for free and forced vibration of the system, ranging from pure harmonic to standardised transient input loads, such as the Dirac delta, Heaviside and various pulse functions [3], no explicit closed-form solution for values of extreme response[1] can be found in the case of type-I or type-II blast excitation. This can be circumvented using efficient and easy-to-use purely numerical routines like the NEWMARK method [4], which are readily available for such complicated time-varying excitations. A second, and for the physical insight into the problem more useful approach, would be the derivation of an appropriate analytical approximation method. Such a method for linear systems, based on the principle of superposition, is presented herein.

For structural systems with geometrical and/or material nonlinearities it is almost impossible to obtain closed-form, hence analytical expressions describing the time or frequency domain response behaviour of the structure due to transient load input such as shock waves. As a result, this makes it entirely impossible to derive closed-form solutions for extreme response values. Two basic methods, which are heavily employed for linear systems, namely the principle of superposition and the Laplace transformation, are both not feasible anymore[2]. Furthermore, numerical solution procedures, mainly based on optimised Runge-Kutta algorithms [5], are less simple and require far more computational resources than their complements in the linear world. However, early studies suggested the possibility of describing the nonlinear system's response due to certain types of transient excitation in terms of extreme values of an equivalent conservative nonlinear SDOF oscillator subjected to an applied impulse or step function. First analytical results for rather simple nonlinear configurations are limited to very few special cases [6–8], but reveal the potential and ease-of-use of the proposed method.

Scope of the Report

The main focus of this report is aimed at exploring and evaluating two different methods for predicting the extreme response of conservative SDOF systems to the standardised blast wave profile in [2]. Both approaches are analytical approximations and rely on the principle of energy conservation. Additionally, the first method, suitable for *linear* systems only, uses the superposition theorem to produce expressions for extreme displacement and velocity due to blast excitation without the need for calculating the entire time history. The second method, covering both, *linear* and *nonlinear* SDOF systems, is split into two parts. Part one consists of finding robust and reliable analytical expressions for extreme response values due to standard excitations (Dirac impulse and Heaviside step functions) as mentioned above. Secondly, special criteria must be developed taking the applied load (blast wave) and the oscillatory system (geometrical nonlinear SDOF) into account in order to establish an equivalent approximate system having the scaled standard excitation functions as applied external load.

Chapter 1 presents merely an introduction into the blast excitation of simple structures and analyses the general characteristics of two empirical model types of shock wave profiles. Numerous parame-

[1] Minimum and maximum values together are called *extreme* values. Primary *response* parameters of a structural dynamic system are usually displacement, velocity and acceleration.

[2] The Laplace transformation is a *linear* integral operation.

ters of the mathematical blast profile equations are compared and their effects on time and frequency domain content of the shock wave are examined.

Although **chapter 2** investigates the response of *linear* SDOF systems to both blast profiles, type-I and type-II as derived in chapter 1, the first two sections 2.1 and 2.2 deal with general aspects of shock excitation problems and define clear reasons for the problem approach as presented in this report. Section 2.3 then derives results for the damped/undamped *linear* SDOF oscillation in the frequency domain using Laplace transformations. Two different solutions, a time-explicit and time-normalised formulation, are presented. Using these results, equivalent expressions for the time domain are obtained in section 2.4 by inverse Laplace transformation. Using well-established numerical solution procedures such as the Newmark-β-method for comparison reveals significant computational performance improvements of these uniquely derived expressions. Section 2.5 describes the derivation of the so called shock spectra - a plot of the normalised[3] displacement versus structural system natural frequency - for both blast type excitations with different profile parameters. Along with the conventional method for searching for the minimum and maximum values in the displacement $u(t)$ and velocity $v(t)$ time history (direct method), the first of two above mentioned new approaches is established. Using the superposition principle simple expressions for extreme values of $u(t)$ and $v(t)$ are found. As will be seen, by reducing the computational expenses to a fraction to those required for Newmark and similar algorithms, the new method is applicable to a wide range of force and system parameters.

The first section of **chapter 3** states the fundamental *nonlinear* SDOF system equation of motion. Limitations are introduced in order to establish solutions for autonomous conservative systems. Section 3.3 derives the second key-finding of this work: the extension of a energy-based approach for autonomous conservative SDOF systems previously presented in [7,8]. This significant addition makes the method generally applicable to step and impulse excited systems as well as free vibration without the limitation to zero initial conditions. Explicit, and where not possible to simplify, implicit analytical expressions for extreme values of response can be obtained. A second equally important benefit of generalising [7, 8] lies in the derivation of integral expressions for the SDOF system's nonlinear oscillation periods.

Using two common nonlinear polynomial restoring force types expressing elastic stiffening spring behaviour, complex expressions introduced by the analytical method are simplified and the approach's overall effectiveness and accuracy are examined in section 3.4. Together with a well-established numerical method (Runge-Kutta algorithm) analytically obtained results for both the time and frequency domain are verified. It will be shown that multiple oscillation frequencies found in the discrete Fourier transformation of the numerically obtained time-domain data as a typical characteristic of nonlinear SDOF systems[4] can be predicted by the newly established analytical solutions. In section 3.5 of chapter 3 the effect of adding a viscous damping term into the system's nonlinear equation of motion is discussed. It is well known that most nonlinear systems change their oscillation period with changing

[3] If not stated otherwise, in shock spectra for linear systems the dynamic displacement is always normalised to the static displacement.

[4] Multiple frequencies of oscillation also occur for linear and nonlinear multiple-degree-of-freedom (MDOF) systems. The significance lies in the phenomena that nonlinear systems exhibit many more oscillation frequencies (in terms of sine and cosine participation) than the system has degrees-of-freedom (DOF). Contrary, this is *not* the case for linear systems, where the number of DOFs is equal to the number of natural frequencies (eigenfrequencies). However, as will be seen in a second memorandum, multiple frequencies appear only if the system's response is expressed in terms of sine and cosine. Using higher-order transcendental functions with multiple periodicity such as Jacobian elliptic functions, nonlinear systems appear to retain only one frequency of oscillation.

amplitude, which depends upon the systems entire energy content. Due to the nonconservative nature of damping energy is 'leaking' and both, amplitude *and* vibration frequency change in a nonlinear fashion during the time history until the SDOF comes fully to rest.

Blast wave loading as treated in this work is a highly time varying type of excitation. Therefore, in order to be able to adequately reduce such non-autonomous systems to time-invariant equivalent systems, it is essential to know the behaviour of the far more complex original oscillator before any approximation methods can be established. Section 4.1 in **chapter 4** recalls the equation of motion of the structural system under consideration. Section 4.2 disregards damping and examines the response of conservative SDOF systems due to blast excitation load functions having selected ranges of characteristic parameters. Two examples are chosen with the same polynomial-type, geometrically nonlinear restoring forces as introduced in chapter 3. Using purely numerical analysis tools, results for both time and frequency domain are presented.

With **chapter 5** as the last chapter in this technical memorandum, a short summary and brief discussion of new and important results found in this work are given.

Acknowledgement

The authors would like to acknowledge the financial support of DSTL Fort Halstead who have enabled the project to exist.

CHAPTER 1

Blast Waves

1.1 Characteristic Blast Wave Profiles

The physics of an explosion process itself are highly complex involving non-equilibrium thermodynamics and fluid mechanics and despite the efforts in experimental investigation and numerical simulation some details still remaining obscure. The brief description of a typical blast wave model presented in this chapter does not consider any of these nontrivial aspects of the actual detonation process. It is merely a short introduction into the concept of describing nonlinear structural response well away from the centre of explosion using a travelling shock wave. The development of such an air blast wave out of an initial pressure pulse formed at the detonation centre is described in detail by KINNEY *et al* [2]. Extensive experimental work in the recent years as referred to in [1] and [9] support the statement in [2]

> ... the fully developed explosive blast-wave system is always formed with about the same general configuration no matter what is assumed for the initial positive pulse [the pressure profile at the centre of the explosion]. That is, any initial configuration is lost and all blast waves at reasonable distances from the center of an explosion show similar wave forms. Thus as long as the energy release in an explosion is sufficiently rapid, its precise timing is relatively unimportant as far as the type of blast wave it produces is concerned. Rather, the important item is the amount of energy released.

The main objective of this chapter is therefore to briefly analyse the most commonly used blast wave profile and to describe the effects its parameters have on the time distribution of the energy it imposes on the impinging structure.

1.1.1 Time Domain

The empirical, quasi-exponential form of the time varying dynamic pressure well away from the centre of combustion of a free field detonation originating from high explosives can be expressed by [2]

$$p_I(t) = p_0 \left(1 - \frac{t}{t_d}\right) \mathrm{e}^{-\alpha \frac{t}{t_d}} \tag{1.1.1}$$

where $p_I(t)$ is the instantaneous overpressure at time t, p_0 the maximum or peak overpressure observed when t is equal to zero[1] and t_d expresses the time duration of positive overpressure as shown in Fig. 1.1.1(a). Since there exists virtual no limit for the maximum pressure[2] p_0, the positive pressure phase is in general far more intense than the negative which is limited in magnitude to the atmospheric pressure.

A more appropriate, thus more realistic version of Eq.(1.1.1), taking the finite rise time of the dynamic overpressure into account, is shown in Fig. 1.1.1(b) and can be given by

$$p_{II}(t) = \begin{cases} \frac{p_0}{t_a} t\,, & 0 \le t \le t_a \\ p_0 \left(1 - \frac{t}{t_d}\right) \mathrm{e}^{-\alpha \frac{t}{t_d}}\,, & t_a \le t \le \infty \end{cases} \tag{1.1.2}$$

or, in a more compact form

$$p_{II}(t) = p_0 \left[\mathbb{H}(t_a - t) \frac{t}{t_a} + \mathbb{H}(t - t_a) \left(1 - \frac{t - t_a}{t_d}\right) \mathrm{e}^{-\alpha \frac{t - t_a}{t_d}} \right] \tag{1.1.3}$$

where t_a is the positive overpressure rising time and $\mathbb{H}(t)$ denotes the Heaviside function. Both equations (1.1.1) and (1.1.3) can be rewritten in terms of a normalised time $\tau = \frac{t}{t_d}$ giving

$$p_I(\tau) = p_0 (1 - \tau)\, \mathrm{e}^{-\alpha\tau} \tag{1.1.4}$$

and

$$p_{II}(\tau) = p_0 \left[\mathbb{H}\left(\frac{t_a}{t_d} - \tau\right) \frac{t_d}{t_a} \tau + \mathbb{H}\left(\tau - \frac{t_a}{t_d}\right) \left(1 + \frac{t_a}{t_d} - \tau\right) \mathrm{e}^{-\alpha\left(\tau - \frac{t_a}{t_d}\right)} \right] \tag{1.1.5a}$$

noting that for all $t_d > 0$

$$\mathbb{H}(t_d(\ldots)) \equiv \mathbb{H}(\ldots)\,. \tag{1.1.5b}$$

Using the substitution $\tau_b = \frac{t_a}{t_d}$ Eq.(1.1.5a) can be simplified even further

$$p_{II}(\tau) = p_0 \left[\mathbb{H}(\tau_b - \tau) \frac{\tau}{\tau_b} + \mathbb{H}(\tau - \tau_b)(\tau_b - \tau + 1)\, \mathrm{e}^{-\alpha(\tau - \tau_b)} \right]. \tag{1.1.6}$$

A closer examination of both equations for the type-II shock wave profile, (1.1.3) and (1.1.6), respectively, indicates that for the limiting case $t_a \to 0 \equiv \tau_b \to 0$ the p_{II}-profile changes into the type-I wave profile. Since the dimensionless time is defined as $\tau \ge 0$ the direction of approach for the limiting function lim is from the right to left, e.g. from $\infty \to +0$,

$$\lim_{t_a \to +0} \left[\mathbb{H}(t_a - t) \frac{t}{t_a} \right] \equiv \lim_{\tau_b \to +0} \left[\mathbb{H}(\tau_b - \tau) \frac{\tau}{\tau_b} \right] = 0$$

and

$$\lim_{t_a \to +0} \left[\mathbb{H}(t - t_a) \left(1 - \frac{t - t_a}{t_d}\right) \mathrm{e}^{-\alpha \frac{t - t_a}{t_d}} \right] = p_0 \left(1 - \frac{t}{t_d}\right) \mathrm{e}^{-\alpha \frac{t}{t_d}}$$

$$\lim_{\tau_b \to +0} \left[\mathbb{H}(\tau - \tau_b)(\tau_b - \tau + 1)\, \mathrm{e}^{-\alpha(\tau - \tau_b)} \right] = p_0 (1 - \tau)\, \mathrm{e}^{-\alpha\tau}\,.$$

[1] The time-varying pressure $p_I(t)$ reaches its maximum value p_0 only if $t = 0$ in Eq.(1.1.1). This may not necessarily be true for measuring $p_I(t)$ during experiments. In general, p_0 should merely be regarded as absolute positive magnitude of the entire force-time-history.

[2] It does depend upon in which medium the explosion takes place (air, water, etc.). Due to its compressibility an absolute limit might be given by the physical properties of air. However, generally speaking the maximum overpressure p_0 is directly proportional to the energy released by the explosion.

1.1.2 Frequency Domain

Without loss of generality it is possible to chose an initial time point t_i so that all signals are equal to zero if $t < t_i$ or $\tau < \tau_i$, where $\tau_i = t_i/t_d$, no matter if either written in their explicit form as function of t, $p(t) \equiv p_I(t) \equiv p_{II}(t)$, Eq.(1.1.1) and (1.1.2), or time-normalised by t_d, $p(\tau) \equiv p_I(\tau) \equiv p_{II}(\tau)$, equations (1.1.4) and (1.1.6), respectively. Hence, the following relation between the Fourier and Laplace transform can be established

$$\mathfrak{F}\{p(t),\omega\}\Big|_{t\geq 0} = \int_{t=0}^{\infty} p(t)\,\mathrm{e}^{-\mathrm{i}\omega t}\,\mathrm{d}t \quad \equiv \quad \mathfrak{L}\{p(t),s\to \mathrm{i}\omega\} = \int_{t=0}^{\infty} p(t)\,\mathrm{e}^{-st}\,\mathrm{d}t\,. \tag{1.1.7}$$

Applying Eq.(1.1.7) to both (1.1.1) and (1.1.3) gives

$$\frac{\tilde{p}_I(\omega)}{p_0} = \frac{1}{\mathrm{i}\omega+\frac{\alpha}{t_d}} - \frac{1}{\left(\mathrm{i}\omega+\frac{\alpha}{t_d}\right)^2 t_d} \tag{1.1.8a}$$

and

$$\frac{\tilde{p}_{II}(\omega)}{p_0} = \frac{t_a}{\mathrm{e}^{\mathrm{i}\omega t_a}\,(\alpha+\mathrm{i}\omega t_d)} + \frac{t_d}{\mathrm{e}^{\mathrm{i}\omega t_a}\,(\alpha+\mathrm{i}\omega t_d)} + \ldots \\ - \frac{\alpha t_a + t_d + \mathrm{i}\omega t_a t_d}{\mathrm{e}^{\mathrm{i}\omega t_a}\,(\alpha+\mathrm{i}\omega t_d)^2} + \frac{\left(-1+\frac{1+\mathrm{i}\omega t_a}{\mathrm{e}^{\mathrm{i}\omega t_a}}\right)\mathrm{H}(t_a)}{\omega^2 t_a} \tag{1.1.8b}$$

respectively, with $\mathrm{H}(t_a) = 1$ in Eq.(1.1.8b) since t_a is always greater zero and $\tilde{p}(\omega)$ as the Fourier transform of $p(t)$. Rearranging and substitution of the circular frequency ω by $(2\pi f)$ leads to the final equations for non-normalised type-I and type-II blast profiles in the frequency domain

$$\frac{\tilde{p}_I(f)}{p_0} = \frac{t_d\,(1-2\mathrm{i}f\pi t_d-\alpha)}{(2f\pi t_d-\mathrm{i}\alpha)^2}\,, \tag{1.1.9}$$

and

$$\frac{\tilde{p}_{II}(f)}{p_0} = \frac{\mathrm{e}^{-2\mathrm{i}f\pi t_a}}{4f^2\pi^2 t_a\,(2f\pi t_d-\mathrm{i}\alpha)^2}\Big(4f^2\pi^2 t_a t_d\,[1-2\mathrm{i}f\pi t_d-\alpha]+\ldots \\ -\left[1-\mathrm{e}^{2\mathrm{i}f\pi t_a}+2\mathrm{i}f\pi t_a\right](2f\pi t_d-\mathrm{i}\alpha)^2\Big)\,. \tag{1.1.10}$$

Both equations (1.1.9) and (1.1.10), expressing the frequency content of their appropriate time histories, Eq.(1.1.1) and (1.1.2), respectively, are shown in Fig. 1.2.1 and 1.2.3 on page 7 and 9 for different values of the parameters α, t_a and t_d.

The Laplace (or one-sided Fourier) transformation of the time-normalised versions of p_I and p_{II}, Eq.(1.1.4) and (1.1.6), respectively, is obtained using Eq.(1.1.7) where the dimensionless time τ becomes a dimensionless frequency η due to the transformation

$$\mathfrak{F}\{p(\tau),2\pi\eta\}\Big|_{\tau\geq 0}\,. \tag{1.1.11}$$

It is easy to see that the real frequency f and η are related by $\eta = f\cdot t_d$. Therefore, both equations (1.1.4) and (1.1.6) rewritten in the frequency domain yield

$$\frac{\tilde{p}_I(\eta)}{p_0} = \frac{\alpha+2\mathrm{i}\pi\eta-1}{(\alpha+2\mathrm{i}\pi\eta)^2} \tag{1.1.12}$$

and

$$\frac{\tilde{p}_{II}(\eta)}{p_0} = \frac{-e^{-2i\pi\tau_b}\left[\tau_b\,(2\pi\eta)^2\,(1-\alpha-2i\pi\eta)+(\alpha+2i\pi\eta)^2\left(e^{2i\pi\tau_b\eta}-2i\pi\tau_b\eta-1\right)\right]}{\tau_b\,(2\pi\eta)^2\,(\alpha+2i\pi\eta)^2}. \quad (1.1.13)$$

Both equations are shown in Fig. 1.2.2 and 1.2.4 on pages 8 and 10, respectively.

It should be noted here that all frequency-domain related diagrams shown in this chapter have either the explicit notional frequency of the excitation function $f = \frac{\omega}{2\pi} \equiv f_p = \frac{\omega}{2\pi}$ or the t_d-normalised excitation frequency $\eta = f \cdot t_d$ as abscissa. However, since this work deals solely with transient external force functions the reader should be clear about the fact that transient signals contain a broad range of frequency components[3] and, as far as this work is concerned, their description in the frequency domain is only of use in connection with *linear* structural single or multiple degrees of freedom systems having clearly defined properties which are, unlike *nonlinear* oscillators, frequency, oscillation amplitude, external force, etc., independent .

1.2 Blast Wave Parameter Comparison

In this section time history and frequency content graphs are shown resulting from the two different types of blast wave profiles given in explicit and time normalised form in section 1.1, Eq.(1.1.1), (1.1.3) and Eq.(1.1.4), (1.1.6), respectively. A range of values for the parameters α, t_a and t_d has been selected and numerical Fourier transforms of the excitation functions were produced, which, when compared to analytical obtained results from the above section are in perfect agreement. As will be shown in chapter 2, these transformation functions can be used to calculate the structural response of a linear mass-spring-damper SDOF system in the frequency domain. Inverse Fourier transform or the method of convolution will then give the time-domain solution.

The influence of the parameters t_d and α upon the **type-I** blast wave profile is shown in Fig. 1.2.1(a) on page 7. Whereas t_d defines the time interval of positive overpressure, α determines the absolute magnitude of negative pressure[4] and the interval until the pressure returns to the ambient level. Setting the first derivative of Eq.(1.1.1) with respect to time equal to zero

$$\frac{dp(t)}{dt} = 0 = -p_0 \frac{e^{-\alpha\frac{t}{t_d}}}{t_d}\left[1+\alpha\left(1-\frac{t}{t_d}\right)\right] \quad (1.2.1a)$$

and solving for $t = t_{p_{\min}}$, i.e. the point in time where the maximum negative overpressure (or minimum total pressure) occurs,

$$t_{p_{\min}} = t_d\left(1+\frac{1}{\alpha}\right) \quad (1.2.1b)$$

makes it possible to determine the magnitude of $p_{\min}$ as

$$p_{\min} = -\frac{p_0}{\alpha}\,e^{-1-\alpha} \quad (1.2.1c)$$

and clearly is only dependent upon α. The same result is obtained by differentiating Eq.(1.1.9) with respect to τ. A comparison between graph (b) and (c) in Fig. 1.2.1 indicates, as expected, the very good

[3] Depending upon the type of transient signal this range can extend up to infinity, e.g. unit impulse function.

[4] As mentioned earlier, the maximum absolute negative pressure magnitude is limited to the negative ambient pressure level, i.e. the total absolute pressure cannot be smaller than zero.

agreement between analytical and numerical solution of the Fourier transform of Eq.(1.1.1). Figure 1.2.2(a) on page 8 shows the t_d-normalised version of equation (1.1.1), i.e. Eq.(1.1.4). Replacing t by τ results in a scaling of the abscissa by different factors of t_d. Therefore, all profiles with the same values for α are now represented by a single line regardless values of t_d and as can easily be seen from Eq.(1.1.4) the type-I shock profile is reduced to an expression with two independent parameters, namely p_0 and α. However, in the same way the frequencies of both the analytical and numerical Fourier transformations are now multiple of t_d, given in graph (b) and (c) of Fig. 1.2.2, the magnitudes had to be normalised by the same parameter t_d to be consistent with $\tilde{p}_I(f)$ from Eq.(1.1.9) as presented in Fig. 1.2.1.

As the total energy input into the structural system due to the impinging shock wave is defined by the absolute magnitude p_0 and the shape of the blast profile, it appears logical that an increase in positive overpressure duration t_d as well as a decrease of α give higher overall spectral energy levels. In fact, both methods increase only the signal's power for the (very) low and mid-frequency levels up to 10 Hz as pictured in Fig. 1.2.1(b) and (c). For a normalised frequency $\eta = f \cdot t_d$ equal to 1 the spectral energy content is the same for all blast profiles regardless the values of the parameters t_d and α, see Fig. 1.2.2. Especially for values of $f \leq 1.0$ a doubling of t_d introduces far less power than dividing α by 2.

Explicit and normalised versions of the **type-II** blast profile, Eq.(1.1.3) and (1.1.6), are shown in Fig. 1.2.3 and 1.2.4. Differences between analytical and numerical results are virtually non-existent. In order to allow for comparisons between type-I and type-II results, parameters α and t_d were in both cases allocated with the same values. In terms of magnitude and energy distribution with frequency there is only little or no difference for frequencies $f \leq 200$ Hz if α stays constant, see Fig. 1.2.3(b) and (c). Beyond this critical value ripples occur spaced at distances which are equal to the inverse of the rise time, i.e. $\frac{1}{t_a}$. Again, decreasing values of α means an increase in the energy level at (very) low frequencies up to 10 Hz. The maximum negative overpressure for the type-II profile occurs at time

$$t_{p_{\min}} = t_a + t_d \left(1 + \frac{1}{\alpha}\right) \tag{1.2.2}$$

and the magnitude of $p_{\min}$ is the same as for the type-I profile given in Eq.(1.2.1c).

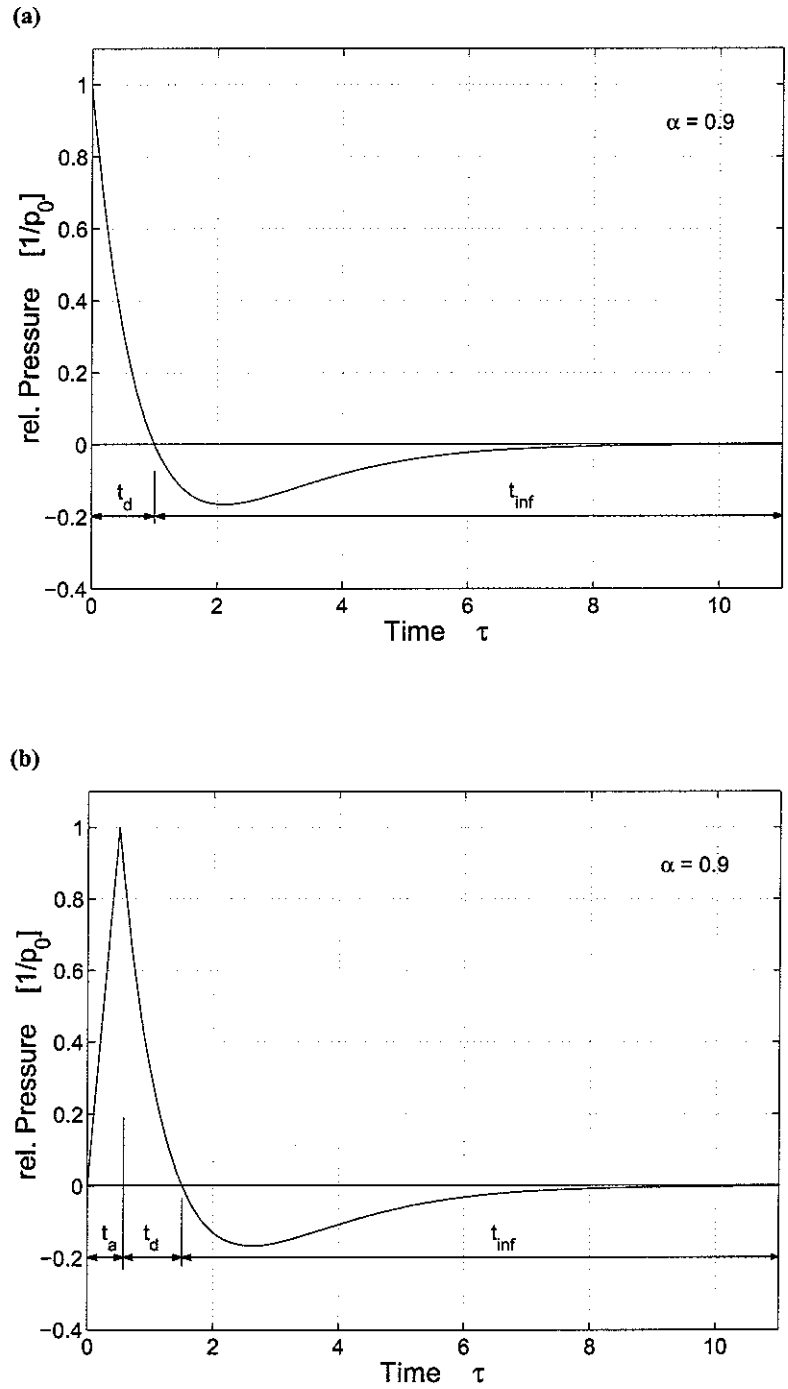

Figure 1.1.1: Blast wave time history profiles: **(a)** Standard blast wave configuration $p_I(t)$ according to KINNEY *et al* [2]. **(b)** Modified configuration $p_{II}(t)$ with finite rising time.

(a)

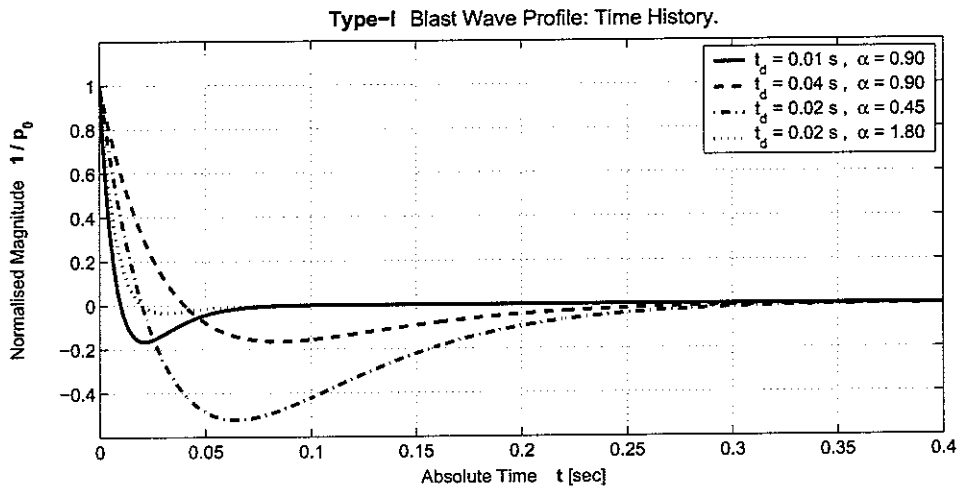

(b)

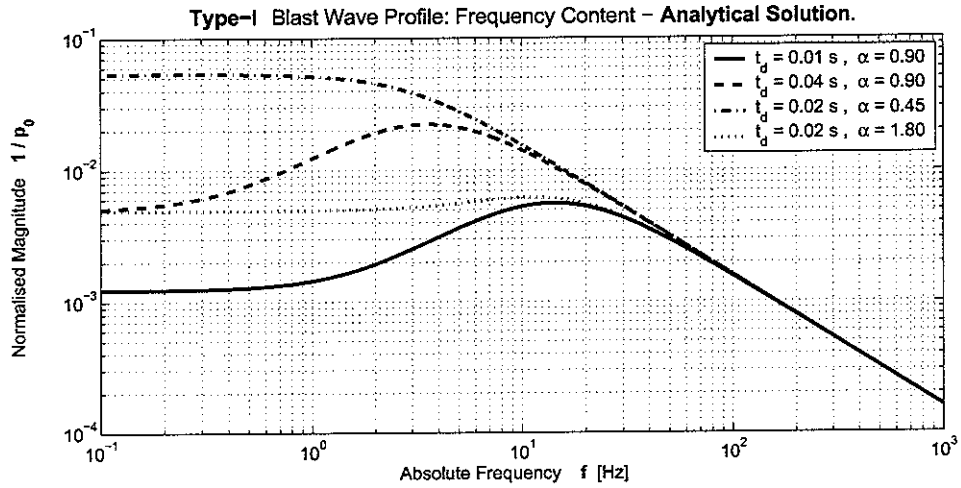

(c)

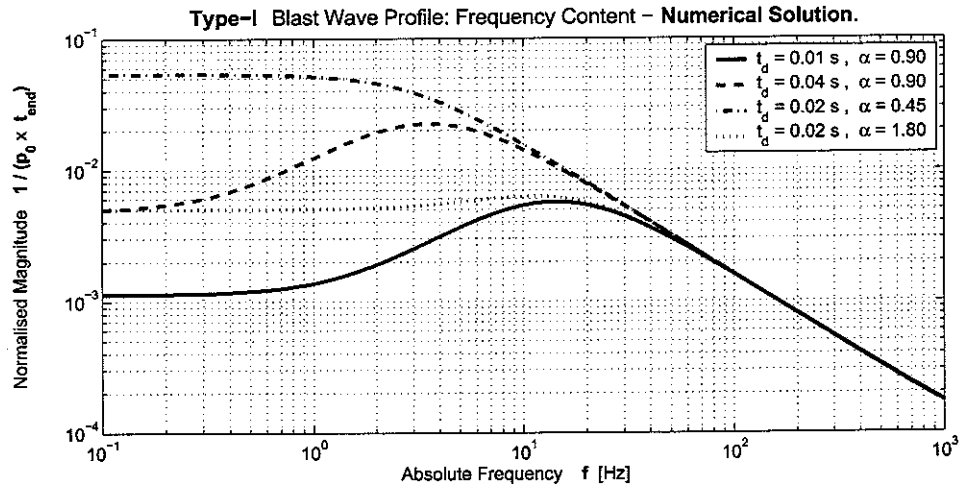

Figure 1.2.1: Blast wave profile type-I: *Explicit Form.* **(a)** Time history. **(b)** Analytical Fourier transform. **(c)** Numerical Fourier transform ($t_{\text{end}} = 2\,\text{s}$). Sampling frequency $f_s = 1.0\,\text{kHz}$.

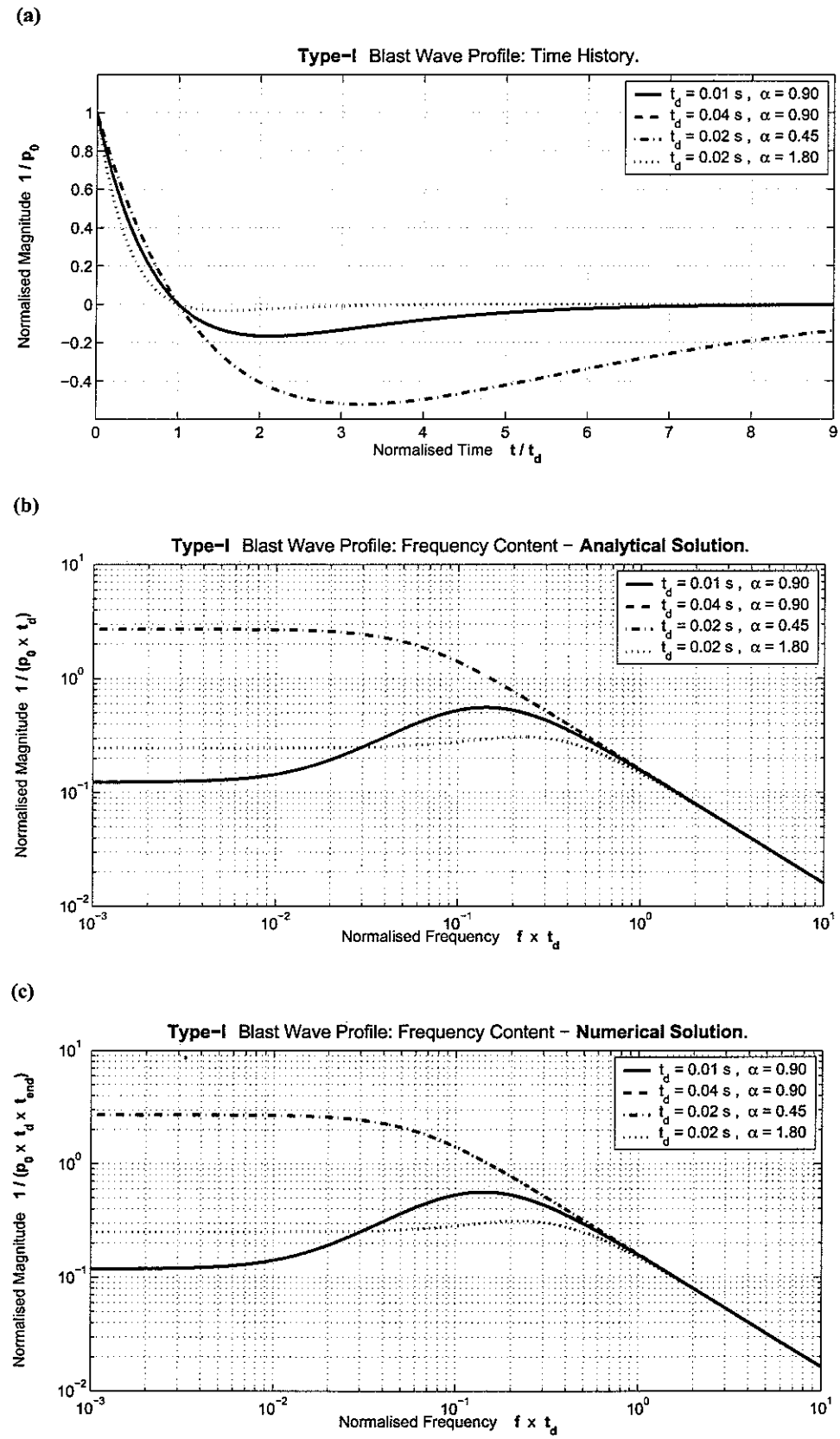

Figure 1.2.2: Blast wave profile type-I: *Normalised Form.* **(a)** Time history. **(b)** Analytical Fourier transform. **(c)** Numerical Fourier transform ($\tau_{\text{end}} = \frac{t_{\text{end}}}{0.01} = 2.0 \cdot 10^2$). Sampling frequency $f_s = 1.0\,\text{kHz}$.

(a)

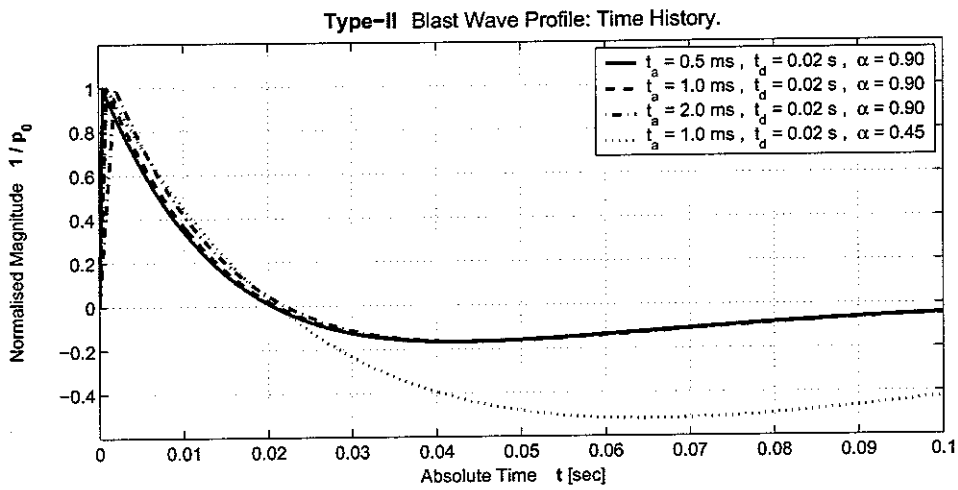

(b)

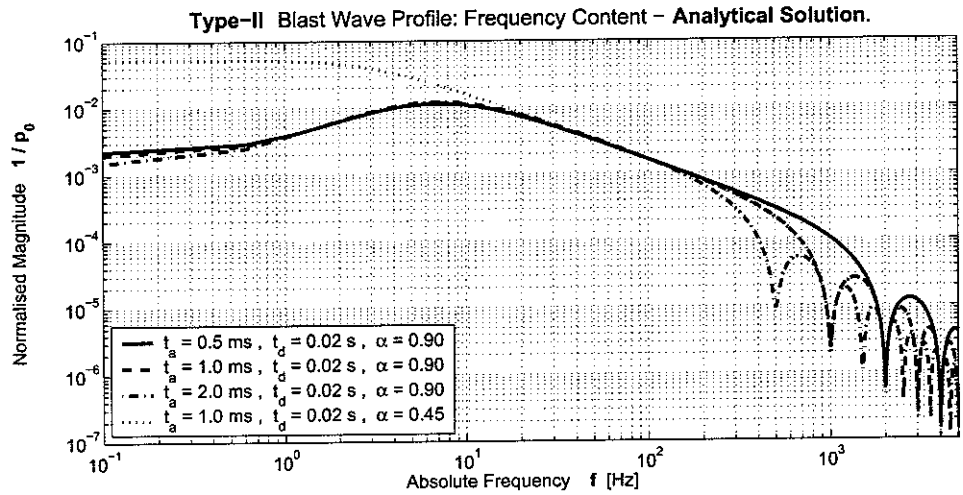

(c)

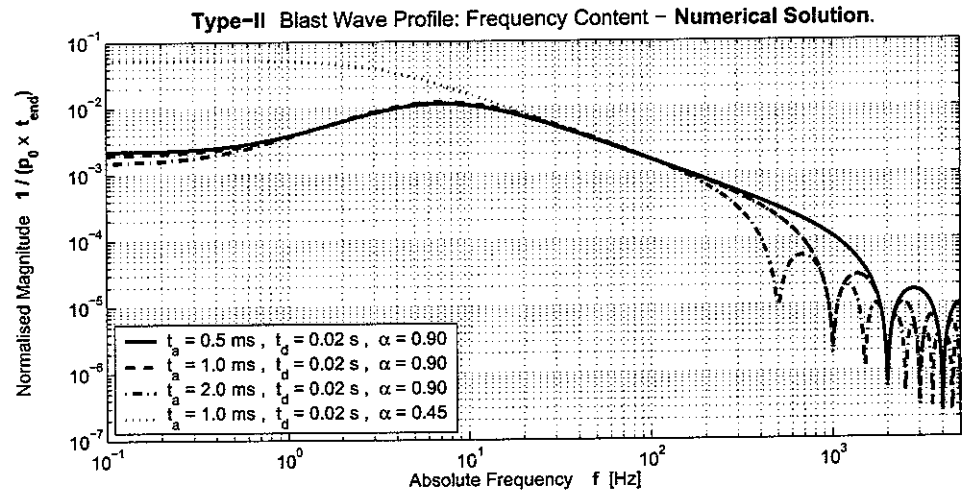

Figure 1.2.3: Blast wave profile type-II: *Explicit Form.* **(a)** Time history. **(b)** Analytical Fourier transform. **(c)** Numerical Fourier transform ($t_{\text{end}} = 2\,\text{s}$). Sampling frequency $f_s = \frac{1}{1 \cdot 10^{-4}\,\text{s}} = 10\,\text{kHz}$.

(a)

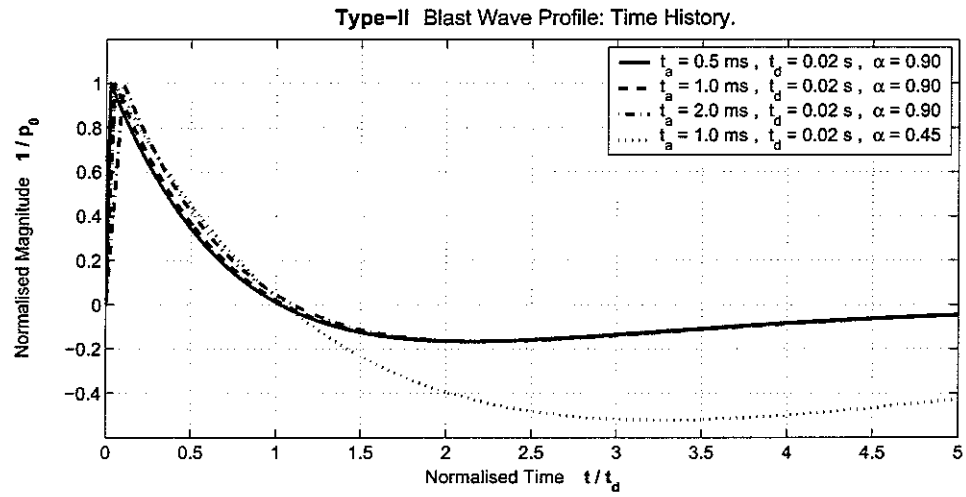

(b)

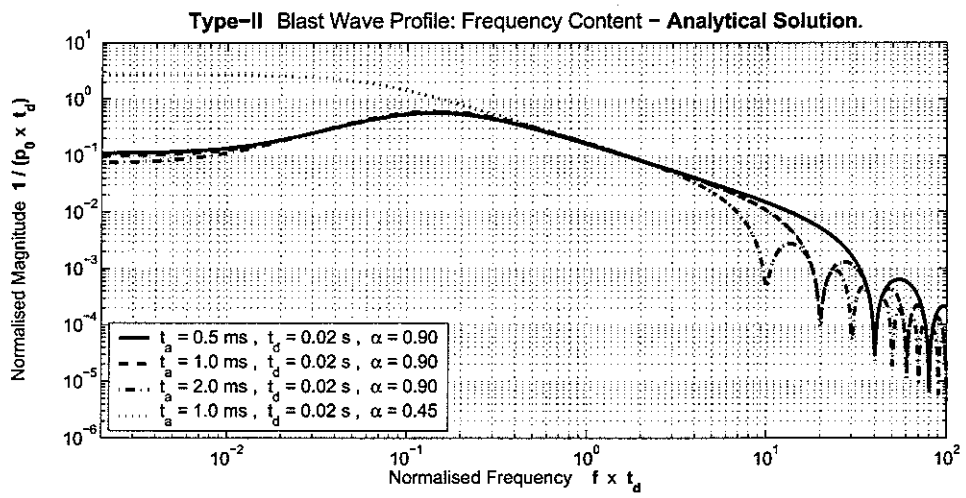

(c)

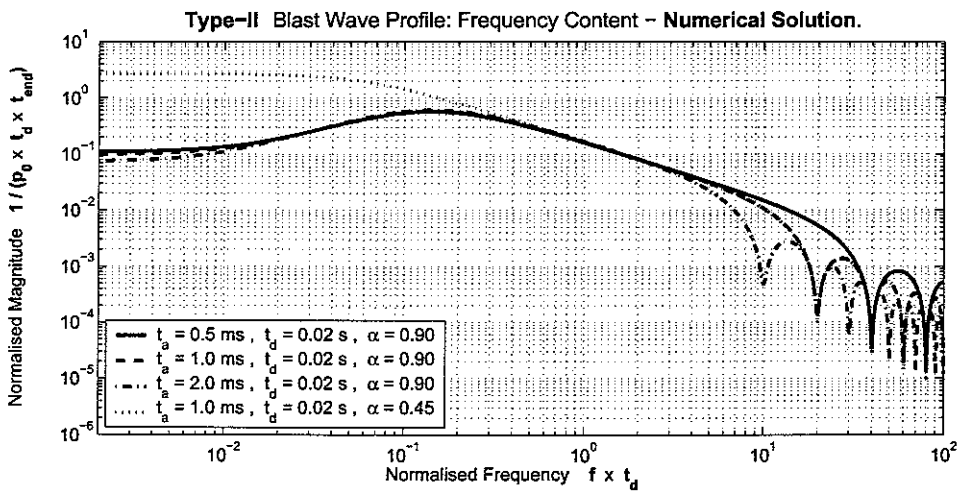

Figure 1.2.4: Blast wave profile type-II: *Normalised Form.* **(a)** Time history. **(b)** Analytical Fourier transform. **(c)** Numerical Fourier transform ($\tau_{\text{end}} = t_{\text{end}} = 5.0 \cdot 10^2$). Sampling frequency $f_s = 500\,\text{Hz}$.

CHAPTER 2

Response of Linear SDOF Systems to Blast Wave Excitation

2.1 Introduction

A comprehensive review of different theoretical analysis methods for predicting the response of various structures to highly transient excitations such as shock waves is given in [1]. The need to solve special types of similar problems in the past gave rise to innovative techniques referred to as the classical methods. In general, the classical methods, such as the exact solution of the governing differential equation, produce results to the problem in closed form which limits their availability to elementary problems. Contrary, numerical methods, which evolved with the development of computational capability, are capable of solving problems involving structures with complex geometries, stiffness and damping properties as well as loading patterns. According to [10] numerical methods can be grouped into three main categories:

(1) Time domain discretisation and numerical solution of the governing equation.

(2) Energy methods for continuous systems.

(3) Spatial discretisation using matrix algebra.

The **first** group produces an approximate solution of the governing differential equation by means of finite difference or numerical integration technique. The latter, a specially tuned Runge-Kutta algorithm [5] is used in chapter 3 to verify newly established analytical results and in chapter 4 for solving the SDOF system's equation of motion where no analytical solution can be found. The limiting factor of method 1 above is given by the fact that for the majority of problems in engineering application the governing differential equation cannot be established. However, it is the preferred method for the solution of simplified problems where the geometrical complex original structure can be reduced to a low order MDOF system or, in special cases, even to a SDOF system.

Group **two** focuses on simple, spatially continuous systems such as beams and plates. Using the sum of kinetic and strain energy which must be for conservative systems at all time equal to the energy done by external forces, leads to closed-form approximation formulations such as Rayleigh-Ritz or Galerkhin method. As will be seen in the next chapter, energy methods, due to their universal physical

appeal, are the basis for finding the exact solution for highly nonlinear, autonomous SDOF systems. The disadvantage can be seen in their limitation to conservative systems, thus making the response prediction of damped structures impossible. However, as long as *positive* damping is present in the problem, the true response magnitude for displacement, velocity and acceleration will always be well below the theoretically predicted result. Caution has to be taken when analysing damped strongly nonlinear systems since the oscillation frequency is dependent on the vibration amplitude.

Method **three** from above is based on the assumption that the entire structural system can be discretised into small elements which are only a small fraction of the size of the original structure. These elements are only connected through points called nodes. In a structural analysis the displacement field is defined separately for each element using, in general, polynomial type functions with unknown coefficients. Using energy methods similar to point 2 above the values of these coefficients and hence the displacement fields for each single element are established leading immediately to the displacement of the entire structure. Advanced computer programs have been developed for this numerical approach, referred to as finite element method (FEM).

However, despite their undeniable advantages in solving complex problems compared to classical analytical exact or approximation methods, numerical procedures do not allow for any significant insight into the physical phenomena of structural blast wave response. Of course, parameter studies can also be carried out using numerical procedures - and most of the time they are the only way due to the complexity of the problem - but this leads to heavy use of computational resources because of the sheer number of independent parameters involved in the problem. Secondly, results obtained usually cover only a small range of possible values for each parameter and hence cannot easily be generalised.

Due to the large amount of uncertainties involved in predicting the blast response of geometrically complicated structures, mainly caused by an uncomplete and inaccurate description of the impinging shock wave, this makes the use of sophisticated and complicated FE models questionable, which often require a lot of user experience, especially if used in connection with such highly transient and nonlinear problems. Furthermore, they are less suitable for quick, routine calculations during various design stages where the outline of the structure is subject to constant changes.

The question to ask must therefore be: Is it possible to establish a simple, analytical approximation method, which predicts the blast response of common basic structures within acceptable limits and provides physical insight, hence making it easy to qualitatively and quantitatively forecast changes in the system's reactions to reasonable changes in either the system or blast load parameters.

2.2 Solution Methods

This question has been addressed already in the past as given in [1], as well as in earlier publications [10]. Hand calculation methods for predicting the net load on a structure at large distances for similar blast profiles as the one in [2] are provided by GLASSTONE *et al* [11]. Based on these findings BAKER *et al* [12] developed a method which delivers closed-form solution of the deformed end state of shock loaded structures, either discrete or continuous, using the energy method as described above. A second simplification approach introduced by BIGGS [13], which transforms MDOF and continuous systems into SDOF systems, can be combined with Baker's method for geometrically complex continuous systems where a closed-form equation of the system's strain energy is often nonexistent.

As with every simplified approach, there are limits on its validity and shortfalls. The main deficiency of Baker's method, which is, without question, at the same time its most strongest asset in terms of simplicity, the transformation of the highly time-dependent process of shock response into an equivalent static loading act. The dynamic effect is then considered by a dynamic amplification factor which is defined as the ratio of dynamic to static response amplitude of the structural system. As will be seen in this and the following chapters, four different key factors can be identified having significant influence on the dynamic response of the structure:[1]

(i) Linear or nonlinear elastic or plastic deformation.

(ii) Natural frequency (or frequencies) of the system.

(iii) Duration t_d and magnitude p_0 of the pressure pulse.

(iv) Shape of the pressure pulse, i.e. rise time (time to reach the pressure maximum p_0) vs. exponential decaying time.

BAKER *et al* [12] proposes in his method approximate solutions by applying energy methods for special loading conditions, namely for

(a) short-duration, and

(b) long-duration

loading processes, relatively to the natural period of the structure. In case (a) above, the structure has only little time to undergo any significant deformation and hence to develop significant restoring force while the load is applied. Therefore, the loading is received similar to a Dirac-δ impulse giving an initial velocity. At points of maximum deflection this initial kinetic energy is entirely stored as strain energy which allows one to solve the governing equation for the maximum or minimum displacement. According to [10] this approach is generally valid for load duration to natural period ratios of *less* than 0.4. Given a positive pressure period t_d of 20 ms from chapter 1 would mean Baker's method for short-loading conditions is only valid for structures with less than 20 Hz natural frequency. Taking only the positive pressure into account might lead to significant errors since a major part of the total blast wave energy is stored in the profiles negative section. Therefore, assuming the entire time history in which $p_I(t)$ (or $p_{II}(t)$) have significant values to be at least 0.5 s would make the method only applicable to systems with less than 0.8 Hz. This renders Baker's method for short-duration processes as completely unsuitable for the combination of systems and load cases considered in this work.

In case (b) above, a long-duration loading relative to the structure's natural oscillation period is referred to as quasi-static. The load applied to the structure changes so slowly that the variation up to the time of maximum response is negligible. At the point of maximum deflection the strain energy stored in the system is equal to the work done by all external forces. According to [9] the range for applicable load duration to natural period ratios is *greater* than 4. Assuming a total time of significant pressure values for either p_I or p_{II} of 0.1 s, cf. chapter 1, the structure's natural frequency must be greater than 40 Hz which leaves the method unfeasible for a wide range of structures in the quasi-static loading case as well.

[1] This listing is more complete than the one given in [10].

It should be noted that all cases defined in [10], for which Baker's method is recommended, based on the assumption of zero reversed blast pressure, i.e. zero negative pressure, see Fig. 1.1.1 on page 6, which makes using the method even more questionable. Additionally, as will be seen in chapter 3, for nonlinear systems the natural oscillation frequency depends on the extreme amplitude of vibration and *none* of the ranges of feasibility as given above can be determined *before* applying the method and hence Baker's method fails completely for strongly nonlinear systems.

This makes it necessary to consider a second, more appropriate approximation method where the structural model, including the loading, is represented by a SDOF system. Based on tables introduced by BIGGS *et al* [13] the parameters and constants of this equivalent SDOF system are evaluated with respect to the characteristic shape of the actual structure at the stage of deformation, which is most likely to occur given the time-varying, spatially equally distributed pressure profile introduced in chapter 1 ensuring equality of work done between both systems. Once the MDOF structure has been transformed into a SDOF system using factors given in [13], the individual deformation stages can have different characteristic internal stiffness and damping mechanism ranging from purely linear elastic to geometrical nonlinear including possible plasticity. The analytical, combined analytical-numerical or purely numerical solution of the governing equation of motion for the SDOF system furnishes the method.

It is justifiable to argue that the assumed shape of deformation for the MDOF system might not represent the true failure mode of the structure and hence the subsequent transformation produces an ill-conditioned SDOF systems. This can be simply overcome by analysing one SDOF system for every anticipated mode of deformation. Moreover, as will be seen in a subsequent technical memo, it is possible to combine two modes of failure into a two-degree-of-freedom system, which can, under certain circumstance, also be solved analytically.

The flexibility of the second approach after [13] and completeness of the phenomena it accounts for makes it the method of choice for the work presented in this report.

2.3 Frequency Domain

The linear ordinary second order differential equation of motion for a SDOF system [14]

$$F(u) = \ddot{u}(t) + 2\zeta\omega_n\dot{u}(t) + \omega_n^2 u(t) - \frac{p(t)}{m} = 0 \tag{2.3.1}$$

can be rewritten as algebraic equation using Laplace transform [15]

$$\begin{aligned}\mathcal{L}\{F(u);s\} = \bar{F}(s) = s^2\bar{u}(s) - su(t=0) - \dot{u}(t=0) + \ldots \\ + 2\zeta\omega_n\left[s\bar{u}(s) - u(t=0)\right] + \omega_n^2\bar{u}(s) - \frac{\bar{p}(s)}{m} = 0\,.\end{aligned} \tag{2.3.2}$$

where $u(t)$ is the displacement in the time domain, $\bar{u}(s)$ the correspondent deformation in the complex Laplace domain, k and m are the system's stiffness and mass, respectively, ζ is the viscous damping ratio given by

$$\zeta = \frac{c}{2\sqrt{km}} \tag{2.3.3}$$

with c as the viscous damping coefficient, $\omega_n = \sqrt{\frac{k}{m}}$ is the system's natural frequency and $p(t)$ is the external applied force as a function of time.[2] Introducing the initial conditions for a system initially at

[2] In this work $p(t)$ is assumed to be of transient nature.

rest

$$u(t=0) = u_0 = 0$$
$$\dot{u}(t=0) = \dot{u}_0 = 0 \tag{2.3.4}$$

simplifies Eq.(2.3.2) to

$$\bar{F}(s) = s^2\bar{u}(s) + 2\zeta\omega_n s\bar{u}(s) + \omega_n^2\bar{u}(s) - \frac{\bar{p}(s)}{m} = 0\,. \tag{2.3.5}$$

Rearranging of (2.3.5) gives the transfer function of the linear SDOF system with respect to the initial conditions in (2.3.4)

$$\bar{h}(s) = \frac{\bar{u}(s)}{\bar{p}(s)} = \frac{1}{m\,(s^2 + 2\zeta\omega_n s + \omega_n^2)}\,. \tag{2.3.6}$$

For the more general case $u_0 \neq 0$, $\dot{u}_0 \neq 0$ Eq.(2.3.2) is rewritten as

$$s^2\,\bar{u}(s) + 2\zeta\omega_n\,(s\,\bar{u}(s) - u_0) + \omega_n^2\,\bar{u}(s) - s\,u_0 - \dot{u}_0 - \frac{\bar{p}(s)}{m} = 0 \tag{2.3.7}$$

which leads to

$$\bar{u}(s) = \frac{1}{m\left(s^2 + 2\zeta\omega_n s + \omega_n^2\right)}\left[\bar{p}(s) + m\left\{u_0\,(s + 2\zeta\omega_n) + \dot{u}_0\right\}\right]. \tag{2.3.8}$$

Using Eq.(2.3.6) this can be simplified to

$$\bar{u}(s) = \bar{h}(s)\left[\bar{p}(s) + \bar{q}_0(s)\right] \tag{2.3.9a}$$

with

$$\bar{q}_0(s) = m\left\{u_0\,(s + 2\zeta\omega_n) + \dot{u}_0\right\} \tag{2.3.9b}$$

being a notional load to the system imposed by the initial conditions.

Substituting for $\bar{p}(s)$ the Laplace transform of the blast wave profiles, Eq.(1.1.9) and (1.1.10) respectively, and letting $(s \longrightarrow \mathrm{i}\omega)$, where $\omega = 2\pi f$ is the circular frequency in $\frac{\mathrm{rad}}{\mathrm{s}}$, i.e. the number of oscillations in an time interval of 2π seconds, the response of the linear system due to the frequency components of the shock excitation is obtained. For the type-I and -II profiles this leads to

$$\tilde{u}_I(\omega) = \tilde{h}(\omega)\left[p_0\,\tilde{p}_I(\omega) + \tilde{q}_0(\omega)\right] \tag{2.3.10a}$$

and

$$\tilde{u}_{II}(\omega) = \tilde{h}(\omega)\left[p_0\,\tilde{p}_{II}(\omega) + \bar{q}_0(\omega)\right] \tag{2.3.10b}$$

where the Laplace transform of the unit impulse response function for the inhomogeneous system in Eq.(2.3.10) is given by

$$\tilde{h}(\omega) = \frac{1}{m\left[(\mathrm{i}\omega)^2 + 2\mathrm{i}\omega_n\omega\zeta + \omega_n^2\right]} = \frac{\omega_n^2 + 2\mathrm{i}\zeta\omega_n\omega - \omega^2}{m\left[\left(\omega^2 - \omega_n^2\right)^2 + \left(2\zeta\omega_n\omega\right)^2\right]} \tag{2.3.10c}$$

and the homogeneous part with $u_0 \neq 0$, $\dot{u}_0 \neq 0$ equates to

$$\tilde{q}_0(\omega) = m\left\{2\zeta\omega_n u_0 + \dot{u}_0 + \mathrm{i}\omega u_0\right\}. \tag{2.3.10d}$$

In the special case of zero initial conditions, i.e. $\bar{q}_0(\omega) = 0$, and together with Eq.(1.1.8a) and (1.1.8b), the frequency response can be expressed by the simplified equations

$$ {}_0\tilde{u}_I(\omega) = \frac{t_d\,(\alpha - 1 + \mathrm{i}\,\omega t_d)}{m(-\mathrm{i}\,\alpha + \omega t_d)^2\,(\omega^2 - 2\,\mathrm{i}\,\zeta\omega\omega_n - \omega_n{}^2)} \tag{2.3.11a} $$

and

$$ {}_0\tilde{u}_{II}(\omega) = \frac{e^{-\mathrm{i}\,\omega t_a}\left[\omega^2 t_a t_d\,(-1 + \alpha + \mathrm{i}\,\omega t_d)\right] - \left(-1 + e^{\mathrm{i}\,\omega t_a} - \mathrm{i}\,\omega t_a\right)(\alpha + \mathrm{i}\,\omega t_d)^2}{m\omega^2 t_a\,(\alpha + \mathrm{i}\,\omega t_d)^2\,(-\omega^2 + 2\,\mathrm{i}\,\zeta\omega\omega_n + \omega_n{}^2)}, \tag{2.3.11b} $$

respectively.

In order to obtain the SDOF response in the frequency domain due to the blast excitation in t_d-normalised form, Eq.(1.1.4) and (1.1.6), the equation of motion (2.3.1) of the structural system has to be rewritten as

$$ \frac{\ddot{u}(\tau)}{t_d^2} + 2\zeta\omega_n\frac{\dot{u}(\tau)}{t_d} + \omega_n^2 u(\tau) - \frac{p(\tau)}{m} = 0 \tag{2.3.12a} $$

which can be simplified to

$$ \ddot{u}(\tau) + 2\zeta\rho_n\dot{u}(\tau) + \rho_n^2 u(\tau) - t_d^2\frac{p(\tau)}{m} = 0 \tag{2.3.12b} $$

with $\rho_n = \omega_n \cdot t_d$ as the dimensionless circular natural frequency. The transfer function is similar to equation (2.3.10c)

$$ \tilde{h}(\rho) = \frac{t_d^2}{m\left[(\mathrm{i}\rho)^2 + 2\mathrm{i}\rho_n\rho\zeta + \rho_n^2\right]} \tag{2.3.13} $$

and for zero initial conditions the frequency domain response is given by

$$ {}_0\tilde{u}_I(\rho) = -\frac{t_d^2\,(\alpha - 1 + \mathrm{i}\,\rho)}{m(\alpha + \mathrm{i}\rho)^2\,(\rho^2 - 2\mathrm{i}\zeta\rho\rho_n - \rho_n^2)} \tag{2.3.14a} $$

and

$$ {}_0\tilde{u}_{II}(\rho) = \frac{e^{-\mathrm{i}\rho\tau_b}t_d^2\left[(\alpha - 1 + \mathrm{i}\rho)\rho^2\tau_b + (\alpha + \mathrm{i}\rho)^2\left(1 - e^{\mathrm{i}\rho\tau_b} + \mathrm{i}\rho\tau_b\right)\right]}{m\rho^2\tau_b\,(\rho + \mathrm{i}\alpha)^2\,(\rho^2 - 2\mathrm{i}\zeta\rho\rho_n - \rho_n^2)}, \tag{2.3.14b} $$

respectively. Both dimensionless frequencies are related by $\rho = 2\pi\eta$.

2.4 Time Domain

2.4.1 Analytical Solution

The response of the system in the time domain is obtained as an analytical expression by equating the inverse Laplace transform of Eq.(2.3.9) as defined in [15] and can be written in symbolic form as

$$ u_{I/II}(t) = \mathfrak{L}^{-1}\left\{\bar{u}_{I/II}(s); t\right\} \tag{2.4.1} $$

which equates to

$$ u_{I/II}(t) = p_0\,\mathfrak{L}^{-1}\left\{\bar{p}_{I/II}(s)\,\bar{h}(s); t\right\} + \mathfrak{L}^{-1}\left\{\bar{q}_0(s)\,\bar{h}(s); t\right\} \tag{2.4.2} $$

because of the linear nature of both the transformation and Eq.(2.3.10). Explicit expressions for equation (2.4.2) are given in appendix A.1.

Returning back to Eq.(2.3.1), the system's response in the time domain can alternatively be calculated by direct integration using the convolution integral [16]

$$u(t) = \int_0^t p(t-\hat{t})\,h(\hat{t})\,\mathrm{d}\hat{t} + u_\mathrm{h}(t) \tag{2.4.3a}$$

with $\hat{t}$ as integration variable. The applied pressure load is represented by $p(t)$ whereas $h(t)$ represents the impulse response function due to a unit impulse excitation in the time domain given for an undercritically damped SDOF with initial conditions $u_0 = 0$ and $\dot{u}_0 = \frac{1}{m}$ as

$$h(t) = \mathfrak{L}^{-1}\left\{\bar{h}(s);t\right\} = \frac{1}{m\omega_d}\,\mathrm{e}^{-\zeta\omega_n t}\sin(\omega_d t)\,, \qquad t > 0 \tag{2.4.3b}$$

where $\omega_d = \sqrt{1-\zeta^2}\,\omega_n$ is the damped natural frequency of the system. The term $u_\mathrm{h}(t)$ in (2.4.3a) expresses the solution obtained by solving the homogeneous version of Eq.(2.3.1) and equates to

$$u_\mathrm{h}(t) = \mathrm{e}^{-\zeta\omega_n t}\left[u_0\left(\cos(\omega_d t) + \frac{\zeta}{\omega_d}\sin(\omega_d t)\right) + \frac{\dot{u}_0}{\omega_d}\sin(\omega_d t)\right]. \tag{2.4.3c}$$

Substitution of Eq.(2.4.3b) and (2.4.3c) into Eq.(2.4.3a) gives the shock wave response of the SDOF oscillator in the time domain with two equations depending upon the blast wave type, Eq.(1.1.9) and (1.1.10) respectively,

$$u_I(t) = \frac{1}{m\omega_d}\int_0^t p_I(t-\hat{t})\,\mathrm{e}^{-\zeta\omega_n\hat{t}}\sin(\omega_d\hat{t})\,\mathrm{d}\hat{t} + u_\mathrm{h}(t)\,, \tag{2.4.4a}$$

$$u_{II}(t) = \frac{1}{m\omega_d}\int_0^t p_{II}(t-\hat{t})\,\mathrm{e}^{-\zeta\omega_n\hat{t}}\sin(\omega_d\hat{t})\,\mathrm{d}\hat{t} + u_\mathrm{h}(t)\,. \tag{2.4.4b}$$

Analytical evaluation of (2.4.4) leads to the same results as given in (A.1.2) and (A.1.3) since the convolution of two inverse Laplace transforms is equal to the inverse transform of their product in the Laplace domain [17]. The same method can be employed in finding the time domain response of the SDOF normalised by t_d. Again, results obtained are the same as those shown in appendix A.1.

Graphical representations of results for both equations (2.4.4), Eq.(A.1.2) and (A.1.3), respectively, are given in graphs (a) and (b) of Fig. 2.4.1 and 2.4.2 on page 27 and 28. The blast wave profile parameters are $t_a = 1.0\,\mathrm{ms}$, $t_d = 20\,\mathrm{ms}$ and $\alpha = 0.9$. The system's natural frequency f_n was set to 3 Hz in graph (a) and 30 Hz in graph (b). Furthermore, a viscous damping coefficient ζ equal to 0.01 has been assumed. A closer examination of the transient response behaviour in both figures 2.4.1 and 2.4.2 reveals only little difference in the maximum displacement amplitude of the SDOF oscillator if subjected to type-I or type-II blast profiles for the given excitation force and system parameters. In general terms, due to the larger amount of energy introduced into the structure by type-II profiles, the amplitudes of the first few half-cycles (transient response state) are slightly higher compared to the type-I excitation. However, after a few oscillation cycles (steady-state response) both displacement response plots are identical.

2.4.2 Numerical Solution

Equation (2.4.3a) can also be solved approximately by numerical integration. A fast and efficient algorithm for this linear problem providing an unconditionally stable solution is the Newmark β-method [4]. For two different natural frequencies of the linear system Fig. 2.4.1 shows a direct comparison between analytically obtained results using Eq.(A.1.2) and numerically computed data utilising the Newmark algorithm. Fig. 2.4.2 features exactly the same comparison for the response of the SDOF due to type-II blast wave excitation as given in Eq.(1.1.3) and in its explicit form in (A.1.3). By choosing the appropriate time step size in the non-adaptive integration algorithm, both figures easily verify the good agreement between analytical and numerical solution methods for the transient-type shock excitation of a linear single-degree-of-freedom system.

2.5 Shock Spectra for Blast Wave Excitation

The plot of the peak response of an undamped SDOF (mass-spring) system to a given shock load as a function of the natural frequency of the system is known as the shock spectrum [16]. Although a few examples of spectra for exponential pulses of infinite duration are given in [3], no analytical explicit relationship between the blast wave profiles (1.1.1) and (1.1.3), respectively, and the maximum deformation of the linear system $u_{\max}$ as a function of the natural frequency f_n has been found in literature.

As shown in appendix A.2 the maximum values of displacement ($n = 0$), velocity ($n = 1$) or acceleration ($n = 2$) can be obtained by setting the appropriate $(n+1)$ derivative with respect to t equal to zero, solving for t_{Ex} at which u_{Ex}, $\dot{u}_{Ex}$ or $\ddot{u}_{Ex}$ occur, re-inserting t_{Ex} into the equations for $u(t)$, $\dot{u}(t)$ or $\ddot{u}(t)$ and solving for the extreme values. There are two major limitations connected to this procedure. (i) first, the SDOF must be conservative, which can easily be achieved by setting ζ equal to zero, and (ii) second, this procedure is only applicable for special cases of (relatively simple) applied load functions.

2.5.1 Direct Solution Methods

A compilation of shock spectra for various types of time-varying excitation forces $P(t)$ as given in [3] suggest that it might be impossible to find the response spectra for a linear SDOF system if $P(t)$ exhibits alternating positive and negative values and the appropriate regions can not be modelled by sequences of impulse, step or linear ramping functions. A comparison of Fig. 2.4.1 with Fig. 2.4.2 underlines the problem of finding analytical expressions for minimum/maximum values of the state vector in the case of such arbitrary excitation functions as type-I and type-II blast waves, Eq.(1.1.1) and (1.1.3) respectively. Although damping is present and (i) is violated the problem still exists even in the case of $\zeta = 0$. It is not clear without ambiguity at which time t_{Ex} the extreme displacement will occur. This does depend upon both sets of parameters, the one for the excitation function and the one for the SDOF.

Taking the version of Eq.(A.1.2) from page 157 for the undamped SDOF system, i.e. $\zeta = 0$,

$$u_I(t) = \frac{p_0}{m\,\omega_n\left(\alpha^2 + t_d^2\,\omega_n^2\right)^2}\left(\mathrm{e}^{-\alpha\frac{t}{t_d}}\,t_d\Big[\alpha t_d\,\omega_n(\alpha-2) - \alpha^2\,\omega_n t + t_d^2\,\omega_n^3(t_d - t) + \ldots \right.$$
$$+ \mathrm{e}^{\alpha\frac{t}{t_d}}\Big(\left\{\alpha^3 - \alpha^2 + t_d^2\,\omega^2\,(\alpha+1)\right\}\sin(\omega_n t) + \ldots \qquad (2.5.1a)$$
$$\left. - t_d\,\omega_n\left\{\alpha^2 - 2\alpha + t_d^2\,\omega_n^2\right\}\cos(\omega_n t)\Big)\Big]\right),$$

the first derivative $\dot{u}_I(t) = \frac{\mathrm{d}u_I(t)}{\mathrm{d}t}$ with respect to time t

$$\dot{u}_I(t) = \frac{1}{m\left(\alpha^2 + t_d^2\,\omega_n^2\right)^2}\left(\mathrm{e}^{-\alpha\frac{t}{t_d}}\Big[\alpha^2\,(t_d + \alpha t - \alpha t_d) - t_d^2\,\omega_n^2\,(t_d - \alpha t + \alpha t_d) + \ldots \right.$$
$$+ \mathrm{e}^{\alpha\frac{t}{t_d}}\,t_d\Big(t_d\,\omega_n\left\{\alpha^2 - 2\alpha + t_d^2\,\omega_n^2\right\}\sin(\omega_n t) + \ldots \qquad (2.5.1b)$$
$$\left. + \left\{\alpha^3 - \alpha^2 + t_d^2\,\omega_n^2\,(\alpha+1)\right\}\cos(\omega_n t)\Big)\Big]\right) = 0$$

has to be equal to zero. One way of finding a solution is rewriting Eq.(2.5.1b) as a coupled set of two linear algebraic equations

$$\begin{aligned} &(i) \quad \alpha^2\,(t_d + \alpha t - \alpha t_d) - t_d^2\,\omega_n^2\,(t_d - \alpha t + \alpha t_d) &&= 0 \\ &(ii) \quad b_s\sin(\omega_n t) + b_c\cos(\omega_n t) &&= 0 \end{aligned} \qquad (2.5.1c)$$

where

$$b_s = t_d\,\omega_n\left\{\alpha^2 - 2\alpha + t_d^2\,\omega_n^2\right\} \quad \text{and} \quad b_c = \left\{\alpha^3 - \alpha^2 + t_d^2\,\omega_n^2\,(\alpha+1)\right\}. \qquad (2.5.1d)$$

It is easy to see that (i) gives

$$t = t_d\left(1 + \frac{1}{\alpha} - \frac{2\alpha}{\alpha^2 + t_d^2\,\omega_n^2}\right) \qquad (2.5.1e)$$

which can be reinserted into (ii) and eliminates t completely. Hence, Eq.(2.5.1c) has apparently no solution for the time $t_{\max}$ at which $u_{\max}$ from (2.5.1a) occurs.[3]

A second attempt to solve Eq.(2.5.1b) in an analytical manner, now by means of approximation, starts with reformulating equation (2.5.1b) as

$$\dot{u}(t) = \frac{1}{C}\left(\mathrm{e}^{-\alpha\frac{t}{t_d}}\,A_p(t) + t_d\,b_s\sin(\omega_n t) + t_d\,b_c\cos(\omega_n t)\right) \qquad (2.5.2a)$$

where

$$C = m\left(\alpha^2 + (t_d\omega_n)^2\right)^2 \quad \text{and} \quad A_p(t) = \alpha^2\,(t_d + \alpha t - \alpha t_d) - (t_d\omega_n)^2\,(t_d - \alpha t + \alpha t_d)\,. \qquad (2.5.2b)$$

The expressions $\left[\mathrm{e}^{-\alpha\frac{t}{t_d}}\,A_p(t)\right]$ and $\left[t_d\,b_s\sin(\omega_n t) + t_d\,b_c\cos(\omega_n t)\right]$ in Eq.(2.5.2a) are the first derivatives with respect to time of the particular integral and the complementary function, respectively.

[3] It should be noted that this method of setting each of the two addends of Eq.(2.5.1b) separately equal to zero confines the possible solution space for $t_{\max}$. The ill-conditioned remaining equation resulting from insertion of (i) into Eq.(ii) shows that there exists no $t \in \mathbb{R}$ which fulfills the artificially introduced requirement of having both addends in Eq.(2.5.1b) equal zero at the same time t. However, by plotting $\dot{u}_I(t)$ against t it becomes clear that time points $t_{\max,i}$ exist at which $\dot{u}_I(t) = 0$.

No closed form solution exists for the zeros of the function in equation (2.5.2a). For SDOF linear natural frequencies of $1 \leq f_n \leq 100\,\text{Hz}$ the point of time $t_{\max}$ can usually be found within the limits $0 < t_{\max} \leq 1\,\text{s}$. Therefore, a Taylor series expansion around the point $t = 0$ would transform the exponential-transcendental Eq.(2.5.2a) into a polynomial of maximum order $n \leq 4$ to be solvable analytically.[4] The Euler or exponential function can be expressed as [15]

$$e^{\alpha \frac{t}{t_d}} \approx \sum_{k=0}^{4} \frac{\left(\alpha \frac{t}{t_d}\right)^k}{k!} \tag{2.5.2c}$$

whereas sine and cosine functions are approximately rewritten as

$$\sin(\omega_n t) = \omega_n t - \frac{(\omega_n t)^3}{3!} \quad \text{and} \quad \cos(\omega_n t) = 1 - \frac{(\omega_n t)^2}{2} + \frac{(\omega_n t)^4}{4!}. \tag{2.5.2d}$$

Unfortunately, plotting the original function, Eq.(2.5.2a), against its Taylor approximations in (2.5.2c) and (2.5.2d) shows that the series expansion terminates far too early to model the original equation at the point $t_{\max}$ and more terms would be required in the expansion in (2.5.2c) and (2.5.2d). This in turn makes (2.5.2a) again analytically unsolvable.

A third way to find the extreme values of Eq.(2.5.1a) is based on the fact that for linear systems the oscillation frequency is a fundamental property of the system itself and stays constant as long as the oscillator remains unaltered. However, this is only fully true for the steady-state solution of the dynamic system, not for the preceding transient oscillation phase where the system moves with a combined frequency consisting of two components, the natural frequency f_n and the forcing frequency f_p. In case of harmonic or periodic applied force functions this combined frequency can be obtained in a rather straightforward way. In the case of transient system input such as the blast profiles introduced, this is hardly possible. Therefore, the real oscillation frequency of the non-steady-state remains unknown. However, for a wide range of blast profile parameters α, t_a and t_d as introduced in chapter 1 the actual oscillation frequency in the transient response state varies approximately up to 15% from the systems natural frequency f_n if $f_n \leq 10\,\text{Hz}$. For larger f_n the error increases significantly. Moreover, there is no clear pattern in which direction, positive or negative, the real frequency differs from f_n. Therefore, a proposed method of inserting multiples of $\frac{1}{2} f_n$ into equation (2.5.1a) in order to obtain a global maximum displacement $u_{\max}$ is unsuitable.

Finally, the last resort of solving Eq.(2.5.1b) in order to obtain maxima solutions for (2.5.1a) has to be purely numerical. Thus, employing Newton's method [15], with the appropriate calculation starting point $t_{N,0}$ sufficiently close to an existing root of (2.5.1b), its value can easily be determined.

2.5.2 Linear Approximation

Instead of attempting to solve equation (2.5.1b) directly the blast wave profile (1.1.1) is approximated in a piecewise linear manner as shown in Fig. 2.5.1 on page 29. The linear approximation profile is obtained with respect to energy conservation rather than a least square curve fitting. Furthermore, in order to obey a causal response in the substituted system the two critical time points t_d and t_{A2} have

[4] Equation (2.5.2a) or (2.5.1b), respectively, could be approximated by a Taylor series of any desired order n. However, as shown in appendix B on page 185, closed form solutions for polynomials of order > 4 can only be obtained in special circumstances dependent on the nature of the equation to be solved.

been retained. The first, t_d, marks the time span of positive overpressure whereas the latter, t_{A2}, gives the time point of maximum negative pressure of the original profile (1.1.1) and is obtained by simply setting its first derivative with respect to time equal zero

$$\frac{\mathrm{d}p(t)}{\mathrm{d}t} = -\frac{p_0}{t_d^2}\,\mathrm{e}^{-\alpha\frac{t}{t_d}}\,(t_d - \alpha t + \alpha t_d) \stackrel{!}{=} 0 \tag{2.5.3a}$$

and solving for t

$$t_{A2} = t_d\left(1+\frac{1}{\alpha}\right). \tag{2.5.3b}$$

The new positive and negative magnitudes, $p_{0\Delta}$ and $p_{1\Delta}$, are calculated from the constraint that the area under the straight lines is equal to the area under the original profile curve for each time segment 1 to 3 (equal energy input). Therefore, t_E is adjusted accordingly. Integration of Eq.(1.1.1) for the intervals $(0;t_d)$, $(t_d;t_{A2})$ and $(t_{A2};t_E)$ gives

$$p_{0\Delta} = 2\frac{p_0}{\alpha^2}\left(\mathrm{e}^{-\alpha}+\alpha-1\right) \tag{2.5.4a}$$

$$p_{1\Delta} = -2\frac{p_0}{\alpha}\left(\mathrm{e}^{-\alpha}-2\mathrm{e}^{-\alpha-1}\right) \tag{2.5.4b}$$

$$t_E = t_d\left(1+\frac{1}{\alpha}+\frac{2}{\alpha p_0\,(\mathrm{e}-2)}\right) \tag{2.5.4c}$$

which are required for the three piecewise linear forces

$$p_1(t) = p_{0\Delta}\left(1-\frac{t}{t_d}\right), \qquad 0 \le t \le t_d \tag{2.5.5a}$$

$$p_2(t) = p_{1\Delta}\left(\frac{t-t_d}{t_{A2}-t_d}\right), \qquad t_d \le t \le t_{A2} \tag{2.5.5b}$$

$$p_3(t) = p_{1\Delta}\left(1-\frac{t-t_{A2}}{t_E-t_{A2}}\right), \qquad t_{A2} \le t \le t_E \tag{2.5.5c}$$

as shown in Fig. 2.5.1. The SDOF response for each time segment r with $r = 1,2,3,4$ is obtained by using Eq.(2.4.3a) from page 17 with zero damping ($\zeta = 0$)

$$u_r(t) = \int_{\hat{t}_r}^{t} p_r(t-\hat{t})\,h(\hat{t})\,\mathrm{d}\hat{t} + u_{\mathrm{h},r}(t), \qquad \begin{matrix} r &=& 1,2,3,4 \\ \hat{t}_r &=& 0,t_d,t_{A2},t_E \end{matrix} \tag{2.5.6}$$

leading for the unit impulse response $h(t)$ to

$$h(t) = \frac{1}{m\omega_n}\sin(\omega_n t) \tag{2.5.7}$$

and the initial conditions u_h to

$$u_{\mathrm{h},r}(t) = u_{0,r}\cos(\omega_n t) + \frac{\dot{u}_{0,r}}{\omega_n}\sin(\omega_n t), \qquad r = 1,2,3,4 \tag{2.5.8}$$

with $u_{0,1} = \dot{u}_{0,1} = 0$. Setting the first derivative of each solution equal zero

$$\frac{\mathrm{d}u_r(t)}{\mathrm{d}t} := 0 \tag{2.5.9}$$

allows closed-form solutions to be found for time points t_{max} where $u_{r,max}$ occurs. Each section 1 to 4 in Fig. 2.5.1 has to be treated independently since the shock excitation force is represented by a discontinuous non-smooth function. The connective link between each segment is given by the appropriate

initial conditions at the start of each time segment, $u_{0,r+1} = u_r(t_r)$ and $v_{0,r+1} = u_r(t_r)$, respectively, with $t_r = t_d$, t_{A2} and t_E as $r = 1,2,3$. A detailed description of the solution procedure is given in appendix A.1.2 on page 176.

The motivation for the method lies in its superior efficiency compared to the much less advanced procedure of calculating the entire time history for a given natural frequency f_n and subsequently finding the appropriate extreme displacements (minima/maxima) in order to obtain the shock spectra of the linear undamped SDOF system. Roughly, with about 25% of the calculation steps used by the exact method to calculate the time history at *one* specific natural frequency, the approximate procedure is capable of obtaining the entire response spectra. But, as with most simplification, the gain in calculation speed has to be paid by less accurate results. However, the next section compares both methods and shows that spectra obtained by the approximation method tend to overestimate the actual system deformation u_{Ex} and proves therefore the method to be a fast and reliable alternative to the time and resource consuming exact solution method, especially for early design stage application.

2.5.3 Results

Exact Solution

Using the simplified, undamped version of Eq.(A.1.2) and (A.1.3), different shock spectra graphs for type-I and type-II blast excitation were produced. As explained above, no explicit analytical formula expressing the maximum displacement at a single frequency in terms of the blast wave and system parameters could be found. Therefore, complete time series at single frequencies had to be calculated and the maximum values were obtained. Because of the very good agreement between analytical and numerical solution, see Fig. 2.4.1 and 2.4.2, this can be done using either of them. However, the authors suggest employing the analytical formulas for the computation of time histories prior to shock spectra if computer resources are limited and studies conducted involve a broad range of system and blast wave parameters. Although implementation of the analytical solutions especially Eq.(A.1.3) can be difficult and erroneous, it is about 3 times faster and requires 80% less memory than the Newmark algorithm.

In all of the following shock spectra plots Fig. 2.5.2 to 2.5.8 the natural frequency f_n of the linear SDOF was chosen as independent parameter. It should be noted here that all spectra can also be given in terms of a normalised natural frequency, preferably $\eta_n = f_n \times t_d = \frac{\rho_n}{2\pi}$, see Eq.(2.3.12b) on page 16. The angular natural frequency is given by $\omega_n = 2\pi f_n$ and the system's stiffness equates to $k = m\omega_n^2$ with the mass m set equal to unity. The influence of the two blast wave types I and II on the SDOF response behaviour has been examined by allocating the parameters α, t_a and t_d with different values obtained from [18].

Figure 2.5.2 on page 30 shows the normalised maximum dynamic displacement of the SDOF system over its natural frequency f_n due to a type-I blast wave with $\alpha = 0.9$ and different values for t_d. Each curve in Fig. 2.5.2 exhibits the same jump phenomena at a certain frequency f_J and can therefore be divided into two regions, one with negative maximum displacement and one with positive displacement only.[5] Both Fig. 2.5.2 and 2.5.3 clearly show the independence of the maximum negative displacement amplitude from the SDOF's natural frequency f_n. All negative maxima occur at different

[5] In case it would be possible to find a closed-form solution for Eq.(2.5.1b), i.e. t_{max}, the function for u_{max}, Eq.(2.5.1a), would exhibit a discontinuity at f_J, i.e. the first derivative with respect to the natural frequency $\frac{du_{max}(f_n)}{df_n}$ would not exist as $f_n \to f_J$.

f_n but their absolute magnitudes stay constant regardless of the value of f_n. This can be explained by returning to Fig. 1.2.1(a) on page 7. Changing the positive overpressure time t_d within a range of $0.01\,\mathrm{s} \leq t_d \leq 0.04\,\mathrm{s}$ has no influence on the negative pressure amplitude and only a little influence on the total energy provided by the negative part of the blast wave. Therefore, as shown in Fig. 1.2.1, increasing α decreases the total amount of energy input into the SDOF significantly. Hence, increasing α reduces the negative deformation amplitude of the system as seen in Fig. 2.5.3.

Comparing Fig. 1.2.1(a) and 1.2.3(a) on page 7 against Fig. 2.4.1 and 2.4.2 by plotting the time history of the blast wave profile as applied load versus the displacement response $u(t)$ of the SDOF shows that for all frequencies below f_J the system is just too slow to react with its positive maximum displacement to the positive force $p(t)$ provided during $0 \leq t \leq t_d$. Instead, on returning from a point of positive displacement back to the equilibrium position, the SDOF absorbs all energy provided by the negative overpressure, which immediately leads to the overall but negative maximum displacement. In the second half of the full cycle, by passing again through the static equilibrium position into the positive half-plane, the system is still subjected to negative pressure. This leads now to a reduction of the positive amplitude and after several oscillation periods the SDOF motion becomes steady-state.[6]

After passing the discontinuity in the shock spectra, i.e. the point where the system has either a maximum negative or positive displacement, it is clear in Fig. 2.5.3 (type-I, $\alpha = 2.7$) that for SDOF systems with natural frequencies $f_n = 1/t_d$, the positive maximum dynamic displacement u_{dyn} is about equal to the static displacement, i.e. $u_{\mathrm{dyn}}/u_{\mathrm{stat,lin}} = 1$. This is not true for type-I $\alpha = 0.9$ blast profiles in Fig. 2.5.2 where the positive maximum u_{dyn} is about $1.3 \times u_{\mathrm{stat}}$. However, for low to moderate natural frequencies, about up to 600 Hz, u_{dyn} varies significantly with respect to t_d. At $f_n = 200\,\mathrm{Hz}$, for example, a doubling of the positive overpressure time from $t_d = 0.005\,\mathrm{s}$ to $0.01\,\mathrm{s}$ leads to a 40% higher dynamical response of the SDOF in Fig. 2.5.3, whereas for type-I and $\alpha = 0.9$, Fig. 2.5.2, the increase is only about 20%. In contrast, at high and very high natural frequencies, $f_n > 750\,\mathrm{Hz}$, doubling of t_d becomes less critical for the system's response and insignificant for increasing absolute values beyond $0.04\,\mathrm{s}$, i.e. at $f_n = 800\,\mathrm{Hz}$ the change in the ratio $u_{\mathrm{dyn}}/u_{\mathrm{stat}}$ by doubling t_d from $0.005\,\mathrm{s}$ to $0.01\,\mathrm{s}$ is much larger than the change by doubling t_d from $0.02\,\mathrm{s}$ to $0.04\,\mathrm{s}$. Although the graph for $\alpha = 2.7$ in Fig. 2.5.3 shows a slightly different response behaviour of the SDOF, both figures can be summarised by the following statements:

(a) for undamped SDOF natural frequencies below a certain frequency f_J determined by the blast wave profile parameters t_d and α, the linear oscillator responds with a maximum negative displacement, which can, subject to the value of parameter α, exceed the static displacement significantly, see Fig. 2.5.2,

(b) for frequencies $f_n > f_J$ the oscillator exhibits only maximum positive displacement,

(c) for high to very high natural frequencies $f_n > 600\,\mathrm{Hz}$ and values for

$$t_d > 0.02\,\mathrm{s} \quad \text{and} \quad 3.0 \geq \alpha \geq 1.0$$

[6] It should be noted here that Fig. 2.4.1 and 2.4.2 show the response of the damped single-degree-of-freedom oscillator. However, omitting the fact that for $\zeta \neq 0$ the amplitudes of the steady-state solution become smaller during each cycle, the fact that the maximum negative or positive displacement occurs during the transient response state holds also true for the undamped oscillator, which is not pictured here.

the system's maximum dynamic displacement can be approximated by the SDOF response to a scaled unit step function $p(t) = p_0 \times \mathbb{H}(t)$, with p_0 as the maximum overpressure, which is equal to twice the static displacement, see appendix A.2.2,

(d) for large values of $t_d \gg 0.02\,\mathrm{s}$ and small values of $\alpha \ll 1.0$ the SDOF maximum dynamic response is equal to twice the static displacement as in (c) but for the entire range of natural frequencies $f_J \leq f_n \leq \infty$, i.e. the system's response to the applied load (blast wave profile) can be modelled using $p_0 \times \mathbb{H}(t)$ instead.

Referring to Fig. 1.2.1(b), taking into account that the SDOF frequency behaviour can be calculated using multiplication of Laplace transforms of the time domain formulations of the applied force and the structural system, and, knowing that the undamped SDOF has a single resonance point at is natural frequency, the conclusions drawn in (c) and (d) are supported. Larger values of t_d and smaller values of α shift the energy content of the type-I and II blast wave profile into regions of lower frequency. However, a closer examination of Fig. 2.5.4 and 2.5.5 makes it necessary to add a fifth statement only valid for the SDOF shock spectra due to a type-II blast wave profile.

(e) depending upon the finite rising time t_a the response of the SDOF oscillator can significantly vary between $u_{\mathrm{stat}} \leq u_{\mathrm{dyn}} \leq 2 \times u_{\mathrm{stat}}$ for all natural frequencies $f_n \geq f_J$. Therefore, the approximation for the maximum dynamic displacement being twice the static as proposed in (c) and (d) above is only valid, if the positive overpressure rising time t_a is sufficiently small.

In case of the spectra shown in Fig. 2.5.4 and 2.5.5 on page 31 with $t_a \leq 0.1\,\mathrm{ms}$ one is able to approximate the maximum dynamic displacement u_{dyn} by $2 \times u_{\mathrm{stat}}$ over the whole frequency range $f_J \leq f_n \leq 1.0\,\mathrm{kHz}$. If, say, only the range $0.2 \leq f_n \leq 0.6\,\mathrm{kHz}$ is of immediate interest the statements made in (c) and (d) would still apply. Clearly, the dips noticed in the SDOF's response pictured in both Figures 2.5.4 and 2.5.5 originate from the roll-off of energy as shown in the power spectrum for blast wave type-II in Fig. 1.2.3 on page 9.

By comparing Fig. 2.5.2 with 2.5.4 and Fig. 2.5.3 with 2.5.5 two more similarities between type-I and type-II response can be identified. First, the absolute maximum oscillation amplitudes in both the negative and positive region (before the roll-off) are equal. Secondly, the jump phenomena in the shock spectra occurs at exactly the same frequency, which proves it is independent of t_a. To summarise, the type-II blast wave profile parameter t_a only accounts for significantly reduced maximum dynamic displacement of the SDOF at certain natural 'resonance' frequencies $f_{n,R_i} = i \times \frac{1}{t_a}$ where $i = 1, 2, \ldots$ as given in Fig. 1.2.3(b). As one would expect, in the case $t_a \to 0$ the SDOF shock spectra response is exactly the same form as due to an excitation by a type-I blast.

As mentioned before, not only the vertical ordinate axis can be plotted in a normalised manner, e.g. $u_{\mathrm{dyn}}/u_{\mathrm{stat,lin}}$, the same is possible for the abscissa. Using t_d as normalisation factor gives the response solution to the equation of motion for a normalised SDOF system as derived in Eq.(2.3.12a) on page 16. For the graphs in both figures 2.5.2 and 2.5.3 on page 30 in particular, this would result in an overlay of all four lines similar to Fig. 2.5.4 and 2.5.5.

In order to verify both analytical and numerical methods as before, Fig. 2.5.6 has been included, which shows the time domain numerical response of the linear system with natural frequencies of 520 Hz and 1.0 kHz respectively. Direct comparison between Fig. 2.5.2, 2.5.4 and Fig. 2.5.6 shows, for

Table 2.5.1: Approximation profile time parameter: Negative maximum overpressure time t_{A2} and total forcing time t_E in seconds as a function of the positive overpressure time t_d. Graphical explanation is provide in Fig. 2.5.1 on page 29. Approximate positive and negative pressure amplitude stay constant with changing t_d, see Eq.(2.5.4), at $p_{0\Delta} = 0.75696 \times p_0$ and $p_{1\Delta} = -0.23874 \times p_0$, respectively, for $\alpha = 0.9$.

t_d [s]	t_{A2} [s]	t_E [s]
5.0E-3	1.0556E-2	2.6025E-2
1.0E-2	2.1111E-2	5.2049E-2
2.0E-2	4.2222E-2	1.0409E-1
4.0E-2	8.4444E-2	2.0819E-1

example, the normalised maximum displacement for $f_n = 520\,\text{Hz}$ and $f_n = 1.0\,\text{kHz}$ does not exceed the magnitude of 1.0 for a positive pressure build-up time of 2 ms.

Using the fast analytical solution procedure as explained above, Eq.(A.1.2) and (A.1.3), respectively, with $\zeta = 0$, three dimensional plots showing the influence of t_d and f_n upon the maximum displacement for the type-I shock wave and t_a in case of type-II shock were obtained, see Figures 2.5.7 and 2.5.8.

Piecewise Linear Approximation

Figure 2.5.9 on page 35 shows results obtained using the approximation method in comparison to the exact solution. Table 2.5.1 gives the values for the individual segment time parameters t_{A2} and t_E, respectively. Despite the fact that the approximation method predicts negative extreme displacement, see graph (a), at natural frequencies f_n when u_{Ex} is actual positive (exact solution), it will *always* overestimate the absolute value $|u_{Ex}|$. In the case of Fig. 2.5.9 the approximate extreme displacement is up to 25% higher than the one calculated using Eq.(2.5.1a), i.e. the real blast profile. Furthermore, the shift of the frequency point f_J where u_{Ex} changes sign from negative to positive values is proportional to t_d for all graphs. Multiplication of all 8 lines in Fig. 2.5.9(a) would give one single frequency f_J for all four values of t_d at around 0.645 for the exact solution and 0.841 for the approximate profile solution.[7]

Figure 2.5.9(b) shows time points t_{Ex} in seconds at which u_{Ex} from graph (a) occurs. It is important to note that at f_J, i.e. the SDOF system's natural frequency where u_{Ex} changes sign from negative values u_{min} to positive values u_{max}, a drop of t_{Ex} takes place. For the exact profile this is a rather abrupt one where as for the approximate solution there is first an increase before f_n reaches f_J and than a significant decline to the same level as produced by the exact blast profile. However, for both methods the value of t_{max} lies well below t_d. As an important consequence, for applied force/SDOF system configurations as given in Fig. 2.5.9 the maximum deformation u_{max} above the jump frequency f_J

[7]The values are obtained by multiplying the frequency point f_J times t_d. Examining Fig. 2.5.9(a) at a higher graphical resolution this gives for the type-I profile

$$129.0 \times 5.0\text{E-}3 = 6.45\text{E-}1 \approx 64.5 \times 1.0\text{E-}2 = 6.45\text{E-}1 \approx 32.25 \times 2.0\text{E-}2 = \ldots$$

and for the approximate excitation force

$$168.2 \times 5.0\text{E-}3 = 8.41\text{E-}1 \approx 84.2 \times 1.0\text{E-}2 = 8.42\text{E-}1 \approx 42.1 \times 2.0\text{E-}2 = \ldots.$$

occurs always within the time interval $0 \leq t \leq t_d$, i.e. during the positive overpressure phase. Whereas if the system's natural frequency stays below f_J the maximum negative displacement $u_{\min}$ can occur up to 0.5 seconds after the excitation has initially been applied.

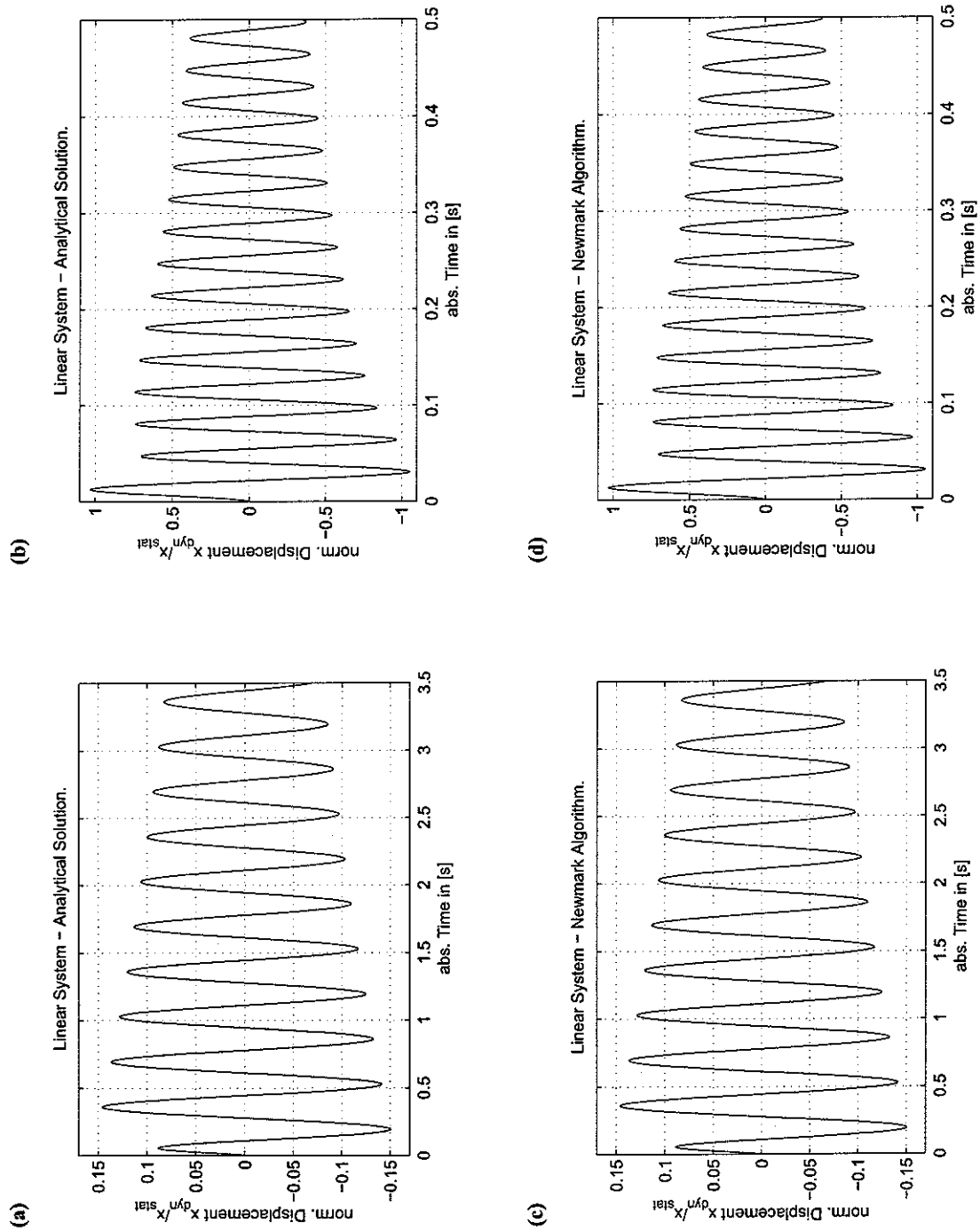

Figure 2.4.1: Response of damped linear SDOF-oscillator with natural frequency f_n due to **type-I** blast wave profile ($t_d = 0.02\,\mathrm{s}$, $\alpha = 0.9$): Comparison between analytical results and Newmark β-method. **(a),(c)**: $f_n = 3.0\,\mathrm{Hz}$, $\zeta = 0.01$. **(b),(d)**: $f_n = 30.0\,\mathrm{Hz}$, $\zeta = 0.01$.

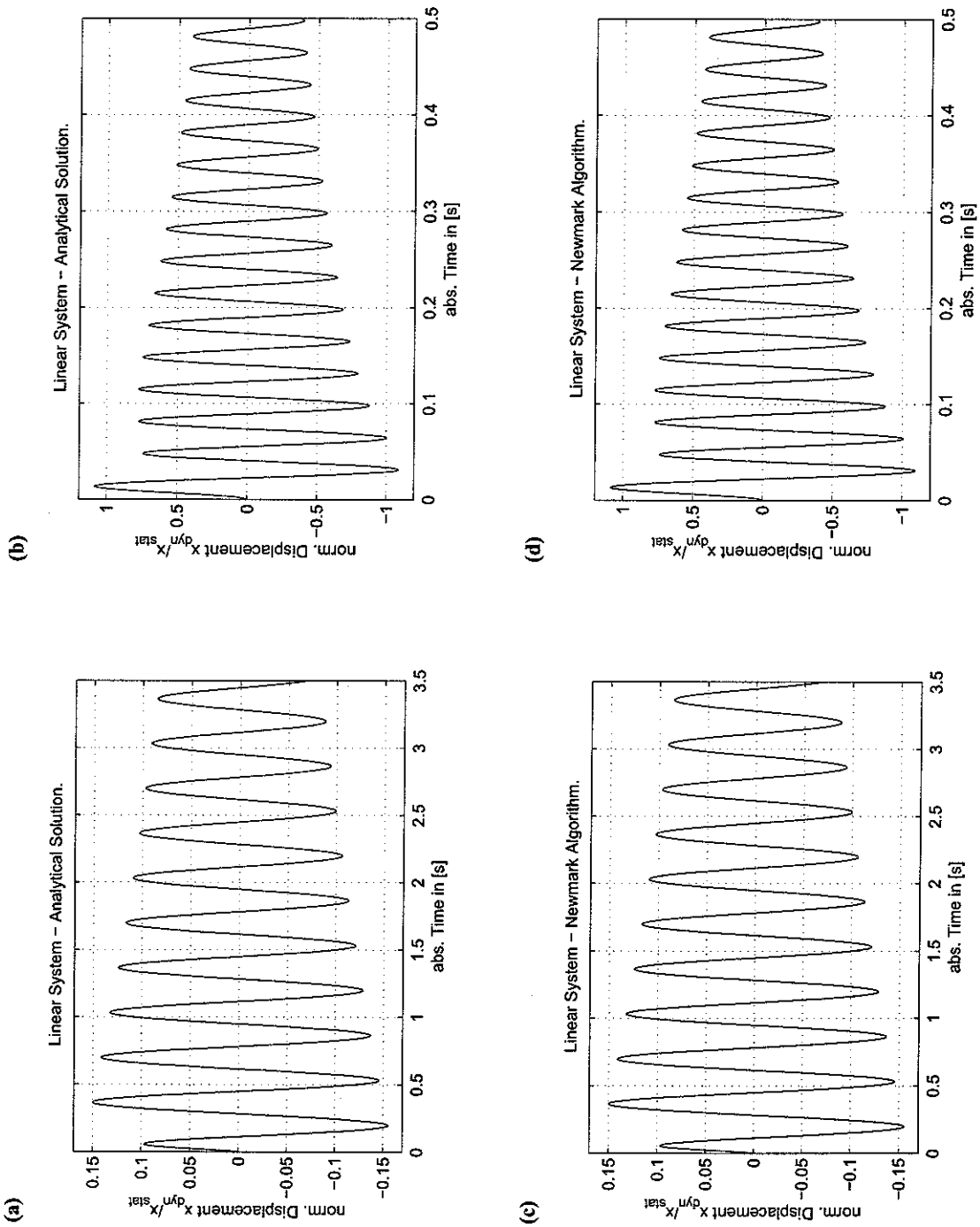

Figure 2.4.2: Response of damped linear SDOF-oscillator with natural frequency f_n due to **type-II** blast wave profile ($t_a = 1.0\,\text{ms}$, $t_d = 0.02\,\text{s}$, $\alpha = 0.9$): Comparison between analytical results and Newmark β-method. **(a),(c)**: $f_n = 3.0\,\text{Hz}$, $\zeta = 0.01$. **(b),(d)**: $f_n = 30.0\,\text{Hz}$, $\zeta = 0.01$.

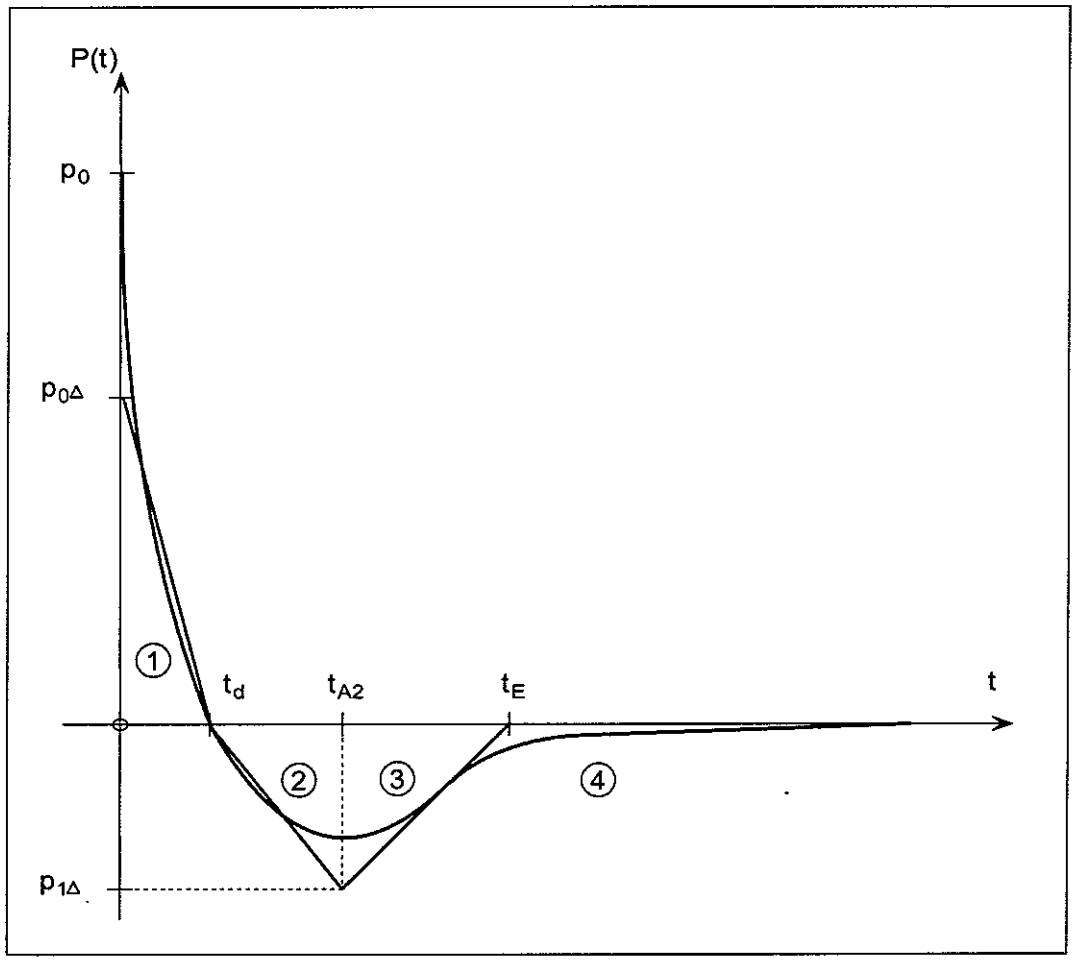

Figure 2.5.1: Piecewise linear approximation of type-I blast wave profile.

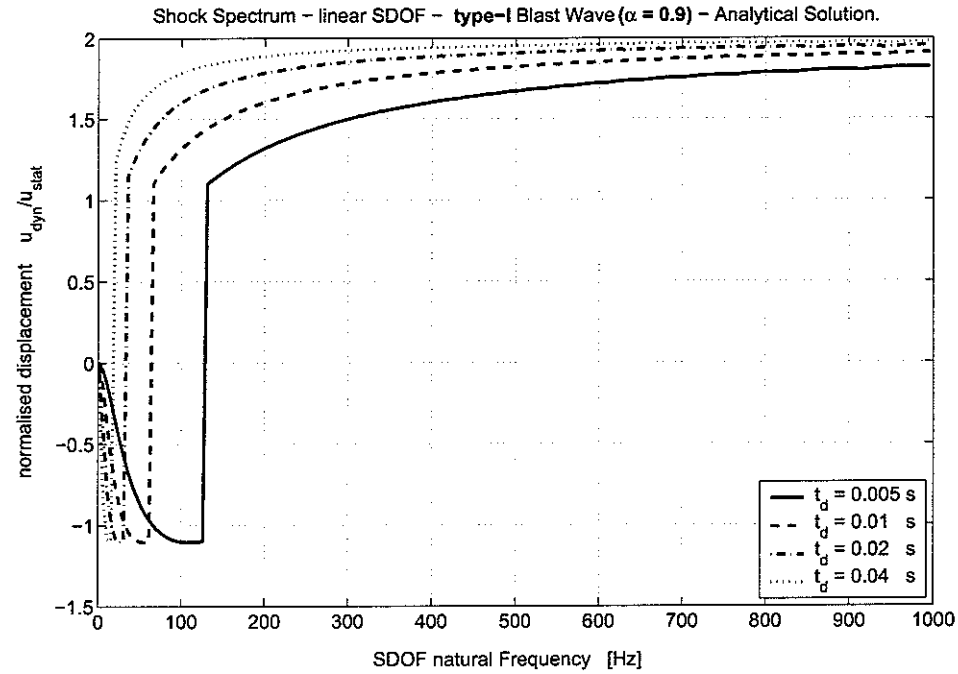

Figure 2.5.2: Shock spectra of SDOF-oscillator with natural frequency $0 \leq f_n \leq 1.0\,\text{kHz}$ due to **type-I** blast wave profile for different values of t_d. ($\alpha = 0.9$, $\zeta = 0.0$).

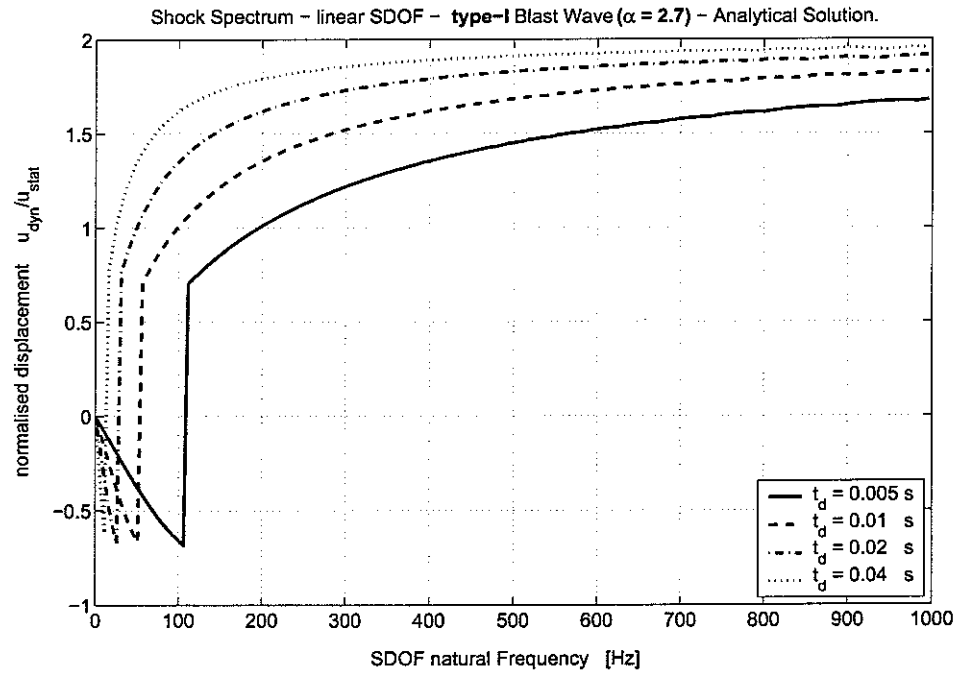

Figure 2.5.3: Shock spectra of SDOF-oscillator with natural frequency $0 \leq f_n \leq 1.0\,\text{kHz}$ due to **type-I** blast wave profile for different values of t_d. ($\alpha = 2.7$, $\zeta = 0.0$).

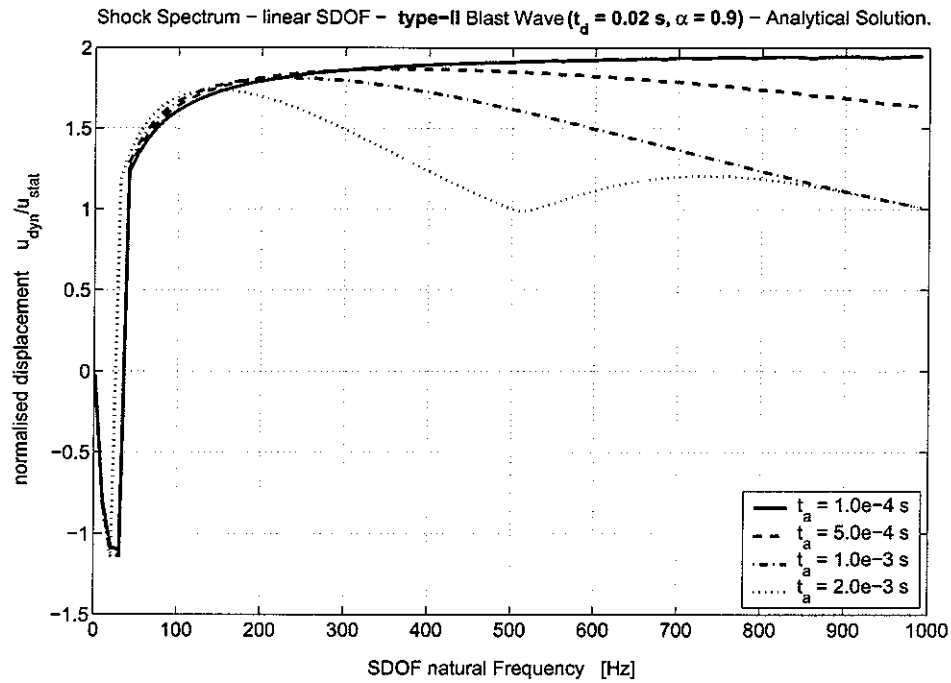

Figure 2.5.4: Shock spectra of SDOF-oscillator with natural frequency $0 \leq f_n \leq 1.0\,\text{kHz}$ due to **type-II** blast wave profile for different values of t_a. ($t_d = 0.02\,\text{s}$, $\alpha = 0.9$, $\zeta = 0.0$).

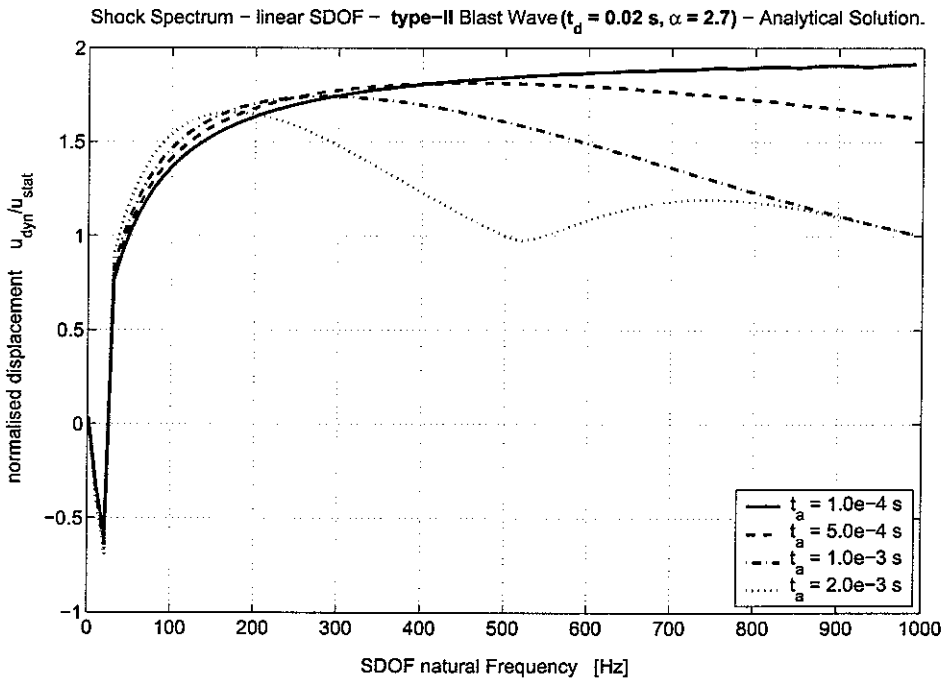

Figure 2.5.5: Shock spectra of SDOF-oscillator with natural frequency $0 \leq f_n \leq 1.0\,\text{kHz}$ due to **type-II** blast wave profile for different values of t_a. ($t_d = 0.02\,\text{s}$, $\alpha = 2.7$, $\zeta = 0.0$).

(a)

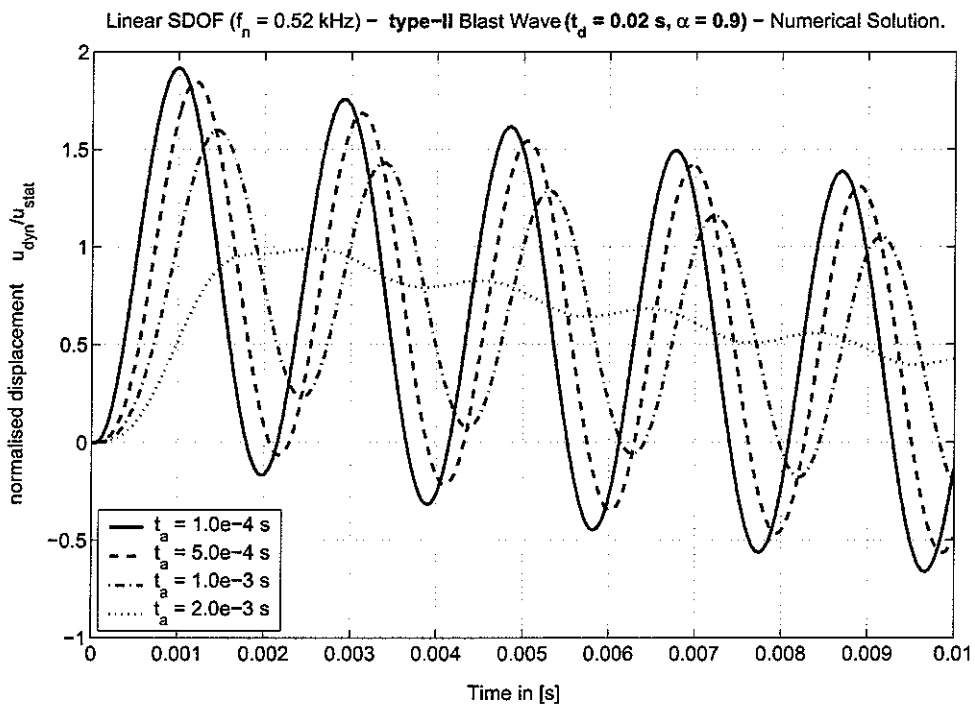

(b)

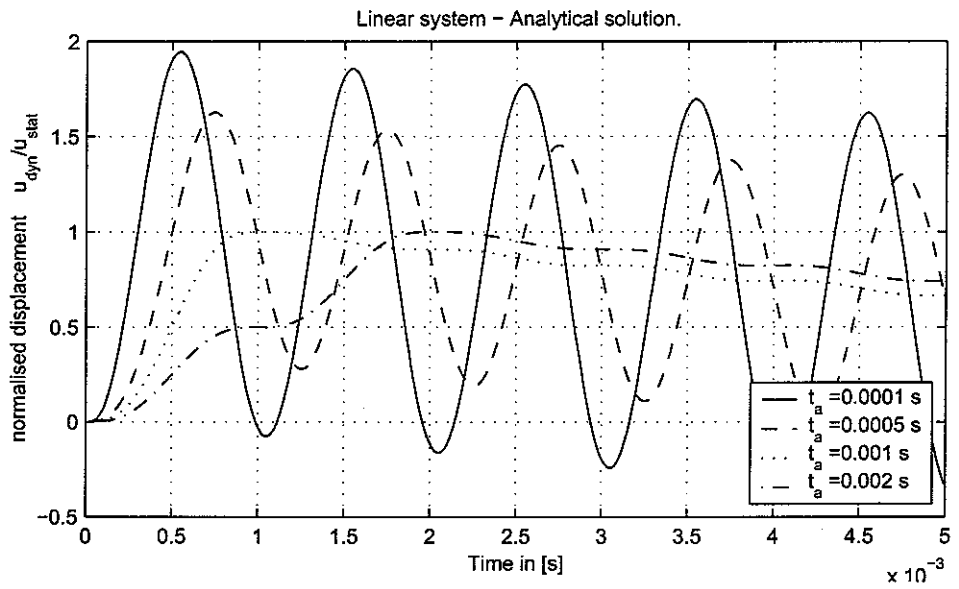

Figure 2.5.6: Time-displacement history of the linear SDOF oscillator at two different natural frequencies of (**a**) $f_n = 520.0\,\text{Hz}$ and (**b**) $f_n = 1.0\,\text{kHz}$ due to a **type-II** blast wave profile for different values of the finite rise times t_a. ($\alpha = 0.9, t_d = 0.02\,\text{s}, \zeta = 0.0$).

(a)

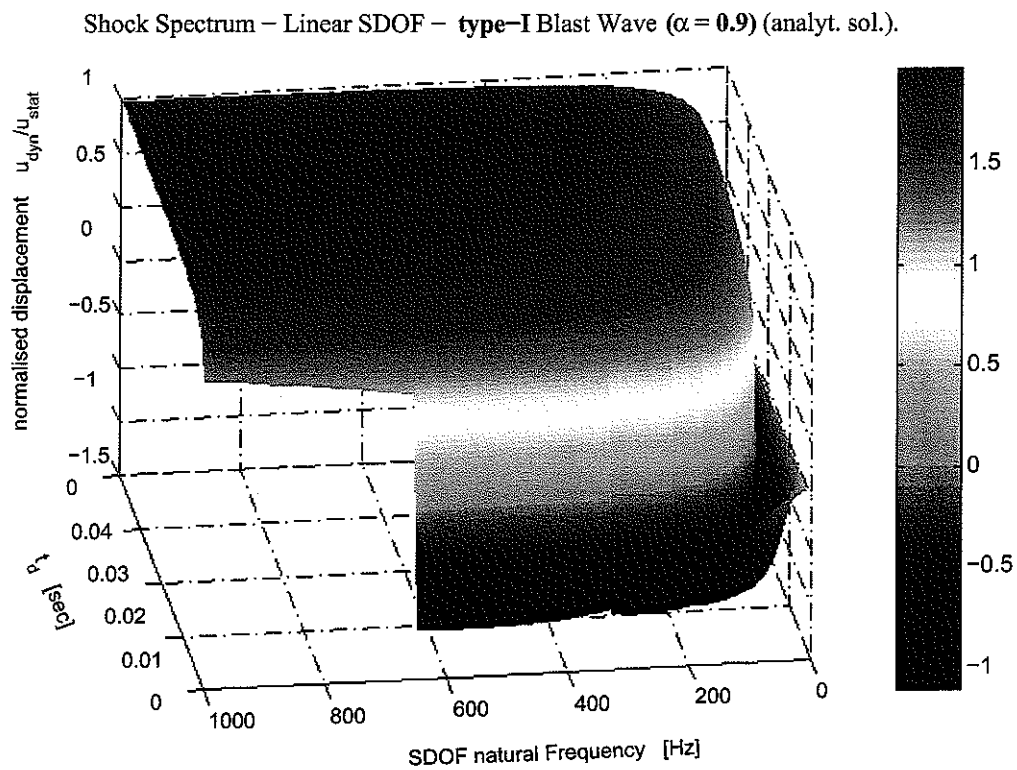

(b)

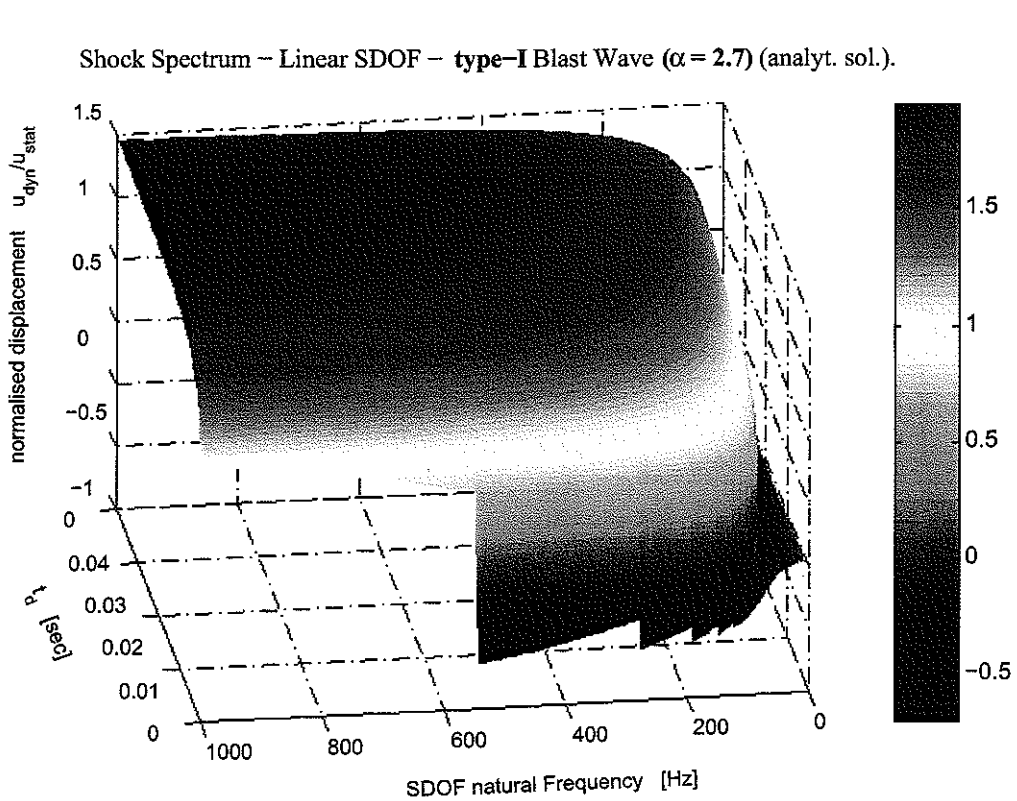

Figure 2.5.7: Shock spectra of linear SDOF-oscillator with natural frequency f_n due to **type-I** blast wave profile for two different values of α: **(a)** $\alpha = 0.9$, **(b)** $\alpha = 2.7$.

(a)

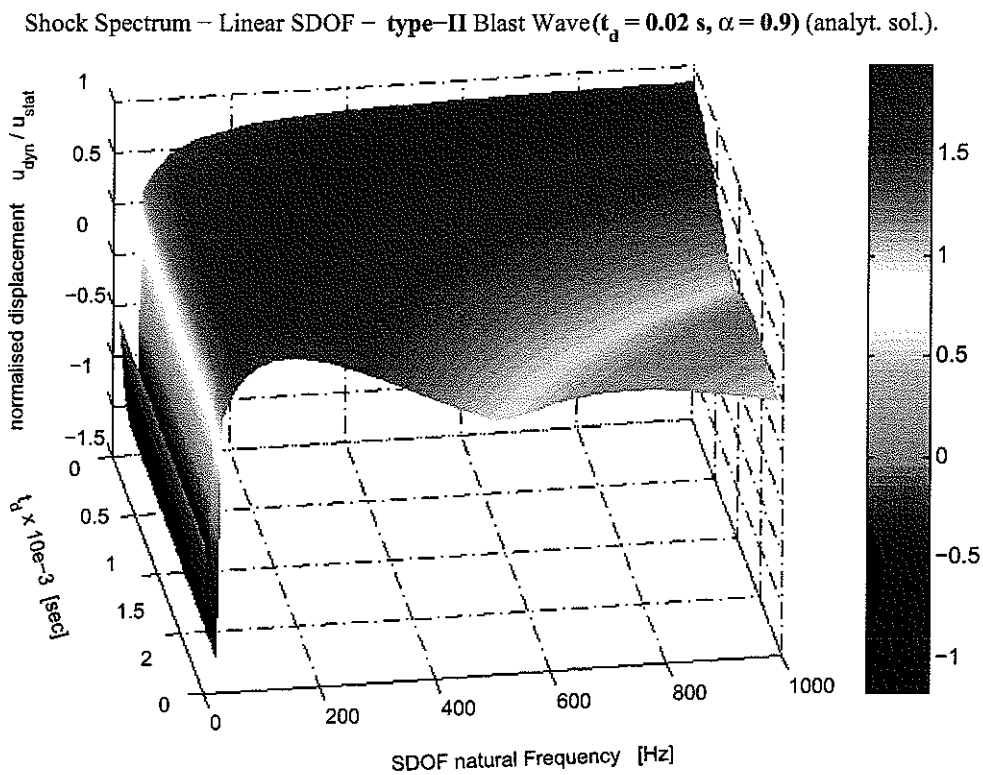

(b)

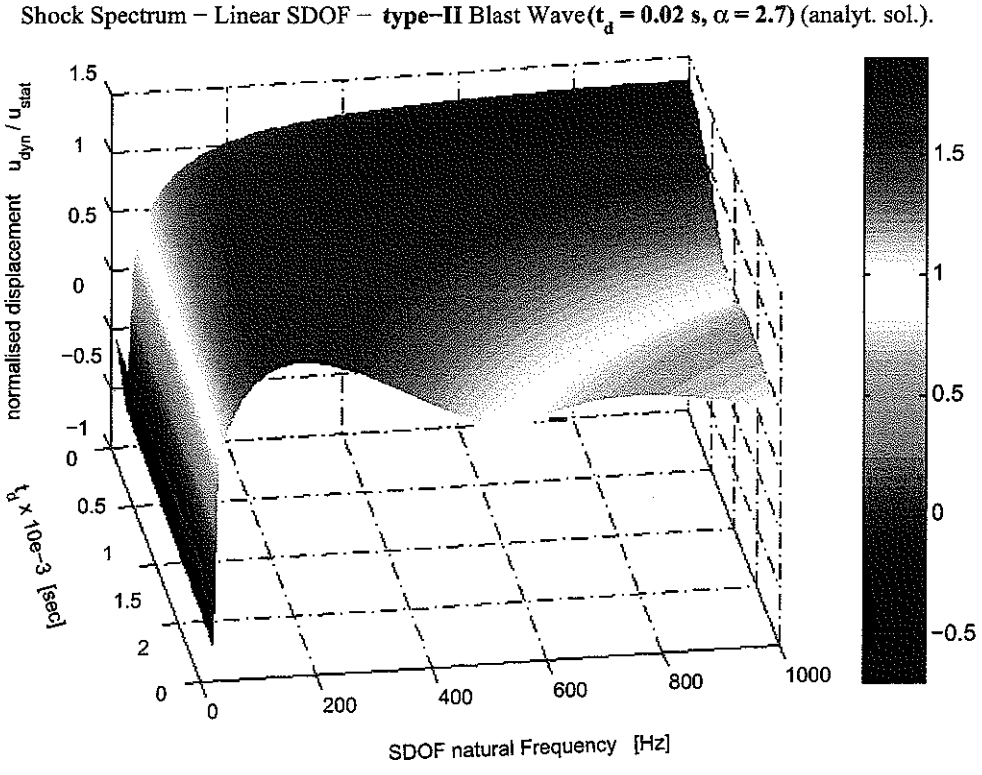

Figure 2.5.8: Shock spectra of linear SDOF-oscillator with natural frequency f_n due to **type-II** blast wave profile for two different values of α: **(a)** $\alpha = 0.9$, **(b)** $\alpha = 2.7$; $t_d = 0.02\,\mathrm{s}$.

(a)

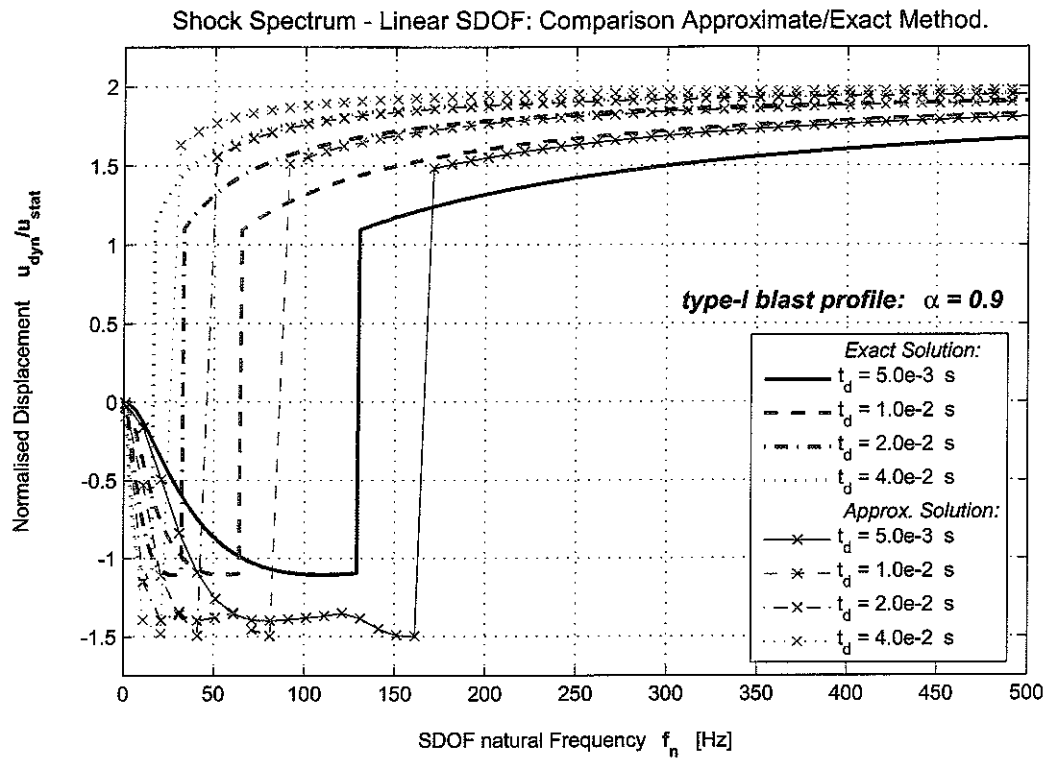

(b)

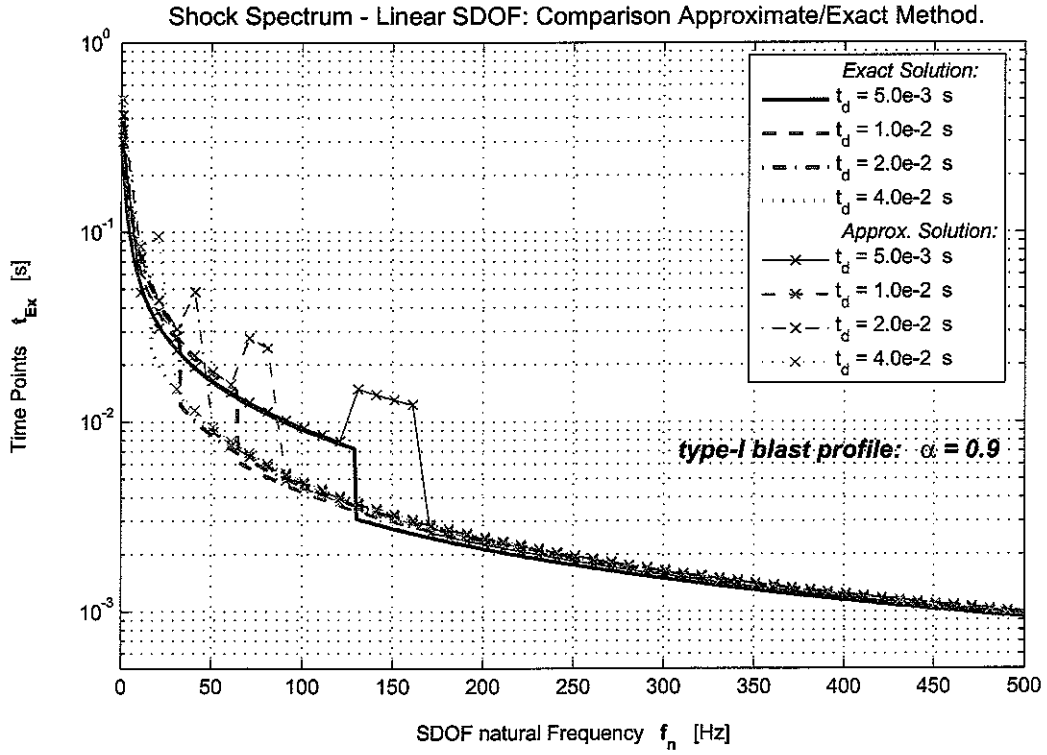

Figure 2.5.9: Shock spectra of SDOF-oscillator with natural frequency $0 \leq f_n \leq 500\,\text{Hz}$ due to **type-I** blast wave profile for different values of t_d. Comparison between exact solution and piecewise linear approximation. ($\alpha = 0.9, \zeta = 0.0$).

CHAPTER 3

Autonomous Nonlinear SDOF Systems

3.1 Introduction

In the last thirty years of research into the subject of structural nonlinear response of autonomous and non-autonomous systems to transient excitation, numerous solution procedures for obtaining extreme values of response have been developed. The majority of these algorithms base on numerical approximation as described in section 2.1 of the previous chapter. Some incorporate a mixed numerical-analytical approach, e.g. [6], and very few only solve the problem entirely analytically [7,8]. However, regarding the latter, no unified approach exists and results presented by various authors are limited to special cases of nonlinear oscillators such as special loading parameters or zero initial conditions.

The appealing clarity and elegance of analytical solutions to physical problems is always defeated by its limited ability of solving nontrivial tasks. In terms of structural dynamics this manifests itself in the attempt to describe geometrically complex vibrating structures, even in two-dimensional space such as nonuniform lattice or frames or plates with various cut-outs. No closed-form description of such problems exists, neither for static nor dynamic excitation, let alone an analytical solution can be obtained. Things worsen in three-dimensional space with structures assembled from a mixture of numerous basic elements such as beams, plates and shells.

So far, only geometry was concerned. Nonlinear restoring forces[1] or highly time-varying excitation loads can leave even the geometrical most simple structure, the SDOF system, without a closed-form solution despite the fact that an analytical description of the problem in terms of first or higher order differential equations can be established. This makes it necessary to simplify the problem and hence the governing equation if results are sought as analytical expressions.

The work presented in this chapter assumes the method of BIGGS [13] can be used to reduce the MDOF system under consideration into an equivalent SDOF system. As within the preceding chapter, the focus lies on solution methods for the newly obtained SDOF rather than on the procedures of how the transformation is achieved.

[1] The term 'restoring force' as used in this work incorporates the sum of all forces exhibit by the structural system due to *damping* and *stiffness*.

3.2 The Equation of Motion

The nonlinear equation of motion of an non-autonomous, dissipative SDOF system can be written as

$$m\ddot{u}(t) + f\big(t, \dot{u}(t), u(t)\big) = P(t) \tag{3.2.1}$$

where m is the oscillating mass, $u(t)$, $\dot{u}(t)$, $\ddot{u}(t)$ denote displacement, velocity and acceleration, respectively, and $f(t,\dot{u},u)$ represents the nonlinear restoring force due to any kind of damping and elastic or nonelastic/plastic stiffness mechanism occurring in the system. The expression on the right hand side can in its most simplest form be written as $P(t) = p_0 \times p_t(t)$ where p_0 is the constant force amplitude and $p_t(t)$ is a pure time-varying function. If time t is eliminated as explicit independent variable Eq.(3.2.1) reduces to the equation of motion for an autonomous system

$$m\ddot{u}(t) + f\big(\dot{u}(t), u(t)\big) = p_0\,. \tag{3.2.2}$$

Furthermore, letting f be independent of $\dot{u}(t)$, i.e. $f = f(u)$ is a function of the displacement only, gives the equation of motion for an autonomous energy conserving system as

$$m\ddot{u}(t) + f(u) = p_0\,, \tag{3.2.3}$$

subjected to arbitrary initial conditions

$$u(t=0) = u_0 \qquad \text{and} \qquad \dot{u}(t=0) = \dot{u}_0\,. \tag{3.2.4}$$

3.3 Response of Conservative Systems

The most important information regarding the system response from an engineer's viewpoint, is the maximum value of displacement as well as the oscillation frequency. In the case of Eq.(3.2.3) determination of the extreme values of displacement is straightforward for the majority of restoring force - displacement relationships. A first integration of (3.2.3) with respect to $u(t)$ expresses the energy balance of the conservative system, which stays constant as $t \to 0$. Assuming that the velocity $\dot{u}(t)$ is equal to zero when the oscillator reaches its minimum or maximum displacement position $u_{\mathsf{Ex}} = \big(u_{\mathsf{min}}; u_{\mathsf{max}}\big)$, this leads to an algebraic equation, which in certain cases can be transformed into an explicit analytical expression for u_{Ex}.

In contrast to linear SDOF systems, which respond to any type of excitation with not more than two different frequencies at the same time[2], nonlinear systems have, generally speaking, a finite significant number of distinctive frequencies in their dynamic response behaviour, independent of the type of vibration, i.e. free oscillation, harmonically or transiently forced. However, separation of variables after a first integration of Eq.(3.2.3) and a subsequent, second integration with respect to time and displacement leads to explicit expressions of the fundamental oscillation period of the periodically vibrating nonlinear SDOF. For most general cases with arbitrary initial conditions this gives rather complex integral equations. Nevertheless, a vast number of these expressions can be solved by means of special tabulated functions which reduce, for special cases of nonlinear restoring forces $f(u)$ or simplified initial conditions, to basic algebraic functions.

[2] An undamped linear system excited by harmonic loading will oscillate with a superposition of its own natural frequency f_n and the frequency imposed by the applied load f_{F}. In the presence of damping the homogeneous part of the solution decays away with increasing time t and the SDOF vibration is purely dominated by f_{F}, i.e. the oscillation becomes harmonic again.

3.3.1 Step Excitation

If the external load $P(t)$ is modelled as an ideal step excitation

$$P(t) = \begin{cases} 0, & t < 0 \\ p_0, & t \geq 0 \end{cases} \tag{3.3.1a}$$

and integration with respect to $u(t)$ is performed, Eq.(3.2.3) can be rewritten as

$$\int_u \left(m \frac{\mathrm{d}}{\mathrm{d}t} \dot{u}(t) + f(u) \right) \mathrm{d}u = \int_u p_0 \, \mathrm{d}u \tag{3.3.1b}$$

which gives together with the substitution in [3]

$$\frac{\mathrm{d}}{\mathrm{d}t} \dot{u}(t) = \frac{\mathrm{d}}{\mathrm{d}u} \left[\frac{1}{2} \left(\frac{\mathrm{d}u}{\mathrm{d}t} \right)^2 \right] \tag{3.3.1c}$$

and the law of conservation of the system's total energy the following condition for potential and kinetic energy of the oscillator as

$$\frac{m}{2} \dot{u}^2(t) + \int_u f(u) \, \mathrm{d}u + C_1 = p_0 \, u(t) \, . \tag{3.3.2a}$$

Herein C_1 is the integration coefficient determined from the initial conditions, m the system's mass, p_0 is the force amplitude, and $f(u)$ expresses the nonlinear stiffness solely depending upon the displacement $u(t)$. Together with Eq.(3.2.4) C_1 is evaluated as

$$C_1 = p_0 \, u_0 - \frac{m}{2} \dot{u}_0^2 - \int_u f(u) \, \mathrm{d}u \Big|_{u=u_0} \, . \tag{3.3.2b}$$

At the point of maximum displacement the velocity $\dot{u}(t)$ in (3.3.2a) is set to zero and the resulting algebraic equation[3] (3.3.3a) is solved for the minimum/maximum values of the displacement

$$\int_u f(u) \, \mathrm{d}u \Big|_{u=u_{\mathrm{Ex}}} - p_0 \, u_{\mathrm{Ex}} = \int_u f(u) \, \mathrm{d}u \Big|_{u=u_0} - p_0 \, u_0 + \frac{m}{2} \dot{u}_0^2 \, . \tag{3.3.3a}$$

where u_{Ex} stands for the set of extreme solutions and

$$u_{\min}, u_{\max} \in u_{\mathrm{Ex}} \qquad \text{so that} \qquad u_{\min} < u_{\max} \, . \tag{3.3.3b}$$

The principle of energy conservation can also be used to obtain an expression for the maximum oscillation velocity as done by TIMOSHENKO *et al* in [19] for a freely vibrating SDOF system. However, the expressions given in here are more general[4] and the new equilibrium position $u_{\mathrm{Ex,eq}}$ of the oscillator does not have to coincide with the position of equilibrium before vibration starts. Combining Eq.(3.3.2a) and (3.3.2b) gives

$$\frac{m}{2} \dot{u}^2(t) + \int_u f(u) \, \mathrm{d}u + p_0 \, u_0 - \frac{m}{2} \dot{u}_0^2 - \int_u f(u) \, \mathrm{d}u \Big|_{u=u_0} = p_0 \, u(t) \, , \tag{3.3.4a}$$

[3] As will be seen in later sections of this chapter, expression given in Eq.(3.3.3a) can result in more than one non-differential equation depending upon the nonlinear restoring force $f(u)$ under consideration.

[4] The formulas derived in [19] do not permit initial conditions other than $u_0 = \dot{u}_0 = 0$.

which expresses the potential and kinetic energy, hence the total energy, stored in the system at any point t_{arbitr} in time. It is straightforward to rearrange (3.3.4a) to yield an explicit expression for the velocity

$$\dot{u}(t) = \sqrt{\frac{2}{m}} \left(p_0 u(t) - \int_u f(u)\,\mathrm{d}u \Big|_{u_{\text{arbitr}}} - p_0 u_0 + \int_u f(u)\,\mathrm{d}u \Big|_{u=u_0} + \frac{m}{2}\dot{u}_0^2 \right)^{\frac{1}{2}}, \tag{3.3.4b}$$

which can be used to calculate $\dot{u}(t)$ at any feasible point of the path of displacement u_{arbitr} of the SDOF oscillator, i.e. u_{arbitr} needs to be within the interval $u_{\min} \leq u_{\text{arbitr}} \leq u_{\max}$. In order to obtain the extreme values of the velocity, u_{arbitr} is replaced by the term $u_{\text{Ex,eq}}$, which denotes the equilibrium position the system oscillates around after excitation by the step function. In contrast to Eq.(3.3.3a), where the velocity was assumed to be zero at points of minimum/maximum displacement, $u_{\text{Ex,eq}}$ is *not* necessarily equal to zero at points of extreme velocity

$$\dot{u}_{\min}, \dot{u}_{\max} \in \dot{u}_{\text{Ex}} \qquad \text{with} \qquad \dot{u}_{\min} < \dot{u}_{\max}. \tag{3.3.4c}$$

Hence, if Eq.(3.3.4b) gives extreme solutions at the point $u_{\text{Ex,eq}}$ the first derivative with respect to u at this point

$$\frac{\mathrm{d}\dot{u}(t)}{\mathrm{d}u} := 0 = \frac{[p_0 - f(u)]}{\sqrt{2m}} \left(p_0 u(t) - \int_u f(u)\,\mathrm{d}u \Big|_{u_{\text{Ex,eq}}} - p_0 u_0 + \int_u f(u)\,\mathrm{d}u \Big|_{u=u_0} + \frac{m}{2}\dot{u}_0^2 \right)^{-\frac{1}{2}} \tag{3.3.4d}$$

must be zero, which is only the case if

$$f(u) = p_0\,, \tag{3.3.4e}$$

i.e. at the point of nonlinear static deflection after excitation due to the step function. Furthermore, if Eq.(3.3.4d) yields global minima or maxima, the second derivative of (3.3.4b) must *not* be equal zero

$$\begin{aligned} \frac{\mathrm{d}^2\dot{u}(t)}{\mathrm{d}u^2} = \frac{[p_0 - f(u)]^2}{m} & \left(p_0 u(t) - \int_u f(u)\,\mathrm{d}u \Big|_{u_{\text{Ex,eq}}} - p_0 u_0 + \int_u f(u)\,\mathrm{d}u \Big|_{u=u_0} + \frac{m}{2}\dot{u}_0^2 \right)^{-\frac{3}{2}} + \dots \\ & - \frac{1}{\sqrt{2m}} \frac{\mathrm{d}f(u)}{\mathrm{d}u} \left(p_0 u(t) - \int_u f(u)\,\mathrm{d}u \Big|_{u_{\text{Ex,eq}}} - p_0 u_0 + \int_u f(u)\,\mathrm{d}u \Big|_{u=u_0} + \frac{m}{2}\dot{u}_0^2 \right)^{-\frac{1}{2}} \neq 0. \end{aligned} \tag{3.3.4f}$$

For the special value of $u(t) = u_{\text{Ex,eq}}$ the first part of the above equation (3.3.4f) yields together with (3.3.4e) zero. Furthermore, assuming for a moment $p > 0$, $u \geq 0$ and $\dot{u}_0 \geq 0$ the terms in brackets in the second part of (3.3.4f) will be greater zero. In fact, by comparing (3.3.3a) with the expressions under the square root in (3.3.4f) it becomes evident both equations consists of almost the same terms. Only the nonlinear stiffness function $f(u)$ and the step magnitude p_0 are evaluated at different points of displacement. In Eq.(3.3.3a) at u_{Ex} and in (3.3.4f) at $u_{\text{Ex,eq}}$, respectively. Moreover, since (3.3.3a) yields zero only at u_{Ex}, but $u_{\text{Ex}} \neq u_{\text{Ex,eq}}$, Eq.(3.3.4f) will always be non-zero and hence (3.3.4d) gives global minima or maxima.

Because $f(u)$ is a general term for the restoring force of the nonlinear system, no explicit expression from (3.3.4e) for the displacement, which then could be inserted into Eq.(3.3.4b), can be given at this

point and (3.3.4b) is rewritten in its final time-invariant form

$$\dot{u}_{\mathrm{Ex}} = \sqrt{\frac{2}{m}} \left(p_0 u_{\mathrm{Ex,eq}} - \int_0^{u_{\mathrm{Ex,eq}}} f(u)\,\mathrm{d}u - p_0 u_0 + \int_0^{u_0} f(u)\,\mathrm{d}u + \frac{m}{2}\dot{u}_0^2 \right)^{\frac{1}{2}} \tag{3.3.4g}$$

where the new point of equilibrium $u_{\mathrm{Ex,eq}}$ is obtained from (3.3.4e) and

$$\dot{u}_{\mathrm{min/max}} = \mp \dot{u}_{\mathrm{Ex}}\,. \tag{3.3.4h}$$

In order to derive an expression for the oscillation frequency of the SDOF the nonlinear differential equation describing the motion of the system needs to be integrated twice. Returning back to (3.3.2a), separation of variables and integration of both sides, one with respect to $u(t)$ and the other with respect to t, yields for the period $T_{\frac{1}{2}}$ of the half-cycle

$$_{\mathbb{H}}T_{\frac{1}{2}} = \int_{t_{\mathrm{min}}}^{t_{\mathrm{max}}} \mathrm{d}t = \int_{u_{\mathrm{min}}}^{u_{\mathrm{max}}} \frac{\mathrm{d}u}{\sqrt{\frac{2}{m}\left(p_0 u(t) - \int_u f(u)\,\mathrm{d}u - C_1 \right)}} \tag{3.3.5}$$

where t_{min} and t_{max} mark the time points of successive u_{min} and u_{max}, respectively. Since for the conservative system the maximum values of displacement u_{Ex} stay constant as $t \to \infty$ the two time instances can be evaluated at arbitrary points in the time-domain. Assuming symmetry of the time-displacement curve of the oscillator, i.e. the integral of the interval $(u_{\mathrm{min}}, u_{\mathrm{max}})$ is equal to the integral over $(u_{\mathrm{max}}, u_{\mathrm{min}})$, the total oscillation period is given by $_{\mathbb{H}}T = 2 \times {}_{\mathbb{H}}T_{\frac{1}{2}}$ and Eq.(3.3.5) can be rewritten as

$$_{\mathbb{H}}T = \sqrt{2m} \int_{u_{\mathrm{min}}}^{u_{\mathrm{max}}} \frac{\mathrm{d}u}{\sqrt{p_0 u(t) - \int_u f(u)\,\mathrm{d}u - C_1}}\,. \tag{3.3.6}$$

The index $\mathbb{H}$ is introduced here to refer to the Heaviside step-excitation function as external applied load as defined in Eq.(3.3.1a).

3.3.2 Impulse Excitation

The Dirac delta function $\delta(t - t_0)$ is defined as[5] [16]

$$\delta(t - t_0) = \begin{cases} \infty & \text{if} \quad t = t_0 \\ 0 & \text{if} \quad t \neq t_0 \end{cases} \tag{3.3.7a}$$

with the important property of a distribution [21]

$$\int_{-\infty}^{\infty} \delta(t - t_0)\,\mathrm{d}t = 1\,. \tag{3.3.7b}$$

[5]The δ-function is not a function by classical means, it is a so-called generalised function. The definition of generalised functions or distributions extends the narrow-spaced classical definition of the term function, see [15], [20].

If the shifting property of Eq.(3.3.7a) is disregarded, i.e. the applied force acts at $t_0 = 0$ upon the system, the otherwise infinite impulse can be approximated by a rectangular finite one of duration Δt with the amplitude

$$\delta(t) = \begin{cases} \lim\limits_{\Delta t \to 0} \frac{1}{\Delta t} & , \quad t = \Delta t \\ 0 & , \quad t \neq \Delta t . \end{cases} \tag{3.3.8}$$

It should be noted here that property (3.3.7b) of the δ-distribution is preserved

$$\int_{-\infty}^{\infty} \delta(t)\,\mathrm{d}t = \lim_{\Delta t \to 0} \int_{0}^{\Delta t} \frac{1}{\Delta t}\,\mathrm{d}t = \lim_{\Delta t \to 0} \left[\frac{t}{\Delta t}\right]_0^{\Delta t} = 1 \tag{3.3.9}$$

giving for the classical mathematical function in Eq.(3.3.8) the total impulse input during the finite time Δt into the system as equal to 1. Using the definitions given in (3.3.8) and (3.3.9) and substituting an arbitrary scaled unit impulse, e.g. $p_0 \times \delta(t)$, into the equation of motion of the SDOF system, Eq.(3.2.3) takes the form

$$\lim_{\Delta t \to 0} \int_{0}^{\Delta t} \left(m \frac{\mathrm{d}}{\mathrm{d}t} \dot{u}(t) + f(u) \right) \mathrm{d}t = \lim_{\Delta t \to 0} \int_{0}^{\Delta t} p_0\, \delta(t)\,\mathrm{d}t \tag{3.3.10a}$$

which gives

$$\lim_{\Delta t \to 0} m\,[\dot{u}(\Delta t) - \dot{u}(0)] \qquad \text{and} \qquad \lim_{\Delta t \to 0} \int_{0}^{\Delta t} f(u)\,\mathrm{d}t \tag{3.3.10b}$$

for both terms on the left-hand-side of Eq.(3.3.10a), and

$$\lim_{\Delta t \to 0} p_0 \int_{0}^{\Delta t} \delta(t)\,\mathrm{d}t = p_0 \tag{3.3.10c}$$

for the applied force term on the right. Since there can be no actual displacement change in an interval of infinite length $\Delta t \to 0$, the second term in (3.3.10b) equates to zero. Combining then Eq.(3.3.10c) and the remainder of (3.3.10b) leads to

$$\lim_{\Delta t \to 0} [\dot{u}(\Delta t)] - \dot{u}_0 = \frac{p_0}{m} . \tag{3.3.10d}$$

The transient excitation problem has now transformed into a free vibration one with revised initial conditions for the velocity of the system, namely a contribution of the acting transient impulse load added to the existing initial velocity $\dot{u}_0$ at the time of application of the impulse

$$\dot{u}(0+) = \dot{u}_{0+} = \frac{p_0}{m} + \dot{u}_0 \tag{3.3.11a}$$

at the time point

$$t_{0+} = t_0 + \lim_{\Delta t \to 0} \Delta t ,$$

i.e. after the impulse interval Δt. With respect to Eq.(3.3.10b) the displacement initial conditions can be rewritten as the existing displacement at the time of application of the impulse

$$u(0+) = u_{0+} = u_0 . \tag{3.3.11b}$$

A simpler application of the above shown method with $u_0 = \dot{u}_0 = 0$ is shown in [16] for a linear system. The system's new equation of motion is now rewritten as

$$m\frac{\mathrm{d}}{\mathrm{d}t}\dot{u}(t) + f(u) = 0 \tag{3.3.12}$$

subjected to the new initial conditions given in Eq.(3.3.11a) and (3.3.11b). Following the same procedure as in the preceding section integration with respect to $u(t)$ leads to

$$\frac{m}{2}\dot{u}^2(t) + \int_u f(u)\,\mathrm{d}u + C_2 = 0 \tag{3.3.13a}$$

with the integration constant C_2 determined by the magnitude of the applied force p_0, and $\dot{u}_0$, u_0 unequal zero

$$C_2 = -\frac{m}{2}\left(\frac{p_0}{m} + \dot{u}_0\right)^2 - \int_u f(u)\,\mathrm{d}u\Big|_{u=u_0}. \tag{3.3.13b}$$

Again, at minimum/maximum displacement the velocity $\dot{u}(t_{\mathrm{Ex}})$ in Eq.(3.3.13a) is set to zero and u_{Ex} is obtained from

$$\int_u f(u)\,\mathrm{d}u\Big|_{u=u_{\mathrm{Ex}}} = \frac{m}{2}\left(\frac{p_0}{m} + \dot{u}_0\right)^2 + \int_u f(u)\,\mathrm{d}u\Big|_{u=u_0}. \tag{3.3.14}$$

In order to derive an expression for the extreme values of velocity defined as $\dot{u}_{\mathrm{min}}, \dot{u}_{\mathrm{max}} \in \dot{u}_{\mathrm{Ex}}$ where $\dot{u}_{\mathrm{min}} < \dot{u}_{\mathrm{max}}$, equation (3.3.13a) is rewritten

$$\dot{u}(t) = \sqrt{\frac{2}{m}}\left(\int_u f(u)\,\mathrm{d}u\Big|_{u=u_0} + \frac{m}{2}\left(\frac{p_0}{m} + \dot{u}_0\right)^2 - \int_u f(u)\,\mathrm{d}u\right)^{\frac{1}{2}} \tag{3.3.15a}$$

and its first derivative set to zero

$$\frac{\mathrm{d}\dot{u}(t)}{\mathrm{d}u} := 0 = -2\sqrt{\frac{2}{m}}f(u)\left(\int_u f(u)\,\mathrm{d}u\Big|_{u=u_0} + \frac{m}{2}\left(\frac{p_0}{m} + \dot{u}_0\right)^2 - \int_u f(u)\,\mathrm{d}u\right)^{-\frac{1}{2}} \tag{3.3.15b}$$

which holds only true if

$$f(u) = 0, \tag{3.3.15c}$$

i.e. the equilibrium position of the system remains unchanged due to a Dirac impulse excitation. Hence, Eq.(3.3.15a) can be stated in its final form as

$$\dot{u}_{\mathrm{Ex}} = \sqrt{\frac{2}{m}}\left(\int_0^{u_0} f(u)\,\mathrm{d}u + \frac{m}{2}\left(\frac{p_0}{m} + \dot{u}_0\right)^2\right)^{\frac{1}{2}} \tag{3.3.15d}$$

with the minimum/maximum values as given by Eq.(3.3.4h). The second derivative of the velocity $\dot{u}_{\mathrm{Ex}}$, Eq.(3.3.15a),

$$\frac{d^2\dot{u}(t)}{du^2} = -\left(\frac{f(u)}{m}\right)^2\left[\frac{2}{m}\left(\int_0^{u_0} f(u)\,du + \frac{m}{2}\left(\frac{p_0}{m} + \dot{u}_0\right)^2\right)\right]^{-\frac{3}{2}} + \ldots$$
$$- \frac{1}{\sqrt{2m}}\frac{d}{du}f(u)\left(\int_0^{u_0} f(u)\,du + \frac{m}{2}\left(\frac{p_0}{m} + \dot{u}_0\right)^2\right)^{-\frac{1}{2}} \neq 0 \tag{3.3.15e}$$

must again be non-zero if (3.3.15b) represents global extrema. The solution of Eq.(3.3.4f) shows that the first part of the second derivative of the oscillator's velocity $\dot{u}(t)$ is equal to zero at $u(t) = u_{\text{Ex,eq}}$ in case of impulse excitation because of (3.3.15c). However, the first derivative of the nonlinear restoring force[6] $f(u)$ will always be non-zero. Therefore, Eq.(3.3.15e) holds true and (3.3.15d) gives global minimum/maximum values for the system's oscillation velocity.

The oscillation period of the impulse response is derived in the same way as Eq.(3.3.5). Separation of variables and integration with respect to t and $u(t)$ gives together with Eq.(3.3.13a)

$$ {}_{\delta}T_{\frac{1}{2}} = \sqrt{2m} \int_{u_{\text{Ex}}} \frac{du}{\sqrt{-\int_{u} f(u)\,du - C_2}} \tag{3.3.16} $$

the period of oscillation for a half-cycle. Assuming symmetry as in section 3.3.1 this can be written as $2 \times {}_{\delta}T_{\frac{1}{2}}$

$$ {}_{\delta}T = 2\sqrt{2m} \int_{u_{\text{min}}}^{u_{\text{max}}} \frac{du}{\sqrt{-\int_{u} f(u)\,du - C_2}}. \tag{3.3.17} $$

The index δ refers to the nature of the system excitation being a Dirac impulse.

In most cases it is impossible to find a closed form solution for T due to the nature of the integrand on the right hand site of (3.3.6) and (3.3.17). However, there are some special forms of nonlinear spring characteristics, which permit the evaluation of frequency, in terms of tabulated special functions. The authors BAPAT and SRINIVASAN [7] investigated the transient response of an undamped nonlinear spring mass system subjected to a forcing function with constant amplitude, which reflects the structural response of an autonomous, conservative system excited by a step function of amplitude p_0. Analytical expressions are given for the maximum displacement and the oscillation frequency of the system considering two different types of nonlinear restoring forces, namely a single term polynomial force $f(u) = ku^a(t)$ and cubic force of the type $f(u) = bu(t) + cu^3(t)$, $b > 0$, where $u(t)$ is the deflection of the system and b, c and k being arbitrary constants whereas a is an odd integer. In a subsequent paper [8] the authors broaden the range of analytical solutions for nonlinear restoring force characteristics to the additional types:

(i) $f(u) = au + b\,\text{sign}[u]\,|u|^2$,

(ii) $f(u) = b\,\text{sign}[u]\,|u|^2 + cu^3$,

(iii) $f(u) = au + b\,\text{sign}[u]$.

Only the maximum displacement u_{max} and the period of vibration of the half-cycle of the system response are established as complex integral expressions, both depending solely upon the force amplitude p_0 and the coefficients a, b, c. Expressions for u_{min} are absent. To summarise, many of the results given in the literature lack a certain level of explicitness and no comparisons of the outcomes obtained with findings from other methods, e.g. numerical simulations or experimental investigations, are drawn. Moreover, a major disadvantage of [7,8] is the assumption of zero initial conditions, i.e.

[6] This holds also true if $f(u)$ is linear given by $ku(t)$. In this case $\frac{df(u)}{du} = k$.

$u_0 = \dot{u}_0 = 0$, which significantly narrows the range of real structural problems to which the solutions can be applied.

Using the same energy-based approach as described above, TIMOSHENKO *et al* [19] derive analytical expressions for the displacement, velocity and natural oscillation frequency of the SDOF for two different nonlinear restoring forces of polynomial-type. Limitations of the work are given by the following three restrictions: (i) results are only valid for specific types of exponents (odd integer) of the internal nonlinear force, (ii) all initial conditions are set to zero, and (iii) free vibration is assumed.

The far more general method derived in section 3.3.1 and 3.3.2 above will be used in the next section to obtain analytical expressions for scalar quantities such as maximum displacement and velocity describing the response of SDOF oscillators with various nonlinear restoring forces.

3.4 Autonomous Conservative Systems - Examples

Selecting two nonlinear restoring forces $f_1(u)$ and $f_2(u)$ similar to the ones used in [7] demonstrates the ability of the above derived method to obtain values of extreme displacement u_{Ex}, velocity $\dot{u}_{Ex}$ and nonlinear oscillation frequency f_{NL} for the most general cases of free vibration and impulse or step excitation. A number of high-order embedded Runge-Kutta adaptive integrations are used to verify the analytical results numerically.

3.4.1 The Nonlinear Restoring Force $f_1(u) = k\,\mathrm{sign}(u)\,|u|^b$

The normalised characteristics of the nonlinear restoring force

$$f_1(u) = k\,\mathrm{sign}(u)\,|u|^b\,, \qquad b \in \mathbb{R},\ b > 0 \tag{3.4.1}$$

where k is a force-deformation relating constant obtained from, e.g. static deformation test, and sign (.) is the signum function (cf. table of notation) are plotted in Figure 3.4.1 for different integer values of b. Integration of Eq.(3.4.1) leads to two solutions depending upon the sign of $u(t)$

$$\int_u f_1(u)\,\mathrm{d}u = k\int_u \mathrm{sign}(u)\,|u|^b\,\mathrm{d}u = \begin{cases} -\frac{k(-u)^b u}{(b+1)}, & u(t) \le 0 \\ \\ \frac{k u^{(b+1)}}{(b+1)}, & u(t) > 0 \end{cases}. \tag{3.4.2}$$

3.4.1.1 Free Vibration

For reasons of consistency as well as verification of experimental data in part II of this technical memorandum, free vibration of a nonlinear single-degree-of-freedom system is briefly outlined here, although this was not explicitly analysed in section 3.3. In order to determine the extreme values of displacement ${}_0u_{Ex}$ due to given initial conditions, Eq.(3.3.3a) is used with all terms involving p_0 set to zero. Introducing $f_1(u)$ for $f(u)$ and evaluation of the integral with respect to Eq.(3.4.2) leads to four equations for ${}_0u_{Ex}$, two for the minimum and two for the maximum value of $u(t)$, respectively, depending upon the sign of u_0. However, a closer examination of Eq.(3.4.2a) and the fact that u_0 is a

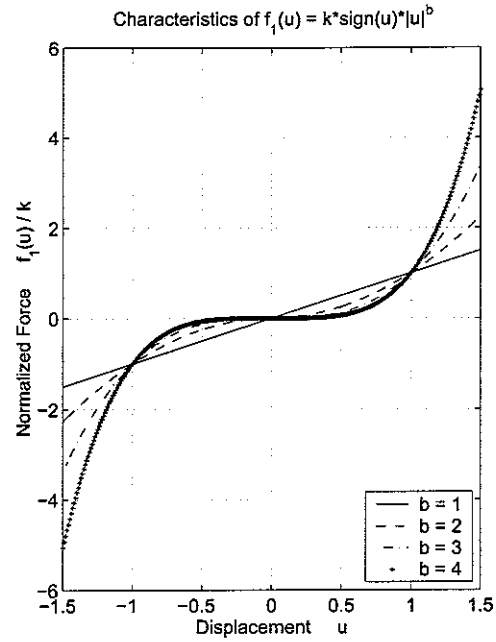

Figure 3.4.1: Normalised nonlinear restoring force characteristics $f_1(u) = k\,\mathrm{sign}(u)\,|u|^b$ for different values of the exponent b. For understanding results presented in subsequent sections of this chapter it is important to note that for any values of b within the range $1 \leq b \leq \infty$ the linear exponent $b = 1$ gives the most resistant force for non-normalised displacement $u(t)$ within the range $-1 \leq u \leq 1$.

simple constant allows rewriting (3.4.2) as

$$k \int_u \mathrm{sign}(u)\,|u|^b\,\mathrm{d}u\Big|_{u=u_0} = \frac{k\,|u_0|^{(b+1)}}{(b+1)}, \qquad u_0 \in \mathbb{R} \tag{3.4.3}$$

which reduces the number of equations for ${}_0u_{\mathrm{Ex}_{f_1}}$ to two, namely

$$-\frac{k}{b+1}\left(-{}_0u_{\mathrm{min}_{f_1}}\right)^b {}_0u_{\mathrm{min}_{f_1}} = \frac{k}{b+1}\,|u_0|^{(b+1)} + \frac{m}{2}\dot{u}_0^2, \qquad {}_0u_{\mathrm{min}_{f_1}} \leq 0 \tag{3.4.4a}$$

$$\frac{k}{b+1}\,{}_0u_{\mathrm{max}_{f_1}}^{(b+1)} = \frac{k}{b+1}\,|u_0|^{(b+1)} + \frac{m}{2}\dot{u}_0^2, \qquad {}_0u_{\mathrm{max}_{f_1}} > 0. \tag{3.4.4b}$$

The extreme values of displacement ${}_0u_{\mathrm{Ex}_{f_1}}$ with ${}_0u_{\mathrm{min}_{f_1}}, {}_0u_{\mathrm{max}_{f_1}} \in {}_0u_{\mathrm{Ex}_{f_1}}$ are not independent variables any more and therefore be treated like constants. With the substitution

$${}_0\overset{(\cdot)}{u}_{\mathrm{min}_{f_1}} = -{}_0u_{\mathrm{min}_{f_1}}, \qquad {}_0u_{\mathrm{min}_{f_1}} \leq 0 \tag{3.4.5}$$

equation (3.4.4a) becomes identical to (3.4.4b) and a single expression for the extreme displacement can be given

$${}_0u_{\mathrm{Ex}_{f_1}} = \left\{|u_0|^{(b+1)} + \frac{(b+1)}{2\,\omega_n^2}\,\dot{u}_0^2\right\}^{\frac{1}{(b+1)}} \tag{3.4.6a}$$

with the minimum and maximum values

$${}_0u_{\mathrm{min/max}_{f_1}} = \mp\,{}_0u_{\mathrm{Ex}_{f_1}} \tag{3.4.6b}$$

where the left-hand-side index '0' refers to the free vibration and ω_n^2 is defined as a reference system natural frequency

$$\omega_n^2 = \frac{k}{m} \tag{3.4.7}$$

in the same way as for linear systems. The velocity of vibration for the SDOF is derived using Eq.(3.3.15d) together with (3.4.3) and $p_0 = 0$

$$\dot{u}_{\mathrm{Ex}} = \sqrt{\frac{2}{m}}\left(\frac{k}{(b+1)}|u_0|^{(b+1)} + \frac{m}{2}\dot{u}_0^2\right)^{\frac{1}{2}} = \omega_n\sqrt{\frac{2}{b+1}}\left(|u_0|^{(b+1)} + \frac{(b+1)}{2\omega_n^2}\dot{u}_0^2\right)^{\frac{1}{2}} \tag{3.4.8a}$$

where

$$\dot{u}_{\mathrm{min/max}} = \mp\dot{u}_{\mathrm{Ex}} \tag{3.4.8b}$$

are the minimum and maximum values of $\dot{u}(t)$, respectively.

The oscillation period for the free vibrating system is obtained in the same manner as Eq.(3.3.17) leading to

$${}_0T_{f_1} = \sqrt{2m}\int\limits_{{}_0u_{\mathrm{Ex}f_1}} \frac{du}{\sqrt{-\int\limits_u f(u)\,\mathrm{d}u - C_0}} \tag{3.4.9a}$$

with the new integration constant C_0, which equates together with Eq.(3.4.3) to

$$C_0 = -\frac{m}{2}\dot{u}_0^2 - \int\limits_u f(u)\,\mathrm{d}u\Big|_{u=u_0} = -\frac{m}{2}\dot{u}_0^2 - \frac{k}{(b+1)}|u_0|^{(b+1)}\,. \tag{3.4.9b}$$

Because of the nature of solutions for the expression $\left[\int\limits_u f(u)\,du\right]$ depending upon the sign of $u(t)$, Eq.(3.4.9a) has to be a sum for the two ranges of integration

$${}_0T_{f_1} = \frac{\sqrt{2(b+1)}}{\omega_n}\left\{\int\limits_{{}_0u_{\mathrm{min}f_1}}^{0} \frac{\mathrm{d}u}{\sqrt{-\left((-u)^b(-u)\right) + {}_0\alpha_{f_1}}} + \int\limits_0^{{}_0u_{\mathrm{max}f_1}} \frac{\mathrm{d}u}{\sqrt{-u^{(b+1)} + {}_0\alpha_{f_1}}}\right\},$$

$${}_0u_{\mathrm{min}f_1} \le 0, \quad {}_0u_{\mathrm{max}f_1} > 0 \tag{3.4.9c}$$

with a constant comprising of all the initial conditions

$${}_0\alpha_{f_1} = |u_0|^{(b+1)} + \frac{(b+1)}{2\omega_n^2}\dot{u}_0^2. \tag{3.4.10}$$

The first integral in (3.4.9c) is valid only in the range of $-\left|{}_0u_{\mathrm{min}f_1}\right| \le u(t) \le 0$ and can be rewritten using the substitution

$$u(t) = -\overset{(-)}{u}(t), \qquad \frac{\mathrm{d}u}{\mathrm{d}\overset{(-)}{u}} = -\frac{\mathrm{d}\left(\overset{(-)}{u}\right)}{\mathrm{d}\overset{(-)}{u}} = -1, \qquad u(t) \le 0 \tag{3.4.11a}$$

as

$$-\int\limits_{\left|{}_0u_{\mathrm{min}f_1}\right|}^{0} \frac{\mathrm{d}\overset{(-)}{u}}{\sqrt{-\overset{(-)}{u}^{(b+1)} + {}_0\alpha_{f_1}}} = \int\limits_0^{\left|{}_0u_{\mathrm{min}f_1}\right|} \frac{\mathrm{d}\overset{(-)}{u}}{\sqrt{-\overset{(-)}{u}^{(b+1)} + {}_0\alpha_{f_1}}}, \qquad \overset{(-)}{u}(t) \ge 0. \tag{3.4.11b}$$

This leads together with $\left|{}_0u_{\min_{f_1}}\right| = {}_0u_{\max_{f_1}}$ from Eq.(3.4.6b) to a final form for the integral equation of the oscillation period

$$ {}_0T_{f_1} = 2\frac{\sqrt{2(b+1)}}{\omega_n}\int_0^{{}_0u_{\max_{f_1}}} \frac{\mathrm{d}u}{\sqrt{-u^{(b+1)}+{}_0\alpha_{f_1}}}, \qquad {}_0u_{\max_{f_1}} > 0 \tag{3.4.11c} $$

with the solution obtained using handbook [17] or MATHEMATICA® [20]

$$ {}_0T_{f_1} = 2\frac{\sqrt{2(b+1)}}{\omega_n}\left[\frac{u\sqrt{1-\frac{u^{(b+1)}}{{}_0\alpha_{f_1}}}}{\sqrt{{}_0\alpha_{f_1}-u^{(b+1)}}}\,{}_2\mathcal{F}_1\left(\frac{1}{1+b},\frac{1}{2};1+\frac{1}{1+b};\frac{u^{(b+1)}}{{}_0\alpha_{f_1}}\right)\right]_0^{{}_0u_{\max_{f_1}}}. \tag{3.4.11d} $$

Evaluated at the limits $\left(0,{}_0u_{\max_{f_1}}\right)$ this gives an algebraic expression for the oscillation period of the freely vibrating nonlinear SDOF system having $f_1(u)$ as restoring force

$$ {}_0T_{f_1} = 2\frac{{}_0u_{\max_{f_1}}}{\omega_n}\sqrt{\frac{2(b+1)}{{}_0\alpha_{f_1}}}\,{}_2\mathcal{F}_1\left(\frac{1}{2},\frac{1}{1+b};1+\frac{1}{1+b};\frac{{}_0u_{\max_{f_1}}^{(b+1)}}{{}_0\alpha_{f_1}}\right), \qquad {}_0u_{\max_{f_1}} > 0 \tag{3.4.11e} $$

with the term ${}_2\mathcal{F}_1(\ldots)$ being the so called *hypergeometric function*, see appendix B.1. Comparison of Eq.(3.4.6) with (3.4.10) gives for the ratio

$$ \frac{{}_0u_{\max_{f_1}}^{(b+1)}}{{}_0\alpha_{f_1}} = 1 $$

which simplifies Eq.(3.4.11e) to

$$ {}_0T_{f_1} = 2\frac{{}_0u_{\max_{f_1}}}{\omega_n}\sqrt{\frac{2\pi(b+1)}{{}_0\alpha_{f_1}}}\,\frac{\Gamma\left(1+\frac{1}{1+b}\right)}{\Gamma\left(\frac{1}{2}+\frac{1}{1+b}\right)} \tag{3.4.12} $$

where $\Gamma(\ldots)$ is the EULER Gamma function defined in appendix B.1 and ${}_0u_{\max_{f_1}}$ and ${}_0\alpha_{f_1}$ are given by Eq.(3.4.6) and (3.4.10), respectively. This leaves the oscillation period solely as a function of the SDOF's properties, namely stiffness coefficient k, order of stiffness element nonlinearity b and mass m, where k and m can be expressed in terms of ω_n, see Eq.(3.4.7), and the initial conditions u_0 and $\dot{u}_0$, given by ${}_0\alpha_{f_1}$ in Eq.(3.4.10)

$$ {}_0T_{f_1} = {}_0T_{f_1}\left(k,m,b,{}_0\alpha_{f_1}\right) = {}_0T_{f_1}\left(\omega_n,b,u_0,\dot{u}_0\right). $$

Although solution Eq.(3.4.12) is valid for any arbitrary b it suggest that the nonlinear SDOF system oscillates with one single frequency $1/{}_0T_{f_1}$ only. As will be seen in section 3.4.3, a Fourier analysis of numerically computed time-domain data reveals multiple oscillation frequencies for the case $b \neq 1$. This phenomena, typical for nonlinear systems becomes more apparent, if one uses for the solution of Eq.(3.4.11c) elliptic functions rather than hypergeometric ones. Returning to the integral equation (3.4.11c) and setting $b = 2$ gives an elliptic integral of the form

$$ {}_0T_{f_1} = 2\frac{\sqrt{6}}{\omega_n}\int_0^{{}_0u_{\max_{f_1}}} \frac{du}{\sqrt{-u^3+{}_0\alpha_{f_1}}} \tag{3.4.13} $$

where the equation under the square root is the same as Eq.(3.4.6), hence has three solutions, one real, namely ${}_0u_{\max_{f_1}}$ and two conjugate complex

$$\chi_1 = \sqrt[3]{{}_0\alpha_{f_1}} = {}_0u_{\max_{f_1}} \tag{3.4.14a}$$

$$\chi_2 = -(-1)^{\frac{1}{3}}\,{}_0u_{\max_{f_1}} = \left(-\frac{1}{2} - \mathrm{i}\frac{\sqrt{3}}{2}\right){}_0u_{\max_{f_1}} \tag{3.4.14b}$$

$$\chi_3 = (-1)^{\frac{2}{3}}\,{}_0u_{\max_{f_1}} = \left(-\frac{1}{2} + \mathrm{i}\frac{\sqrt{3}}{2}\right){}_0u_{\max_{f_1}}\,. \tag{3.4.14c}$$

The solution for Eq.(3.4.13) is given by case $\{243.00\}$ in [22]

$${}_0T_{f_1} = 2\frac{\sqrt{6}}{\omega_n}\eta_{\mathsf{E}}\,\mathcal{F}(\psi,\kappa) \tag{3.4.15a}$$

where $\sqrt{-u^3 + {}_0\alpha_{f_1}}$ from (3.4.13) is rewritten as

$$\sqrt{(\chi_1 - u)\left[(u-\chi_b)^2 + \chi_a^2\right]} \tag{3.4.15b}$$

with

$$\chi_a = \sqrt{-\frac{(\chi_2-\chi_3)^2}{4}} = \frac{\sqrt{3}}{2}\chi_1\,,\quad \chi_b = \frac{\chi_2+\chi_3}{2} = -\frac{\chi_1}{2}\,,\quad A = \sqrt{(\chi_b-\chi_1)^2+\chi_a^2} = \sqrt{3}\chi_1 \tag{3.4.15c}$$

and

$$\eta_{\mathsf{E}} = \frac{1}{\sqrt{{}_0u_{\max_{f_1}}\sqrt{3}}}\,,\quad \kappa^2 = \frac{1}{4}\left(2+\sqrt{3}\right),\quad \cos\psi = \left(\frac{A-a}{A+a}\right) = 2-\sqrt{3}\,. \tag{3.4.15d}$$

It is easy to see that for

$$\psi_{\frac{1}{2}(j+1)} = (j-1)\pi \mp \psi_0\,,\qquad j = 1,3,5,\ldots \tag{3.4.16a}$$

Eq.(3.4.15d) has multiple solutions with $\psi_0 = \arccos\left(2-\sqrt{3}\right)$ as fundamental one. Using the identity [22]

$$\mathcal{F}(n\pi \pm \theta,\kappa) = 2n\,\mathcal{K}(\kappa) \pm \mathcal{F}(\theta,\kappa) \tag{3.4.16b}$$

equation (3.4.15a) can be written as

$${}_0T_{f_1} = 2\frac{\sqrt{6}}{\omega_n}\eta_{\mathsf{E}}\left(2(j-1)\,\mathcal{K}(\kappa) \mp \mathcal{F}(\psi_0,\kappa)\right) \tag{3.4.17}$$

Setting $b = 2$, ${}_0u^3_{\max_{f_1}} = {}_0\alpha_{f_1}$ and rearranging Eq.(3.4.12) gives

$${}_0T_{f_1} = \frac{2\sqrt{6}}{\omega_n\sqrt{{}_0u_{\max_{f_1}}}}\sqrt{\pi}\,\frac{\Gamma\left(\frac{4}{3}\right)}{\Gamma\left(\frac{5}{6}\right)} \approx 1.40218\,\frac{2\sqrt{6}}{\omega_n\sqrt{{}_0u_{\max_{f_1}}}} \tag{3.4.18}$$

which is identical to Eq.(3.4.15a)

$${}_0T_{f_1} = j\,\frac{2\sqrt{6}}{\omega_n\sqrt{{}_0u_{\max_{f_1}}}}\,\frac{\mathcal{F}(\psi_0,\kappa)}{\sqrt[4]{3}} \approx 1.40218\,j\,\frac{2\sqrt{6}}{\omega_n\sqrt{{}_0u_{\max_{f_1}}}}\,. \tag{3.4.19}$$

Similar results are obtained if $b = 3$. However, for values of b greater than 3 employing elliptic functions becomes difficult. The resulting integral equation (3.4.11c) can only be solved for polynomials with order higher than 4 in a limited number of special cases. For example, if $b = 2n+1$ where $n = 2,3$ the substitution

$$\nu = \left(\frac{u}{{}_0u_{\max_{f_1}}} \right)^2 \tag{3.4.20a}$$

is introduced leading to

$$\mathrm{d}u = \frac{{}_0u^2_{\max_{f_1}}}{2u}\,\mathrm{d}\nu \qquad \text{and} \qquad u = {}_0u_{\max_{f_1}}\sqrt{\nu}, \tag{3.4.20b}$$

and the integral (3.4.11c) is rewritten as

$${}_0T_{f_1} = \frac{\sqrt{2\,(2n+2)}}{\omega_n\,{}_0u^n_{\max_{f_1}}} \int_0^1 \frac{\mathrm{d}\nu}{\sqrt{\nu\left(1-\nu^{(n+1)}\right)}} \tag{3.4.20c}$$

which can be solved using $\{259.50\}$ and $\{259.61\}$ in [22] for $n = 2$ and $n = 3$, respectively. Examples of substitutions other than Eq.(3.4.20a) can be found in [22–24].

For the special case of $b = 1$ Eq.(3.4.6b) and (3.4.12) expressing the free vibration of a linear system, cf. appendix A.2.1

$${}_0u_{\mathrm{Ex}_{f_1},\mathrm{lin}} = \left\{ |u_0|^2 + \frac{\dot{u}_0^2}{\omega_n^2} \right\}^{\frac{1}{2}} \tag{3.4.21a}$$

which in turn leads to the equality

$$\sqrt{{}_0\alpha_{f_1}} = {}_0u_{\max_{f_1},\mathrm{lin}}\,. \tag{3.4.21b}$$

The maximum oscillation velocity $\dot{u}_{\max}$ from Eq.(3.4.8b) becomes in the linear case

$$\dot{u}_{\mathrm{Ex,lin}} = \sqrt{(\omega_n u_0)^2 + \dot{u}_0^2}, \tag{3.4.21c}$$

which corresponds to the result given in appendix A.2.1 on page 180. Making use of Eq.(B.1.8) and (3.4.21b) the special function in (3.4.11e) simplifies to

$$\begin{aligned} {}_2\mathcal{F}_1\left(\frac{1}{2},\frac{1}{2};\frac{3}{2};\frac{{}_0u^2_{\max_{f_1},\mathrm{lin}}}{{}_0\alpha_{f_1}}\right) &= \frac{\sqrt{{}_0\alpha_{f_1}}}{{}_0u_{\max_{f_1},\mathrm{lin}}} \arcsin\left(\frac{{}_0u_{\max_{f_1},\mathrm{lin}}}{\sqrt{{}_0\alpha_{f_1}}}\right) \\ &= \frac{\pi}{2} \end{aligned} \tag{3.4.21d}$$

and the linear oscillation period ${}_0T_{f_1,\mathrm{lin}}$ becomes, as one would expect, the inverse of the natural frequency

$${}_0T_{f_1,\mathrm{lin}} = \frac{1}{f_n}\,. \tag{3.4.21e}$$

Results - Free Vibration

For the special case $\dot{u}_0 = 0$ the minimum/maximum displacement of the freely vibrating nonlinear SDOF with $f_1(u) = k\,\mathrm{sign}(u)\,|u|^b$, Eq.(3.4.6), simplifies to the trivial, linear expression

$${}_0u_{\mathrm{Ex}_{f_1}} = \mp|u_0|\,. \tag{3.4.22}$$

Considering now u_0 to be constant in (3.4.6) one can plot the **maximum** absolute **displacement** ${}_0u_{\max_{f_1}}$ depending on the SDOF equivalent natural frequency f_n and the initial velocity $\dot{u}_0$ for different values of the nonlinear restoring force exponent b as shown in Fig. 3.4.2 on page 94.[7]

For the linear SDOF ($b = 1$) in (a) the influence of initial velocity $v_0 = \dot{u}_0$ within the range of $0.5 \leq v_0 \leq 6.0$ becomes insignificant for natural frequencies higher than 20 Hz. This reverses with increasing values for b, as pictured in graphs (c) to (d). At 100 Hz the maximum displacement difference between $v_0 = 2.5$ and $v_0 = 6.0$ is still about 20% whereas at one tenth of this frequency, i.e. 10 Hz, this difference has already reduced to 25%. However, in general it can be concluded that for low initial velocity and high natural frequencies $f_n \gg 100$ Hz the minimum/maximum response is purely defined by the initial displacement u_0. Furthermore, at large values of b the maximum dynamic overall displacement $u_{\text{dyn}} = {}_0u_{\max_{f_1}}$ at low frequencies up to 10 Hz is much more influenced by higher values of v_0. As an example, for $b = 4$, $f_n = 5$ Hz and $v_0 = 0.5$, the solid line in Fig. 3.4.2(d), the maximum displacement u_{dyn} is equal to 0.25. In contrast for $b = 2$ in part (b) of Fig. 3.4.2, u_{dyn} at $f_n = 5$ Hz and $v_0 = 0.5$ it is equal to $u_0 = 0.1$. This effect is reinforced due to the circumstance that u_0 is smaller than 1, see Eq.(3.4.6). For $u_0 \geq 1$ and the same or slightly higher values for v_0 this implication is much less, which is clearly emphasised in Fig. 3.4.3 on page 95. For large values of u_0 the maximum displacement is nearly constant with frequency f_n. For $u_0 = 0.05$ and increasing b the maximum displacement decreases with f_n to the minimum value of 0.05 despite the given initial velocity $v_0 = 2.5$.

The **normalised nonlinear oscillation frequency** f_{NL}/f_n where f_{NL} is the inverse of the analytically obtained oscillation period ${}_0T_{f_1}$, Eq.(3.4.12), depending upon the SDOF's stiffness coefficient k, mass m and on the initial conditions, is shown in Fig. 3.4.4 for a constant value of $u_0 = 0.1$ and in Fig. 3.4.5 for $v_0 = 2.5 = \text{const.}$. Both figures have (a) as the linear case where the oscillation period is exact the reciprocal of the systems's natural frequency f_n as defined in Eq.(3.4.7) and independent of any initial condition u_0 or v_0.

As the order of nonlinearity b increases, the four lines in Fig. 3.4.4 plotted for four different initial velocities from 0.5 to 6.0 begin to separate, first at low natural frequencies $f_n \leq 10$ Hz, see Fig. (b) and later at moderate and high f_n, i.e. over the entire given frequency range. At low initial velocity (solid and dashed lines) the real oscillation frequency decreases significantly with increasing order of nonlinearity b. In figure (d) for $f_n \geq 20$ Hz the nonlinear frequency f_{NL} for $v_0 = 0.5$ and 1.5 is only a fraction of the value of the linear system's natural frequency f_n.

Closer examination of Fig. 3.4.5 reveals the graphs first split up at the upper end of the spectrum as b increases, see (b) to (d). In general, at larger initial displacement $u_0 \geq 1.00$, increasing values for b and constant initial velocity $v_0 = 2.5$ the change in the actual oscillation frequency f_{NL} is negligible compared to small u_0. For u_0 equal to 0.05 and 0.5, f_{NL} gets smaller with increasing values for f_n and b, whereas for $u_0 = 1.25$ it stays constant. This is due to the fact that $u_0 < 1$, which can additionally be verified by looking back to Fig. 3.4.4 where the drop in frequency for all graphs is much bigger than for the lines in Fig. 3.4.5 as the nonlinearity exponent b increases.

It should be noted here that all results in this subsection, Fig. 3.4.2 to 3.4.5, have been verified using a numerical time domain integration method. This applies as well for subsection 3.4.1.2 and 3.4.1.3.

[7] The plot for ${}_0u_{\min_{f_1}}$ would look like a mirror image of Fig. 3.4.2 with the mirror axis being the abscissa, i.e. with negative values on the ordinate, see Eq.(3.4.6b).

However, a detailed verification for the results of section 3.4.1 and 3.4.2 including remarks on the numerical algorithm will be given in 3.4.3.

3.4.1.2 Step Response

Substituting the nonlinear restoring force $f_1(u)$ from equation (3.4.1) into Eq.(3.3.3a)

$$k \int_u \operatorname{sign}(u)\,|u|^b\,\mathrm{d}u\Big|_{u={}_{\mathrm{H}}u_{\mathrm{Ex}f_1}} - p_0\,{}_{\mathrm{H}}u_{\mathrm{Ex}f_1} = k \int_u \operatorname{sign}(u)\,|u|^b\,\mathrm{d}u\Big|_{u=u_0} - p_0 u_0 + \frac{m}{2}\dot{u}_0^2 \tag{3.4.23}$$

and evaluating the integrals on both sides obeying Eq.(3.4.2) gives the following four nonlinear algebraic polynomial equation for the extreme values of displacement ${}_{\mathrm{H}}u_{\mathrm{Ex}f_1}$ depending upon the sign of ${}_{\mathrm{H}}u_{\mathrm{min}f_1}$, ${}_{\mathrm{H}}u_{\mathrm{max}f_1}$ and u_0

(a): $\boxed{{}_{\mathrm{H}}u_{\mathrm{Ex}f_1} \le 0,\ u_0 \le 0}$

$$-(-{}_{\mathrm{H}}u_{\mathrm{Ex}f_1})^b\,{}_{\mathrm{H}}u_{\mathrm{Ex}f_1} - \frac{p_0(b+1)}{k}\,{}_{\mathrm{H}}u_{\mathrm{Ex}f_1} = -(-u_0)^b u_0 - \frac{p_0(b+1)}{k}u_0 + \frac{(b+1)}{2\omega_n^2}\dot{u}_0^2 \tag{3.4.24a}$$

(b): $\boxed{{}_{\mathrm{H}}u_{\mathrm{Ex}f_1} \le 0,\ u_0 > 0}$

$$-(-{}_{\mathrm{H}}u_{\mathrm{Ex}f_1})^b\,{}_{\mathrm{H}}u_{\mathrm{Ex}f_1} - \frac{p_0(b+1)}{k}\,{}_{\mathrm{H}}u_{\mathrm{Ex}f_1} = u_0^{(b+1)} - \frac{p_0(b+1)}{k}u_0 + \frac{(b+1)}{2\omega_n^2}\dot{u}_0^2 \tag{3.4.24b}$$

(c): $\boxed{{}_{\mathrm{H}}u_{\mathrm{Ex}f_1} > 0,\ u_0 \le 0}$

$${}_{\mathrm{H}}u_{\mathrm{Ex}f_1}^{(b+1)} - \frac{p_0(b+1)}{k}\,{}_{\mathrm{H}}u_{\mathrm{Ex}f_1} = -(-u_0)^b u_0 - \frac{p_0(b+1)}{k}u_0 + \frac{(b+1)}{2\omega_n^2}\dot{u}_0^2 \tag{3.4.24c}$$

(d): $\boxed{{}_{\mathrm{H}}u_{\mathrm{Ex}f_1} > 0,\ u_0 > 0}$

$${}_{\mathrm{H}}u_{\mathrm{Ex}f_1}^{(b+1)} - \frac{p_0(b+1)}{k}\,{}_{\mathrm{H}}u_{\mathrm{Ex}f_1} = u_0^{(b+1)} - \frac{p_0(b+1)}{k}u_0 + \frac{(b+1)}{2\omega_n^2}\dot{u}_0^2\,. \tag{3.4.24d}$$

It is easy to see that the terms on the right-hand side in Eq.(3.4.24) incorporating the initial conditions can be rewritten as a single expression

$${}_{\mathrm{H}}\alpha_{f_1} = |u_0|^{(b+1)} - \operatorname{sign}(u_0)\frac{(b+1)p_0}{k}|u_0| + \frac{(b+1)}{2\omega_n^2}\dot{u}_0^2\,. \tag{3.4.25}$$

Furthermore, a simple substitution similar to Eq.(3.4.5)

$${}_{\mathrm{H}}\overset{(\cdot)}{u}_{\mathrm{Ex}f_1} = -\,{}_{\mathrm{H}}u_{\mathrm{Ex}f_1}\,, \qquad {}_{\mathrm{H}}u_{\mathrm{Ex}f_1} \le 0 \tag{3.4.26}$$

reduces the number of possible cases from four to two

(1) $\boxed{{}_{\mathrm{H}}u_{\mathrm{Ex}_{f_1}} \leq 0 \rightarrow {}_{\mathrm{H}}\overset{(\cdot)}{u}_{\mathrm{Ex}_{f_1}} \geq 0}$

$$ {}_{\mathrm{H}}\overset{(\cdot)}{u}{}^{(b+1)}_{\mathrm{Ex}_{f_1}} + \frac{p_0(b+1)}{k}\, {}_{\mathrm{H}}\overset{(\cdot)}{u}_{\mathrm{Ex}_{f_1}} - {}_{\mathrm{H}}\alpha_{f_1} = 0 \tag{3.4.27a} $$

(2) $\boxed{{}_{\mathrm{H}}u_{\mathrm{Ex}_{f_1}} > 0}$

$$ {}_{\mathrm{H}}u^{(b+1)}_{\mathrm{Ex}_{f_1}} - \frac{p_0(b+1)}{k}\, {}_{\mathrm{H}}u_{\mathrm{Ex}_{f_1}} - {}_{\mathrm{H}}\alpha_{f_1} = 0. \tag{3.4.27b} $$

Since it is unknown what sign ${}_{\mathrm{H}}u_{\mathrm{min}_{f_1}}, {}_{\mathrm{H}}u_{\mathrm{max}_{f_1}} \in {}_{\mathrm{H}}u_{\mathrm{Ex}_{f_1}}$ will possess, both equations need to be evaluated in order to retrieve a unique solution. Although mathematically feasible, complex solutions are in general without any physical meaning. However, as will be seen in the next section 3.4 they are required for solving the oscillation period integral expressions.

It should be noted that both equations in (3.4.27) above can be written in *one single* expression

$$ \left|{}_{\mathrm{H}}u_{\mathrm{Ex}_{f_1}}\right|^{(b+1)} - \frac{p_0(b+1)}{k}\, {}_{\mathrm{H}}u_{\mathrm{Ex}_{f_1}} - {}_{\mathrm{H}}\alpha_{f_1} = 0. \tag{3.4.28} $$

However, solutions for (3.4.28) can be only obtained numerically and multiple negative and positive roots, given b is large enough, do not clearly indicate the sought solution. Splitting (3.4.28) into (3.4.27) leads to two positive values if $-\infty < u(t) < \infty$. After applying (3.4.26) the result from (a) is the negative extreme value of the SDOF displacement.

The step response oscillation period ${}_{\mathrm{H}}T_{f_1}$ is obtained using (3.3.6), which now has to be grouped into three different cases (I), (II) and (III) as follows.

(I) $\boxed{{}_{\mathrm{H}}u_{\mathrm{max}_{f_1}} < {}_{\mathrm{H}}u_{\mathrm{min}_{f_1}} \leq 0}$

The maxima displacement obtained from Eq.(3.4.27) has only negative values. Together with Eq.(3.4.2) this gives

$$ {}_{\mathrm{H}}\overset{(\cdot)}{T}_{f_1} = \frac{\sqrt{2(b+1)}}{\omega_n} \left\{ \int_{{}_{\mathrm{H}}u_{\mathrm{max}_{f_1}}}^{{}_{\mathrm{H}}u_{\mathrm{min}_{f_1}}} \frac{\mathrm{d}u}{\sqrt{-\left((-u)^b(-u)\right) + \frac{(b+1)p_0}{k}u + {}_{\mathrm{H}}\alpha_{f_1}}} \right\}, \qquad u(t) \leq 0 \tag{3.4.29a} $$

which can be rewritten using the substitution from Eq.(3.4.11a) as

$$ = -\frac{\sqrt{2(b+1)}}{\omega_n} \left\{ \int_{\left|{}_{\mathrm{H}}u_{\mathrm{max}_{f_1}}\right|}^{\left|{}_{\mathrm{H}}u_{\mathrm{min}_{f_1}}\right|} \frac{\mathrm{d}\overset{(\cdot)}{u}}{\sqrt{-\overset{(\cdot)}{u}{}^{(b+1)} - \frac{(b+1)p_0}{k}\overset{(\cdot)}{u} + {}_{\mathrm{H}}\alpha_{f_1}}} \right\}, \qquad \overset{(\cdot)}{u}(t) \geq 0 \tag{3.4.29b} $$

and after interchanging the integration limits leading to the final result

$$ {}_{\mathrm{H}}\overset{(\cdot)}{T}_{f_1} = \frac{\sqrt{2(b+1)}}{\omega_n} \left\{ \int_{\left|{}_{\mathrm{H}}u_{\mathrm{min}_{f_1}}\right|}^{\left|{}_{\mathrm{H}}u_{\mathrm{max}_{f_1}}\right|} \frac{\mathrm{d}\overset{(\cdot)}{u}}{\sqrt{-\overset{(\cdot)}{u}{}^{(b+1)} - \frac{(b+1)p_0}{k}\overset{(\cdot)}{u} + {}_{\mathrm{H}}\alpha_{f_1}}} \right\}, \qquad \overset{(\cdot)}{u}(t) \geq 0 \tag{3.4.29c} $$

(II) $\boxed{{}_{\mathbb{H}}u_{\min_{f_1}} < 0,\ {}_{\mathbb{H}}u_{\max_{f_1}} > 0}$ or $\boxed{{}_{\mathbb{H}}u_{\max_{f_1}} < 0,\ {}_{\mathbb{H}}u_{\min_{f_1}} > 0}$

The oscillation period is now a sum of the two integration intervals ranging from the domain of negative displacement $u(t) < 0$ to the positive. The formulas to follow assume ${}_{\mathbb{H}}u_{\min_{f_1}} < 0$, ${}_{\mathbb{H}}u_{\max_{f_1}} > 0$ but are easily modified for the case ${}_{\mathbb{H}}u_{\min_{f_1}} > 0$, ${}_{\mathbb{H}}u_{\max_{f_1}} < 0$ by changing the limits on the appropriate integration expressions. Again, using (3.3.6) together with (3.4.2) leads to

$$
{}^{(-/+)}_{\mathbb{H}}T_{f_1} = \frac{\sqrt{2(b+1)}}{\omega_n}\left\{ \int_{{}_{\mathbb{H}}u_{\min_{f_1}}}^{0} \frac{\mathrm{d}u}{\sqrt{-\left((-u)^b(-u)\right) + \frac{(b+1)p_0}{k}u + {}_{\mathbb{H}}\alpha_{f_1}}} + \int_{0}^{{}_{\mathbb{H}}u_{\max_{f_1}}} \frac{\mathrm{d}u}{\sqrt{-u^{(b+1)} + \frac{(b+1)p_0}{k}u + {}_{\mathbb{H}}\alpha_{f_1}}} \right\}, \quad (3.4.30a)
$$

and hence

$$
{}^{(-/+)}_{\mathbb{H}}T_{f_1} = \frac{\sqrt{2(b+1)}}{\omega_n}\left\{ \int_{0}^{\left|{}_{\mathbb{H}}u_{\min_{f_1}}\right|} \frac{\mathrm{d}\overset{(-)}{u}}{\sqrt{-\overset{(-)}{u}^{(b+1)} - \frac{(b+1)p_0}{k}\overset{(-)}{u} + {}_{\mathbb{H}}\alpha_{f_1}}} + \int_{0}^{{}_{\mathbb{H}}u_{\max_{f_1}}} \frac{\mathrm{d}u}{\sqrt{-u^{(b+1)} + \frac{(b+1)p_0}{k}u + {}_{\mathbb{H}}\alpha_{f_1}}} \right\}, \quad \overset{(-)}{u}(t), u(t) > 0. \quad (3.4.30b)
$$

(III) $\boxed{0 \leq {}_{\mathbb{H}}u_{\min_{f_1}} < {}_{\mathbb{H}}u_{\max_{f_1}}}$

The displacement of the system is purely positive. The integral equation for the oscillation period is therefore

$$
{}^{(+)}_{\mathbb{H}}T_{f_1} = \frac{\sqrt{2(b+1)}}{\omega_n}\left\{ \int_{{}_{\mathbb{H}}u_{\min_{f_1}}}^{{}_{\mathbb{H}}u_{\max_{f_1}}} \frac{\mathrm{d}u}{\sqrt{-u^{(b+1)} + \frac{(b+1)p_0}{k}u + {}_{\mathbb{H}}\alpha_{f_1}}} \right\}, \quad u(t) > 0. \quad (3.4.31)
$$

All terms in curly brackets in Eq.(3.4.29) to (3.4.31) are known as *elliptic integrals* [22], see appendix B.2 for details.

An expression for the extreme values of velocity can be found using Eq.(3.3.4g) on page 41 together with (3.4.3) on page 46

$$
\dot{u}_{\mathrm{Ex}} = \sqrt{\frac{2}{m}}\left(p_0 u_{\mathrm{Ex,eq}} - \frac{k}{(b+1)}\left|u_{\mathrm{Ex,eq}}\right|^{(b+1)} - p_0 u_0 + \frac{k}{(b+1)}\left|u_0\right|^{(b+1)} + \frac{m}{2}\dot{u}_0^2 \right)^{\frac{1}{2}} \quad (3.4.32a)
$$

where the new equilibrium position is given by (3.3.4e)

$$
u_{\mathrm{Ex,eq}} = \mathrm{sign}\,(p_0)\left(\frac{|p_0|}{k}\right)^{\frac{1}{b}} \quad (3.4.32b)
$$

and therefore corresponds to the nonlinear static displacement caused by the step load with magnitude p_0. Equation (3.4.32) can be rearranged and leads together with (3.4.25) to a more compact form

$$\dot{u}_{\mathrm{Ex}} = \omega_n \sqrt{\frac{2}{b+1}} \left(\frac{p_0(b+1)}{k} u_{\mathrm{Ex,eq}} - \left| u_{\mathrm{Ex,eq}} \right|^{(b+1)} + {}_{\mathbb{H}}\alpha_{f_1} \right)^{\frac{1}{2}} \tag{3.4.32c}$$

where minimum and maximum values of are given by (3.3.4h).

For any arbitrary value of the exponent b, i.e. $b \in \mathbb{R}$, equations (3.4.29) to (3.4.31) can only be solved numerically in their current complex form. However, examining three simplified cases (i) $u_0 = \dot{u}_0 = 0$, (ii) $b = 2$, and (iii) $b = 3$, analytical solutions become available. In addition, for $b = 1$ Eq.(3.4.27) to (3.4.31) reduce to the well known solutions for a linear step-excited SDOF system, see appendix A.2.2, with

$${}_{\mathbb{H}}\overset{(-)}{u}_{\mathrm{Ex}_{f_1},\mathrm{lin}} = -\frac{p_0}{k} + \sqrt{\left(\frac{p_0}{k}\right)^2 + {}_{\mathbb{H}}\alpha_{f_1,\mathrm{lin}}} \tag{3.4.33a}$$

and

$${}_{\mathbb{H}}u_{\mathrm{Ex}_{f_1},\mathrm{lin}} = \frac{p_0}{k} \pm \sqrt{\left(\frac{p_0}{k}\right)^2 + {}_{\mathbb{H}}\alpha_{f_1,\mathrm{lin}}} \tag{3.4.33b}$$

for the minimum/maximum linear displacement due to $P(t) = p_0 \mathbb{H}(t)$. The constant ${}_{\mathbb{H}}\alpha_{f_1,\mathrm{lin}}$ is easily derived from Eq.(3.4.25) by setting $b = 1$. Because of the condition

$${}_{\mathbb{H}}\overset{(-)}{u}_{\mathrm{Ex}_{f_1},\mathrm{lin}} \,,\; {}_{\mathbb{H}}u_{\mathrm{Ex}_{f_1},\mathrm{lin}} \overset{!}{\geq} 0 \tag{3.4.34}$$

Eq.(3.4.33a) is only valid if

$$\frac{p_0}{k} \leq \sqrt{\left(\frac{p_0}{k}\right)^2 + {}_{\mathbb{H}}\alpha_{f_1,\mathrm{lin}}}$$

and (3.4.33b) only if

$$\frac{p_0}{k} \geq \sqrt{\left(\frac{p_0}{k}\right)^2 + {}_{\mathbb{H}}\alpha_{f_1,\mathrm{lin}}} \,.$$

Furthermore, for any type of initial conditions the expression underneath the square root in (3.4.33) will always be greater zero which can be proved as follows. The inequality

$$\left(\frac{p_0}{k}\right)^2 + |u_0|^2 - \mathrm{sign}\,(u_0)\, \frac{2p_0}{k} |u_0| + \frac{\dot{u}_0^2}{\omega_n^2} \overset{!}{\geq} 0 \tag{3.4.35}$$

reaches a its global minima if $u_0 > 0$, hence $\mathrm{sign}\,(u_0) = +$, $\dot{u}_0 = 0$ and $p_0 \geq 0$ leading to

$$\begin{aligned} \left(\frac{p_0}{k}\right)^2 + u_0^2 - \frac{2p_0}{k} u_0 &\geq 0 \\ \left(\frac{p_0}{k}\right)^2 + u_0^2 &\geq \frac{2p_0}{k} u_0 \\ \frac{1}{2}\left(\frac{p_0}{k u_0} + \frac{k u_0}{p_0}\right) &\geq 1 \end{aligned}$$

which holds true for

$$u_0, k, p_0 \in \mathbb{R}$$

and is already implied in the small proof of Eq.(3.4.35),

$$u_0, k, p_0 \geq 0.$$

For zero initial conditions Eq.(3.4.33) gives the same result as (A.2.12)

$${}_{\mathbb{H}}u_{\min_{f_1},\text{lin}} = 0$$

and

$${}_{\mathbb{H}}u_{\max_{f_1},\text{lin}} = 2 \times u_{\text{stat,lin}} = 2\frac{p_0}{k}.$$

Equation (3.4.32c) leads for the linear case with $b = 1$ to

$$\dot{u}_{\text{Ex,lin}} = \omega_n \sqrt{u_{\text{stat,lin}}^2 + u_0 - 2\frac{p_0}{k}u_0 + \left(\frac{\dot{u}_0}{\omega_n}\right)^2} \tag{3.4.36}$$

as the systems velocity with $u_{\text{stat,lin}}$ given by Eq.(3.4.32b), see above. Equation (3.4.36) is the very same expression as obtained in appendix A.2.2 on page 181 and demonstrates once more the ability of the proposed method to cover linear and nonlinear SDOF systems in an equal manner.

The linear oscillation period in case (II) derived from Eq.(3.4.30) is

$${}_{\mathbb{H}}T_{f_1,\text{lin}} = \frac{2}{\omega_n}\left\{ \int_0^{\left|{}_{\mathbb{H}}u_{\min_{f_1}}\right|} \frac{\mathrm{d}\overset{(\cdot)}{u}}{\sqrt{-\overset{(\cdot)}{u}^2 - \frac{2p_0}{k}\overset{(\cdot)}{u} + {}_{\mathbb{H}}\alpha_{f_1}}} + \int_0^{{}_{\mathbb{H}}u_{\max_{f_1}}} \frac{\mathrm{d}u}{\sqrt{-u^2 + \frac{2p_0}{k}u + {}_{\mathbb{H}}\alpha_{f_1}}} \right\} \tag{3.4.37a}$$

which equates to the algebraic expression

$$\begin{aligned} {}_{\mathbb{H}}T_{f_1,\text{lin}} = \frac{2}{\omega_n}\Bigg\{ &-\arctan\left(\frac{p_0}{k\sqrt{{}_{\mathbb{H}}\alpha_{f_1}}}\right) + \arctan\left(\frac{\frac{p_0}{k} + \left|{}_{\mathbb{H}}u_{\min_{f_1}}\right|}{\sqrt{-\left|{}_{\mathbb{H}}u_{\min_{f_1}}\right|\left(2\frac{p_0}{k} + \left|{}_{\mathbb{H}}u_{\min_{f_1}}\right|\right) + {}_{\mathbb{H}}\alpha_{f_1}}}\right) \\ &+ \arctan\left(\frac{p_0}{k\sqrt{{}_{\mathbb{H}}\alpha_{f_1}}}\right) + \arctan\left(\frac{\frac{p_0}{k} - {}_{\mathbb{H}}u_{\max_{f_1}}}{\sqrt{2\frac{p_0}{k}\,{}_{\mathbb{H}}u_{\max_{f_1}} - {}_{\mathbb{H}}u_{\max_{f_1}}^2 + {}_{\mathbb{H}}\alpha_{f_1}}}\right)\Bigg\} \end{aligned} \tag{3.4.37b}$$

and simplifies together with (3.4.33), the definition of the natural frequency of the linear system

$$\omega_n = 2\pi f_n, \tag{3.4.37c}$$

and the inverse trigonometrical limit

$$\lim_{x \to +\infty} \arctan(x) = \frac{\pi}{2}$$

to

$$\begin{aligned} {}_{\mathbb{H}}T_{f_1,\text{lin}} &= \frac{2}{\omega_n}\left\{\frac{\pi}{2} + \frac{\pi}{2}\right\} \\ &= \frac{1}{f_n} \end{aligned} \tag{3.4.37d}$$

the well-known relationship of oscillation period and frequency of the linear system for the general case $u_0 \neq 0$, $\dot{u}_0 \neq 0$. If $p_0 = 0$, Eq.(3.4.33) becomes

$$ {}_{\mathbb{H}}^{(\cdot)}u_{\mathrm{Ex}_{f_1},\mathrm{lin}} = {}_{\mathbb{H}}u_{\mathrm{Ex}_{f_1},\mathrm{lin}} = \pm\sqrt{|u_0|^2 + \frac{\dot{u}_0^2}{\omega_n^2}}\,. \tag{3.4.37e} $$

For the oscillation period the term is always, as one would expect, $\frac{1}{f_n}$, regardless initial conditions u_0, $\dot{u}_0$ and step force amplitude p_0. The results obtained in (3.4.33) to (3.4.37) are an indicator of the consistency of the method derived in this chapter. By changing only a single equation parameter, the linear and nonlinear dynamic behaviour of the SDOF can be expressed.

Returning back to the special cases (i) to (iii) mentioned above, Eq.(3.4.27) reduces with

(i) $\mathbf{u_0 = \dot{u}_0 = 0}$ to the two following nonlinear algebraic equations for the extreme values of displacement ${}_{\mathbb{H}}u_{\mathrm{Ex}_{f_1}}$ depending solely upon the systems nonlinear stiffness coefficient k and the magnitude and direction of the applied load p_0

$$ {}_{\mathbb{H}}^{(\cdot)}u_{\mathrm{Ex}_{f_1}}\left({}_{\mathbb{H}}^{(\cdot)}u_{\mathrm{Ex}_{f_1}}^{b} + \frac{(b+1)p_0}{k}\right) = 0 \tag{3.4.38a} $$

$$ {}_{\mathbb{H}}u_{\mathrm{Ex}_{f_1}}\left({}_{\mathbb{H}}u_{\mathrm{Ex}_{f_1}}^{b} - \frac{(b+1)p_0}{k}\right) = 0 \tag{3.4.38b} $$

with the only feasible solutions

$$ -{}_{\mathbb{H}}^{(\cdot)}u_{\mathrm{Ex}_{f_1}} = {}_{\mathbb{H}}u_{\mathrm{Ex}_{f_1}} = \begin{cases} 0 & = {}_{\mathbb{H}}^{[u_0]}u_{\min_{f_1}} \quad \text{if} \quad p_0 > 0, \\ -\left[\dfrac{(b+1)\,|p_0|}{k}\right]^{\frac{1}{b}} & = {}_{\mathbb{H}}^{[u_0]}u_{\max_{f_1}} \quad \text{if} \quad p_0 < 0 \end{cases} \tag{3.4.39a} $$

for Eq.(3.4.38a) obeying condition (3.4.26) and

$$ {}_{\mathbb{H}}u_{\mathrm{Ex}_{f_1}} = \begin{cases} \left[\dfrac{(b+1)\,|p_0|}{k}\right]^{\frac{1}{b}} & = {}_{\mathbb{H}}^{[u_0]}u_{\max_{f_1}} \quad \text{if} \quad p_0 > 0, \\ 0 & = {}_{\mathbb{H}}^{[u_0]}u_{\min_{f_1}} \quad \text{if} \quad p_0 < 0 \end{cases} \tag{3.4.39b} $$

for Eq.(3.4.38b). The index $[u_0]$ used in the upper left corner of the symbols for minimum and maximum displacement refers to the case of zero initial conditions. It should be noted here that obtaining an explicit expression for ${}_{\mathbb{H}}^{[u_0]}u_{\mathrm{Ex}_{f_1}}$ as done by BAPAT *et al* [7] discharges the solution for ${}_{\mathbb{H}}^{[u_0]}u_{\min_{f_1}}$ and leads to a somewhat ambiguous derivation of the minimum displacement ${}_{\mathbb{H}}^{[u_0]}u_{\min_{f_1}}$, which is fundamental for obtaining the oscillation period since it presents the lower limit of integration as will be seen below.

For $u_0 = \dot{u}_0 = 0$ Eq.(3.4.32) and (3.4.32b) reduces together with the equality

$$ p_0 \times \mathrm{sign}\,(p_0) = |p_0| $$

to

$$ \begin{aligned} \dot{u}_{\mathrm{Ex}} &= \sqrt{2}\sqrt{\frac{|p_0|}{m}\left(\frac{|p_0|}{k}\right)^{\frac{1}{b}} - \frac{\omega_n^2}{(b+1)}\,\mathrm{sign}\,(p_0)\left(\frac{|p_0|}{k}\right)^{\frac{(b+1)}{b}}} \\ &= \omega_n\left(\frac{|p_0|}{k}\right)^{\left(\frac{1}{2}+\frac{1}{2b}\right)}\sqrt{2\left(1 - \frac{\mathrm{sign}\,(p_0)}{b+1}\right)} \end{aligned} \tag{3.4.40} $$

as the extreme values of the system's oscillation velocity for zero initial conditions.

With the constant ${}_{\mathbb{H}}\alpha_{f_1}$ from Eq.(3.4.25) equal to zero and assuming[8] $p_0 > 0$ and case (III), i.e. $0 \leq {}^{[u_0]}_{\mathbb{H}}u_{\min_{f_1}} < {}^{[u_0]}_{\mathbb{H}}u_{\max_{f_1}}$, the oscillation period ${}_{\mathbb{H}}T_{f_1}$ derived in (3.4.31) can now be written as

$$ {}^{[u_0]}_{\mathbb{H}}{}^{(+)}T_{f_1} = \frac{\sqrt{2(b+1)}}{\omega_n} \int_0^{{}^{[u_0]}_{\mathbb{H}}u_{\max_{f_1}}} \frac{\mathrm{d}u}{\sqrt{-u^{(b+1)} + \frac{(b+1)p_0}{k}u}}, \qquad p_0 > 0 \tag{3.4.41a} $$

or, since the lower integration limit ${}^{[u_0]}_{\mathbb{H}}u_{\min_{f_1}} = 0$, as[9]

$$ {}^{[u_0]}_{\mathbb{H}}T_{f_1} = \frac{\sqrt{2(b+1)}}{\omega_n} \int_0^{{}^{[u_0]}_{\mathbb{H}}u_{\max_{f_1}}} \frac{\mathrm{d}u}{\sqrt{u}\sqrt{-u^b + \frac{(b+1)p_0}{k}}} \tag{3.4.41b} $$

which leads to

$$ \begin{aligned} {}^{[u_0]}_{\mathbb{H}}T_{f_1} &= \frac{2\sqrt{2(b+1)}}{\omega_n} \left[\sqrt{u}\sqrt{\frac{1-\frac{ku^b}{(b+1)p_0}}{\frac{(b+1)p_0}{k}-u^b}}\ {}_2\mathcal{F}_1\left(\frac{1}{2b},\frac{1}{2};1+\frac{1}{2b};\frac{ku^b}{(b+1)p_0}\right)\right]_0^{{}^{[u_0]}_{\mathbb{H}}u_{\max_{f_1}}} \\ &= \frac{2\sqrt{2(b+1)}}{\omega_n}\sqrt{\frac{k\,{}^{[u_0]}_{\mathbb{H}}u_{\max_{f_1}}}{(b+1)p_0}}\ {}_2\mathcal{F}_1\left(\frac{1}{2b},\frac{1}{2};1+\frac{1}{2b};\frac{k\left({}^{[u_0]}_{\mathbb{H}}u_{\max_{f_1}}\right)^b}{(b+1)p_0}\right). \end{aligned} $$

Finally, together with Eq.(3.4.39) one has the oscillation period as

$$ {}^{[u_0]}_{\mathbb{H}}T_{f_1} = \frac{-2\sqrt{2}}{\omega_n}\sqrt{\frac{k}{p_0}}\left[\frac{(b+1)p_0}{k}\right]^{\frac{1}{2b}} \frac{\sqrt{\pi}\,\Gamma\left(\frac{1}{2b}\right)}{(b-1)\,\Gamma\left(\frac{1}{2b}-\frac{1}{2}\right)}, \qquad p_0 > 0 \tag{3.4.42} $$

where $\Gamma(\ldots)$ denotes the Gamma function outlined in appendix B.1 and [21]. In case of $p < 0$ the period ${}^{[u_0]}_{\mathbb{H}}T_{f_1}$ is given by Eq.(3.4.29c)

$$ {}^{[u_0]}_{\mathbb{H}}{}^{(-)}T_{f_1} = \frac{\sqrt{2(b+1)}}{\omega_n} \int_{\left|{}_{\mathbb{H}}u_{\min_{f_1}}\right|}^{\left|{}_{\mathbb{H}}u_{\max_{f_1}}\right|} \frac{\mathrm{d}\overset{(-)}{u}}{\sqrt{-\overset{(-)}{u}{}^{(b+1)} - \frac{(b+1)(-p_0)}{k}\overset{(-)}{u}}} \tag{3.4.43a} $$

which simplifies with $\left|{}_{\mathbb{H}}u_{\min_{f_1}}\right| = 0$ to Eq.(3.4.41a)

$$ = \frac{\sqrt{2(b+1)}}{\omega_n} \int_0^{\left|{}^{[u_0]}_{\mathbb{H}}u_{\max_{f_1}}\right|} \frac{\mathrm{d}\overset{(-)}{u}}{\sqrt{-\overset{(-)}{u}{}^{(b+1)} + \frac{(b+1)p_0}{k}\overset{(-)}{u}}}, \qquad {}^{[u_0]}_{\mathbb{H}}u_{\max_{f_1}} < 0 \tag{3.4.43b} $$

[8] In the case of a nonlinear step-excited SDOF system which is at rest at the time the load is applied, i.e. zero initial conditions, minimum and maximum displacement will always have the same sign, i.e. either positive or negative depending solely on the direction of action of the force $P(t) = p_0\,\mathbb{H}(t)$.

[9] It should be noted here that the results for Eq.(3.4.41a) and (3.4.41b) are exactly the same. However, the second equation was introduced because the integration algorithm of the algebraic manipulation software MATHEMATICA® [20] converged more rapidly to a stable solution. Using Eq.(3.4.41a) for integration between the limits $0 \leq u(t) \leq {}^{[u_0]}_{\mathbb{H}}u_{\max_{f_1}}$ leads to an indeterminate expression since $u(t)$ will appear in the denominator. Therefore, the simplification made above before integrating has to be introduced prior to application of the integration limits if Eq.(3.4.41a) is used.

and hence yields the same solution as (3.4.42).

It should be mentioned here that the expressions derived in (3.4.39) and (3.4.42) for the special case of zero initial conditions are essentially the same as those obtained by BAPAT *et al* [7] using an integration-by-substitution method. However, neither a clear interpretation of the minimum displacement ${}^{[u_0]}_{\mathbb{H}}u_{\min_{f_1}}$ as the solution of Eq.(3.4.38) nor the possibility of a negative acting force constant $p_0 < 0$ were given. Both equations (3.4.39) and (3.4.42) hold also true for the linear case $b = 1$ giving for ${}_{\mathbb{H}}u_{\mathsf{Ex}_{f_1}}$

$$
{}_{\mathbb{H}}u_{\max_{f_1}} = \pm 2\,\frac{|p_0|}{k}\begin{cases}\text{if} & p_0 > 0,\\ \text{if} & p_0 < 0\end{cases}
$$

$$
{}_{\mathbb{H}}u_{\min_{f_1}} = 0
$$

and with

$$
\lim_{b\to 1}\left[\frac{\sqrt{\pi}\,\Gamma\left(\frac{1}{2b}\right)}{(b-1)\,\Gamma\left(\frac{1}{2b}-\frac{1}{2}\right)}\right] = -\frac{\pi}{2}
$$

for the oscillation period

$$
{}_{\mathbb{H}}T_{f_1,\mathsf{lin}} = \frac{1}{f_n}
$$

as shown in A.2.2.

(ii) $\mathbf{b = 2}$: Considering a restoring force proportional to the square of the displacement, Eq.(3.4.27) simplifies to two third order polynomials

$$
(1)\qquad {}^{[2]}_{\mathbb{H}}\overset{(\cdot)3}{u}_{\mathsf{Ex}_{f_1}} + \frac{3p_0}{k}\,{}^{[2]}_{\mathbb{H}}\overset{(\cdot)}{u}_{\mathsf{Ex}_{f_1}} - {}^{[2]}_{\mathbb{H}}\alpha_{f_1} = 0, \qquad {}^{[2]}_{\mathbb{H}}\overset{(\cdot)}{u}_{\mathsf{Ex}_{f_1}} \geq 0 \qquad (3.4.44a)
$$

$$
(2)\qquad {}^{[2]}_{\mathbb{H}}u^3_{\mathsf{Ex}_{f_1}} - \frac{3p_0}{k}\,{}^{[2]}_{\mathbb{H}}u_{\mathsf{Ex}_{f_1}} - {}^{[2]}_{\mathbb{H}}\alpha_{f_1} = 0, \qquad {}^{[2]}_{\mathbb{H}}u_{\mathsf{Ex}_{f_1}} \geq 0 \qquad (3.4.44b)
$$

with a constant consisting of all initial conditions

$$
{}^{[2]}_{\mathbb{H}}\alpha_{f_1} = |u_0|^3 - \operatorname{sign}(u_0)\,\frac{3p_0}{k}\,|u_0| + \frac{3\dot{u}_0^2}{2\omega_n^2} \qquad (3.4.45)
$$

and an index [2] referring to the special case of $b = 2$. It is easy to see that for $p < 0$ case (1) and (2) can be interchanged since both of them posses the same condition $u_{\mathsf{Ex}} > 0$. Equation (3.4.44) can be solved using the algorithm given in [15], see appendix B.3 for details. The solution indicator D equates for case (1) as

$$
D_{(1)} = \left(\frac{p_0}{k}\right)^3 + \left(-{}^{[2]}_{\mathbb{H}}\alpha_{f_1}\right)^2 \qquad (3.4.46a)
$$

and for (2) in Eq.(3.4.44)

$$
D_{(2)} = -\left(\frac{p_0}{k}\right)^3 + \left(-{}^{[2]}_{\mathbb{H}}\alpha_{f_1}\right)^2. \qquad (3.4.46b)
$$

where the sign of D constitutes the nature of solutions, see Table B.3.1. Since this cannot be determined without prior knowledge of the direction of action of the force p_0, the force-stiffness ratio and all initial conditions, it is necessary to distinguish between the two different cases (a) $D \leq 0$ and (b) $D > 0$ for $D_{(1)}$ and $D_{(2)}$. It should be noted here, that the following paragraph is of more general nature. The term D will refer to $D_{(1)}$ as well as $D_{(2)}$. Likewise, the term ${}^{[2]}_{\mathbb{H}}u_{\mathsf{Ex}_{f_1}}$ refers to ${}^{[2]}_{\mathbb{H}}\overset{(\cdot)}{u}_{\mathsf{Ex}_{f_1}}$ and ${}^{[2]}_{\mathbb{H}}u_{\mathsf{Ex}_{f_1}}$ at the same time.

(a) $\mathbf{D \leq 0}$: All solutions will be real and can be obtained using Eq.(B.3.3b)

$$ {}^{[2]}_{\mathbb{H}}u_{\mathrm{Ex}_{f_1},i} = 2\sqrt{\frac{p_0}{k}}\cos\left[\frac{\varphi_p}{3}+\frac{2\pi}{3}(i-1)\right], \quad (i=1,2,3) \tag{3.4.47a} $$

where the constant φ_p equates to

$$ \varphi_p = \arccos\left[\frac{{}^{[2]}_{\mathbb{H}}\alpha_{f_1}}{2\sqrt{\left(\frac{p_0}{k}\right)^3}}\right]. \tag{3.4.47b} $$

The solutions ${}^{[2]}_{\mathbb{H}}u_{\mathrm{Ex}_{f_1},i}$ obtained by Eq.(3.4.47a) are not sorted by any means, see appendix B.3, but can always be rearranged in a way to fulfill the following two conditions

$$ {}^{[2]}_{\mathbb{H}}u_{\mathrm{Ex}_{f_1},1} + {}^{[2]}_{\mathbb{H}}u_{\mathrm{Ex}_{f_1},2} = -{}^{[2]}_{\mathbb{H}}u_{\mathrm{Ex}_{f_1},3} \tag{3.4.47c} $$

and

$$ {}^{[2]}_{\mathbb{H}}u_{\mathrm{Ex}_{f_1},1} > {}^{[2]}_{\mathbb{H}}u_{\mathrm{Ex}_{f_1},2}\,. \tag{3.4.47d} $$

(b) $\mathbf{D > 0}$: According to Table B.3.1 equation (3.4.44) has one real

$$ {}^{[2]}_{\mathbb{H}}u_{\mathrm{Ex}_{f_1},1} = s_1 + s_2 \tag{3.4.48a} $$

and two conjugate complex solutions

$$ {}^{[2]}_{\mathbb{H}}u_{\mathrm{Ex}_{f_1},2/3} = -\frac{s_1+s_2}{2} \pm \frac{s_1-s_2}{2}\,\mathrm{i}\sqrt{3} \tag{3.4.48b} $$

where, cf. appendix B.3,

$$ s_1 = \sqrt[3]{\frac{{}^{[2]}_{\mathbb{H}}\alpha_{f_1}}{2}+\sqrt{D}} \tag{3.4.48c} $$

and

$$ s_2 = \frac{p_0}{k\sqrt[3]{\frac{{}^{[2]}_{\mathbb{H}}\alpha_{f_1}}{2}+\sqrt{D}}}. \tag{3.4.48d} $$

It is important to note here, that all solutions obtained in both cases (a) and (b) have to fulfill conditions (3.4.44), i.e. must be equal or greater zero. Negative real solutions are discarded.

The following derivation of the oscillation period ${}^{[2]}_{\mathbb{H}}T_{f_1}$ is constrained to case (II) and (III) above, i.e. Eq.(3.4.30b) and (3.4.31). Additionally, $p_0 > 0$ will be assumed. All other possible cases can be derived from these. Substituting $b = 2$ into Eq.(3.4.30b) gives a sum of third-order elliptic integrals in their non-canonical form [24]

$$ {}^{(-/+)}_{[2]}T_{f_1} = \frac{\sqrt{6}}{\omega_n}\left\{\int_0^{\left|{}^{[2]}_{\mathbb{H}}u_{\min_{f_1}}\right|}\frac{d\overset{(-)}{u}}{\sqrt{-\overset{(-)}{u}^3-\frac{3p_0}{k}\overset{(-)}{u}+{}^{[2]}_{\mathbb{H}}\alpha_{f_1}}}+\int_0^{{}^{[2]}_{\mathbb{H}}u_{\max_{f_1}}}\frac{du}{\sqrt{-u^3+\frac{3p_0}{k}u+{}^{[2]}_{\mathbb{H}}\alpha_{f_1}}}\right\}. \tag{3.4.49} $$

A solution in terms of special tabulated functions is only possible if all zeros and poles of the integral expressions are known. If multiplied by (-1) the expressions under the square roots in each of the denominators in Eq.(3.4.49) are identical to (3.4.44). Hence, solutions for all zeros are available and (3.4.49) can be rewritten in Legendre canonical form [23] using

$$-\overset{(\cdot)}{u}^3 - \frac{3p_0}{k}\overset{(\cdot)}{u} + \overset{[2]}{\mathbb{H}}\alpha_{f_1} = \left(\xi_1 - \overset{(\cdot)}{u}\right)\left(\overset{(\cdot)}{u} - \xi_2\right)\left(\overset{(\cdot)}{u} - \xi_3\right)$$

$$= (\xi_1 - u)(u - \xi_2)(u - \xi_3) \tag{3.4.50a}$$

$$= -u^3 + (\xi_1 + \xi_2 + \xi_3)u^2 - (\xi_1\xi_2 + \xi_1\xi_3 + \xi_2\xi_3)u + \xi_1\xi_2\xi_3 \tag{3.4.50b}$$

and

$$-u^3 + \frac{3p_0}{k}u + \overset{[2]}{\mathbb{H}}\alpha_{f_1} = (\chi_1 - u)(u - \chi_2)(u - \chi_3) \tag{3.4.50c}$$

$$= -u^3 + (\chi_1 + \chi_2 + \chi_3)u^2 + (-\chi_1\chi_2 - \chi_1\chi_3 - \chi_2\chi_3)u + \chi_1\chi_2\chi_3 \tag{3.4.50d}$$

where

$$\xi_i = \overset{[2]}{\mathbb{H}}\overset{(\cdot)}{u}_{\mathrm{Ex}_{f_1},i} \quad \text{and} \quad \chi_i = \overset{[2]}{\mathbb{H}}u_{\mathrm{Ex}_{f_1},j}, \qquad (i,j = 1,2,3) \tag{3.4.50e}$$

are the solutions of the third-order polynomials, Eq.(3.4.44a) and (3.4.44b), respectively. Using the inverse of substitution (3.4.26) on page 52 the oscillation period is then

$$\overset{(-/+)}{\overset{[2]}{\mathbb{H}}T_{f_1}} = \frac{\sqrt{6}}{\omega_n}\left\{ \int_0^{\left|\overset{[2]}{\mathbb{H}}u_{\min_{f_1}}\right|} \frac{\mathrm{d}u}{\sqrt{(\xi_1 - u)(u - \xi_2)(u - \xi_3)}} + \int_0^{\overset{[2]}{\mathbb{H}}u_{\max_{f_1}}} \frac{\mathrm{d}u}{\sqrt{(\chi_1 - u)(u - \chi_2)(u - \chi_3)}} \right\}. \tag{3.4.51}$$

Selection of case (II) on page 54 implies the solution of (3.4.44) for the following cases:

$$\text{(A)} \qquad y_1 > 0 > y_2 > y_3; \qquad y_1, y_2, y_3 \in \mathbb{R} \tag{3.4.52a}$$

$$\text{(B)} \qquad y_1 > 0, y_2 = y_3^*; \qquad y_1 \in \mathbb{R};\ y_2, y_3 \in \mathbb{C} \tag{3.4.52b}$$

depending upon the sign of D in (3.4.46) and

$$y_i = \xi_i \quad \text{or} \quad y_i = \chi_i, \qquad (i = 1,2,3),$$

which need to be taken into account for the solution of the integral terms in (3.4.51). Since the solution behaviour of both terms in (3.4.51) is essentially the same, only the first one will be examined closer. Considering case (A), i.e. Eq.(3.4.50a) has three real solutions and the indicator D in (3.4.46a) is greater zero, the solution for the first part of Eq.(3.4.51) can be obtained using case number $\{236.00\}$ in [22]

$$\int_0^{\left|\overset{[2]}{\mathbb{H}}u_{\min_{f_1}}\right| = \xi_1} \frac{\mathrm{d}u}{\sqrt{(\xi_1 - u)(u - \xi_2)(u - \xi_3)}} = \eta_{\mathrm{E},(A)}\,\mathcal{F}\left(\psi_{(A)}, \kappa_{(A)}\right) \tag{3.4.53a}$$

with $\mathcal{F}(\psi,\kappa)$ being the *incomplete elliptic integral of the first kind*, see appendix B.2, and the constants for case (A)

$$\eta_{\mathrm{E},(A)} = \frac{2}{\sqrt{\xi_1-\xi_3}}, \qquad \psi_{(A)} = \arcsin\left(\sqrt{\frac{\xi_1}{\xi_1-\xi_2}}\right), \qquad \kappa_{(A)} = \sqrt{\frac{\xi_1-\xi_2}{\xi_1-\xi_3}}, \tag{3.4.53b}$$

whereas for (B) solution case $\{243.00\}$ [22] applies, leading to

$$\int_0^{\left|{}^{[2]}_{\mathrm{H}}u_{\min_{f_1}}\right|=\xi_1} \frac{\mathrm{d}u}{\sqrt{(\xi_1-u)\left[(u-\xi_a)^2+\xi_b^2\right]}} = \eta_{\mathrm{E},(B)}\,\mathcal{F}\left(\psi_{(B)},\kappa_{(B)}\right) \tag{3.4.54a}$$

with

$$\xi_a = \frac{\xi_2+\xi_3}{2} \qquad \text{and} \qquad \xi_b^2 = -\frac{(\xi_2-\xi_3)^2}{4}. \tag{3.4.54b}$$

and appropriate constants defined as [22]

$$\eta_{\mathrm{E},(B)} = \frac{1}{\sqrt{A_{(B)}}}, \qquad A_{(B)}^2 = (\xi_a-\xi_1)^2+\xi_b^2,$$
$$\psi_{(B)} = \arccos\left(\frac{A_{(B)}-\xi_1}{A_{(B)}+\xi_1}\right), \qquad \kappa_{(B)}^2 = \frac{A_{(B)}-\xi_a+\xi_1}{2A_{(B)}}. \tag{3.4.54c}$$

Substituting ξ_i with χ_i in (3.4.53) and (3.4.54) leads to the solution for the second integral term in Eq.(3.4.51). Finally, the oscillation period (3.4.51) can be written as

$${}^{(-/+)}_{[2]}T_{f_1} = \frac{\sqrt{6}}{\omega_n}\left\{\eta_{\mathrm{E},\xi}\,\mathcal{F}\left(\psi_\xi,\kappa_\xi\right)+\eta_{\mathrm{E},\chi}\,\mathcal{F}\left(\psi_\chi,\kappa_\chi\right)\right\} \tag{3.4.55}$$

where the indexes ξ and χ refer to the first and second integral in (3.4.51) and can be solved using Eq.(3.4.53) and (3.4.54) as given above.

Assuming case (III) from page 54, the system of two equations in (3.4.44) has no feasible solution when equating (1) and three real solutions, two positive and one negative, respectively, when solving equation (2), namely

$$\chi_1 > \chi_2 > \chi_3, \qquad \chi_3 < 0, \qquad \chi_1+\chi_2+\chi_3 = 0.$$

Hence, for determining the oscillation frequency ${}^{(+)}_{[2]}T_{f_1}$ due to purely positive displacement equation (3.4.31) is required. Using (3.4.50c) together with (3.4.50e) this can be written in its canonical form

$${}^{(+)}_{[2]}T_{f_1} = \frac{\sqrt{6}}{\omega_n}\int_{{}^{[2]}_{\mathrm{H}}u_{\min_{f_1}}}^{{}^{[2]}_{\mathrm{H}}u_{\max_{f_1}}} \frac{\mathrm{d}u}{\sqrt{(\chi_1-u)(u-\chi_2)(u-\chi_3)}}, \tag{3.4.56a}$$

with the integration limits

$${}^{[2]}_{\mathrm{H}}u_{\min_{f_1}} = \chi_2 \qquad \text{and} \qquad {}^{[2]}_{\mathrm{H}}u_{\max_{f_1}} = \chi_1.$$

Referring to case $\{236.00\}$ in [22], Eq.(3.4.56a) equates to

$$ {}^{(+)}_{[2]}_{\mathbb{H}}T_{f_1} = \frac{\sqrt{6}}{\omega_n}\eta_{\mathsf{E}}\,\mathcal{F}(\psi,\kappa) \tag{3.4.56b} $$

with

$$ \eta_{\mathsf{E}} = \frac{2}{\sqrt{\chi_1-\chi_3}}, \qquad \psi = \arcsin\left(\sqrt{\frac{\chi_1-\chi_2}{\chi_1-\chi_2}}\right), \qquad \kappa = \sqrt{\frac{\chi_1-\chi_2}{\chi_1-\chi_3}}. \tag{3.4.56c} $$

It is easy to see, ψ reduces to $\arcsin(\pm 1)$ and hence, to odd integer multiples of $\frac{\pi}{2}$. With the identity [22]

$$ \mathcal{F}(n\pi\pm\theta,\kappa) = 2n\,\mathcal{K}(\kappa) \pm \mathcal{F}(\theta,\kappa) \tag{3.4.56d} $$

Eq.(3.4.56b) can be simplified to

$$ {}^{(+)}_{[2]}_{\mathbb{H}}T_{f_1} = (2j-1)\,\frac{\sqrt{6}}{\omega_n}\eta_{\mathsf{E}}\,\mathcal{K}(\kappa) \qquad \text{with} \quad j=1,2,3,\ldots \tag{3.4.56e} $$

and $\mathcal{K}(\kappa)$ as the *complete elliptic integral of the first kind*, cf. appendix B.2.

(iii) $\mathbf{b=3}$: In the case of a cubic power in the displacement in the restoring force of the autonomous conservative system Eq.(3.4.27) can be rewritten as

$$ (1) \qquad {}^{[3]^{(-)}4}_{\mathbb{H}}u_{\mathsf{Ex}_{f_1}} + \frac{4p_0}{k}\,{}^{[3]^{(-)}}_{\mathbb{H}}u_{\mathsf{Ex}_{f_1}} - {}^{[3]}_{\mathbb{H}}\alpha_{f_1} = 0, \qquad {}^{[3]^{(-)}}_{\mathbb{H}}u_{\mathsf{Ex}_{f_1}} = -\,{}^{[3]}_{\mathbb{H}}u_{\mathsf{Ex}_{f_1}}, \quad {}^{[3]^{(-)}}_{\mathbb{H}}u_{\mathsf{Ex}_{f_1}} \geq 0 \tag{3.4.57a} $$

$$ (2) \qquad {}^{[3]}_{\mathbb{H}}u^4_{\mathsf{Ex}_{f_1}} - \frac{4p_0}{k}\,{}^{[3]}_{\mathbb{H}}u_{\mathsf{Ex}_{f_1}} - {}^{[3]}_{\mathbb{H}}\alpha_{f_1} = 0, \qquad {}^{[3]}_{\mathbb{H}}u_{\mathsf{Ex}_{f_1}} \geq 0 \tag{3.4.57b} $$

with a constant consisting of all initial conditions

$$ {}^{[3]}_{\mathbb{H}}\alpha_{f_1} = |u_0|^4 - \operatorname{sign}(u_0)\,\frac{4p_0}{k}\,|u_0| + \frac{2\dot{u}_0^2}{\omega_n^2} \tag{3.4.58} $$

and an index [3] referring to the special case of $b=3$. Again, for $p_0<0$ case (1) and (2) can be interchanged since both of them possess the same condition $u_{\mathsf{Ex}}>0$. Finding the solution of (3.4.57) is not as straightforward as shown in the preceding section (ii) with $b=2$. Making use of the formulations given in appendix B.4 analytical results can be obtained in a non-iterative way.

With $p_0>0$ the oscillation period for the case ${}^{[3]}_{\mathbb{H}}u_{\min_{f_1}}<0$, ${}^{[3]}_{\mathbb{H}}u_{\max_{f_1}}>0$ is derived from Eq.(3.4.30b)

$$ {}^{(-/+)}_{[3]}_{\mathbb{H}}T_{f_1} = \frac{\sqrt{8}}{\omega_n}\left\{ \int_0^{\left|{}^{[3]}_{\mathbb{H}}u_{\min_{f_1}}\right|} \frac{\mathrm{d}u}{\sqrt{-u^4-\frac{4p_0}{k}u+{}^{[3]}_{\mathbb{H}}\alpha_{f_1}}} + \int_0^{{}^{[3]}_{\mathbb{H}}u_{\max_{f_1}}} \frac{\mathrm{d}u}{\sqrt{-u^4+\frac{4p_0}{k}u+{}^{[3]}_{\mathbb{H}}\alpha_{f_1}}} \right\}. \tag{3.4.59} $$

Both terms under the square roots are rewritten in their canonical form as

$$ -u^4 - \frac{4p_0}{k}u + {}^{[3]}_{\mathbb{H}}\alpha_{f_1} = (\xi_1-u)(u-\xi_2)(u-\xi_3)(u-\xi_4) \tag{3.4.60a} $$

and

$$-u^4+\frac{4p_0}{k}u+{}^{[3]}_{\mathbb{H}}\alpha_{f_1}=(\chi_1-u)(u-\chi_2)(u-\chi_3)(u-\chi_4) \tag{3.4.60b}$$

where

$$\xi_i={}^{[3]}_{\mathbb{H}}u_{\mathrm{Ex}_{f_1},i}^{(\text{-})} \quad \text{and} \quad \chi_i={}^{[3]}_{\mathbb{H}}u_{\mathrm{Ex}_{f_1},i}, \qquad (i=1,2,3) \tag{3.4.60c}$$

are the solutions of the fourth-order polynomials Eq.(3.4.57a) and (3.4.57b), respectively. Again, two different cases for the system (3.4.60) have to be analysed, namely

$$\text{(A)} \qquad y_1>0>y_2>y_3>y_4; \qquad y_1,y_2,y_3,y_4\in\mathbb{R} \tag{3.4.61a}$$

$$\text{(B)} \qquad y_1>0>y_2,y_3=y_4^*; \qquad y_1,y_2\in\mathbb{R};\ y_3,y_4\in\mathbb{C} \tag{3.4.61b}$$

with

$$y_i=\xi_i \quad \text{or} \quad y_i=\chi_i, \qquad (i=1,2,3).$$

Supposing Eq.(3.4.57a) has four real zeros as indicated in case (A). Then the first term in curly brackets in Eq.(3.4.59) can be solved using $\{257.00\}$ in [22]

$$\int_0^{\left|{}^{[3]}_{\mathbb{H}}u_{\min_{f_1}}\right|}\frac{\mathrm{d}u}{\sqrt{(\xi_1-u)(u-\xi_2)(u-\xi_3)(u-\xi_4)}}=\eta_{\mathrm{E},(A)}\,\mathcal{F}\left(\psi_{(A)},\kappa_{(A)}\right) \tag{3.4.62a}$$

provided $\xi_1={}^{[3]}_{\mathbb{H}}u_{\min_{f_1}}$ which is always the case since ${}^{[3]}_{\mathbb{H}}u_{\min_{f_1}}$ is a solution of Eq.(3.4.57a). The constants for (3.4.62a) are then given as

$$\eta_{\mathrm{E},(A)}=\frac{2}{\sqrt{(\xi_1-\xi_3)(\xi_2-\xi_4)}}, \qquad \psi_{(A)}=\arcsin\left(\sqrt{\frac{(\xi_2-\xi_4)\xi_1}{(\xi_1-\xi_2)(-\xi_4)}}\right), \tag{3.4.62b}$$

and

$$\kappa_{(A)}=\sqrt{\frac{(\xi_1-\xi_2)(\xi_3-\xi_4)}{(\xi_1-\xi_3)(\xi_2-\xi_4)}}. \tag{3.4.62c}$$

If Eq.(3.4.57a) has four solutions according to (B) above, i.e. two real and two conjugate complex zeros, case number $\{259.00\}$ [22] must be rewritten as

$$\begin{aligned}\int_0^{\left|{}^{[3]}_{\mathbb{H}}u_{\min_{f_1}}\right|}\frac{\mathrm{d}u}{\sqrt{\cdots}} &= \int_0^{\xi_1}\frac{\mathrm{d}u}{\sqrt{\cdots}} = \int_{\xi_2}^{\xi_1}\frac{\mathrm{d}u}{\sqrt{\cdots}}-\int_{\xi_2}^{0}\frac{\mathrm{d}u}{\sqrt{\cdots}}\\ &=\left[\eta_{\mathrm{E},(B)}\,\mathcal{F}\left(\psi_{(B)},\kappa_{(B)}\right)\right]_{\xi_2}^{\xi_1}-\left[\eta_{\mathrm{E},(B)}\,\mathcal{F}\left(\psi_{(B)},\kappa_{(B)}\right)\right]_{\xi_2}^{0}\end{aligned} \tag{3.4.63}$$

since [22] does not contain an explicitly solution for the integration interval $[0;\xi_1]$. The expression under the square roots in (3.4.63) is identical to Eq.(3.4.62a) but can be expressed as

$$\sqrt{(\xi_1-u)(u-\xi_2)\left[(u-\xi_a)^2+\xi_b^2\right]} \tag{3.4.64a}$$

with

$$\xi_a = \frac{\xi_3 + \xi_4}{2} \qquad \text{and} \qquad \xi_b^2 = -\frac{(\xi_3 - \xi_4)^2}{4}. \tag{3.4.64b}$$

Denoting the upper limit of integration in (3.4.63) as ε the solution is given by the following expressions

$$\eta_{\mathrm{E},(B)} = \frac{1}{\sqrt{A \times B}}, \qquad A_{(B)}^2 = (\xi_a - \xi_1)^2 + \xi_b^2, \qquad B_{(B)}^2 = (\xi_b - \xi_a)^2 + \xi_b^2,$$

$$\psi_{(B)} = \arccos\left(\frac{(\xi_1 - \varepsilon)B_{(B)} - (\varepsilon - \xi_2)A_{(B)}}{(\xi_1 - \varepsilon)B_{(B)} + (\varepsilon - \xi_2)A_{(B)}}\right), \qquad \kappa_{(B)} = \sqrt{\frac{(\xi_1 - \xi_2)^2 - \left(A_{(B)} - B_{(B)}\right)^2}{4A_{(B)}B_{(B)}}}. \tag{3.4.65}$$

with ε being either ξ_1 or 0. Substituting ξ_i with χ_i in Eq.(3.4.62) to (3.4.65) gives the solution for the second integral term in Eq.(3.4.59). Finally, the oscillation period can be written as

$$\overset{(-/+)}{\underset{\mathbb{H}}{[3]}}T_{f_1} = \frac{\sqrt{8}}{\omega_n}\left\{\eta_{\mathrm{E},\xi}\,\mathcal{F}\left(\psi_\xi, \kappa_\xi\right) + \eta_{\mathrm{E},\chi}\,\mathcal{F}\left(\psi_\chi, \kappa_\chi\right)\right\} \tag{3.4.66}$$

where the indexes ξ and χ refer to the first and second integral term in equation (3.4.59) respectively.

A closer examination of (3.4.57) reveals both equations are identical to Eq.(3.4.28) on page 53 for the special case of $b = 3$. Hence, (3.4.59) can be rewritten as a single integral expression

$$\overset{(-/+)}{\underset{\mathbb{H}}{[3]}}T_{f_1} = \frac{\sqrt{8}}{\omega_n}\int_{\overset{[3]}{\mathbb{H}}u_{\min_{f_1}}=\xi_2}^{\overset{[3]}{\mathbb{H}}u_{\max_{f_1}}=\xi_1} \frac{\mathrm{d}u}{\sqrt{(\xi_1 - u)(u - \xi_2)(u - \xi_3)(u - \xi_4)}} \tag{3.4.67}$$

with $u(t)$ bounded between $[-\infty;\infty]$ and either entirely negative, positive or a combination of both. Thus, given case (A) from above, i.e. four real solutions,

$$\xi_1 > \xi_2 > \xi_3 > \xi_4, \qquad \xi_1 + \xi_2 + \xi_3 + \xi_4 = 0,$$

equation (3.4.67) can be solved using either case $\{256.00\}$ or $\{257.00\}$ in [22] leading to

$$\overset{(-/+)}{\underset{\mathbb{H}}{[3]}}T_{f_1} = \frac{\sqrt{8}}{\omega_n}\eta_{\mathrm{E},(A)}\,\mathcal{F}\left(\psi_{(A)}, \kappa_{(A)}\right) \tag{3.4.68a}$$

but now with the constants

$$\eta_{\mathrm{E},(A)} = \frac{2}{\sqrt{(\xi_1 - \xi_3)(\xi_2 - \xi_4)}}, \qquad \kappa_{(A)} = \sqrt{\frac{(\xi_1 - \xi_2)(\xi_3 - \xi_4)}{(\xi_1 - \xi_3)(\xi_2 - \xi_4)}}, \tag{3.4.68b}$$

and

$$\psi_{(A)} = \arcsin\left(\sqrt{\frac{(\xi_1 - \xi_3)(\xi_1 - \xi_2)}{(\xi_1 - \xi_2)(\xi_1 - \xi_3)}}\right) = \arcsin(\pm 1) \tag{3.4.68c}$$

simplifying (3.4.68a) in the same manner as (3.4.56d)

$$\overset{(-/+)}{\underset{\mathbb{H}}{[3]}}T_{f_1} = (2j-1)\,\frac{\sqrt{8}}{\omega_n}\eta_{\mathrm{E},(A)}\,\mathcal{K}\left(\kappa_{(A)}\right) \qquad \text{with} \quad j = 1,2,3,\ldots. \tag{3.4.69}$$

With two real and two complex solutions, equation (b) in (3.4.61), the square root in (3.4.67) is rewritten in the same manner as (3.4.64a) and therefore (3.4.67) equates to the same constants as given in Eq.(3.4.65) except

$$\psi_{(B)} = \arccos(-1) \tag{3.4.70}$$

rendering the solution of (3.4.67) to

$$\overset{(-/+)}{\underset{\mathbb{H}}{[3]}}T_{f_1} = (2j-1)\,\frac{\sqrt{32}}{\omega_n}\,\eta_{\mathsf{E},(B)}\,\mathfrak{K}\left(\kappa_{(B)}\right) \qquad \text{with} \quad j = 1,2,3,\ldots . \tag{3.4.71}$$

A third case where (3.4.67) has only complex solutions

$$\text{(C)} \qquad y_1 = y_2^{\,*}; y_3 = y_4^{\,*}; \qquad y_1, y_2, y_3, y_4 \in \mathbb{C}$$

as listed in [22] is irrelevant for the determination of $\overset{(-/+)}{\underset{\mathbb{H}}{[3]}}T_{f_1}$ since the associated equation in (3.4.57) would have no valid solution if all roots are complex and can therefore be discarded.

It should be noted that the second way of deriving the oscillation period from *one* integral expression (3.4.67) covering the entire domain of possible solutions for the extreme displacement $u(t)$ is only valid in the special case of odd integer values of b. The calculation for obtaining T simplify considerably. However, for implementing the above derived method into machine executable code the first way with (3.4.59) might be the preferred one since the algorithm does not vary with the value of b, i.e. the method is also applicable for cases $b \neq 3$ as demonstrated in the previous section where $b = 2$.

Results - Step Excitation

Zero initial conditions. The maximum dynamic **displacement** of a step function excited SDOF system with zero initial conditions, Eq.(3.4.39), normalised to the static displacement of the linear oscillator

$$u_{\mathsf{stat,lin}} = \frac{p_0}{k} = \frac{p_0}{m\,(2\pi f_n)^2},$$

is plotted in Fig. 3.4.6 on page 98. As shown in appendix A.2.2 for the linear SDOF, $b = 1$ in (3.4.39), the ratio $u_{\mathsf{dyn}}/u_{\mathsf{stat,lin}}$ is exactly 2.0 regardless of natural frequency f_n and load amplitude p_0. Contrary, as the restoring force $f_1(u)$ of the system becomes nonlinear, this ratio changes with both natural frequency and load level. For $b = 2$ the dynamic displacement at a load amplitude of $p_0 = 10.0\,\mathsf{N}$ and a natural frequency of $f_n = 10\,\mathsf{Hz}$ (system stiffness factor $k = 3.9478 \times 10^3\,\mathsf{N/m^2}$ if $m = 1\,\mathsf{kg}$), for example, exceeds the linear static displacement by a factor of 35. If $b = 3$ and $b = 4$ this factor takes the values 85 and 125, respectively. However, only for the solid line in Fig. 3.4.6 (a)-(d) representing the step force amplitude of $p_0 = 10.0\,\mathsf{N}$ the normalised displacement constantly exceeds the factor of 2 in the range $1 \leq f_n \leq 100\,\mathsf{Hz}$. For higher load levels, e.g. $p_0 = 100.0\,\mathsf{N}$ to $1000.0\,\mathsf{N}$, the ratio $u_{\mathsf{dyn}}/u_{\mathsf{stat,lin}}$ can be significantly smaller than 2 at low to moderate natural frequencies $f_n < 20\,\mathsf{Hz}$, i.e. the absolute dynamic displacement of the nonlinear system is less than the dynamic displacement of linear SDOF in figure (a). Nevertheless, with increasing order of nonlinearity the system's dynamic displacement increases significantly compared to the linear case up to several orders of magnitude even for relatively small load amplitudes, see Fig. 3.4.6 (d).

The ratio of **nonlinear oscillation frequency** f_{NL} and SDOF natural frequency f_n as a function the system's restoring force $f_1(u)$ and the magnitude of the applied step load function p_0, as given in Eq.(3.4.42), is shown in Fig. 3.4.7. As expected for the linear case $b = 1$ in (a) this ratio must be a constant. For $b \neq 1$ and load levels greater than 10 N the nonlinear frequency is higher for low natural frequencies and significantly lower at moderate to large f_n. An interesting point to note is the fact that no matter what value b possesses each line crosses the $f_{\mathrm{NL}}/f_n = 1.0$ amplitude at around the same frequency in all figures (b) to (d). In general, for higher values of b and constant load amplitude the oscillation frequency f_{NL} of the step response decreases with increasing natural frequency f_n of the system, i.e. increasing stiffness k or decreasing mass m, which is consistent with the results found by BAPAT and SRINIVASAN [7] for the special case of zero initial conditions. Furthermore, for constant values of b the effective oscillation frequency increases with increasing forcing magnitude.

3.4.1.3 Impulse Response

Substitution of the nonlinear restoring force $f_1(u)$ from Eq.(3.4.1) into (3.3.14) gives

$$k \int_u \operatorname{sign}(u)\,|u|^b\,du\Big|_{u={}_{\delta}u_{\mathrm{Ex}_{f_1}}} = k \int_u \operatorname{sign}(u)\,|u|^b\,du\Big|_{u=u_0} + \frac{m}{2}\left(\frac{p_0}{m} + \dot{u}_0\right). \tag{3.4.72}$$

Taking Eq.(3.4.2) into account leads to four nonlinear algebraic equations similar to (3.4.24) on page 52. Again, this can be reduced to two cases, see Eq.(3.4.27a) and (3.4.27b), giving

(1) $\boxed{{}_{\delta}u_{\mathrm{Ex}_{f_1}} \leq 0 \rightarrow {}_{\delta}\overset{(\cdot)}{u}_{\mathrm{Ex}_{f_1}} \geq 0}$

$$ {}_{\delta}\overset{(\cdot)}{u}{}^{(b+1)}_{\mathrm{Ex}_{f_1}} - {}_{\delta}\alpha_{f_1} = 0 \tag{3.4.73a}$$

(2) $\boxed{{}_{\delta}u_{\mathrm{Ex}_{f_1}} > 0}$

$$ {}_{\delta}u^{(b+1)}_{\mathrm{Ex}_{f_1}} - {}_{\delta}\alpha_{f_1} = 0. \tag{3.4.73b}$$

with the term ${}_{\delta}\alpha_{f_1}$ containing both initial conditions and applied force

$${}_{\delta}\alpha_{f_1} = |u_0|^{(b+1)} + \frac{(b+1)}{2\omega_n^2}\left(\frac{p_0}{m} + \dot{u}_0\right)^2. \tag{3.4.74}$$

Further simplification of Eq.(3.4.73) leads to a single equation for determination of the minimum and maximum displacement due to impulse excitation

$${}_{\delta}u_{\mathrm{Ex}_{f_1}} = {}_{\delta}u_{\mathrm{min/max}_{f_1}} = \mp \sqrt[(b+1)]{{}_{\delta}\alpha_{f_1}} = \mp \left[|u_0|^{(b+1)} + \frac{(b+1)}{2\omega_n^2}\left(\frac{p_0}{m} + \dot{u}_0\right)^2\right]^{\frac{1}{(b+1)}} \tag{3.4.75}$$

for all initial conditions and applied forces bounded within

$$-\infty < u_0,\ \dot{u}_0,\ p_0 < \infty \qquad u_0,\ \dot{u}_0,\ p_0 \in \mathbb{R}.$$

An expression for the extreme values of velocity can be derived from Eq.(3.3.15d) on page 43

$$\dot{u}_{\mathrm{Ex}} = \sqrt{\frac{2}{m}}\left(\frac{k}{(b+1)}\,|u_0|^{(b+1)} + \frac{m}{2}\left(\frac{p_0}{m} + \dot{u}_0\right)^2\right)^{\frac{1}{2}} \tag{3.4.76a}$$

which simplifies together with Eq.(3.4.74) to

$$\dot{u}_{\mathrm{Ex}} = \omega_n \sqrt{\frac{2\,{}_\delta\alpha_{f_1}}{(b+1)}}\,. \tag{3.4.76b}$$

Minimum and maximum values of (3.4.76b) are given by (3.3.4h) on page 41.

The oscillation period is obtained from Eq.(3.3.17) and equates with the substitution (3.4.5) in exact the same manner as (3.4.9c) to

$${}_\delta T_{f_1} = 2\frac{\sqrt{2(b+1)}}{\omega_n} \int_0^{{}_\delta u_{\max f_1}} \frac{\mathrm{d}u}{\sqrt{-u^{(b+1)} + {}_\delta\alpha_{f_1}}}, \qquad {}_\delta u_{\max f_1} > 0 \tag{3.4.77a}$$

with the solution

$${}_\delta T_{f_1} = 2\frac{\sqrt{2(b+1)}}{\omega_n} \left[\frac{u\sqrt{1-\frac{u^{(b+1)}}{{}_\delta\alpha_{f_1}}}}{\sqrt{{}_\delta\alpha_{f_1} - u^{(b+1)}}}\, {}_2\mathcal{F}_1\left(\frac{1}{1+b}, \frac{1}{2}; 1+\frac{1}{1+b}; \frac{u^{(b+1)}}{{}_\delta\alpha_{f_1}}\right)\right]_0^{{}_\delta u_{\max f_1}} \tag{3.4.77b}$$

evaluated within the limits $\left[0, {}_\delta u_{\max f_1}\right]$, thus obtaining an algebraic expression similar to Eq.(3.4.11e)

$${}_\delta T_{f_1} = 2\frac{{}_\delta u_{\max f_1}}{\omega_n} \sqrt{\frac{2(b+1)}{{}_\delta\alpha_{f_1}}}\, {}_2\mathcal{F}_1\left(\frac{1}{2}, \frac{1}{1+b}; 1+\frac{1}{1+b}; \frac{{}_\delta u_{\max f_1}^{(b+1)}}{{}_\delta\alpha_{f_1}}\right), \qquad {}_\delta u_{\max f_1} > 0. \tag{3.4.77c}$$

A comparison of Eq.(3.4.74) and (3.4.75) equates the ratio ${}_\delta u_{\mathrm{Ex}f_1}^{(b+1)} \big/ {}_\delta\alpha_{f_1}$ to 1, which in turn leads for Eq.(3.4.77c) to

$${}_\delta T_{f_1} = 2\frac{{}_\delta u_{\max f_1}}{\omega_n} \sqrt{\frac{2\pi(b+1)}{{}_\delta\alpha_{f_1}}}\, \frac{\Gamma\left(1+\frac{1}{1+b}\right)}{\Gamma\left(\frac{1}{2}+\frac{1}{1+b}\right)} \tag{3.4.78}$$

as shown in subsection 3.4.1.1 on page 48. With ${}_\delta u_{\max f_1}$ and ${}_\delta\alpha_{f_1}$ given by Eq.(3.4.75) and (3.4.74), respectively, $\Gamma(\ldots)$ as the Euler gamma function, cf. appendix B.1, and the natural frequency of the reference system defined by $\omega_n = \sqrt{\frac{k}{m}}$. Equation (3.4.78) is a function of the system's properties, e.g. stiffness k, mass m, nonlinear order b, the initial conditions u_0, $\dot{u}_0$, and the magnitude of the applied Dirac-impulse p_0

$${}_\delta T_{f_1} = {}_\delta T_{f_1}(\omega_n, b, u_0, \dot{u}_0, p_0)\,. \tag{3.4.79}$$

In order to derive the nonlinear SDOF's multiple oscillation frequencies, an identical approach to the one outlined in section 3.4.1.1 of this chapter can be employed using Jacobian elliptic functions rather than hyperbolic one. A direct comparison between the free vibration and impulse excitation of the SDOF oscillator sees all methods and parameters unchanged except ${}_0\alpha_{f_1} \neq {}_\delta\alpha_{f_1}$, see (3.4.10) and (3.4.74).

The linear case of (3.4.78) is obtained by $b = 1$ and gives together with

$${}_\delta u_{\mathrm{Ex}f_1,\mathrm{lin}} = \sqrt{|u_0|^2 + \frac{1}{\omega_n^2}\left(\frac{p_0}{m} + \dot{u}_0\right)^2} \tag{3.4.80a}$$

and Eq.(B.1.8)

$${}_\delta T_{f_1,\mathrm{lin}} = \frac{1}{f_n} \tag{3.4.80b}$$

the well-known result for the linear SDOF.

Results - Impulse Excitation

The maximum **displacement** of an impulse excited SDOF oscillator with zero initial conditions as a function of the system's natural linear frequency[10] f_n is shown in Fig. 3.4.8 on page 100 for different load levels p_0. For comparison of linear and nonlinear systems as well as with results obtained in the previous sections, the extreme values of displacement are normalised to the static deformation of the linear system, i.e. ${}_\delta u_{\max} = u_{\text{dyn}}/u_{\text{stat,lin}}$. As expected, the linear case in 3.4.8(a) exhibits no dependency on the impulse load magnitude p_0, all four lines coincide. The opposite is true for the nonlinear oscillator with $b \neq 1$. For moderate to high frequencies $f_n \geq 10\,\text{Hz}$ and small load magnitudes ($p_0 = 10$) the normalised displacement increases with increasing values of b, i.e. with increasing order of nonlinearity. For low and very low frequencies $f_n \ll 10\,\text{Hz}$ and $p_0 = 10$ it stays constant. In contrast, for high to very high load levels[11] the opposite is correct - with both increasing p_0 and b the scaled dynamic response $u_{\text{dyn}}/u_{\text{stat,lin}}$ takes significantly smaller values than in the linear case, especially for low natural frequencies $f_n < 20\,\text{Hz}$. Since the static displacement function $u_{\text{stat,lin}}$ is a constant for a specific frequency f_n in all four subfigures (a)-(d) in 3.4.8, decreasing normalised displacement implies decreasing absolute dynamic displacement u_{dyn}.

For the same initial conditions ($u_0 = \dot{u}_0 = v_0 = 0.0$) and load levels p_0 of the impulse function, Fig. 3.4.9 shows the normalised **nonlinear oscillation frequency** f_{NL}/f_n as a function of the linear system's reference natural frequency $f_n = \frac{1}{2\pi}\sqrt{\frac{k}{m}}$, i.e. the ratio of stiffness to mass. Clearly, for the linear case $b = 1$ in picture (a) f_{NL} is identical to f_n and the ratio f_{NL}/f_n must therefore be equal to one.

As b increases the lines representing different load amplitudes start to separate. Although the graphs seem to be equally spaced on the log-scale in Fig. 3.4.9, they differ by factors of several orders of magnitude. For very low frequencies $f_n \leq 5\,\text{Hz}$ and $p_0 = 10.0$ the solid line in all four figures (a) to (d) remains nearly constant whereas the graphs for all other load levels shift rapidly towards higher ratios of f_{NL}/f_n, i.e. higher effective nonlinear oscillation frequency f_{NL}. However, for the upper end of the natural frequency scale, $f_n \geq 60\,\text{Hz}$ the opposite is true. The dotted and the dashed lines for $p_0 = 1000\,\text{N}$ and $p_0 = 500\,\text{N}$, respectively, stay virtually unchanged whereas for $p_0 = 10\,\text{N}$ the line decreases significantly with increasing b.

A comparison with Fig. 3.4.7, the step excited system with $u_0 = \dot{u}_0 = v_0 = 0$, shows very similar response behaviour of the SDOF for both types of applied force at relatively low natural frequencies $f_n \leq 5\,\text{Hz}$. Although the line spacing for different magnitudes p_0 is similar in both figures for increasing b, the nonlinear frequencies of the step excited system are about ten times smaller than for the impulse driven SDOF, especially for small values of p_0.

In Fig. 3.4.10 on page 102 the ratio f_{NL}/f_n is given as a function of two independent variables, namely f_n and p_0 for different values of b in three-dimensional plots with linear scale. In figure (a), the linear case, again the oscillation frequency is clearly independent of the magnitude of the applied load. In case of the nonlinear SDOF, figures (b) to (d), the ratio f_{NL}/f_n varies notably with varying natural frequency at low values for f_n, especially in the range $1 \leq f_n < 25\,\text{Hz}$. Furthermore, it is in this region

[10] Since f_n does not exist for nonlinear systems it should merely be regarded as a virtual independent variable. In fact, varying f_n and keeping the mass $m = \text{const.}$ leaves the stiffness coefficient k as independent variable due to $k = m(2\pi f_n)^2$. Hence, the diagrams could also have been drawn with k on their x-axis.

[11] With respect to the cases investigated in this work.

of f_n where a change of the load magnitude of the impulse p_0 has the most influence upon f_{NL}/f_n, which reaches its peak amplitudes for the values $f_n = 1\,\text{Hz}$ and $p_0 = 1000\,\text{N}$, i.e. 5.3, 12.8 and 22.4 for $b = 2$, $b = 3$ and $b = 4$, respectively.

Setting in Eq.(3.4.75) the initial velocity $\dot{u}_0 = v_0$ and the load amplitude of the impulse p_0 as specific constant values leaves the maximum nonlinear **displacement** of the SDOF system as a function of f_n, b and the initial displacement u_0 as pictured in Fig. 3.4.11 for $v_0 = 2.5\,\text{m/s}$, $p_0 = 100\,\text{N}$ and various discrete values of u_0 and b. For small values of f_n the initial displacement u_0 is insignificant for the maximum dynamic response of the oscillator, but *not* independent of the order of nonlinearity b of the nonlinear restoring force. If the range of f_n increases beyond a threshold of 10 Hz the influence of u_0 becomes greater but decreases with increasing b. Moreover, for moderate to high natural frequencies and initial displacement $u_0 \geq 1.0\,\text{m}$ the ratio $u_{dyn}/u_{stat,lin}$ stays nearly constant regardless of the values of exponent b.

The normalised nonlinear **oscillation frequency** f_{NL}/f_n in Fig. 3.4.12 shows a different behaviour than the normalised displacement. For small values of f_n, i.e $f_n \leq 10\,\text{Hz}$, the frequency f_{NL} for the nonlinear systems is significantly higher than for their linear complement having f_n. However, for increasing stiffness $k = m(2\pi f_n)^2$ the ratio f_{NL}/f_n decreases rapidly depending mainly on the initial conditions u_0 of the system and its order of nonlinearity expressed by different values of b.

Graphs in Fig. 3.4.13 and 3.4.14 on pages 105 and 106 show ratios of maximum displacement $u_{dyn}/u_{stat,lin}$ and oscillation frequency f_{NL}/f_n for two different values of initial displacement, namely $u_0 = 0.1\,\text{m}$ and $u_0 = 0.5\,\text{m}$, and different values of v_0. The applied impulse magnitude is $p_0 = 10\,\text{N}$. In the linear case in Fig. 3.4.13(a) the initial velocity v_0 has the most significant influence on the SDOF system's response. In contrast, Fig. 3.4.14(d) suggests the effect of different values for v_0 on the nonlinear oscillation frequency f_{NL} is greater for higher values of b.

3.4.2 The Nonlinear Restoring Force $f_2(u) = k_\alpha u + k_\beta u^3$

The second nonlinear restoring force $f_2(u)$ used in this report occurs in Duffing-type oscillators, see [3] and [19] for example, and is given by

$$f_2(u) = k_\alpha u + k_\beta u^3\,, \qquad k_\alpha, k_\beta, u \in \mathbb{R}. \tag{3.4.81}$$

A plot of the characteristic of $f_2(u)$ as a function of the ratio of the force-displacement constants k_β/k_α is shown in Fig. 3.4.15. Integration of (3.4.81) with respect to $u(t)$ is straight forward and yields

$$\int_u f_2(u)\,du = \frac{1}{2}k_\alpha u^2 + \frac{1}{4}k_\beta u^4. \tag{3.4.82}$$

3.4.2.1 Free Vibration

The extreme values of displacement of a freely vibrating SDOF having $f_2(u)$ as internal nonlinear restoring force are obtained using Eq.(3.3.3a) and leaving out the terms involving p_0

$${}_0u^4_{Ex_{f_2}} + 2\frac{k_\alpha}{k_\beta}\,{}_0u^2_{Ex_{f_2}} = u_0^4 + 2\frac{k_\alpha}{k_\beta}u_0^2 + \frac{m}{2k_\beta}\dot{u}_0^2 \tag{3.4.83a}$$

which can be rewritten as

$$y^2 + \frac{2}{k_\gamma} y - {}_0\alpha_{f_2} = 0 \qquad \text{where} \qquad y = {}_0u^2_{\mathsf{Ex}_{f_2}}, \tag{3.4.83b}$$

a constant expressing the nonlinear-linear stiffness coefficient ratio

$$k_\gamma = \frac{k_\beta}{k_\alpha} \tag{3.4.83c}$$

and a term consisting of all initial conditions

$${}_0\alpha_{f_2} = u_0^4 + \frac{2}{k_\gamma} u_0^2 + \frac{2\dot{u}_0^2}{\omega_{n,\beta}^2} \tag{3.4.83d}$$

with

$$\omega_{n,\beta}^2 = \frac{k_\beta}{m} \tag{3.4.83e}$$

similar to the definition in Eq.(3.4.7). Equation (3.4.83b) has two real solutions

$$y_{1/2} = -\frac{1}{k_\gamma} \pm \sqrt{\left(\frac{1}{k_\gamma}\right)^2 + {}_0\alpha_{f_2}} \tag{3.4.83f}$$

which are clearly separated

$$0 \le y_1 < \infty \qquad \text{and} \qquad -\infty < y_2 < 0$$

and bounded within $\mathbb{R}\,[-\infty;\infty]$ since

$${}_0\alpha_{f_2} \ge 0 \qquad \text{and} \qquad k_\gamma > 0$$

for all initial conditions u_0, $\dot{u}_0$. This leaves exact two solutions for Eq.(3.4.83a)

$$\begin{aligned} {}_0u_{\mathsf{Ex}_{f_2}} = \pm\sqrt{y_1} = u_{\mathsf{min/max}} &= \pm\sqrt{-\frac{1}{k_\gamma} + \sqrt{\left(\frac{1}{k_\gamma}\right)^2 + {}_0\alpha_{f_2}}} \\ &= \pm\sqrt{\frac{1}{k_\gamma}}\sqrt{\sqrt{1 + {}_0\alpha_{f_2} k_\gamma{}^2} - 1} \end{aligned} \tag{3.4.84}$$

which will always be real regardless of the ratio of $\frac{k_\beta}{k_\alpha}$ and the initial conditions. The system's minimum/maximum velocity is derived from Eq.(3.3.15d) on page 43 setting $p_0 = 0$

$$\dot{u}_{\mathsf{Ex}} = \sqrt{\frac{2}{m}}\left(\frac{1}{2}k_\alpha u_0^2 + \frac{1}{4}k_\beta u_0^4 + \frac{m}{2}\dot{u}_0^2\right)^{\frac{1}{2}}, \tag{3.4.85a}$$

which, together with (3.4.83d) can be written as

$$\dot{u}_{\mathsf{Ex}} = \omega_{n,\beta}\sqrt{\frac{{}_0\alpha_{f_2}}{2}}. \tag{3.4.85b}$$

Equation (3.3.6) is used to obtain the oscillation period of the nonlinear freely vibrating SDOF system with $f_2(u)$ setting $p_0 = 0$

$${}_0T_{f_2} = \sqrt{2m}\int_{u_{\mathsf{min}}}^{u_{\mathsf{max}}} \frac{du}{\sqrt{-\int_u f_2(u)\,\mathrm{d}u - C_0}}. \tag{3.4.86a}$$

Together with Eq.(3.4.82), the constant C_0

$$C_0 = -\frac{1}{2}u_0^2 - \frac{1}{4}u_0^4 - \frac{m}{2}\dot{u}_0^2$$

and the fact $u_{\min} = -u_{\max}$ from Eq.(3.4.84) this can be written as

$$_0T_{f_2} = \frac{4\sqrt{2}}{\omega_{n,\beta}} \int_{u_{\min}}^{u_{\max}} \frac{\mathrm{d}u}{\sqrt{-u^4 - \frac{2}{k_\gamma}u^2 + {}_0\alpha_{f_2}}} \tag{3.4.86b}$$

and is known from the previous section 3.4.1 as a fourth-order elliptic integral. It has been shown that the solution of (3.4.86b) is only possible, if all poles and zeros of the integrand are known. These solutions are given by Eq.(3.4.83f)

$$\begin{aligned} &\chi_1 = u_{\max} = \sqrt{y_1}\,, && \chi_2 = u_{\min} = -\sqrt{y_1} && \chi_1\,,\ \chi_2 \in \mathbb{R} \\ &\chi_3 = \sqrt{y_2} && \chi_4 = \chi_3{}^* = -\sqrt{y_2} && \chi_3\,,\ \chi_4 \in \mathbb{C} \end{aligned} \tag{3.4.86c}$$

and hence, the term under the square root in (3.4.86b) can be rewritten in the same manner as (3.4.60) in Legendre's canonical form

$$\begin{aligned} -u^4 - \frac{2}{k_\gamma}u^2 + {}_0\alpha_{f_2} &= (\chi_1 - u)(u - \chi_2)(u - \chi_3)(u - \chi_4) \\ &= (\chi_1 - u)(u + \chi_1)(u - \chi_3)(u + \chi_3) \\ &= -u^4 - \left(-\chi_1^2 - \chi_3^2\right)u^2 + \left(-\chi_1^2\chi_3^2\right). \end{aligned} \tag{3.4.86d}$$

It should be noted here that the real part of the solutions χ_3 and χ_4 in Eq.(3.4.86c) is equal to zero since y_2 as given in (3.4.83f) is purely negative. A comparison of the coefficients in (3.4.86d) shows the equality of

$$-\chi_1^2 - \chi_3^2 = \frac{2}{k_\gamma} \qquad \text{and} \qquad -\chi_1^2\chi_3^2 = {}_0\alpha_{f_2}$$

which can be proved by substitution from Eq.(3.4.86c). The oscillation period from (3.4.86b) can now be written as

$$_0T_{f_2} = \frac{8\sqrt{2}}{\omega_{n,\beta}} \int_{u_{\min}}^{0} \frac{\mathrm{d}u}{\sqrt{(\chi_1 - u)(u - \chi_2)\left[(u - \chi_a)^2 + \chi_b^2\right]}} \tag{3.4.86e}$$

with the solution, see section 3.4.1 Eq.(3.4.54a) and [22],

$$_0T_{f_2} = \frac{8\sqrt{2}}{\omega_{n,\beta}}\eta_{\mathrm{E}}\,\mathcal{F}(\psi, \kappa) \tag{3.4.87a}$$

where

$$\chi_b = \frac{\chi_3 + \chi_3{}^*}{2} \qquad \text{and} \qquad \chi_a^2 = -\frac{(\chi_3 - \chi_3{}^*)^2}{4} \tag{3.4.87b}$$

and

$$\begin{aligned} &\eta_{\mathrm{E}} = \frac{1}{\sqrt{AB}}, \qquad A^2 = (\chi_1 - \chi_b)^2 + \chi_a^2, \qquad B^2 = (\chi_2 - \chi_b)^2 + \chi_a^2, \\ &\psi = \arccos\left(\frac{\chi_1 B + \chi_2 A}{\chi_1 B - \chi_2 A}\right), \qquad \kappa^2 = \frac{(\chi_1 - \chi_2)^2 - (A - B)^2}{4AB}. \end{aligned} \tag{3.4.87c}$$

It should be noted that the upper integration limit in (3.4.86e) has to be set to zero although oscillation around zero equilibrium position is symmetrical for a freely vibrating SDOF. However, [22] does not offer an explicit solution for the interval $[\chi_2;\chi_1]$. Making use of the relations given in Eq.(3.4.86c), namely $\chi_2 = -\chi_1$ and $\chi_3{}^* = -\chi_3$, the constants in Eq.(3.4.87c) can be simplified significantly to yield

$$\chi_b = 0, \quad \chi_a^2 = \chi_3^2, \quad A^2 = \chi_1^2 - \chi_3^2, \quad B^2 = \chi_1^2 - \chi_3^2 \quad \longrightarrow \quad B = A$$
$$\psi = \arccos(0) = j\frac{\pi}{2} \quad \text{with} \quad (j = 1,3,5,\ldots), \qquad \eta_E = \frac{1}{A} \quad \text{and} \quad \kappa = \frac{\chi_1}{A}. \tag{3.4.88a}$$

Furthermore, with ψ equals to odd multiple of $\frac{\pi}{2}$ the incomplete elliptic integral $\mathcal{F}\left(j\frac{\pi}{2},\kappa^2\right)$ in equation (3.4.87a) can be reduced using the identity relation Eq.(3.4.16b) to the complete elliptic function $j\,\mathcal{K}(\kappa)$ giving as final result for the nonlinear oscillation period

$${}_0T_{f_2,j} = j\frac{8\sqrt{2}}{\omega_{n,\beta}}\eta_E\,\mathcal{K}(\kappa), \qquad (j = 1,3,5,\ldots). \tag{3.4.88b}$$

As will be shown in section 3.4.3 on page 82, for values of the initial conditions u_0 and $\dot{u}_0$ above a certain minimum threshold, the nonlinear SDOF system responds visibly with more than one frequency, even in the case of zero applied load, i.e. free vibration. In fact, all higher harmonics of the system's response signal are odd multiples of ${}_0T_{f_2,j=1}$ as obtained in (3.4.88b).

Results - Free Vibration

The displacement of a linear freely vibrating SDOF oscillator depends only on three independent variables, namely stiffness to mass ratio, i.e. the systems natural frequency, and the two initial conditions u_0 and $\dot{u}_0$, see appendix A.2.1. However, for a nonlinear SDOF, equations (3.4.84) and (3.4.83d), the minimum/maximum displacement of the system with restoring force $f_2(u)$ is a function of five independent terms

$${}_0u_{Ex_{f_2}} = {}_0u_{Ex_{f_2}}\left(k_\gamma, {}_0\alpha_{f_2}\right) = {}_0u_{Ex_{f_2}}\left(k_\alpha, k_\beta, m, u_0, \dot{u}_0\right) \tag{3.4.89}$$

where k_α, k_β are the linear and cubic stiffness coefficients, respectively, m is the system's inertia and u_0, $\dot{u}_0$ are the initial conditions. Retaining three out of five terms constant enables one to plot ${}_0u_{Ex_{f_2}}$ as a function of two independent variables in a three-dimensional coordinate system. If not stated explicitly, all figures presented in this section have been obtained setting $m = 1$ and $k_\alpha = 1$, hence obtaining the non-dimensional stiffness ratio $k_\gamma = \frac{k_\beta}{k_\alpha}$ by variation of k_β. Regarding the initial conditions, for an alternating u_0 the velocity is kept constant and vice versa.

Plots (a) and (b) in Fig. 3.4.16 on page 108 show the **maximum displacement** as a function of the stiffness ratio k_γ and the initial displacement u_0 for a constant initial velocity $\dot{u}_0 = v_0$ equal to 2.5 m/s and 15 m/s, respectively. For graph (a) the maximum deformation amplitude ${}_0u_{max_{f_2}}$ of the SDOF oscillator stays virtually constant with changing ratio of k_γ. Contrary, for a higher value of v_0 equal to 15 m/s, graph (b) in 3.4.16, ${}_0u_{max_{f_2}}$ decreases by nearly 50% with increasing k_γ. Furthermore, the initial velocity contributes more significantly to the total displacement amplitude in plot (b) compared to (a) due to its higher value and therefore higher energy input into the system. This manifests itself by the fact that the values for ${}_0u_{max_{f_2}}$ at zero initial displacement differ by an approximate factor of 5 from graph (a) to (b). However, for ratios of k_γ equal to 1.5 and initial displacements $u_0 = 2$ m (or -2 m) the

amplitudes of ${}_0u_{\max f_2}$ for both graphs are nearly identical suggesting that in this case a higher initial velocity becomes insignificant with increasing initial displacement and nonlinearity, i.e. larger values of k_γ. This can easily be verified by referring to Eq.(3.4.83d) where u_0 has significantly more influence on the initial energy level than v_0, provided that $|u_0| > 1$.

For fixed initial displacement of 0.5 m and 1.25 m both graphs (c) and (d) in 3.4.16 show the absolute maximum deformation of the SDOF as a function of both, the initial velocity and the stiffness coefficient ratio k_γ. Again, for increasing k_γ influence of v_0 diminishes.

For the identically configured SDOF system Fig. 3.4.17 on page 109 gives the non-normalised **nonlinear frequencies** f_{NL} in Hz. As can be seen in all four graphs (a) to (d), at very low values of $k_\gamma \leq 0.1$ increasing initial displacement u_0 or velocity v_0 has virtually no effect on the oscillation frequency. This can be explained by the fact that at such small ratios of k_β / k_α the part in $f_2(u)$ with k_α dominates the restoring force and hence, the system is of quasi-linear nature. Furthermore, for the smaller values of the fixed variables, $v_0 = 2.5\,\mathrm{m/s}$ in graph (a) and $u_0 = 0.5\,\mathrm{m}$ in (c), the oscillation frequency stays virtually unchanged for increasing k_γ and very small values of the second independent, complementary variable, i.e. u_0 in (a) and v_0 in (c). A feasible explanation for this behaviour can be given in terms of energy input. Both initial conditions are not large enough to produce a significant "nonlinear" extreme displacement u_{Ex} and the linear term $k_\alpha\, u(t)$ is predominant in $f_2(u)$. Hence, increasing k_γ has only small influence and $u_{\min}/u_{\max}$ as integration limits for Eq.(3.4.86b) stay almost constant as can be seen from the previous figure 3.4.16 graphs (a) and (c) and hence, the nonlinear oscillation period ${}_0T_{f_2}$ remains virtually unchanged.

Contrary, with sufficiently large energy input due to u_0 and v_0, the SDOF system perform nonlinear oscillations even for regions of very low values of the complementary initial condition, i.e. u_0 in Fig. 3.4.17 (b) and v_0 in graph (d), if k_γ is reasonable large.

3.4.2.2 Step Response

The maximum displacement of a system due to step excitation with the nonlinear restoring force $f_2(u)$ is obtained from Eq.(3.3.3a) leading to the algebraic equation

$$\frac{k_\beta}{4}\,{}_{\mathrm{H}}u^4_{\mathrm{Ex}_{f_2}} + \frac{k_\alpha}{2}\,{}_{\mathrm{H}}u^2_{\mathrm{Ex}_{f_2}} - p_0\,{}_{\mathrm{H}}u_{\mathrm{Ex}_{f_2}} = \frac{k_\beta}{4}u_0^4 + \frac{k_\alpha}{2}u_0^2 - p_0 u_0 + \frac{m}{2}\dot{u}_0^2 \tag{3.4.90a}$$

or

$${}_{\mathrm{H}}u^4_{\mathrm{Ex}_{f_2}} + \frac{2}{k_\gamma}\,{}_{\mathrm{H}}u^2_{\mathrm{Ex}_{f_2}} - \frac{4p_0}{k_\beta}\,{}_{\mathrm{H}}u_{\mathrm{Ex}_{f_2}} - {}_{\mathrm{H}}\alpha_{f_2} = 0 \tag{3.4.90b}$$

with the constant

$${}_{\mathrm{H}}\alpha_{f_2} = u_0^4 + \frac{2}{k_\gamma}u_0^2 - \frac{4p_0}{k_\beta}u_0 + \frac{2}{\omega^2_{n,\beta}}\dot{u}_0^2 \tag{3.4.90c}$$

similar to Eq.(3.4.83d). Using appendix B.4 analytical solutions of (3.4.90b) can be derived. By comparison with Eq.(B.4.1b), (3.4.90b) is already a forth-order polynomial in its reduced form. Thus, from Eq.(B.4.2) the cubic resolving term is obtained as

$$z^3 + \frac{4}{k_\gamma}z^2 + 4\left(\frac{1}{{k_\gamma}^2} + {}_{\mathrm{H}}\alpha_{f_2}\right)z - \left(\frac{4p_0}{k_\beta}\right)^2 = 0 \tag{3.4.91a}$$

and can be reduced in the same manner as (B.3.1c) to

$$y^3 + Py + Q = 0 \tag{3.4.91b}$$

where the constants are given by

$$P = 4\left({}_{\mathrm{H}}\alpha_{f_2} - \frac{1}{3k_\gamma{}^2}\right), \qquad Q = -\frac{16}{27}\left(\frac{1}{k_\gamma{}^3} + \frac{27p_0^2}{k_\beta{}^2} + \frac{9\,{}_{\mathrm{H}}\alpha_{f_2}}{k_\gamma}\right) \tag{3.4.91c}$$

and the solution indicator of the third-order polynomial in (3.4.91b) is obtained from Eq.(B.3.1d) as

$$D = \frac{4}{27}\left({}_{\mathrm{H}}\alpha_{f_2} - \frac{1}{3k_\gamma}\right)^3 + \frac{64}{729}\left(\frac{1}{k_\gamma{}^3} + \frac{27p_0^2}{k_\beta{}^2} + \frac{9\,{}_{\mathrm{H}}\alpha_{f_2}}{k_\gamma}\right)^2 \tag{3.4.91d}$$

which clearly extends over the range $-\infty < D < \infty$ with $D \in \mathbb{R}$ and hence Eq.(3.4.90b) can have real and complex roots. A critical situation for the solution of Eq.(3.4.90b) would arise if (3.4.91a), or its reduced form (3.4.91b), possess three real zeros, *one positive* and *two negative*. Referring to Table B.4.1 on page 189 this renders Eq.(3.4.90b) with two pairs of complex conjugate solutions and hence no physical meaningful solution can be extracted. However, obtaining all three roots of (3.4.91b)

$$y_1 = \frac{-6\sqrt[3]{2}P + 2^{\frac{2}{3}}\left(-27Q + \sqrt{108P^3 + 729Q^2}\right)^{\frac{2}{3}}}{6\left(-27Q + \sqrt{108P^3 + 729Q^2}\right)^{\frac{1}{3}}} \tag{3.4.92a}$$

$$y_2 = \frac{\left(3 + 3\,\mathrm{i}\sqrt{3}\right)P + (-3)^{\frac{2}{3}}\sqrt[3]{2}\left(-9Q + \sqrt{12P^3 + 81Q^2}\right)^{\frac{2}{3}}}{3\,2^{\frac{2}{3}}\left(-27Q + \sqrt{108P^3 + 729Q^2}\right)^{\frac{1}{3}}} \tag{3.4.92b}$$

$$y_3 = \frac{-6(-1)^{\frac{2}{3}}\sqrt[3]{2}P - \sqrt[3]{-1}\sqrt[3]{36}\left(-9Q + \sqrt{12P^3 + 81Q^2}\right)^{\frac{2}{3}}}{6\left(-27Q + \sqrt{108P^3 + 729Q^2}\right)^{\frac{1}{3}}} \tag{3.4.92c}$$

with

$$(-3)^{\frac{2}{3}} = \frac{\sqrt[3]{9}}{2}\left(-1 + \mathrm{i}\sqrt{3}\right), \quad (-1)^{\frac{2}{3}} = \frac{1}{2}\left(-1 + \mathrm{i}\sqrt{3}\right) \quad \text{and} \quad (-1)^{\frac{1}{3}} = \frac{1}{2}\left(1 + \mathrm{i}\sqrt{3}\right)$$

is most useful for deriving various limits of (3.4.92) which prove that Eq.(3.4.91b) does not possess two negative real solutions if all independent terms involved stay with appropriate bounds. Rewriting Eq.(3.4.90b) as

$${}_{\mathrm{H}}u^4_{\mathrm{Ex}_{f_2}} + A\,{}_{\mathrm{H}}u^2_{\mathrm{Ex}_{f_2}} + B\,{}_{\mathrm{H}}u_{\mathrm{Ex}_{f_2}} - {}_{\mathrm{H}}\alpha_{f_2} = 0 \tag{3.4.93a}$$

where

$$A = \frac{2}{k_\gamma} \qquad \text{and} \qquad B = -\frac{4p_0}{k_\beta} \tag{3.4.93b}$$

leads to

$$P = 4\,{}_{\mathrm{H}}\alpha_{f_2} - \frac{A^2}{3}, \qquad Q = -\left(\frac{2}{27}A^3 + \frac{8}{3}A\,{}_{\mathrm{H}}\alpha_{f_2} + B^2\right) \tag{3.4.93c}$$

as the constant factors of the reduced third-order polynomial in Eq.(3.4.91b). It is easy to see that substitution of (3.4.93b) into (3.4.93c) yields (3.4.91c). Introducing now (3.4.93c) into the roots of (3.4.91b) yields y_i from (3.4.92) with $i = 1,2,3$ as explicit functions of A, B and ${}_{\mathrm{H}}\alpha_{f_2}$. Hence, in order to ensure not more than *one* y_i is *real and negative*, the following seven limiting cases for A, B and ${}_{\mathrm{H}}\alpha_{f_2}$ have to be considered:

(1) $\boxed{\mathbf{A \to 0}}$

The stiffness coefficient ratio k_γ from Eq.(3.4.83c) is large, hence the system is highly nonlinear. The contrary case $A \to \infty$ in which the system appears linear is of no interest here.

(2) $\boxed{\mathbf{B \to 0}}$

If k_β in (3.4.93b) takes on large values compared to the step force magnitude p_0, than B tends to zero.

(3) $\boxed{\mathbf{B \to +\infty}}$

Contrary, $|p_0|$ is rather large compared to k_β, the constant B is represented by large positive values if $p_0 u_0 < 0$.

(4) $\boxed{\mathbf{B \to -\infty}}$

The constant B tends to large negative values if $|p_0| \gg k_\beta$, as above, but $p_0 u_0 > 0$.

(5) $\boxed{{}_{\mathrm{H}}\alpha_{f_2} \to \mathbf{0}}$

For zero initial conditions $u_0 = v_0 = 0$ the constant ${}_{\mathrm{H}}\alpha_{f_2}$ becomes equal to zero. If both initial displacement and velocity are small, i.e. $|u_0| \ll 1$, $|v_0| \ll 1$, and $|k_\beta| \gg |p_0|$, than ${}_{\mathrm{H}}\alpha_{f_2}$ tends to zero.

(6) $\boxed{{}_{\mathrm{H}}\alpha_{f_2} \to +\infty}$

For large values of u_0, v_0 and p_0, but with $p_0 u_0 < 0$, as well as small values for the ratio k_γ, the constant ${}_{\mathrm{H}}\alpha_{f_2}$ will be rendered as a large positive number.

(7) $\boxed{{}_{\mathrm{H}}\alpha_{f_2} \to -\infty}$

With the same conditions for u_0 and v_0 as above in case (4), but $|k_\beta| \ll |p_0|$ and $p_0 u_0 > 0$, ${}_{\mathrm{H}}\alpha_{f_2}$ becomes a large negative quantity since $|p_0|$ is usually several magnitudes higher than $|u_0|$.

Applying case (1) equation (3.4.92a) simplifies to

$$\lim_{A\to 0} y_1(A,B,{}_{\mathrm{H}}\alpha_{f_2}) = \frac{-8\sqrt[3]{3}\,{}_{\mathrm{H}}\alpha_{f_2} + \sqrt[3]{2}\left(9B^2 + \sqrt{81B^4 + 768\,{}_{\mathrm{H}}\alpha_{f_2}{}^3}\right)^{\frac{2}{3}}}{6^{\frac{2}{3}}\left(9B^2 + \sqrt{81B^4 + 768\,{}_{\mathrm{H}}\alpha_{f_2}{}^3}\right)^{\frac{1}{3}}} \tag{3.4.94a}$$

and is now a function of B and ${}_{\mathrm{H}}\alpha_{f_2}$ only. A subsequent execution of (2) gives

$$\lim_{\substack{A\to 0\\ B\to 0}} y_1(A,B,{}_{\mathrm{H}}\alpha_{f_2}) = \frac{2\left(-\alpha + (\alpha^3)^{\frac{1}{3}}\right)}{\sqrt{3}\,(\alpha^3)^{\frac{1}{6}}} \tag{3.4.94b}$$

and letting ${}_{\mathrm{H}}\alpha_{f_2}$ approach zero yields the final result for the first root y_1 of Eq.(3.4.91b), equation (3.4.92a)

$$\lim_{\substack{A\to 0\\ B\to 0\\ {}_{\mathrm{H}}\alpha_{f_2}\to 0}} y_1(A,B,{}_{\mathrm{H}}\alpha_{f_2}) = 0. \tag{3.4.94c}$$

Similar results for y_1 and the other two roots, y_2 and y_3, are obtained by applying different combinations of (1)-(7) from above to Eq.(3.4.92). A complete listing of all possible results is given in Table 3.4.1,

Table 3.4.1: Limits of zero solutions of the third-order reduced polynomial in Eq.(3.4.91b) depending on the asymptotic value behaviour of A, B and ${}_{\mathrm{H}}\alpha_{f_2}$.

Case	Sub-Cases I	Sub-Case II	y_1	y_2	y_3
$\mathbf{A \to 0}$	$\mathbf{B \to 0}$	${}_{\mathrm{H}}\alpha_{f_2} \to 0$	0	0	0
		${}_{\mathrm{H}}\alpha_{f_2} \to +\infty$	0	$\mathrm{i}\infty$	$-\mathrm{i}\infty$
		${}_{\mathrm{H}}\alpha_{f_2} \to -\infty$	∞	$-\infty$	0
$\mathbf{A \to 0}$	$\mathbf{B \to +\infty}$	${}_{\mathrm{H}}\alpha_{f_2} \to 0$	∞	$-\infty+\mathrm{i}\infty$	$-\infty-\mathrm{i}\infty$
		${}_{\mathrm{H}}\alpha_{f_2} \to +\infty$	∞	$-\infty+\mathrm{i}\infty$	$-\infty-\mathrm{i}\infty$
		${}_{\mathrm{H}}\alpha_{f_2} \to -\infty$	∞	$-\infty+\mathrm{i}\infty$	$-\infty-\mathrm{i}\infty$
$\mathbf{A \to 0}$	$\mathbf{B \to -\infty}$	${}_{\mathrm{H}}\alpha_{f_2} \to 0$	∞	$-\infty+\mathrm{i}\infty$	$-\infty-\mathrm{i}\infty$
		${}_{\mathrm{H}}\alpha_{f_2} \to +\infty$	∞	$-\infty+\mathrm{i}\infty$	$-\infty-\mathrm{i}\infty$
		${}_{\mathrm{H}}\alpha_{f_2} \to -\infty$	∞	$-\infty+\mathrm{i}\infty$	$-\infty-\mathrm{i}\infty$

which clearly shows that the condition from above, not more than one y_i is at any time a real negative number for all possible combinations of A, B and ${}_{\mathrm{H}}\alpha_{f_2}$. Hence, equation (3.4.90b) will always lead to at least two real solutions.

The system's vibration velocity can be derived from (3.3.4g) on page 41 leading together with (3.4.90c) to

$$\dot{u}_{\mathrm{Ex}} = \frac{\omega_{n,\beta}}{\sqrt{2}}\left(-u_{\mathrm{Ex,eq}}^4 - \frac{2}{k_\gamma}u_{\mathrm{Ex,eq}}^2 + \frac{4p_0}{k_\beta}u_{\mathrm{Ex,eq}} + {}_{\mathrm{H}}\alpha_{f_2}\right)^{\frac{1}{2}} \tag{3.4.95a}$$

where $u_{\mathrm{Ex,eq}}$ is the deflection point with maximum absolute velocity. According to Eq.(3.3.4e) this is the point of nonlinear static displacement, obtained for $f_2(u)$ analytically from

$$u_{\mathrm{Ex,eq}}^3 + \frac{u_{\mathrm{Ex,eq}}}{k_\gamma} - \frac{p_0}{k_\beta} = 0 \tag{3.4.95b}$$

by using the formulas given in appendix B.3. From equation (3.3.6) on page 41 the oscillation period for step excitation is obtained

$${}_{\mathrm{H}}T_{f_2} = \frac{2\sqrt{2}}{\omega_{n,\beta}} \int\limits_{{}_{\mathrm{H}}u_{\mathrm{Ex}f_2}} \frac{du}{\sqrt{-u^4 - \frac{2}{k_\gamma}u^2 + \frac{4p_0}{k_\beta}u + {}_{\mathrm{H}}\alpha_{f_2}}} \tag{3.4.96a}$$

and rewritten in Legrende canonical form

$${}_{\mathrm{H}}T_{f_2} = \frac{2\sqrt{2}}{\omega_{n,\beta}} \int\limits_{{}_{\mathrm{H}}u_{\mathrm{min}f_2}}^{{}_{\mathrm{H}}u_{\mathrm{max}f_2}} \frac{du}{\sqrt{(\chi_1 - u)(u-\chi_2)(u-\chi_3)(u-\chi_4)}} \tag{3.4.96b}$$

with

$$\chi_i = {}_{\mathrm{H}}u_{\mathrm{Ex}f_2,i}, \qquad (i = 1,2,3,4)$$

as the zeros of Eq.(3.4.90b). It has been shown in previous sections that the sign of D in (3.4.91d) determines the nature of the solutions of the characteristic equation (3.4.90b). Therefore, the following two cases have to be distinguished:

- **D < 0 :** If equation (3.4.90b) has four real solutions

$$\chi_1 > \chi_2 > \chi_3 > \chi_4\,, \qquad \chi_1+\chi_2+\chi_3+\chi_4 = 0\,, \qquad \chi_i \in \mathbb{R},\ (i=1,2,\ldots,4) \tag{3.4.97a}$$

then Eq.(3.4.96b) can be solved by employing case number $\{257.00\}$ in [22]

$$_{\mathbb{H}}T_{f_2} = \frac{2\sqrt{2}}{\omega_{n,\beta}}\,\eta_{\mathsf{E}}\,\mathcal{F}(\psi,\kappa) \tag{3.4.97b}$$

with the constants

$$\eta_{\mathsf{E}} = \frac{2}{\sqrt{(\chi_1-\chi_3)(\chi_2-\chi_4)}}\,, \qquad \kappa = \sqrt{\frac{(\chi_1-\chi_2)(\chi_3-\chi_4)}{(\chi_1-\chi_3)(\chi_2-\chi_4)}}\,, \tag{3.4.97c}$$

and the argument ψ determined by the integration limits χ_1 and χ_2 as

$$\psi = \arcsin(\pm 1) \quad \rightarrow \quad \psi = (2j-1)\,\frac{\pi}{2} \qquad \text{with} \quad j = 1,2,3,\ldots\,. \tag{3.4.97d}$$

As already demonstrated in Eq.(3.4.71) the value $j\frac{\pi}{2}$ simplifies (3.4.97b) to

$$_{\mathbb{H}}T_{f_2} = (2j-1)\,\frac{2\sqrt{2}}{\omega_{n,\beta}}\,\eta_{\mathsf{E}}\,\mathcal{K}(\kappa)\,, \qquad j = 1,2,3,\ldots \tag{3.4.98}$$

with the complete elliptic integral $\mathcal{K}(\kappa)$.

- **D ≥ 0 :** If the solution indicator (3.4.91d) of the cubic polynomial in (3.4.91a) is greater zero, the fourth-order polynomial (3.4.90b) has two real and two conjugate complex solutions

$$\chi_1 > \chi_2\,, \quad \chi_1,\chi_2 \in \mathbb{R}; \qquad \chi_3\,,\,\chi_4 = \chi_3{}^*\,, \quad \chi_3,\chi_4 \in \mathbb{C} \tag{3.4.99a}$$

which leads to case $\{259.00\}$ (with $y \equiv a$) in [22]

$$_{\mathbb{H}}T_{f_2} = \frac{2\sqrt{2}}{\omega_{n,\beta}} \int_{_{\mathbb{H}}u_{\min_{f_2}}}^{_{\mathbb{H}}u_{\max_{f_2}}} \frac{du}{\sqrt{(\chi_1-u)(u-\chi_2)\left[(u-\chi_a)^2+\chi_b^2\right]}} = \frac{2\sqrt{2}}{\omega_{n,\beta}}\,\eta_{\mathsf{E}}\,\mathcal{F}(\psi,\kappa) \tag{3.4.99b}$$

where

$$\chi_a = \frac{\chi_3+\chi_3{}^*}{2} \qquad \text{and} \qquad \chi_b^2 = -\frac{(\chi_3-\chi_3{}^*)^2}{4}\,.$$

and

$$\eta_{\mathsf{E}} = \frac{1}{\sqrt{A\times B}}\,, \qquad A^2 = (\chi_1-\chi_a)^2+\chi_b^2\,, \qquad B^2 = (\chi_2-\chi_a)^2+\chi_b^2\,,$$

$$\kappa = \sqrt{\frac{(\chi_1-\chi_2)^2-(A-B)^2}{4AB}}\,. \tag{3.4.99c}$$

The argument ψ of Eq.(3.4.99b) is obtained as

$$\psi = \arccos(-1) \quad \rightarrow \quad \psi = (2j-1)\,\pi \qquad \text{with} \quad j = 1,2,3,\ldots\,. \tag{3.4.99d}$$

Substitution of ψ back into Eq.(3.4.99b) gives

$$_{\mathbb{H}}T_{f_2} = (2j-1)\,\frac{2\sqrt{2}}{\omega_{n,\beta}}\,\eta_{\mathsf{E}}\,\mathcal{K}(\kappa)\,, \qquad j = 1,2,3,\ldots\,. \tag{3.4.100}$$

System initially at rest. For the special case of ${}_{\mathrm{H}}\alpha_{f_2} = 0$, i.e. zero initial conditions, equation (3.4.90b) simplifies to

$$ {}_{\mathrm{H}}u_{\mathrm{Ex}_{f_2}} \left({}_{\mathrm{H}}u^3_{\mathrm{Ex}_{f_2}} + \frac{2}{k_\gamma} {}_{\mathrm{H}}u_{\mathrm{Ex}_{f_2}} - \frac{4p_0}{k_\beta} \right) = 0 \tag{3.4.101a} $$

with

$$ {}_{\mathrm{H}}u_{\mathrm{min}_{f_2}} = 0 \tag{3.4.101b} $$

and

$$ {}_{\mathrm{H}}u_{\mathrm{max}_{f_2}} = \frac{1}{\sqrt[3]{\frac{2p_0}{k_\beta} + \sqrt{D}}} \left[\left(\frac{2p_0}{k_\beta} + \sqrt{D} \right)^{\frac{2}{3}} - \frac{2}{3k_\gamma} \right] \tag{3.4.101c} $$

according to appendix B.3. The solution indicator for the third-order polynomial equates to

$$ D = \left(\frac{2}{3k_\gamma} \right)^3 + \left(-\frac{2p_0}{k_\beta} \right)^2 \tag{3.4.101d} $$

and is for all possible values of k_β k_γ and p_0 always greater zero. This in turn gives for the term in brackets in Eq.(3.4.101a) only one real solution, Eq.(3.4.101c), and two complex conjugate, see Table B.3.1 in section B.3. The oscillation period is obtained in the same way as for ${}_{\mathrm{H}}\alpha_{f_2} \neq 0$, i.e. by using Eq.(3.4.99b) together with the appropriate constants in (3.4.99c) setting $\chi_2 = 0$. A similar solution for the special case ${}_{\mathrm{H}}\alpha_{f_2} = 0$ is also given by BAPAT and SRINIVASAN in [7].

Results - Step Response

For the special case of the step excited SDOF system with zero initial conditions both normalised maximum displacement

$$ \frac{u_{\mathrm{dyn}} \equiv {}_{\mathrm{H}}u_{\mathrm{max}_{f_2}}}{u_{\mathrm{stat,lin}}} $$

and nonlinear oscillation frequency

$$ \frac{f_{\mathrm{NL}}}{f_{n,\alpha}}, \qquad \text{where} \qquad f_{\mathrm{NL}} = \frac{1}{{}_{\mathrm{H}}T_{f_2}} \qquad \text{and} \qquad f_{n,\alpha} = \frac{1}{2\pi}\sqrt{\frac{k_\alpha}{m}} $$

are plotted in Fig. 3.4.18 on page 110. The maximum displacement as a function of the stiffness coefficients k_α, k_β and the applied step magnitude p_0

$$ {}_{\mathrm{H}}u_{\mathrm{max}_{f_2}} = {}_{\mathrm{H}}u_{\mathrm{max}_{f_2}}\left(k_\alpha, k_\beta, p_0\right) $$

has been calculated using Eq.(3.4.101c) and (3.4.101d). The linear stiffness coefficient k_α was set to the default value of 1.0 and the stiffness ratio was defined between $0 \leq k_\gamma \leq 1.5$, hence $k_\beta = k_\alpha \times k_\gamma$. The static deformation of the linear system has been obtained by dividing step force magnitude by linear stiffness coefficient, e.g.

$$ u_{\mathrm{stat,lin}} = \frac{p_0}{k_\alpha} $$

giving with $k_\alpha = 1$ for $u_{\mathrm{stat,lin}}$ a purely linear function.

Graph (a) in Fig. 3.4.18 clearly indicates the dependance of the **maximum displacement** ${}_{\mathrm{H}}u_{\mathrm{max}_{f_2}}$ on both the SDOF system's stiffness ratio k_γ and the load amplitude p_0. For small values of k_γ and p_0 the dynamic displacement amplitude does not exceed two times the static displacement of the linear system with a restoring force

$$ f_{\mathrm{lin}}(u) = k_\alpha\, u(t). $$

For the stiffness coefficient ratio $k_\gamma = k_\beta / k_\alpha = 0$ the actual dynamic displacement is exactly twice the static, i.e. the well-known solution for the linear system. For small values of $k_\gamma \leq 0.01$ this linear behaviour is explained by the fact that the term $k_\alpha\, u(t)$ still dominates the stiffness force $f_2(u)$ in Eq.(3.4.81). Despite increasing nonlinearity in the system, e.g. $k_\gamma \rightarrow 1.5$, the oscillator can still be regarded as linear for step loading amplitudes $p_0 \leq 10.0$. As mentioned, a linear oscillator plotted in Fig. 3.4.18(a) would exhibit a flat surface at the ratio ${}_{\mathrm{H}}u_{\mathrm{max}f_2} / u_{\mathrm{stat,lin}} = 2$ for the normalised maximum displacement. However, the nonlinear system as given in 3.4.18(a) indicates a rapidly decreasing of this ratio with both, increasing nonlinear stiffness and step load magnitude to fractions of the ratio ${}_{\mathrm{H}}u_{\mathrm{max}f_2} / u_{\mathrm{stat,lin}}$ of the equivalent linear SDOF. Hence, for obtaining displacement values close to the true response of the nonlinear system it is highly misleading to neglect the nonlinear term in Eq.(3.4.81) even for small ratios of $k_\gamma = k_\beta / k_\alpha \leq 0.1$ as sometimes suggested in literature.

This fact is underlined by graph (b) of Fig. 3.4.18. At points for very small values for k_γ and p_0 the ratio $\frac{f_{\mathrm{NL}}}{f_n}$ is about equal to one which indicates the system is almost linear. However, even a small growth of either k_γ or p_0, or both, rapidly leads to **oscillation frequencies** f_{NL} substantially higher than in the linear case.

3.4.2.3 Impulse Response

Substitution of equation(3.4.82) into (3.3.14) yields

$$\frac{k_\beta}{4}\,{}_\delta u^4_{\mathrm{Ex}f_2} + \frac{k_\alpha}{2}\,{}_\delta u^2_{\mathrm{Ex}f_2} = \frac{k_\beta}{4}u_0^4 + \frac{k_\alpha}{2}u_0^2 + \frac{m}{2}\left(\frac{p_0}{m} + \dot{u}_0\right)^2 \tag{3.4.102a}$$

which is rewritten as

$${}_\delta u^4_{\mathrm{Ex}f_2} + \frac{2}{k_\gamma}\,{}_\delta u^2_{\mathrm{Ex}f_2} - {}_\delta\alpha_{f_2} = 0 \tag{3.4.102b}$$

with

$${}_\delta\alpha_{f_2} = u_0^4 + \frac{2}{k_\gamma}u_0^2 + \frac{2}{\omega^2_{n,\beta}}\left(\frac{p_0}{m} + \dot{u}_0\right)^2 . \tag{3.4.102c}$$

It is easy to see that Eq.(3.4.102a) is identical to (3.4.83a) with a similar term ${}_0\alpha_{f_2}$, which is irrelevant to the solution behaviour of Eq.(3.4.102b). Hence, extreme displacement

$${}_\delta u_{\mathrm{Ex}f_2} = u_{\mathrm{min/max}} = \pm\sqrt{-\frac{1}{k_\gamma} + \sqrt{\left(\frac{1}{k_\gamma}\right)^2 + {}_\delta\alpha_{f_2}}} = \pm\sqrt{\frac{1}{k_\gamma}}\sqrt{\sqrt{1 + {}_\delta\alpha_{f_2}k_\gamma{}^2} - 1} \tag{3.4.103}$$

and oscillation velocity

$$\dot{u}_{\mathrm{Ex}} = \omega_{n,\beta}\sqrt{\frac{{}_\delta\alpha_{f_2}}{2}} \tag{3.4.104}$$

are obtained in the same manner as the solutions for free vibration on page 70 but with ${}_\delta\alpha_{f_2}$ from equation (3.4.102c). The oscillation period for an impulse excited nonlinear SDOF system with a nonlinear restoring force $f_2(u)$ as given in Eq.(3.4.81) is obtained from

$${}_\delta T_{f_2} = \frac{4\sqrt{2}}{\omega_{n,\beta}}\eta_{\mathrm{E}}\,\mathcal{F}(\psi,\kappa) \tag{3.4.105}$$

with the coefficients as derived in Eq.(3.4.87) on page 72. Furthermore, all simplification introduced by Eq.(3.4.88) are also applicable to (3.4.105) thus giving

$${}_\delta T_{f_2} = j\frac{4\sqrt{2}}{\omega_{n,\beta}}\eta_{\mathrm{E}}\,\mathcal{K}(\kappa)\,, \qquad (j = 1,3,5,\ldots) \tag{3.4.106}$$

as solution for predicting the fundamental and higher order oscillation periods of the SDOF system as introduced in section 3.4.2.1.

It should be noted here that the equilibrium position of the system stays unchanged during the oscillation process, regardless of acting force direction and initial conditions introduced, as can be deduced from Eq.(3.4.103). The minimum displacement is the negative maximum displacement value, which applies also for the case of free vibration as shown in (3.4.84). However, as already encountered for linear systems, application of a step load always results in shift of the neutral oscillation position determined by $\frac{1}{2}(u_{\min}+u_{\max})$ as shown in section 3.4.2.2 and appendix A.2.2.

Zero initial conditions. In the case of $u_0 = \dot{u}_0 = 0$ the term ${}_\delta\alpha_{f_2}$ is rewritten as

$$ {}_\delta\alpha_{f_2} = \frac{2}{\omega_{n,\beta}^2}\left(\frac{p_0}{m}\right)^2 \tag{3.4.107a} $$

and equation (3.4.102b) is solved by the substitution $z = {}_\delta u_{\mathrm{Ex}_{f_2}}^2$

$$ z^2 + \frac{2}{k_\gamma} z - {}_\delta\alpha_{f_2} = 0 \tag{3.4.107b} $$

which leads to exact the same expression as Eq.(3.4.103) except ${}_\delta\alpha_{f_2}$ is now determined by (3.4.107a).

Results - Impulse Response

Assuming a SDOF system initially at rest the normalised maximum displacement ${}_\delta u_{\max_{f_2}}/u_{\mathrm{stat,lin}}$ and oscillation frequency due to an impulse excitation with a total amplitude of p_0 are shown in Fig. 3.4.19, see page 111. The stiffness ratio was set to $0 \le k_\gamma \le 1.5$ and with k_α and m equal to unity, k_β has been computed. The static linear displacement is given by

$$ u_{\mathrm{stat,lin}} = \frac{p_0}{k_\alpha} $$

as defined in section 3.4.2.2. For $k_\alpha \neq 0$, $k_\beta = 0$ the SDOF would be purely linear with a maximum dynamic elongation amplitude of

$$ u_{\mathrm{stat,dyn}} = \frac{p_0}{m\,\omega_{n,\alpha}} $$

see appendix A.2.3 Eq.(A.2.17) for $u_0 = \dot{u}_0 = 0$. Hence, normalising the linear dynamic displacement $u_{\mathrm{stat,dyn}}$ to the linear static $u_{\mathrm{stat,lin}}$ gives

$$ \frac{u_{\mathrm{stat,dyn}}}{u_{\mathrm{stat,lin}}} = \omega_{n,\alpha} = \sqrt{\frac{k_\alpha}{m}} = 1\,. $$

This explains why in Fig. 3.4.19 (a) the maximum **normalised displacement** amplitude of the quasi-linear system at either very small load magnitudes $p_0 < 10.0$ or small ratios of k_β/k_α as $k_\beta \to 0$ reaches the magnitude of 1. It is easy to verify that for other values of k_α and m than unity the ratio ${}_\delta u_{\max_{f_2}}/u_{\mathrm{stat,lin}}$ would be considerably different. It should be noted once more that even for small values of k_γ or p_0 the ratio ${}_\delta u_{\max_{f_2}}/u_{\mathrm{stat,lin}}$ differs considerably from 1, thus the system cannot be referred to as linear.

Comparing the **oscillation frequency** ratio f_{NL}/f_n in both figures 3.4.18 and 3.4.19 suggest similar behaviour of the nonlinear system despite the fact of completely different excitation functions.[12]

[12] This also applies to the normalised displacement ${}_\delta u_{\max_{f_2}}/u_{\mathrm{stat,lin}}$ in graph (a) of both figures.

However, the nonlinear frequency for an impulse excited systems varies in a range almost twice the size of that for a step excited SDOF with the parameters as given above.

3.4.3 Explicit Time and Frequency Domain Behaviour

The results presented in the preceding sections of this work are somewhat limited in their use for establishing a complete picture of the response of nonlinear oscillators excited by various forms of shock and impulse forces. The major difficulty in describing nonlinear dynamic systems in the time and frequency domain is the fact that the superposition principle, well known from the linear theory in section 2, no longer holds true. Therefore, linear integral transformations, e.g. Laplace and Fourier transforms, are not helpful.

Analytical approximate methods exist modelling the nonlinear system as piecewise linear, depending upon the displacement u and velocity $\dot{u}$ at time t, which determine the nonlinear restoring force characteristics. This is likely to result in complex and intricate formulations, especially if, apart from large deflection or rotation, the systems exhibits material nonlinearities (e.g. hysteresis) as well. Moreover, these methods are limited to oscillators with small linearities only, because otherwise the linearisation error would become too large in the restoring force approximation, even if the piecewise linear sections $\Delta f_{\text{approx}}(\Delta u)$ are kept small. The only remaining option is the direct integration of the nonlinear equation of motion of the system in the time domain.

In sections 3.4.1 and 3.4.2 rather complex integral expression were derived and analytical solutions were obtained for only special cases of nonlinear oscillators. In order to find a solution for equations such as (3.2.3) or even (3.2.1) in terms of $u = u(t)$ no analytical method exists which could be used.[13] Hence, the nonlinear differential equation is rewritten as a nonlinear algebraic difference equation using either linear or nonlinear interpolation. In fact, for numerical approximations such as finite or boundary element methods, Rayleigh-Ritz or Galerkin approximation, direct numerical integration in the time domain is the only feasible approach.

Numerical methods for solving systems of nonlinear differential equations of second and higher order have been investigated for more than a century [5], [25]. However, the conversion from numerical mathematics into computer programs and the consideration of practical aspects arising from the implementation of these algorithms started in 1960's and 1970's when growing numbers of digital computer resources became readily available. Although a number of methods have been proposed, only a few studies were devoted to a direct comparison of these methods [26–28]. As a conclusion, drawn from the literature review, the Runge-Kutta method was chosen giving an unconditionally stable algorithm and very high convergence rate toward the exact solution with decreasing time step. The drawback of the method is the higher execution time compared to algorithms such as average acceleration method, central difference method or Wilson method. This negative aspect was significantly reduced by introducing an adaptive time step concept into the algorithm [29].

The data presented graphically in this section has been obtained using explicit adaptive time stepping algorithms for the solution of ordinary differential equation (ODE) initial value problems (IVP)

[13] As will be shown in a second part of this memorandum series, analytical solutions exist for nonlinear autonomous systems as given in Eq.(3.2.3) having Duffing-type restoring forces, e.g. $f(u) = f_2(u) = k_\alpha u + k_\beta u^3$, by using a new class of periodic functions.

and the numerical software manipulation package MATLAB® [14].

Several different configurations of the Runge-Kutta [5] integration method have been employed. Rather than using step-doubling for error determination in each time step, embedded methods with higher order error predictors were selected. Usually they are twice as fast as the step-doubling approach [29]. In general, they can be grouped into two classes with respect to the remaining numerical error of each method [27].

The first category are fifth-order algorithms with a fourth-order accurate calculation step and a fifth-order error step. The routine `RK54_v3a` uses the CASH-KARP coefficients [30] whereas the MATLAB® internal routine `ode45` uses the DORMAND-PRINCE [31] pair coefficients. Both routines perform equally accurate but in favour of greater flexibility[15], data handling and proven stability `ode45` was chosen for further numerical simulation with a 5th order algorithm.

A second, higher-order algorithm written by GOVORUKHIN (also based on DORMAND-PRINCE [32]), was found on `www.mathworks.com/matlabcentral/fileexchange/`. A comparison of performance between both routines results in general findings already given in [29] for different pairs of high-order numerical integration algorithms. In general, higher order does not necessarily mean higher accuracy. As herein, `ode45` results were much more accurate compared to the exact analytical solution than those produced by `ode87` when using the same overall and relative error tolerance parameters. However, the trade off lay in calculation speed. For a 10 second time frame and rather moderate error values (relative 10^{-5}, absolute 10^{-8}) `ode87` was about three times faster than `ode45`. This ratio increased with a more stringent error tolerance up to a factor of 15 to 20.

Common to all introduced numerical ODE solvers is the fact that they are only applicable to first-order systems. In general, this is no problem since every ODE of order n

$$\frac{\mathrm{d}^n u(t)}{\mathrm{d}t^n} = \mathbf{F}\left[t, P(t), u(t), \frac{\mathrm{d}u(t)}{\mathrm{d}t}, \ldots, \frac{\mathrm{d}^{(n-1)}u(t)}{\mathrm{d}t^{(n-1)}}\right], \tag{3.4.108}$$

where $\mathbf{F}[\ldots]$ is a general function, in this case of the variables $\left(t, P(t), u(t), \frac{\mathrm{d}u(t)}{\mathrm{d}t}, \ldots, \frac{\mathrm{d}^{(n-1)}u(t)}{\mathrm{d}t^{(n-1)}}\right)$, can be rewritten as a set of n coupled *first-order* ODEs, see [33]

$$\begin{aligned}
\frac{\mathrm{d}z_1(t)}{\mathrm{d}t} &= z_2(t), \\
\frac{\mathrm{d}z_2(t)}{\mathrm{d}t} &= z_3(t), \\
&\vdots \\
\frac{\mathrm{d}z_n(t)}{\mathrm{d}t} &= \mathbf{F}[t, P(t), z_1(t), z_2(t), \ldots, z_n(t)]
\end{aligned} \tag{3.4.109}$$

using the substitution

$$z_1(t) = u(t), \quad z_2(t) = \frac{\mathrm{d}u(t)}{\mathrm{d}t}, \quad z_3(t) = \frac{\mathrm{d}^2 u(t)}{\mathrm{d}t^2}, \ldots, \quad z_n(t) = \frac{\mathrm{d}^{(n-1)}u(t)}{\mathrm{d}t^{(n-1)}}.$$

[14] Version 6.0 - Release 12.

[15] There are many more differential equation solvers available in the MATLAB® environment possessing the same variable reference interface as `ode45`. This was especially useful for using higher-order solver algorithms readily available on `www.mathworks.com`.

Application of this procedure to the equation of motion for the nonlinear autonomous conservative SDOF system (3.2.3) by setting $z_1(t) \equiv u(t)$, $z_2(t) \equiv \dot{u}(t)$ and $P(t) = p_0$ gives two coupled first-order ODEs

$$\begin{aligned} \dot{z}_1 &= z_2 \,, \\ \dot{z}_2 &= \frac{1}{m}\left[p_0 - f(z_1)\right] \end{aligned} \tag{3.4.110a}$$

with the initial conditions from Eq.(3.2.4) equal to

$$z_{1,0} = u_0 \quad , \qquad z_{2,0} = v_0 \,. \tag{3.4.110b}$$

3.4.3.1 Restoring Force $f_1(u) = k\,\mathrm{sign}(u)\,|u|^b$

A first comparison of results produced from both analytical and numerical computation is given in Table 3.4.2 on page 85. All numerical values were acquired using the ode45 - MATLAB® routine as described above with 1.0E-9 and 1.0E-11 as relative and absolute error tolerances, respectively. The very good agreement between both results presented in the table is easily verified. The average absolute error for displacement and velocity values is less than 1.0E-4% and for frequency values less than 2.5E-2%.

Figure 3.4.20 on page 112 shows the **absolute displacement** $u(t)$ as a function of time for three different nonlinear exponents $b = 2,3,4$ (the linear case is given by $b = 1$), and the typical types of oscillation examined in this work: free vibration, step and impulse excitation with the maximum values given in Table 3.4.2. A direct comparison of graph (a) in Fig. 3.4.20, the case of free vibration, with Fig. 3.4.2 and 3.4.3 on page 94 and 95, respectively, shows for a constant natural frequency f_n and increasing values of b an increasing amplitude of the maximum absolute displacement $u_{\max}$ in all three graphs. Since the linear static displacement $u_{\mathrm{stat,lin}}$ is constant at a fixed frequency f_n, the absolute displacement in Fig. 3.4.20(b) and (c) can be compared with the normalised displacement in Fig. 3.4.6 and 3.4.8, respectively, on page 98 and 100. And again, increasing values for the nonlinear exponent b give increasing maximum $u_{\max}$ (see Fig. 3.4.6 in addition) and decreasing minimum displacement $u_{\min}$ for a step excited SDOF system.

An explanation for this seemingly odd behaviour of increasing absolute displacement with increasing order of the restoring force function has been provided earlier and can be found examining Fig. 3.4.1 on page 46. The increase in monotony of function $f_1(u)$ as b takes on larger values, which is responsible for the increased stiffness of the oscillating SDOF system, is only observable if $|u| > 1$. In fact, between $-1 \leq u(t) \leq 1$ monotony and hence restoring force *decrease* as $b \to \infty$. In conclusion, if the absolute (not normalised!) displacement $u(t)$ stays within $[-1;1]$ the system's restoring force exhibits characteristics of an elastic 'softening' spring.

For step excitation the relative dynamic displacement, defined as[16]

$$u_{\mathrm{dyn,rel}} = u_{\max} - u_{\min} \,,$$

decreases as b increases from 1 to 3. If $b = 4$, $u_{\mathrm{dyn,rel}}$ rises again. Furthermore, it is clear to see that for different values of b the system's new equilibrium position, defined by Eq.(3.3.4e) and (3.4.32b), shifts

[16] With the definition given a relative dynamic displacement can also be calculated for free and impulse vibration. However, it would always equate to zero since the equilibrium position stays at $u = 0$.

Table 3.4.2: Nonlinear SDOF $\mathbf{f_I(u) = k\,sign(u)\,|u|^b}$: Extreme displacement u_{min}/u_{max} and velocity $\dot{u}_{min}/\dot{u}_{max}$ obtained from analytical and numerical calculations together with the first three fundamental nonlinear natural frequencies of the oscillator. The system properties are: reference natural frequency $f_n = 15.0\,\text{Hz}$, mass $m = 3.0\,\text{kg}$, $\omega_n = 2\pi f_n = 30\pi\,\text{rad/s}$, stiffness $k = m\omega_n^2\,\frac{\text{N}}{\text{m}}$. Applied load and initial conditions: $p_0 = 100.0\,\text{N}$, $u_0 = 0.15\,\text{m}$ and $\dot{u}_0 = 2.25\,\frac{\text{m}}{\text{s}}$.

Excitation Type	b	Displacement u_{min}/u_{max} analytical	Displacement u_{min}/u_{max} numerical[b]	Velocity $\dot{u}_{min}/\dot{u}_{max}$ analytical	Velocity $\dot{u}_{min}/\dot{u}_{max}$ numerical[b]	Frequency[a] (Hz) 1	2	3	...	$f_{NL,j} = j f_{NL}$ j
free	1	-1.51888E-01 1.51888E-01	-1.51888E-01 1.51888E-01	-1.43151E+01 1.43151E+01	-1.43151E+01 1.43151E+01	15.000	–	–		1
	2	-1.61725E-01 1.61725E-01	-1.61725E-01 1.61725E-01	-5.00484E+00 5.00484E+00	-5.00484E+00 5.00484E+00	5.518	16.553	22.070		
	3	-2.01426E-01 2.01426E-01	-2.01426E-01 2.01426E-01	-2.70387E+00 2.70387E+00	-2.70387E+00 2.70387E+00	2.560	7.679	12.799	...	1,3,5,...
	4	-2.72435E-01 2.72435E-01	-2.72435E-01 2.72435E-01	-2.30918E+00 2.30918E+00	-2.30918E+00 2.30918E+00	1.690	5.071	8.451		
step	1	-1.44429E-01 1.51936E-01	-1.44429E-01 1.51936E-01	-1.39659E+01 1.39659E+01	-1.39659E+01 1.39659E+01	15.000	–	–		1
	2	-1.09405E-01 1.63662E-01	-1.09405E-01 1.63662E-01	-4.21557E+00 4.21557E+00	-4.21557E+00 4.21557E+00	5.191	10.382	15.573		
	3	4.05157E-02 2.31423E-01	4.05157E-02 2.31423E-01	-2.25407E+00 2.25407E+00	-2.25407E+00 2.25407E+00	3.629	7.259	10.888	...	1,2,3,...
	4	[c]7.01056E-02 [c]3.50022E-01	7.01056E-02 3.50022E-01	-2.92106E+00 2.92106E+00	-2.92106E+00 2.92106E+00	3.149	6.297	9.446		
impulse	1	-4.06257E-01 4.06257E-01	-4.06257E-01 4.06257E-01	-3.82888E+01 3.82888E+01	-3.82888E+01 3.82888E+01	15.000	–	–		1
	2	-6.01102E-01 6.01102E-01	-6.01102E-01 6.01102E-01	-3.58631E+01 3.58631E+01	-3.58631E+01 3.58631E+01	10.637	31.912	53.187		
	3	-7.31035E-01 7.31035E-01	-7.31035E-01 7.31035E-01	-3.56149E+01 3.56149E+01	-3.56149E+01 3.56149E+01	9.290	27.870	46.451	...	1,3,5,...
	4	-8.13573E-01 8.13573E-01	-8.13573E-01 8.13573E-01	-3.55871E+01 3.55871E+01	-3.55871E+01 3.55871E+01	8.722	26.167	43.612		

[a] Analytical and numerical computation gave identical results.

[b] All values were obtained using various adaptive Runge-Kutta algorithms as described in the text.

[c] Values are obtained evaluating the analytical expression numerically. There is no closed form solution available.

Table 3.4.3: Nonlinear SDOF system $\mathbf{f_1(u) = k\,sign(u)\,|u|^b}$: Static and dynamic displacement values for the step excited SDOF. The system properties: natural frequency $f_n = 15.0\,\text{Hz}$, mass $m = 3.0\,\text{kg}$, $\omega_n = 2\pi f_n = 30\pi\,\text{rad/s}$, stiffness coefficient $k = m\omega_n^2\,\frac{\text{N}}{\text{m}}$. Applied load and initial conditions: $p_0 = 100.0\,\text{N}$, $u_0 = 0.15\,\text{m}$ and $\dot{u}_0 = 2.25\,\frac{\text{m}}{\text{s}}$. All values are given in m.

b	nonlin. static displacement $u_{\text{stat,NL}}$	relative dynamic displacement[a] $u_{\text{dyn,rel}} = u_{\text{max}} - u_{\text{min}}$	*positive* relative dyn. displacement[a] $u_{\text{max}} - u_{\text{stat,NL}}$	*negative* relative dyn. displacement[a] $u_{\text{stat,NL}} - u_{\text{min}}$
1	3.753E-03	2.964E-01	1.481E-01	-1.481E-01
2	6.126E-02	2.731E-01	1.024E-01	-1.707E-01
3	1.554E-01	1.909E-01	7.602E-02	-1.149E-01
4	2.475E-01	2.799E-01	1.025E-01	-1.774E-01

[a]Values for u_{min} and u_{max} are obtained from Table 3.4.2, see page 85.

significantly from approximately zero ($b = 1$) to 0.25 m for $b = 4$. A summary of static and dynamic displacement values for the SDOF response due to an applied step function is given in Table 3.4.3. A closer examination of column three and four in the table shows that the nonlinear system does not oscillate symmetrically around its new equilibrium position $u_{\text{Ex,eq}} = u_{\text{stat,NL}}$. Compared to the linear case in line 1, absolute values of positive and negative dynamic displacement are not equal anymore.

Whereas the extreme oscillation amplitudes for the displacement increase as the restoring force of the SDOF takes higher order nonlinearity, the opposite is true for the system's **oscillating velocity** $\dot{u}(t)$, especially in the case of free vibration, see Fig. 3.4.21(a). An integer increase in the power b leads to an asymptotic-type decrease in $\dot{u}_{\text{Ex}}$. In Fig. 3.4.21(b), $\dot{u}(t)$ for the step excited SDOF, the same trend as already mentioned for the displacement is observable but now in reversed form. For $b = 1,2,3$ $\dot{u}_{\text{Ex}}$ reduces significantly only to slightly rise again for $b = 4$. If the system with its chosen properties as given above is excited by a scaled Dirac impulse the extreme values of velocity stay virtually constant as suggested by Fig. 3.4.21(c). In fact, $\dot{u}_{\text{Ex}}$ is decreasing exponentially for bigger ratios u_0/p_0 and $u_0/\dot{u}_0$ as stated by Eq.(3.4.76).

Figures 3.4.22 to 3.4.24 on pages 114-116 show **oscillation frequency** magnitude and phase of the SDOF's response due to free vibration, step and impulse excitation. The graphs were obtained by interpolating the non-equally spaced time domain output of the adaptive solver routines into equidistant spaced time and displacement vectors, subsequent windowing by either *Hanning* or *Hamming* functions[17] and Fourier transform using the FFT algorithm [34]. The linear case $b = 1$ with its unique single frequency at $f_n = 15\,\text{Hz}$ is clearly distinguishable in all three pictures. As already predicted by the analytical solutions in figures 3.4.4, 3.4.5, 3.4.7 and 3.4.9 on pages 96, 97, 99 and 101, respectively, increasing values of b result in decreasing nonlinear fundamental oscillation frequencies $f_{\text{NL},1}$. Moreover, the multi-frequency response derived analytically in section 3.4.1 is in perfect agreement with the numerous peaks and phase changes in Fig. 3.4.22 to 3.4.24.

[17]Numerous time-domain windows available in [34] were tested prior to the Fourier transformation. However, the best results were obtained using the two functions named above. The fact that applying two different windowing functions for the same oscillation response type, e.g. free, step or impulse, does only result, in the special case of *Hanning* and *Hamming* functions, in different levels of the frequency-domain magnitude, see Fig. 3.4.22(a) for example.

3.4.3.2 Restoring force $f_2(u) = k_\alpha u + k_\beta u^3$

For the SDOF oscillator with $f_2(u)$ as nonlinear restoring force Table 3.4.4 gives the comparison of analytically and numerically obtained data for a specific set of system parameters. For small numbers of the nonlinear stiffness ratio, e.g. $k_\gamma \leq 1$, **displacement** and **velocity** are virtually equal to the values for the linear case $b = 1$ in Table 3.4.2 for all three types of oscillation. Moreover, even for the upper limit of $k_\gamma = 35$ in Table 3.4.4, the displacement u_{max}/u_{min} differs less than 1.6% (free vibration) and the extreme velocity $\dot{u}_{max}/\dot{u}_{min}$ not more than 18.5% (step excitation) from the values derived for the linear case in section 3.4.3.1 for a free vibrating or step excited SDOF system with $f_1(u)$. An exception is the impulse excited oscillator. As k_γ increases beyond 1.0 the system can no longer be regarded as linear in predicting extreme values of displacement and velocity. Numbers for u_{max}/u_{min} and $\dot{u}_{max}/\dot{u}_{min}$ vary significantly from the data given in Table 3.4.2 for $b = 1$.

These findings are in perfect agreement with diagrams presented in section 3.4.2. Figure 3.4.16(a) on page 108, for example, clearly indicates that there is virtually no change in the maximum absolute displacement of the freely vibrating system at fixed values for u_0 and $\dot{u}_0$ as k_γ increases.

By comparing both graphs showing the normalised **oscillation frequencies** f_{NL}/f_n of the step and impulse excited system, Fig. 3.4.18(b) and 3.4.19(b) on pages 110 and 111, respectively, reveals the same upper limit yielding pattern of both functions. However, for step-type loaded system this limiting value is reached earlier and at a much lower level than for system with an applied Dirac impulse as external load. The values presented in column 7 in Table 3.4.4 strongly support this fact. For $k_\gamma = 35$ the oscillation frequency ratio f_{NL}/f_n of the impulse response is approximately 36% higher than the ratio of the response for the step excited system.

It should be noted here that the pattern for the multiple frequency response listed in the last column of Table 3.4.4, which is typical for nonlinear SDOF systems, is exactly the same as for the restoring force $f_1(u)$ in section 3.4.3.1 and is perfectly predicted by the analytical solution given in section 3.4.2.

For different values of the nonlinear stiffness ratio $k_\gamma = k_\beta/k_\alpha$ the absolute **displacement** of the freely vibrating, step and impulse excited SDOF's with $f_2(u)$ is given in Fig. 3.4.25 on page 117. Minimum and maximum values are given in Table 3.4.4. In contrast to the displacement response of the $f_1(u)$ system shown on page 112, there is virtually no difference in oscillation amplitude in the two graphs of free vibration and step excitation in Fig. 3.4.25(a) and (b). In case of impulse excitation, graph (c), the effect of growing absolute displacement amplitude u_{Ex} with increasing nonlinearity of the restoring stiffness force $f_1(u)$, as demonstrated in Fig. 3.4.20(c) on page 112, is reversed in Fig. 3.4.25(c). Increasing values of k_γ result in decreasing extreme values for the minimum and maximum displacement. This circumstance is due to the fact that $f_2(u)$ truly behaves like a 'stiffening' elastic force throughout the entire range of displacement $-\infty < u(t) < \infty$, i.e. larger values for the coefficients k_α, k_γ and the displacement give higher values for the restoring force. Furthermore, whereas for the restoring force $f_1(u)$ the extreme values of velocity decrease asymptotically with increasing nonlinear stiffness exponent b, see Fig. 3.4.21, $\dot{u}_{Ex}$ increases slightly as k_γ increases in Fig. 3.4.26 on page 118.

It is clear to see in all figures 3.4.25-3.4.29 that for weak nonlinearity of $f_2(u)$, e.g. $k_\gamma \leq 1$, the system behaves very similar in terms of the ratio of the minimum to maximum displacement/velocity and oscillation period as the linear SDOF obtained if $b = 1$ in $f_1(u)$.

Table 3.4.4: Nonlinear SDOF $f_2(u) = k_\alpha u + k_\beta u^3$: Extreme displacement $u_{\min}/u_{\max}$ and velocity $\dot{u}_{\min}/\dot{u}_{\max}$ are obtained from analytical and numerical calculations together with the first three fundamental nonlinear natural frequencies of the oscillator. The system properties are: natural frequency $f_n = 15.0\,\text{Hz}$, mass $m = 3.0\,\text{kg}$, $\omega_n = 2\pi f_n\,\text{rad/s}$, stiffness coefficient $k_\alpha = m\omega_n^2\,\frac{\text{N}}{\text{m}}$, $k_\beta = k_\alpha \times k_\gamma$. Applied load and initial conditions: $p_0 = 100.0\,\text{N}$, $u_0 = 0.15\,\text{m}$ and $\dot{u}_0 = 2.25\,\frac{\text{m}}{\text{s}}$.

Excitation Type	k_γ	Displacement $\frac{u_{\min}}{u_{\max}}$ analytical	Displacement $\frac{u_{\min}}{u_{\max}}$ numerical[b]	Velocity $\frac{\dot{u}_{\min}}{\dot{u}_{\max}}$ analytical	Velocity $\frac{\dot{u}_{\min}}{\dot{u}_{\max}}$ numerical[b]	Frequency[a] (Hz) 1	2	3	...	$f_{\text{NL},j} = j f_{\text{NL}}$ j
free	0.1	-1.51884E-01 1.51884E-01	-1.51884E-01 1.51884E-01	-1.43229E+01 1.43229E+01	-1.43229E+01 1.43229E+01	15.013	45.039	75.065	...	**1,3,5,...**
	0.9	-1.51850E-01 1.51850E-01	-1.51850E-01 1.51850E-01	-1.43856E+01 1.43856E+01	-1.43856E+01 1.43856E+01	15.116	45.349	75.581		
	8.5	-1.51584E-01 1.51584E-01	-1.51584E-01 1.51584E-01	-1.49678E+01 1.49678E+01	-1.49678E+01 1.49678E+01	16.055	48.167	80.278		
	35	-1.51056E-01 1.51056E-01	-1.51056E-01 1.51056E-01	-1.68409E+01 1.68409E+01	-1.68409E+01 1.68409E+01	18.911	56.735	94.559		
step	0.1	-1.44442E-01 1.51931E-01	-1.44442E-01 1.51931E-01	-1.39740E+01 1.39740E+01	-1.39740E+01 1.39740E+01	15.012	30.025	45.037	...	**1,2,3,...**
	0.9	-1.44536E-01 1.51896E-01	-1.44536E-01 1.51896E-01	-1.40382E+01 1.40382E+01	-4.21557E+00 1.40382E+01	15.111	30.222	45.333		
	8.5	-1.45297E-01 1.51617E-01	-1.45297E-01 1.51617E-01	-1.46342E+01 1.46342E+01	-1.46342E+01 1.46342E+01	16.016	32.031	48.047		
	35	-1.46846E-01 1.51071E-01	-1.46846E-01 1.51071E-01	-1.65451E+01 1.65451E+01	-1.65451E+01 1.65451E+01	18.818	37.636	56.454		
impulse	0.1	-4.04635E-01 4.04635E-01	-4.04635E-01 4.04635E-01	-3.82917E+01 3.82917E+01	-3.82917E+01 3.82917E+01	15.093	45.279	75.466	...	**1,3,5,...**
	0.9	-3.93099E-01 3.93099E-01	-3.93099E-01 3.93099E-01	-3.83152E+01 3.83152E+01	-3.83152E+01 3.83152E+01	15.761	47.284	78.807		
	8.5	-3.36100E-01 3.36100E-01	-3.36100E-01 3.36100E-01	-3.85376E+01 3.85376E+01	-3.85376E+01 3.85376E+01	19.602	58.807	98.012		
	35	-2.74096E-01 2.74096E-01	-2.74096E-01 2.74096E-01	-3.93030E+01 3.93030E+01	-3.93030E+01 3.93030E+01	25.620	76.861	128.102		

[a] Analytical and numerical computation gave identical results.

[b] All values were obtained using various adaptive Runge-Kutta algorithms as described in the text.

As documented by analytical results in Table 3.4.4, a rather significant increase of the nonlinear stiffness coefficient $k_\beta = k_\alpha \times k_\gamma$ from values of $0.1\,\mathrm{m}^{-2}$ to $35\,\mathrm{m}^{-2}$ results in an only small rise of the oscillation frequency f_{NL} if the system is either freely oscillating or excited by the step function as shown in Fig. 3.4.27(a) and 3.4.28(a) on page 119 and 120, respectively. For an impulse loaded SDOF increasing the nonlinear stiffness ratio k_γ gives a considerable higher increase of the oscillation frequency f_{NL}, see last main row in Table 3.4.4 and Fig. 3.4.29(a) on page 121.

In fact, the main difference in terms of oscillation frequency between the both SDOF systems either having $f_1(u)$ or $f_2(u)$ as nonlinear stiffness function is the fact that for increasing nonlinearity in $f_1(u)$, e.g. increasing values of b, the true oscillation frequency f_{NL} *falls* rapidly whereas increasing nonlinearity for $f_2(u)$ (increasing values for k_β, hence increasing ratio k_γ) means slight to moderate *increase* of f_{NL}. Nevertheless, as mentioned earlier, this observation for f_1 is entirely due to the resulting extreme values for the displacement, i.e. $|u_{\mathrm{Ex}}| < 1$, which are directly connected to the set of initial system parameters chosen herein.

However, the pattern of **multiple frequency response** with *odd* integer numbers for free and impulse vibration, and *even and odd* integer numbers for step excitation is preserved regardless of the type of nonlinear restoring forces, eg. $f_1(u)$ or $f_2(u)$, comparing Table 3.4.2 and 3.4.4.

3.5 Autonomous Nonconservative Systems

The most general form of the equation of motion for an autonomous nonconservative SDOF system is given by Eq.(3.2.2) on page 38. Assuming the nonlinear restoring force $f(\dot{u}, u)$ can be written as

$$f(\dot{u}, u) = f_{\mathrm{D}}(\dot{u}(t)) + f(u(t)) \tag{3.5.1}$$

where f_{D} denotes a dissipative damping force and f refers to the nonlinear elastic spring element. Thus, the energy balance for the SDOF at a point of maximum displacement u_{Ex} due to a step excitation is

$$\int_u f(u)\Big|_{u=u_{\mathrm{Ex}}} = p_0\,(u_{\mathrm{Ex}} - u_0) + \frac{m}{2}u_0^2 + \int_u f(u)\Big|_{u=u_0} + \Delta \mathrm{E}_{\mathrm{D}} \tag{3.5.2}$$

with $\Delta \mathrm{E}_{\mathrm{D}}$ as the amount of energy dissipated by the system during oscillation from an arbitrary point of displacement u_{arbitr}, i.e. the lower integration limits in Eq.(3.5.2), to the minimum/maximum value of displacement u_{Ex}. Due to energy dissipation the extreme displacement becomes a function of time, e.g. $u_{\mathrm{Ex}}(t)$. Together with (3.5.1) $\Delta \mathrm{E}_{\mathrm{D}}$ is given by

$$\Delta \mathrm{E}_{\mathrm{D}} = -\int_{u_{\mathrm{arbitr}}(t)}^{u_{\mathrm{Ex}}(t)} f_{\mathrm{D}}(\dot{u})\,\mathrm{d}u = -\int_{t_{\mathrm{arbitr}}}^{t_{\mathrm{Ex}}} f_{\mathrm{D}}(\dot{u})\,\dot{u}(t)\,\mathrm{d}t \tag{3.5.3}$$

with the minus sign indicating a loss of energy for the system and the appropriate time limits t_{Ex} and t_{arbitr} defined as $u(t_{\mathrm{Ex}}) = u_{\mathrm{Ex}}$ and $u(t_{\mathrm{arbitr}}) = u_{\mathrm{arbitr}}$, respectively. Hence, without the prior knowledge of $\dot{u}(t)$, and thus $u(t)$, Eq.(3.5.3) cannot be solved and the amount of energy lost by the SDOF moving from $u_{\mathrm{arbitr}}(t)$ to $u_{\mathrm{Ex}}(t)$ remains unknown. Therefore, both quantities velocity and displacement describing the nonlinear system's response have to be determined using approximate methods.

In general, approximation methods can be divided into two classes. The first, so called numerical procedures are standardised algorithms for solving single or multiple algebraic or differential equations using computational resources nowadays readily available. The Runge-Kutta integration scheme

introduced in section 3.4.3 is an example of such methods. If some insight into the character of the solution and its dependence on certain parameters is to be obtained, then numerical calculation must be repeated for many different parameter combinations. Due to the large amount of data obtained in this way, difficulties might arise to identify even relatively simple general relationships between system parameters.

The second type of non-closed-form solution approaches are so called analytical approximation methods, which make it possible to comprehend rather complex relationships approximately by means of much simpler analytical expressions. They often lead to easily manageable and useful results. Higher accuracy can be achieved by increasing the number of terms of an analytical approximation but can reduce the clarity of the result significantly.

However, pure numerical approaches are still very appropriate in obtaining reliable system response data since they rely on proven and tested algorithms established in various research fields for many years. Furthermore, results obtained can be useful to understand both the basic overall behaviour and possible tendencies of the system's response which in turn can be useful in deciding the type and nature of possible analytical approximations.

One of the earliest analytical approximation methods for elastic, nonlinear stiffness forces in mechanical oscillators, and in these days by far the most suitable, is the bilinear solution procedure proposed by ERGIN [35]. The nonlinear restoring force is approximated by a bilinear characteristic expressing the force-displacement relationship subjected to the condition that the mean square error between the two is a minimum. A special case of this general spring-mass system problem has been solved by THOMSON [36]. The restoring force contributing element is assumed to have a constant stiffness for a certain range of deformation. Beyond this pre-defined range of displacement the restoring force-displacement relationship is declared to be invalid. With the method given in [35] the normalised peak response of the system can be found by solving two linear algebraic equations resulting from the two slopes of the two segments of the bilinear characteristic. This leads only to a maximum response spectrum if the first peak of the displacement-time history for each (linear) natural frequency of the system corresponds to the overall maximum response. This is the case for nonlinear SDOF systems, damped or undamped, with a hardening type restoring force characteristic when subjected to step, delta or rectangular pulse function excitation [8]. It is easy to understand that for any other arbitrary type of pulse shape applied to the system the shock spectra obtained in [35] will only be of use if the duration of the pulse is less than the time period the system needs to reach the first maxima. All subsequent peaks will then be either of same amplitude, as in the case for a nonconservative system, or smaller, if the system is dissipative.

The following two subsections present time and frequency domain analyses of dissipative SDOF oscillators with the two nonlinear restoring forces $f_1(u)$ and $f_2(u)$ as introduced in section 3.4. For the sake of simplicity the damping force $f_D(\dot{u})$ is assumed to be linear and of viscous nature [37] with a damping coefficient identical to linear systems

$$f_D = c\dot{u}(t). \tag{3.5.4}$$

All results obtained were derived using the adaptive algorithm presented in 3.4.3 on page 82. The set of first-order differential equations has now to account for the damping force and Eq.(3.4.110a) is

rewritten as

$$\begin{aligned} \dot{z}_1 &= z_2\,, \\ \dot{z}_2 &= \frac{1}{m}\left[p_0 - c z_2 - f(z_1)\right] \end{aligned} \tag{3.5.5}$$

subjected to the same initial conditions introduced in (3.4.110b).

After calculating the time-domain response of the system, $u(t)$ and $\dot{u}(t)$ respectively, the displacement data is used to obtain the frequency spectra of the nonlinear oscillation. Starting at $t = 0$ a distinctive number of n data points $u_1 = u(t = 0) \ldots u_n = u(t = t_n)$ is selected, multiplied by a windowing function $w(t)$ and transformed into the frequency domain using discrete Fourier transformation (DFT) in its most efficient implementation as fast Fourier transform (FFT), see [34]. This gives the frequency response of the system for the windowed time interval $0 \leq t \leq t_n$. In the next step the selection of the same number of n data points starts at $u_2 = u(t = \Delta t)$ and includes $u_{n+1} = u(t = t_n + \Delta t)$ where $1/\Delta t$ is the sampling frequency of the signal, i.e. the FFT window frame moves one data point for each transformation.

The unevenly spaced time domain signal was re-sampled with $1/\Delta t = 500\,\mathrm{Hz}$ since the frequencies of interest ranged from zero to about 150 Hz. It is a known phenomena that increasing the sampling frequency only results in capturing higher harmonics of the oscillation whereas the frequency resolution depends on the length of the sample. This is especially important for transient non-stationary oscillation signals such as the response of damped nonlinear oscillators due to the trade-off between determining the exact frequency f_{NL} of the system at an arbitrary time point t_j and its resolution. For the results presented in what follows a sampling frequency of 500 Hz gives $\Delta t = 0.002\,\mathrm{s}$ which leads with a defined number of $n = 512$ data points to time frames of $t_n = 1.002\,\mathrm{s}$. Each of these frames was multiplied by a specific windowing function and a FFT was performed. In an additional third step, in order to improve the quality of the graphical presentation, the two dimensional spectral data was interpolated using cubic splines [34].

3.5.1 Restoring Force $f_1(u) = k\,\mathrm{sign}(u)\,|u|^b$

The combined restoring force of the oscillator comprises now of the nonlinear elastic stiffness force $f_1(u) = k\,\mathrm{sign}(u)\,|u|^b$ and the linear viscous damping force from Eq.(3.5.4). Due to the dissipation of energy during the oscillation the amplitudes of displacement $u(t)$ and velocity $\dot{u}(t)$ steadily decrease until the system comes fully to rest for $t \to \infty$, as shown in figure 3.5.1(a) on page 122 for a p_0-scaled Dirac impulse excitation with initial conditions as $u_0 = 0.15\,\mathrm{m}$ and $\dot{u}_0 = 2.25\,\mathrm{m/s}$. Therefore, as mentioned earlier in this chapter, the nonlinear oscillation frequency f_{NL} changes constantly with time.

Using the previously described method of spectral analysis results in the two-dimensional contour plot presented in Fig. 3.5.1(c). As indicated by results obtained in previous sections, the response frequencies $f_{\mathrm{NL},j}$ are multiples of f_{NL} with $j = 3, 5, 7, \ldots$ for the case of impulse excitation. The system pictured in Fig. 3.5.1 has a quadratic nonlinear restoring force ($b = 2$) and the properties were selected to be identical to the oscillators given in section 3.4. Hence, comparing the results listed in Table 3.4.2 on page 85 with the values for extreme displacement and oscillation frequency in Fig. 3.5.1 at $t = 0$ shows good agreement. As can be seen in graph 3.5.1(b), the response frequencies for the first time frame $0 \leq t \leq 1.022\,\mathrm{s}$ are slightly lower than to the ones given in Table 3.4.2, which can be ascribed to

two effects independent of each other. First, due to the presence of damping the oscillation frequency is smaller than for the undamped system. Second, recalling the inverse problem of sample length and frequency resolution explained above, the spectra gives the *average* oscillation frequency $\overline{f_{\mathrm{NL}}}$ over a certain time interval, here $0 \leq t \leq 1.022\,\mathrm{s}$, which will be, in case of positive damping[18] always be smaller than the actual frequency f_{NL}. Furthermore, due to the same problem, the main slopes in Fig. 3.5.1 are wider than the ones given for conservative systems in section 3.4. For the latter, sampling lengths are orders of magnitude larger than for the non-steady-state damped system resulting in sharp and distinctive peaks for the multiple oscillation frequencies results.

The spectrum in graph (c) of Fig. 3.5.1 clearly indicates what the time history in picture (a) already suggests: with decreasing amplitude as $t \to 0$ the higher harmonics start to vanish and the system oscillates with one or at most two closely spaced frequencies.

Figure 3.5.2 on page 123 shows the time history of displacement and frequency content for exactly the same SDOF system. The excitation force is now a Heaviside step function with amplitude p_0 rather than a Dirac impulse. The displacement $u(t)$ in picture (a) is given in its non-normalised form and the change of the equilibrium position of the SDOF mass is clearly visible. Minimum and maximum values are $-0.105\,\mathrm{m}$ and $0.1636\,\mathrm{m}$, respectively, which is, considered the rather modest damping of $\zeta = 0.5\%$, in perfect agreement with the results given in Table 3.4.2 on page 85. The first three nonlinear oscillation frequencies for the conservative system are $5.191\,\mathrm{Hz}$, $10.382\,\mathrm{Hz}$ and $15.573\,\mathrm{Hz}$. Comparing these values with graph (b) on page 123 shows that for a lightly damped system the formulas derived in this chapter for undamped nonlinear oscillator are still very useful, bearing in mind that additional deviations introduced into Fig. 3.5.2(b) and (c) originate from the afore mentioned frequency resolution problem of the Fourier transform. A rather noticeable first peak occurs in both graphs, (b) and (c), at a frequency of about $0.35\,\mathrm{Hz}$, which represents an underlying oscillation as the system shifts from the old to new equilibrium position.

The major difference between both spectra, Fig. 3.5.2(c) and 3.5.1(c), is revealed in the nature of the multi-frequency response. In case of impulse excitation the well separated frequencies

$$f_{\mathrm{NL},\frac{1}{2}(j+1)} = j \times f_{\mathrm{NL}}, \quad (j = 3,5,\ldots)$$

decay constantly over time until the system stops oscillating where they reach zero. From zero to almost $15\,\mathrm{s}$, slightly over half the entire recorded time interval, about 6 to 7 single frequencies contribute to the systems periodic deformation. Five seconds later, at $t = 20\,\mathrm{s}$, only two almost coinciding frequencies are remaining, $f_{\mathrm{NL},1}$ and $f_{\mathrm{NL},2}$, respectively. With the frequency resolution chosen for the FFT they are hardly distinguishable. The displacement history in graph 3.5.1(a) indicates that at this point of time the SDOF mass is nearly at rest, the oscillation dies away and hence the frequency (or frequencies) approach zero.

Contrary, for the oscillating SDOF with exactly the same system properties, a step excitation results in response behaviour with nearly constant frequencies $f_{\mathrm{NL},j} = j \times f_{\mathrm{NL}}$, $(j = 2,3,\ldots)$ whose participation on the oscillators total response vanish as $t \to \infty$. Referring to Fig. 3.5.1, at $t = 10\,\mathrm{s}$ the

[18]The term 'positive damping' defines the most common case in nature where the damping force f_{D} constantly opposes the time-varying displacement $u(t)$ and acts in line with the restoring stiffness force. Hence the oscillating system dissipates energy. Contrary, the case where damping counteracts the restoring force, i.e. the system gains energy with each cycle, is called 'negative damping'. An example for the latter is the aerodynamic flutter phenomena, which can lead to instable and chaotic response behaviour.

mass moves with only a single frequency of $f_{NL,1} \approx 5\,Hz$. A direct comparison between the two displacement-time histories in 3.5.1 and 3.5.2 supports the fact suggested by the spectra that, despite decreasing amplitude for both cases, the impulse forced system increases oscillation period $1/f_{NL}$ as t progresses, whereas for the step excited system the oscillation frequency stays virtually constant.

3.5.2 Restoring Force $f_2(u) = k_\alpha u + k_\beta u^3$

A numerical model for a viscously damped Duffing-type oscillator subjected to impulse and step force functions produces time-displacement graphs and frequency spectra as given in Fig. 3.5.3 and 3.5.4. The system properties are similar to the ones given in the previous section 3.5.1. A linear oscillation frequency was defined as $f_n = 15\,Hz$ from which the linear circular frequency $\omega_n = 2\pi f_n$ and the linear stiffness $k_\alpha = m\omega_n^2$ with $m = 3.0\,kg$ have been calculated. The ratio $k_\gamma = k_\beta / k_\alpha$ was set to $8.5\,m^{-2}$ in order to allow for direct comparisons with results from section 3.4.2 on page 70. Furthermore, the initial conditions $u_0 = 0.15\,m$ and $\dot{u}_0 = 2.25\,m/s$ were kept unchanged.

Both graphs of the Fourier transforms of the first time block of displacement data, picture (b) in Fig. 3.5.3 and 3.5.4, respectively, match expectations very well compared to the values given in table 3.4.4 on page 88, section 3.4.2. In each plot for the nonconservative system there are three distinctive peaks at frequencies well below $f_{NL,j} = j \times f_{NL}$ with either $(j = 3,5,\ldots)$ or $(j = 2,3,\ldots)$ as given for the conservative system on page 88. Due to a change of equilibrium position the step excited SDOF exhibits a typical peak at an unrelated frequency of about 0.22 Hz. Again, all frequencies given in the spectra of both figures on pages 124 and 125 are only *average* frequencies over the fixed number of n time points.

In general, the excitation function seems to have less influence on the Duffing-type SDOF system's response behaviour in its given configuration with the parameter from above. One reason, probably the most significant, is the rather low ratio of nonlinear/linear stiffness coefficients $k_\gamma = k_\beta / k_\alpha = 8.5\,m^{-2}$. For values of k_γ orders of magnitude higher the influence of the linear part of the stiffness force vanishes and the SDOF is purely nonlinear with a behaviour similar to what has been shown in section 3.5.1[19]. A second reason is identified as the presence and nature of initial conditions. Different values for u_0 and $\dot{u}_0$ can lead to a significant different time-displacement history, e.g. higher or lower equilibrium shift for step excitation, and hence to entirely different spectra.

[19] In case of a polynomial-type nonlinear elastic restoring force with only one term in the polynomial, such as $f_1(u) = k\,\mathrm{sign}(u)\,|u|^b$, the tendency of dynamic response behaviour of autonomous systems with different exponents b is similar for successive, close spaced values of b.

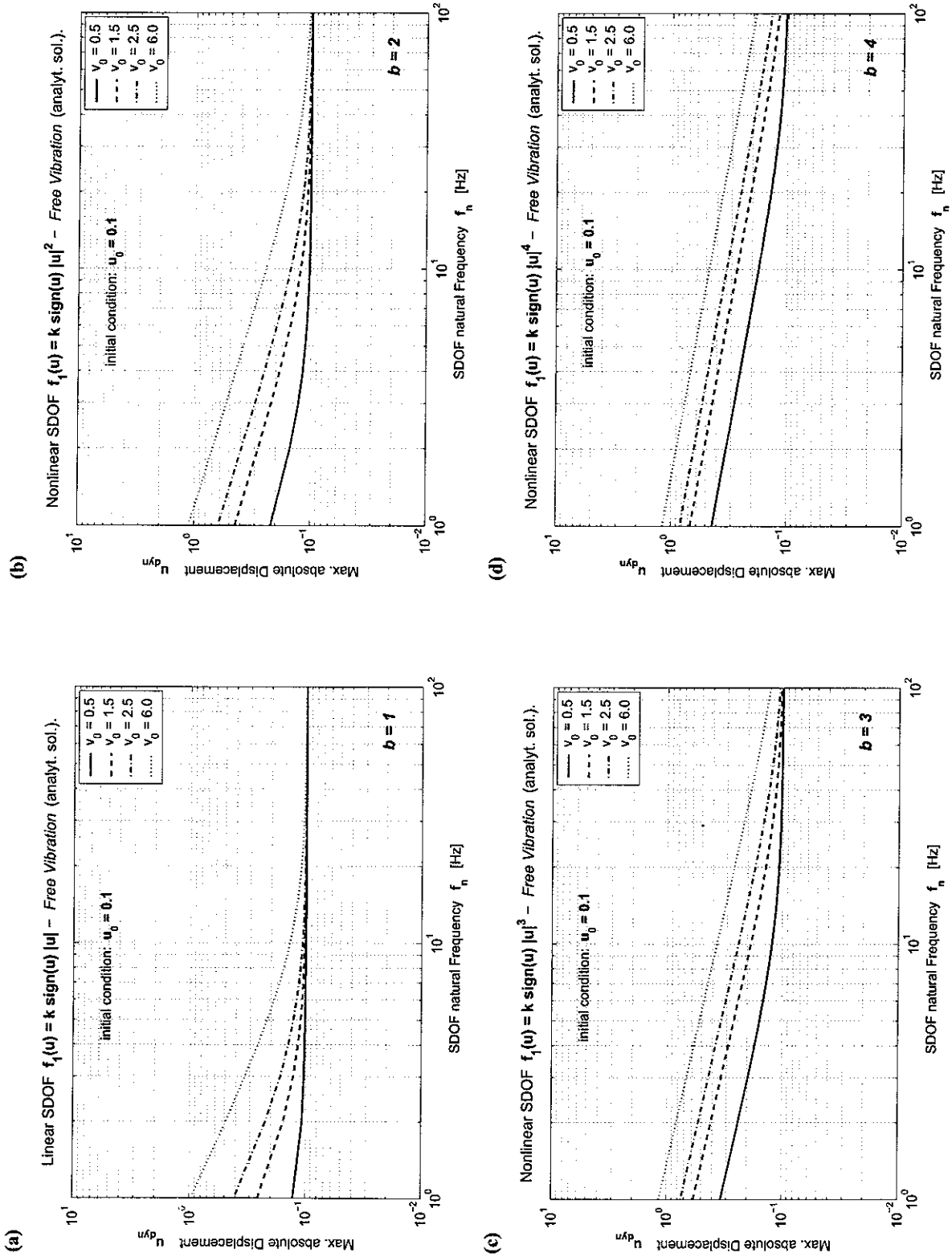

Figure 3.4.2: Nonlinear SDOF system oscillator $f_1(u) = k\,\mathrm{sign}(u)\,|u|^b$ - *Free Vibration:* Maximum absolute displacement for different values of iv_0 and b with $u_0 = 0.1$ m ($k = m\omega_n^2 \frac{\mathrm{N}}{\mathrm{m}^b}$, $\omega_n = 2\pi f_n \frac{\mathrm{rad}}{\mathrm{s}}$ and $m = 1$ kg).

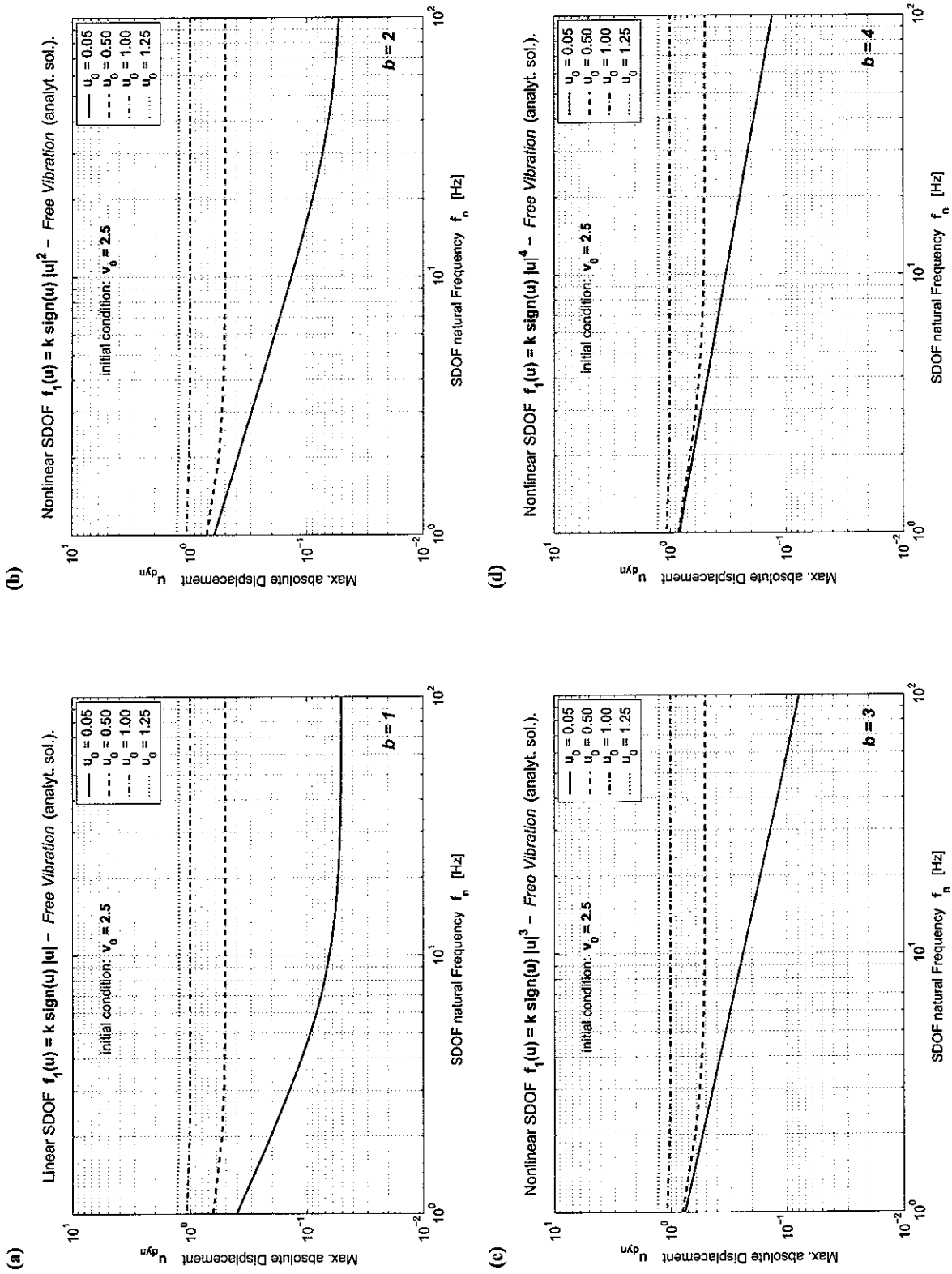

Figure 3.4.3: Nonlinear SDOF system oscillator $f_1(u) = k\,\mathrm{sign}(u)\,|u|^b$ - *Free Vibration*: Maximum absolute displacement for different values of u_0 and b with $\dot{u}_0 = v_0 = 2.5\,\frac{\mathrm{m}}{\mathrm{s}}$ ($k = m\omega_n^2\,\frac{\mathrm{N}}{\mathrm{m}^b}$, $\omega_n = 2\pi f_n\,\frac{\mathrm{rad}}{\mathrm{s}}$ and $m = 1\,\mathrm{kg}$).

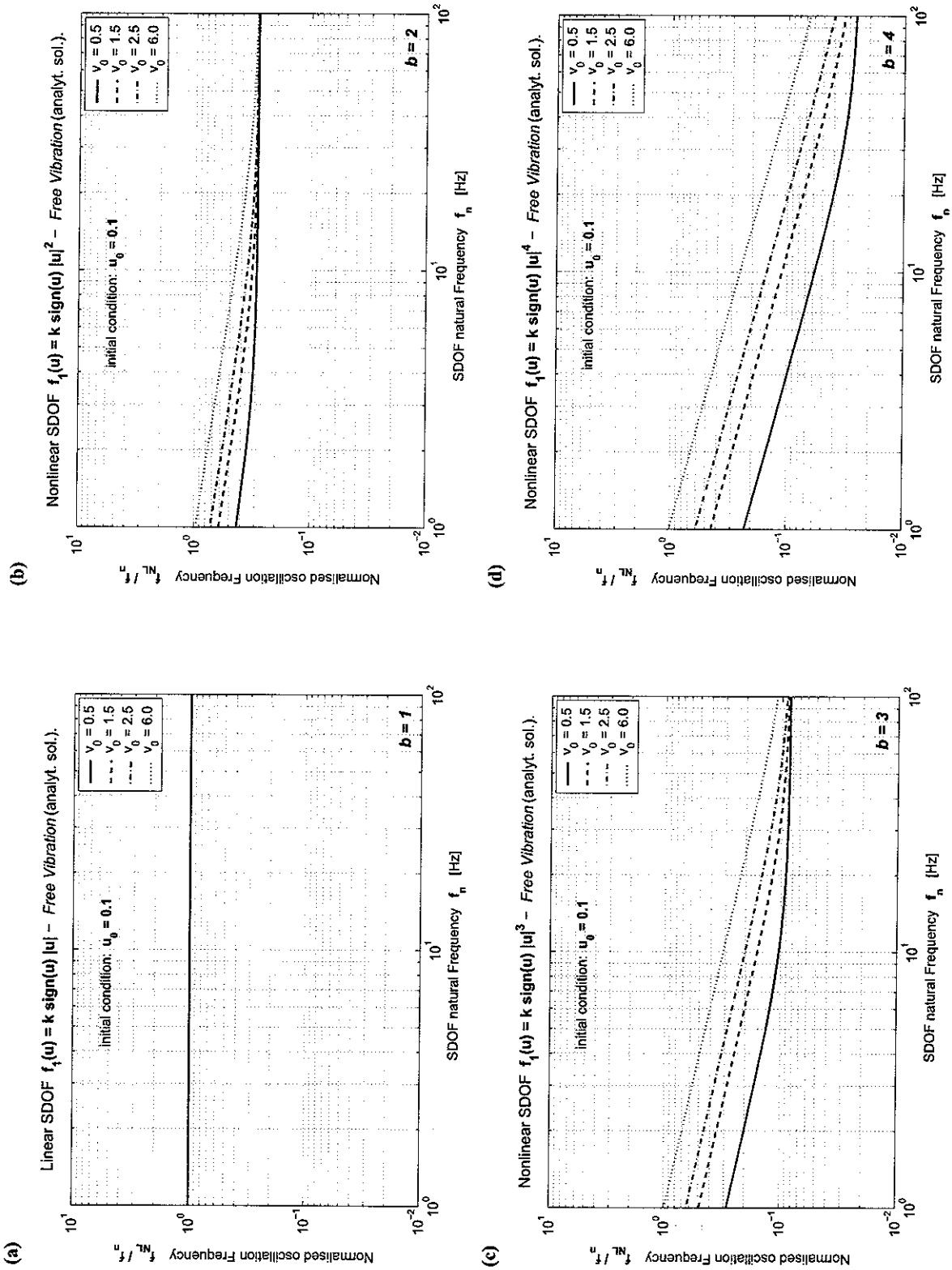

Figure 3.4.4: Nonlinear SDOF system oscillator $f_1(u) = k\ \mathrm{sign}(u)\ |u|^b$ - *Free Vibration*: Nonlinear oscillation frequency $f_{\mathrm{NL}} = \frac{1}{0.T_1}$ for different values of u_0 and b with $u_0 = 0.1\,\mathrm{m}$, $k = m\omega_n^2 \frac{\mathrm{N}}{\mathrm{m}^b}$, $\omega_n = 2\pi f_n \frac{\mathrm{rad}}{\mathrm{s}}$ and $m = 1\,\mathrm{kg}$.

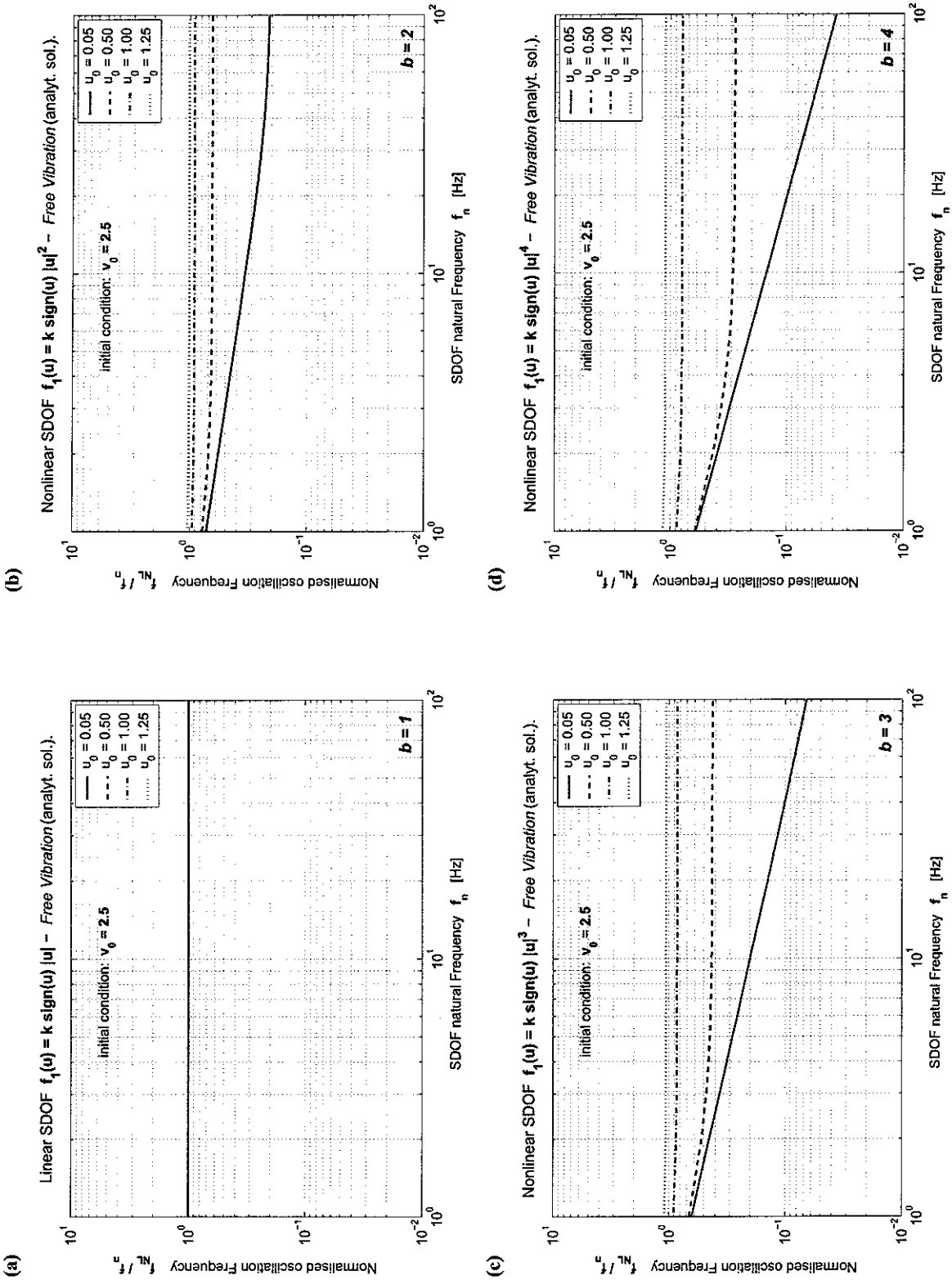

Figure 3.4.5: Nonlinear SDOF system oscillator $f_1(u) = k\,\mathrm{sign}(u)\,|u|^b$ - *Free Vibration:* Nonlinear oscillation frequency $f_{\mathrm{NL}} = \frac{1}{{}_0T_{f_1}}$ for different values of u_0 and b with $\dot{u}_0 = v_0 = 2.5\,\frac{\mathrm{m}}{\mathrm{s}}$ ($k = m\omega_n^2\,\mathrm{N}\,m^b$, $\omega_n = 2\pi f_n\,\frac{\mathrm{rad}}{\mathrm{s}}$ and $m = 1\,\mathrm{kg}$).

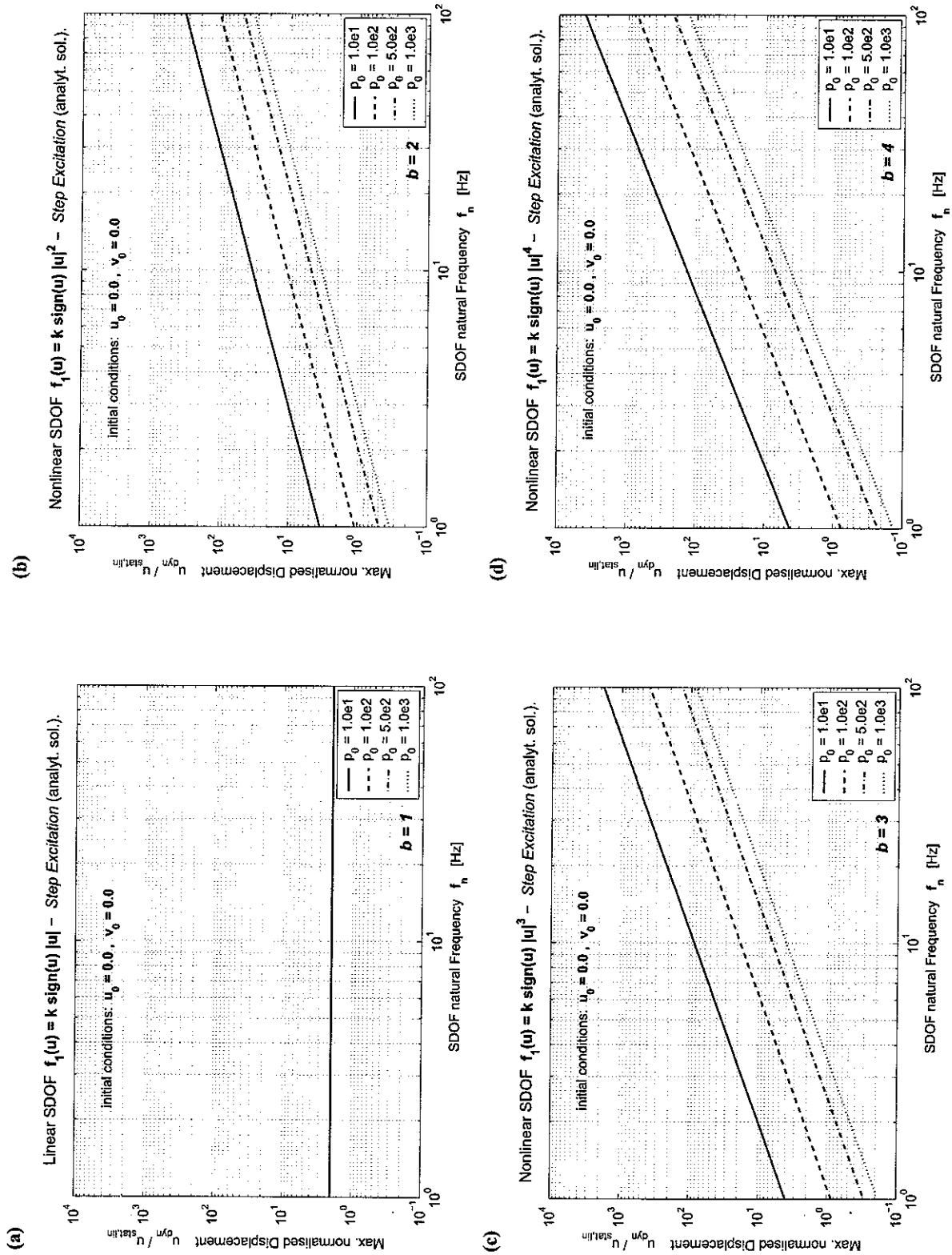

Figure 3.4.6: Nonlinear SDOF system oscillator $f_1(u) = k\,\mathrm{sign}(u)\,|u|^b$ - *Step Excitation:* Maximum normalised displacement for different values of p_0 (in N) and b with $u_0 = \dot{u}_0 = 0.0$ ($k = m\omega_n^2 \frac{\mathrm{N}}{\mathrm{m}^b}$, $\omega_n = 2\pi f_n \frac{\mathrm{rad}}{\mathrm{s}}$ and $m = 1\,\mathrm{kg}$).

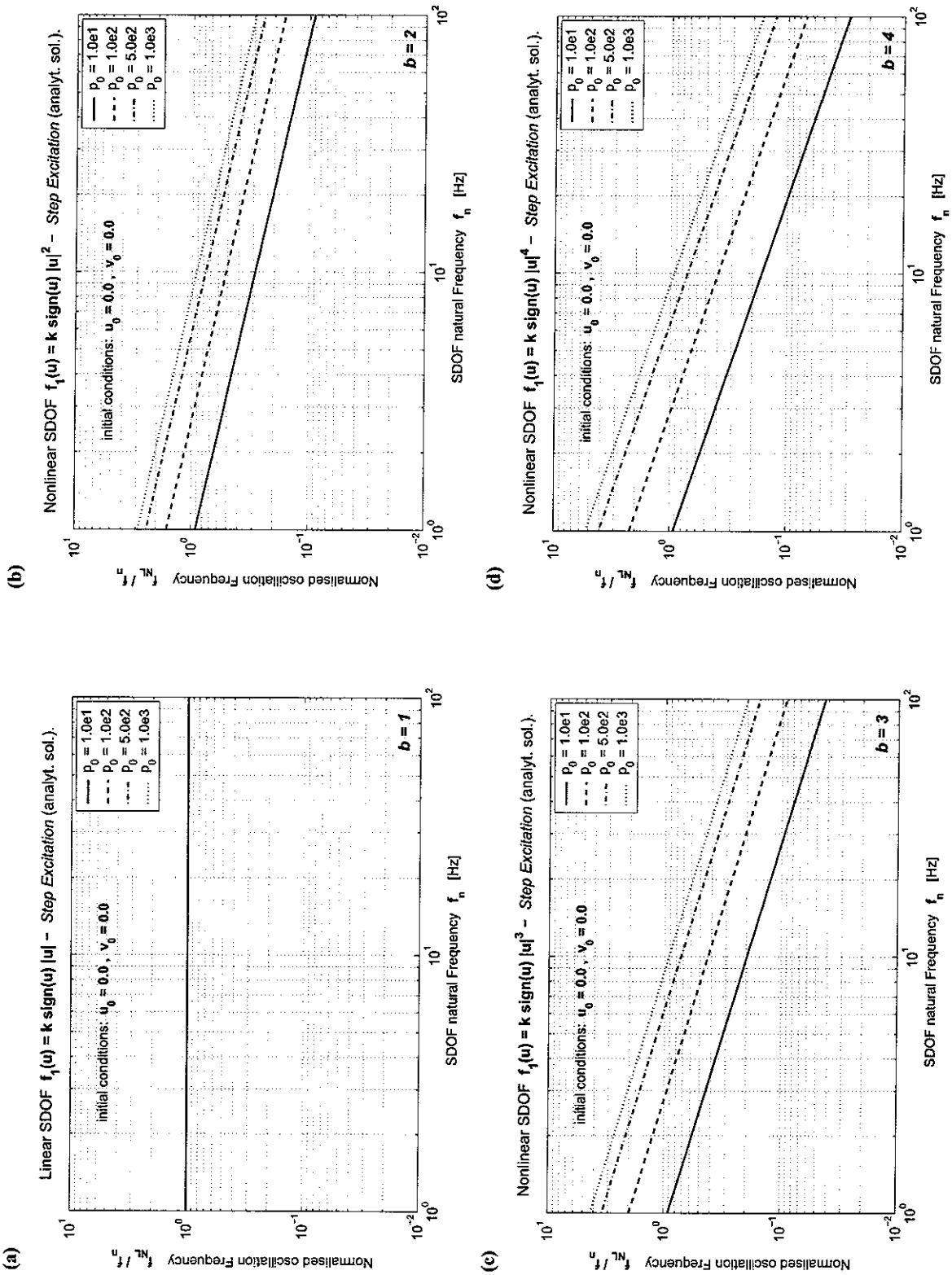

Figure 3.4.7: Nonlinear SDOF system oscillator $f_1(u) = k\ \mathrm{sign}(u)\ |u|^b$ - *Step Excitation:* Nonlinear oscillation frequency $f_{\mathrm{NL}} = \frac{1}{\mathrm{H}\,T_{f_1}}$ for different values of p_0 (in N) and b with $u_0 = \dot{u}_0 = 0.0$ ($k = m\omega_n^2\,\frac{\mathrm{N}}{\mathrm{m}^b}$, $\omega_n = 2\pi f_n\,\frac{\mathrm{rad}}{\mathrm{s}}$ and $m = 1\,\mathrm{kg}$).

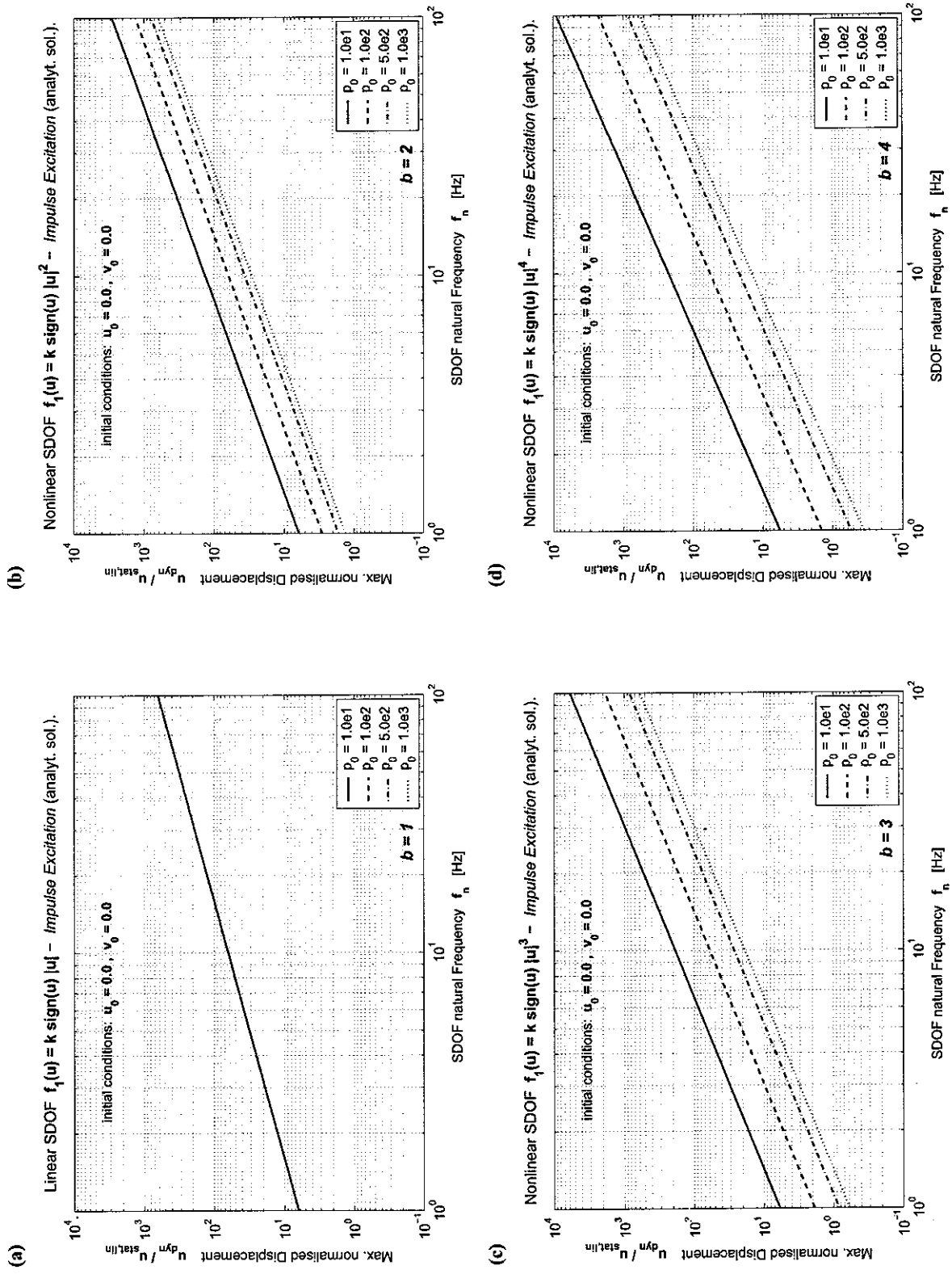

Figure 3.4.8: Nonlinear SDOF system oscillator $f_1(u) = k\,\mathrm{sign}(u)\,|u|^b$ - *Impulse Excitation*: Maximum normalised displacement for different values of p_0 and b with $u_0 = v_0 = \dot{u}_0 = 0.0$ ($k = m\omega_n^2$, $\omega_n = 2\pi f_n$ and $m = 1$).

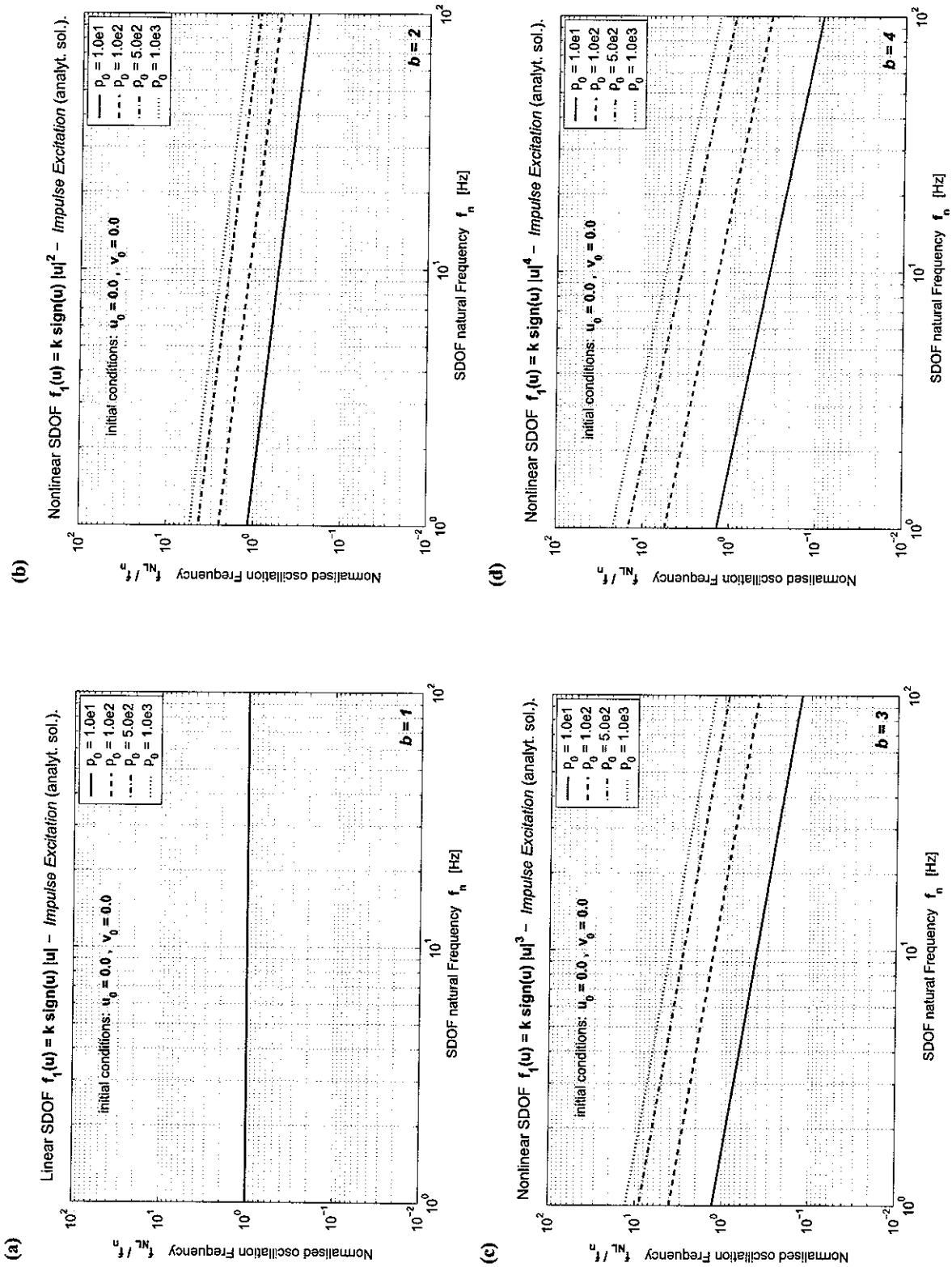

Figure 3.4.9: Nonlinear SDOF system oscillator $f_1(u) = k\,\mathrm{sign}(u)\,|u|^b$ - *Impulse Excitation:* Nonlinear oscillation frequency $f_{\mathrm{NL}} = \frac{1}{\delta T_{f_1}}$ for different values of p_0 and b with $u_0 = v_0 = \dot{u}_0 = 0.0$ ($k = m\omega_n^2$, $\omega_n = 2\pi f_n$ and $m = 1$).

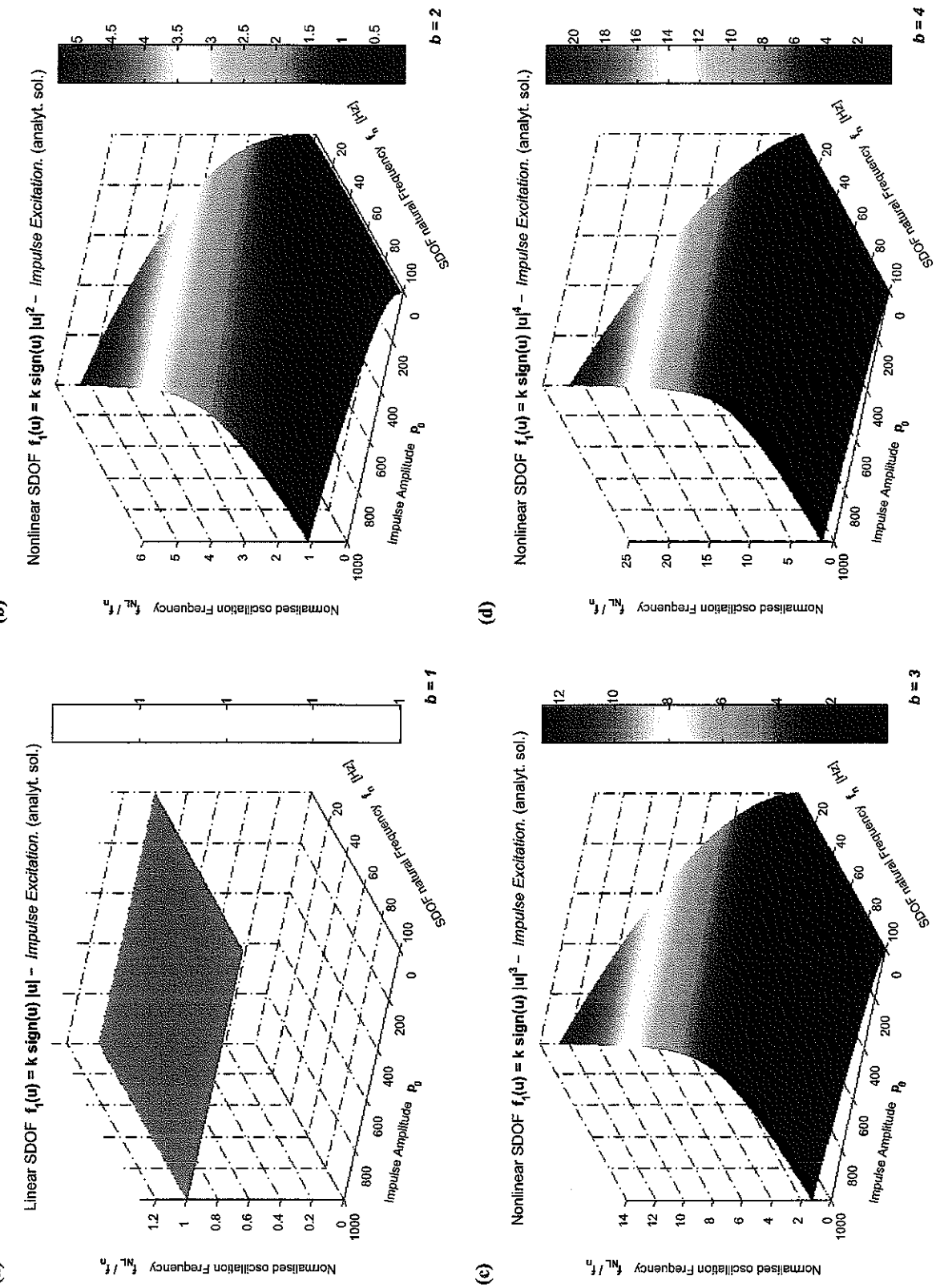

Figure 3.4.10: Nonlinear SDOF system oscillator $f_1(u) = k\,\mathrm{sign}\,(u)\,|u|^b$ - *Impulse Excitation:* Nonlinear oscillation frequency $f_{\mathrm{NL}} = \frac{1}{8T_1}$ as a function of the systems natural frequency f_n and the applied load magnitude p_0 for different values of b with $u_0 = v_0 = \dot{u}_0 = 0.0$ ($k = m\,\omega_n^2\,\frac{\mathrm{N}}{\mathrm{m}^b}$, $\omega_n = 2\pi f_n\,\frac{\mathrm{rad}}{\mathrm{s}}$ and $m = 1\,\mathrm{kg}$).

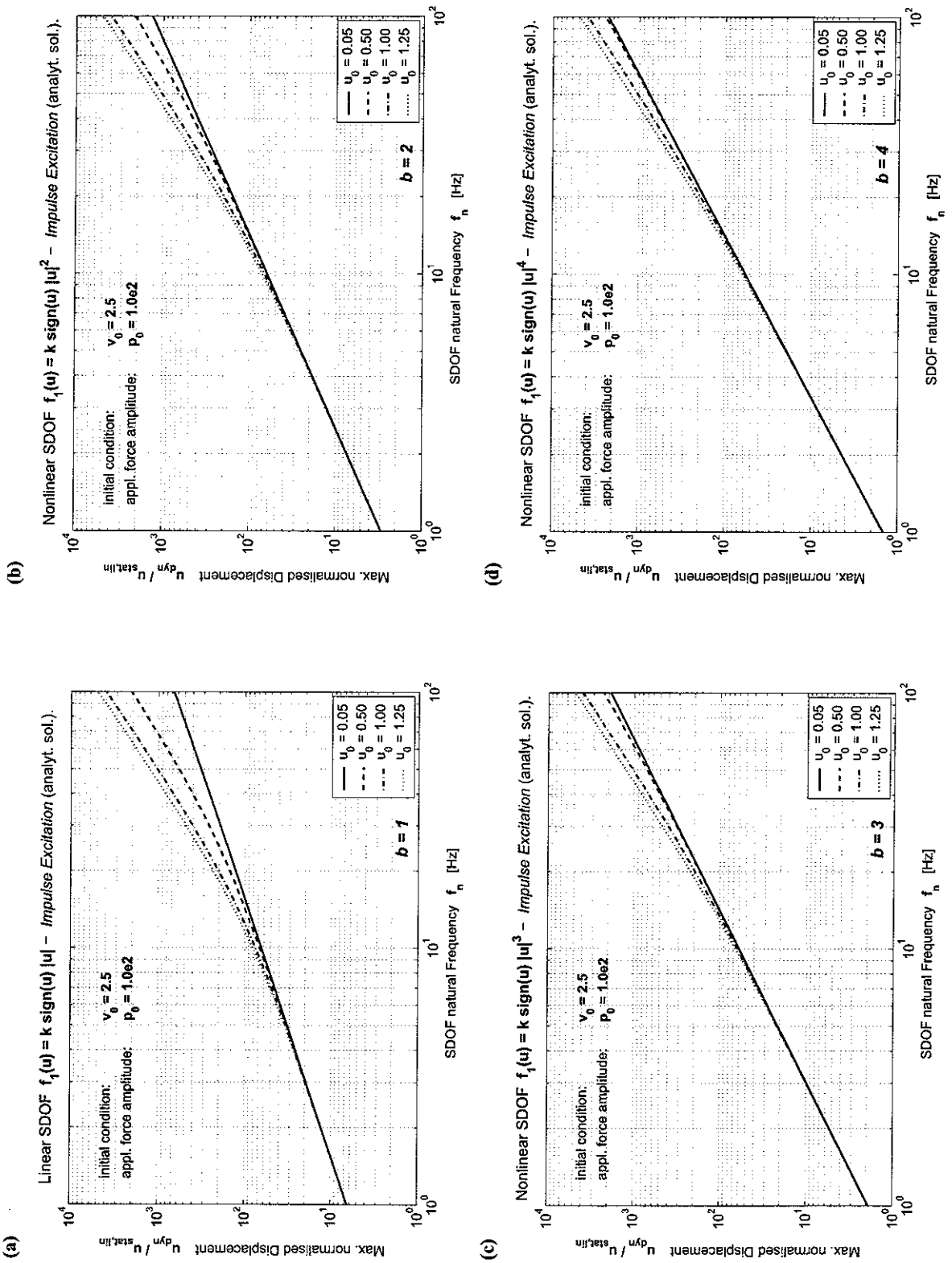

Figure 3.4.11: Nonlinear SDOF system oscillator $f_1(u) = k\,\mathrm{sign}(u)\,|u|^b$ - *Impulse Excitation*: Maximum normalised displacement for different values of u_0 and b with $\dot{u}_0 = v_0 = 2.5\,\frac{\mathrm{m}}{\mathrm{s}}$ and $p_0 = 100.0\,\mathrm{N}$ ($k = m\omega_n^2\,\frac{\mathrm{N}}{\mathrm{m}^b}$, $\omega_n = 2\pi f_n\,\frac{\mathrm{rad}}{\mathrm{s}}$ and $m = 1\,\mathrm{kg}$).

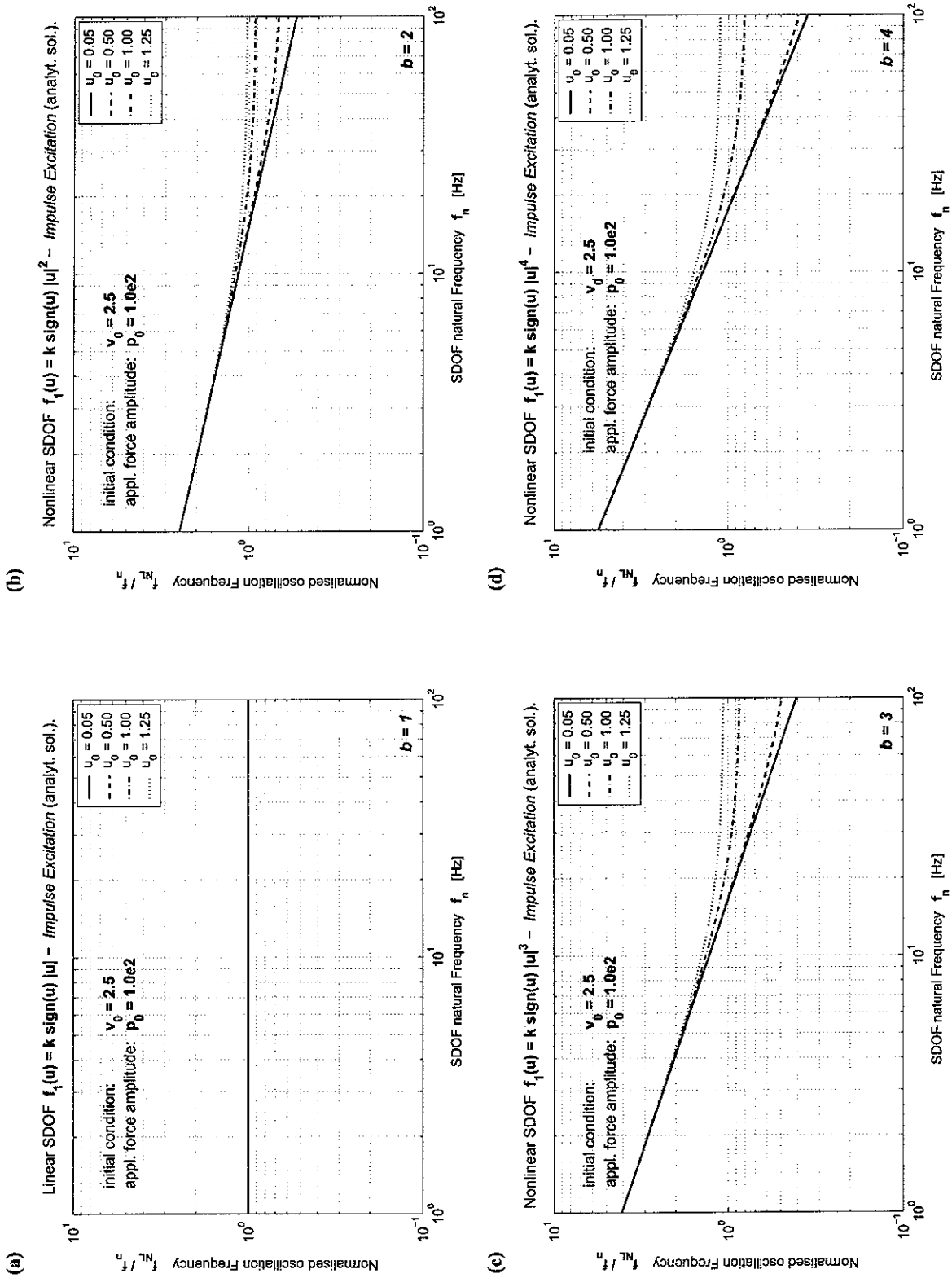

Figure 3.4.12: Nonlinear SDOF system oscillator $f_1(u) = k\,\mathrm{sign}(u)\,|u|^b$ - *Impulse Excitation:* Nonlinear oscillation frequency $f_{\mathrm{NL}} = \frac{1}{\delta T_1}$ for different values of u_0 and b with $\dot{u}_0 = v_0 = 2.5\,\frac{\mathrm{m}}{\mathrm{s}}$ and $p_0 = 100.0\,\mathrm{N}$ ($k = m\omega_n^2\,\frac{\mathrm{N}}{\mathrm{m}^b}$, $\omega_n = 2\pi f_n\,\frac{\mathrm{rad}}{\mathrm{s}}$ and $m = 1\,\mathrm{kg}$).

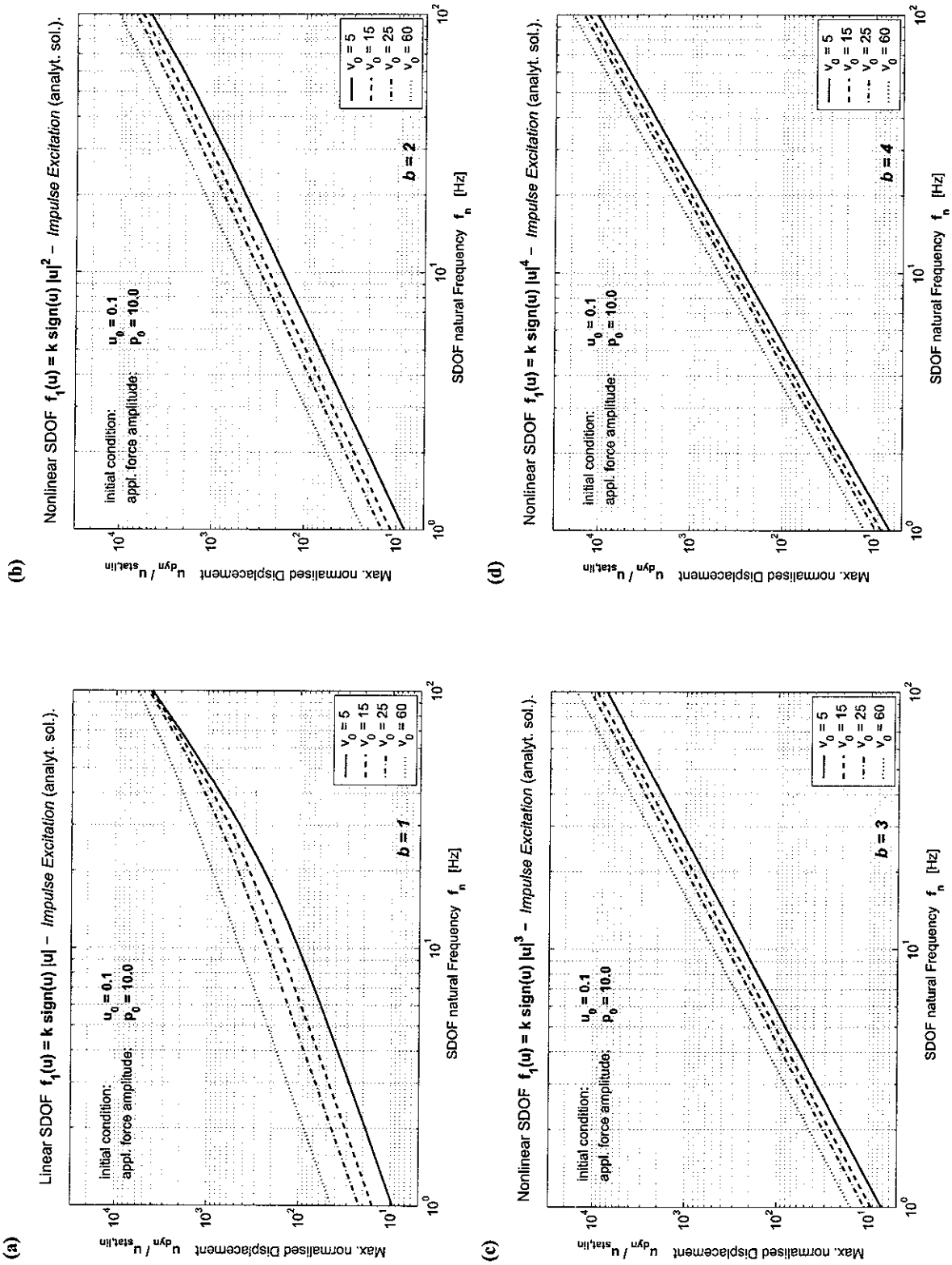

Figure 3.4.13: Nonlinear SDOF system oscillator $f_1(u) = k\,\mathrm{sign}(u)\,|u|^b$ - *Impulse Excitation*: Maximum normalised displacement for different values of v_0 and b with $u_0 = 0.1\,\mathrm{m}$ and $p_0 = 10.0\,\mathrm{N}$ ($k = m\omega_n^2\,\frac{\mathrm{N}}{\mathrm{m}^b}$, $\omega_n = 2\pi f_n\,\frac{\mathrm{rad}}{\mathrm{s}}$ and $m = 1\,\mathrm{kg}$).

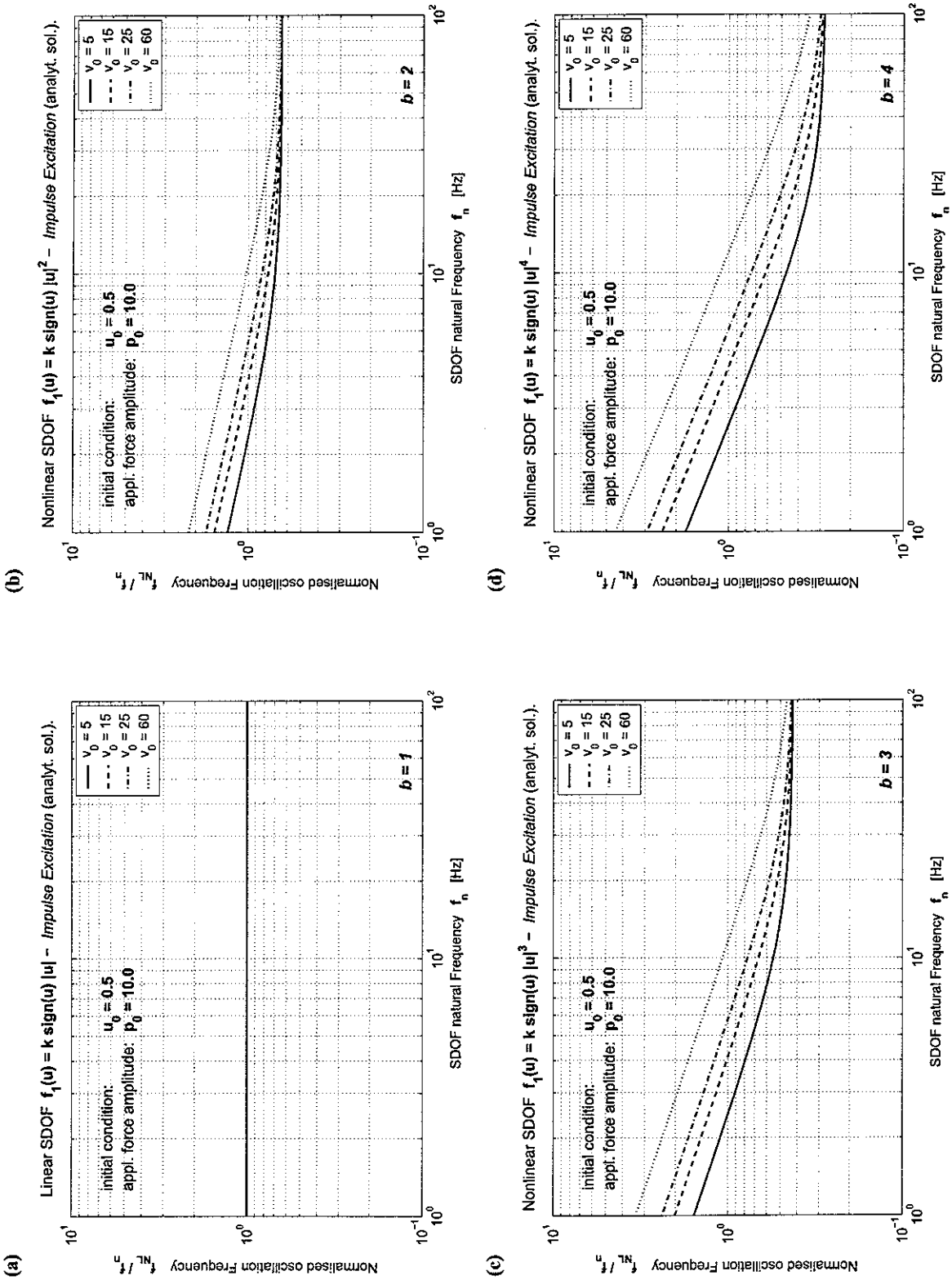

Figure 3.4.14: Nonlinear SDOF system oscillator $f_1(u) = k\,\mathrm{sign}(u)\,|u|^b$ - *Impulse Excitation:* Nonlinear oscillation frequency $f_{\mathrm{NL}} = \frac{1}{\delta T_1}$ for different values of v_0 and b with $u_0 = 0.5\,\mathrm{m}$ and $p_0 = 10.0\,\mathrm{N}$ ($k = m\omega_n^2\,\frac{\mathrm{N}}{\mathrm{m}^b}$, $\omega_n = 2\pi f_n\,\frac{\mathrm{rad}}{\mathrm{s}}$ and $m = 1\,\mathrm{kg}$).

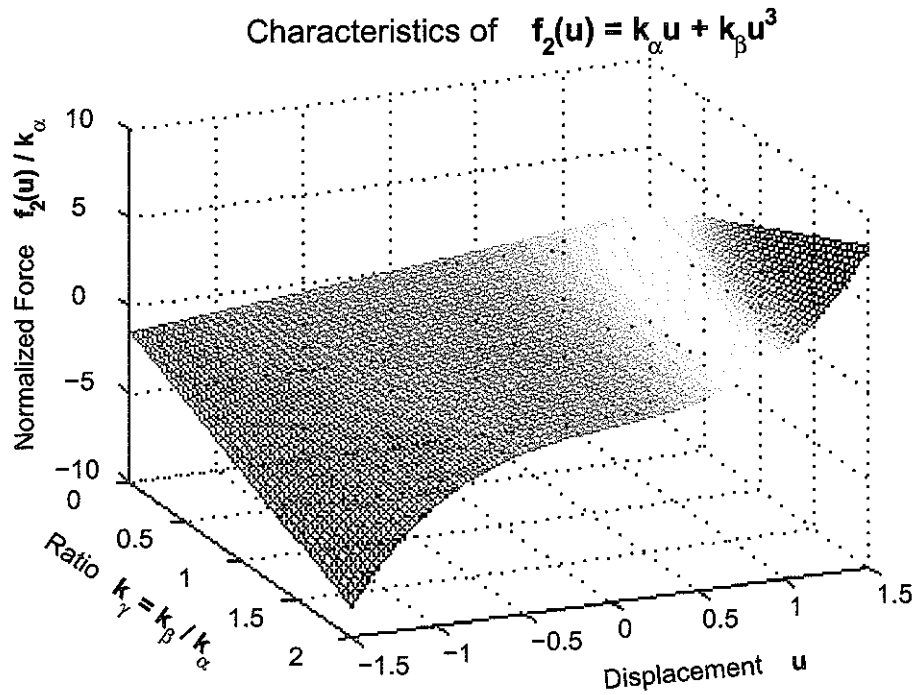

Figure 3.4.15: Normalised nonlinear restoring force characteristics $f_2(u) = k_\alpha u + k_\beta u^3$ for different values of the stiffness coefficient ratio $k_\gamma = \frac{k_\beta}{k_\alpha}$.

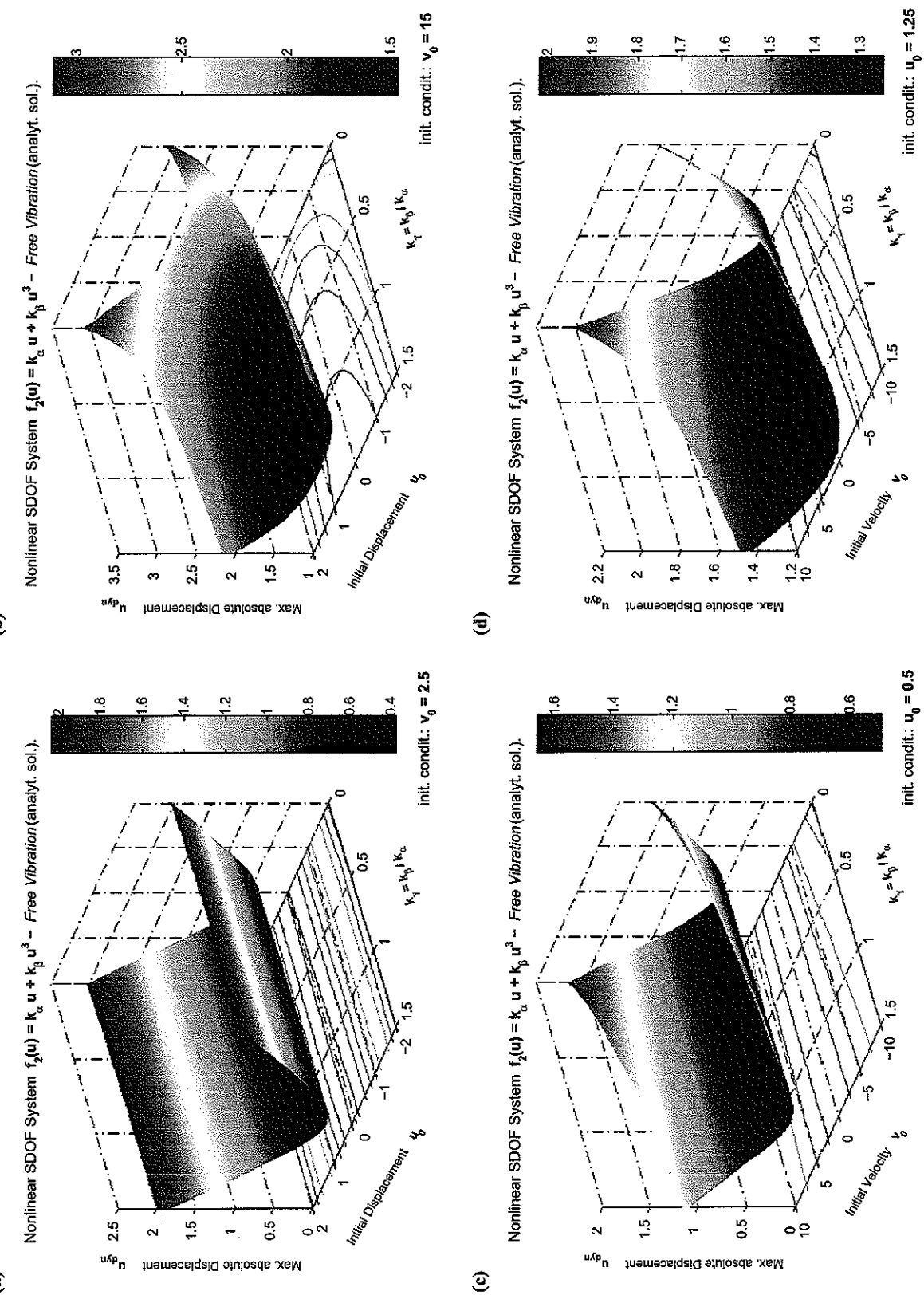

Figure 3.4.16: Nonlinear SDOF system oscillator $f_2(u) = k_\alpha u + k_\beta u^3$ - *Free Vibration:* Maximum absolute displacement as a function of the system's initial conditions u_0 and v_0. ($k_\alpha = m\omega_{n,\alpha}^2$, $\omega_{n,\alpha} = 2\pi f_{n,\alpha}\ \frac{\text{rad}}{\text{s}}$, $f_{n,\alpha} = 1.0\,\text{Hz}$ and $m = 1\,\text{kg}$).

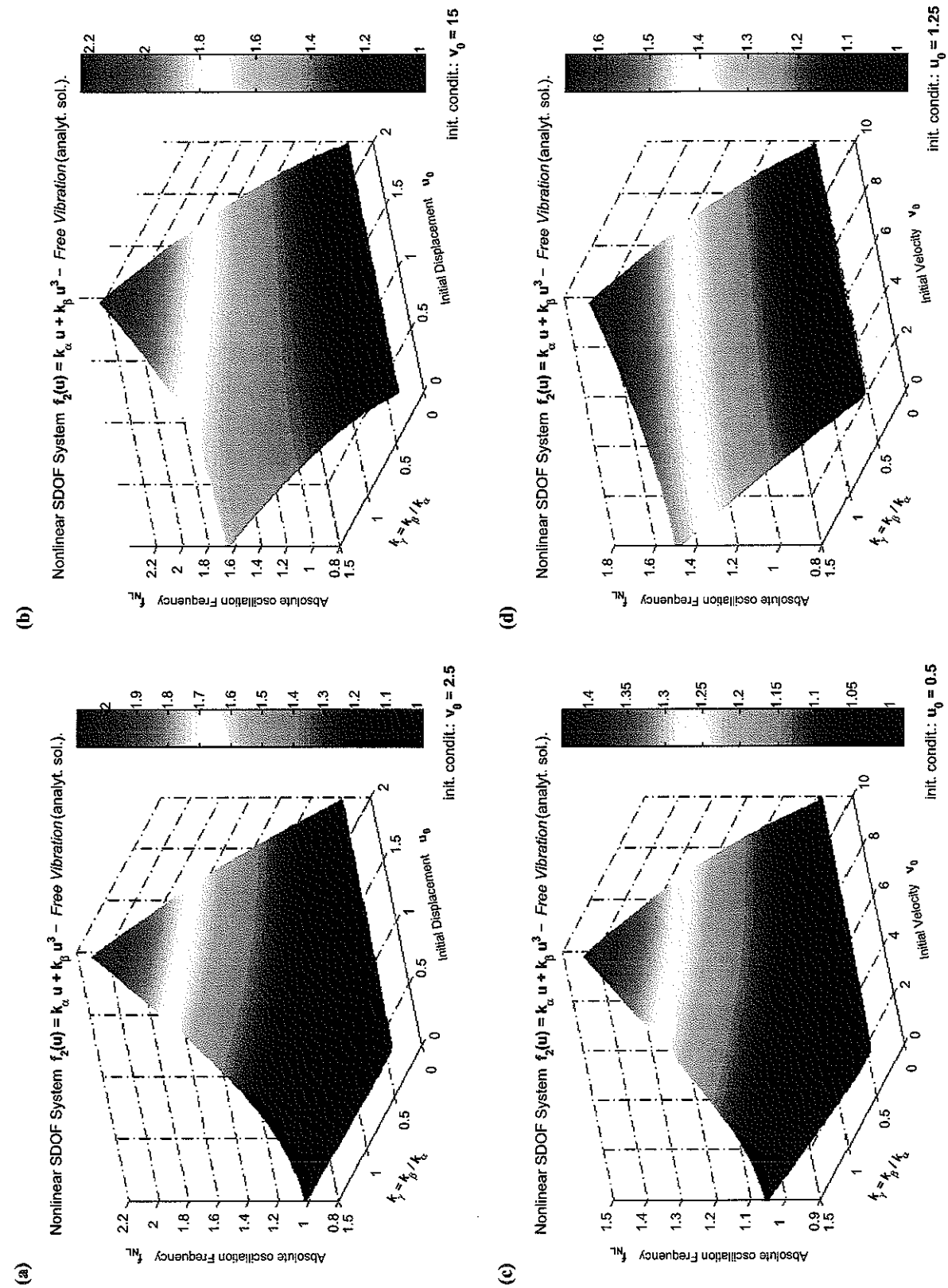

Figure 3.4.17: Nonlinear SDOF system oscillator $f_2(u) = k_\alpha u + k_\beta u^3$ - *Free Vibration*: Absolute nonlinear oscillation frequency as a function of the system's initial conditions u_0 and v_0. ($k_\alpha = m\omega_{n,\alpha}^2$, $\omega_{n,\alpha} = 2\pi f_{n,\alpha}$ $\frac{\text{rad}}{\text{s}}$, $f_{n,\alpha} = 1.0\,\text{Hz}$ and $m = 1\,\text{kg}$).

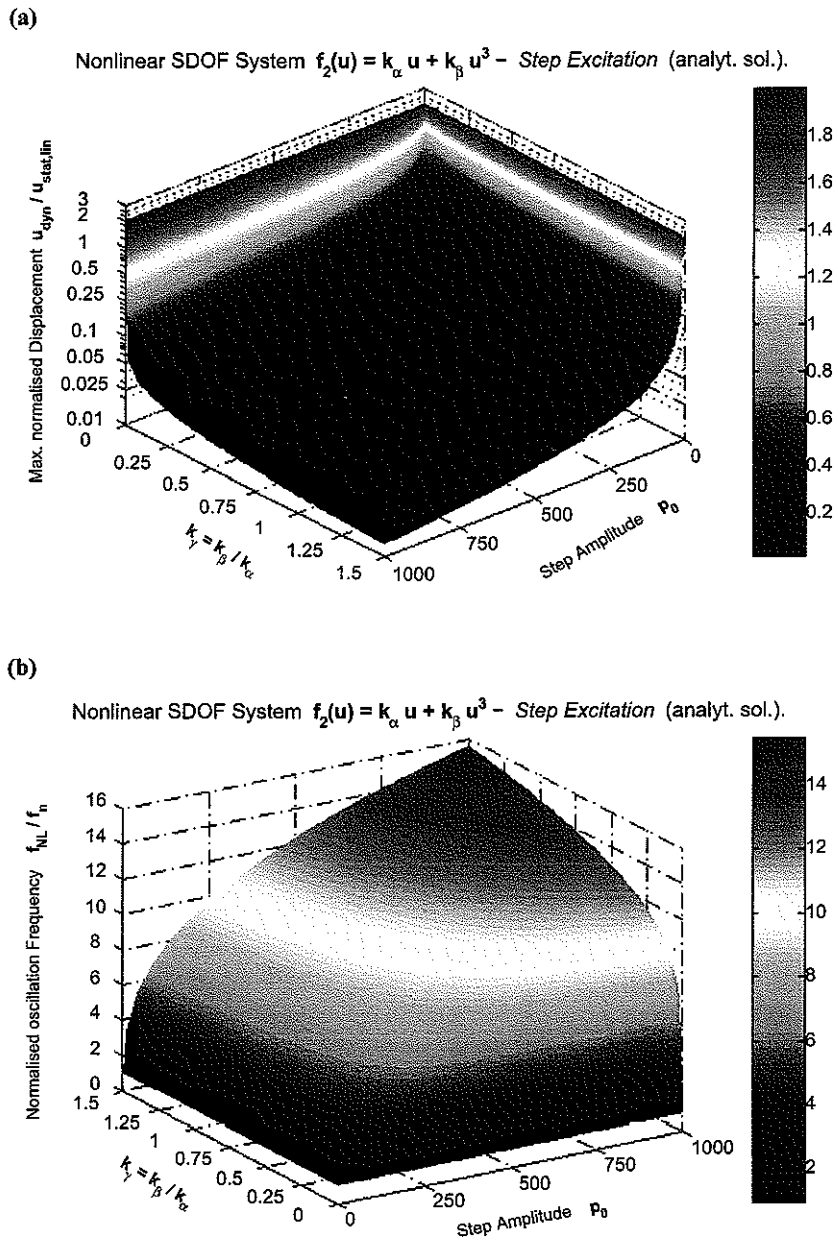

Figure 3.4.18: Nonlinear SDOF system oscillator $f_2(u) = k_\alpha u + k_\beta u^3$ - *Step Excitation*:
(a) Maximum normalised displacement, **(b)** normalised oscillation frequency as functions of the system's stiffness ratio $k_\gamma = \frac{k_\beta}{k_\alpha}$ and the magnitude of the applied step force p_0. Initial conditions $u_0 = 0.0$, $v_0 = 0.0$. ($k_\alpha = 1.0\,\frac{\mathrm{N}}{\mathrm{m}}$, $k_\gamma = 0 \ldots 1.5\,\frac{1}{\mathrm{m}^2}$, $k_\beta = k_\alpha \times k_\gamma$ in $\frac{\mathrm{N}}{\mathrm{m}^3}$, $\omega_{n,\alpha}^2 = \frac{k_\alpha}{m}$ in $\frac{\mathrm{rad}}{\mathrm{s}}$, $\omega_{n,\beta}^2 = \frac{k_\beta}{m}$, $\frac{\mathrm{rad}}{\mathrm{s}}$ and $m = 1\,\mathrm{kg}$).

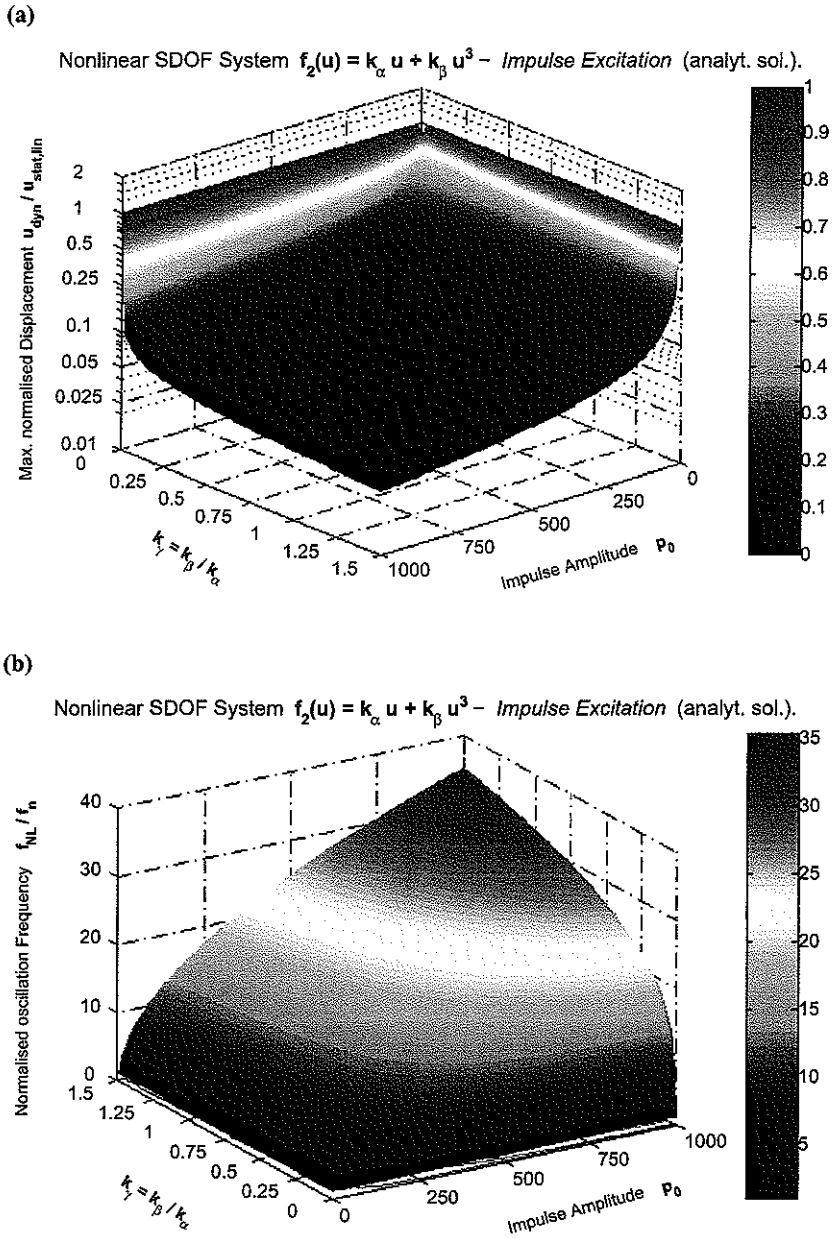

Figure 3.4.19: Nonlinear SDOF system oscillator $f_2(u) = k_\alpha u + k_\beta u^3$ - *Impulse Excitation*:
(a) Maximum normalised displacement, **(b)** normalised oscillation frequency as functions of the system's stiffness ratio $k_\gamma = \frac{k_\beta}{k_\alpha}$ and the magnitude of the applied impulse force p_0. ($k_\alpha = 1.0\,\text{Hz}$, $k_\gamma = 0 \ldots 1.5\,\frac{1}{\text{m}^2}$, $k_\beta = k_\alpha \times k_\gamma$ in $\frac{\text{N}}{\text{m}^3}$, $\omega_{n,\alpha}^2 = \frac{k_\alpha}{m}$ in $\frac{\text{rad}}{\text{s}}$, $\omega_{n,\beta}^2 = \frac{k_\beta}{m}$ in $\frac{\text{rad}}{\text{s}}$ and $m = 1\,\text{kg}$).

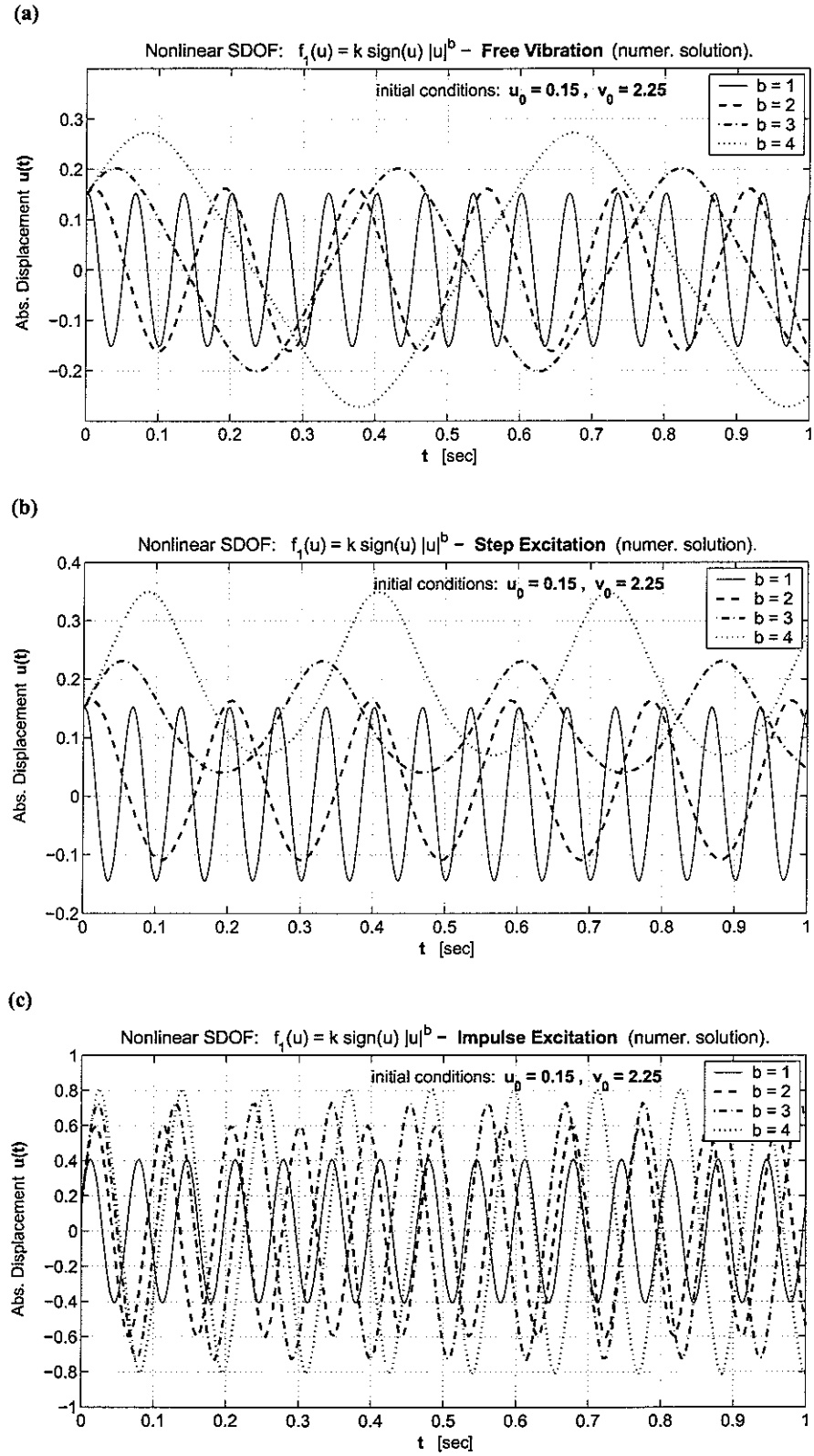

Figure 3.4.20:

Nonlinear SDOF oscillator $f_1(u) = k\,\mathrm{sign}(u)\,|u|^b$ - *Time Domain*: Absolute displacement for **(a)** free vibration, **(b)** step excitation, **(c)** impulse excitation. Maximum values are listed in table 3.4.2 on page 85. System properties: natural frequency $f_n = 15.0\,\mathrm{Hz}$, mass $m = 3.0\,\mathrm{kg}$, $\omega_n = 2\pi f_n\,\mathrm{rad/s}$, stiffness coefficient $k = m\omega_n^2\,\frac{\mathrm{N}}{\mathrm{m}}$. Applied load and initial conditions: $p_0 = 100.0\,\mathrm{N}$, $u_0 = 0.15\,\mathrm{m}$ and $\dot{u}_0 = 2.25\,\frac{\mathrm{m}}{\mathrm{s}}$.

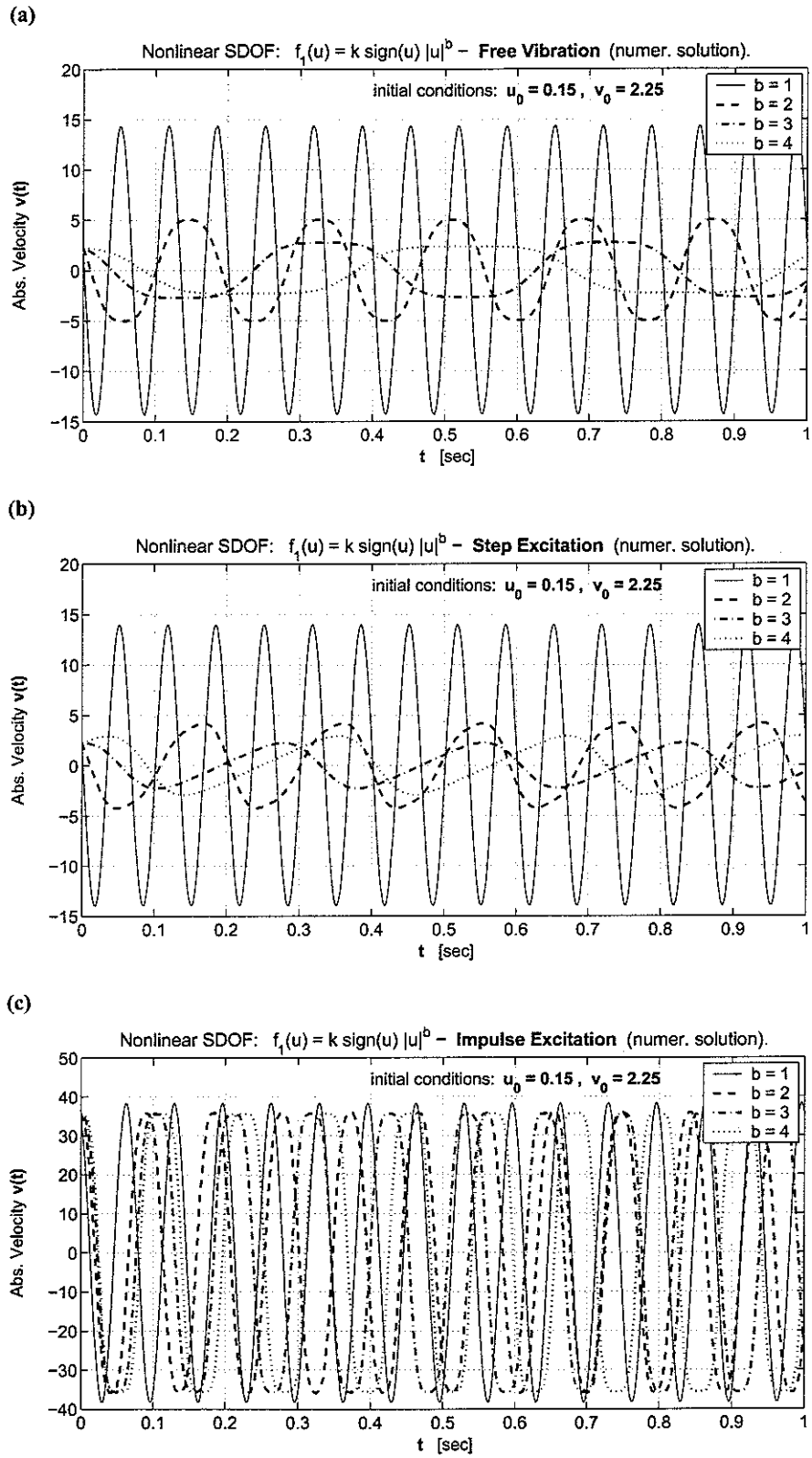

Figure 3.4.21: Nonlinear SDOF oscillator $f_1(u) = k\,\mathrm{sign}(u)\,|u|^b$ - *Time Domain*: Absolute velocity for **(a)** free vibration, **(b)** step excitation, **(c)** impulse excitation. Maximum values are listed in table 3.4.2 on page 85. System properties: natural frequency $f_n = 15.0\,\mathrm{Hz}$, mass $m = 3.0\,\mathrm{kg}$, $\omega_n = 2\pi f_n\,\mathrm{rad/s}$, stiffness coefficient $k = m\omega_n^2\,\frac{\mathrm{N}}{\mathrm{m}}$. Applied load and initial conditions: $p_0 = 100.0\,\mathrm{N}$, $u_0 = 0.15\,\mathrm{m}$ and $\dot{u}_0 = 2.25\,\frac{\mathrm{m}}{\mathrm{s}}$.

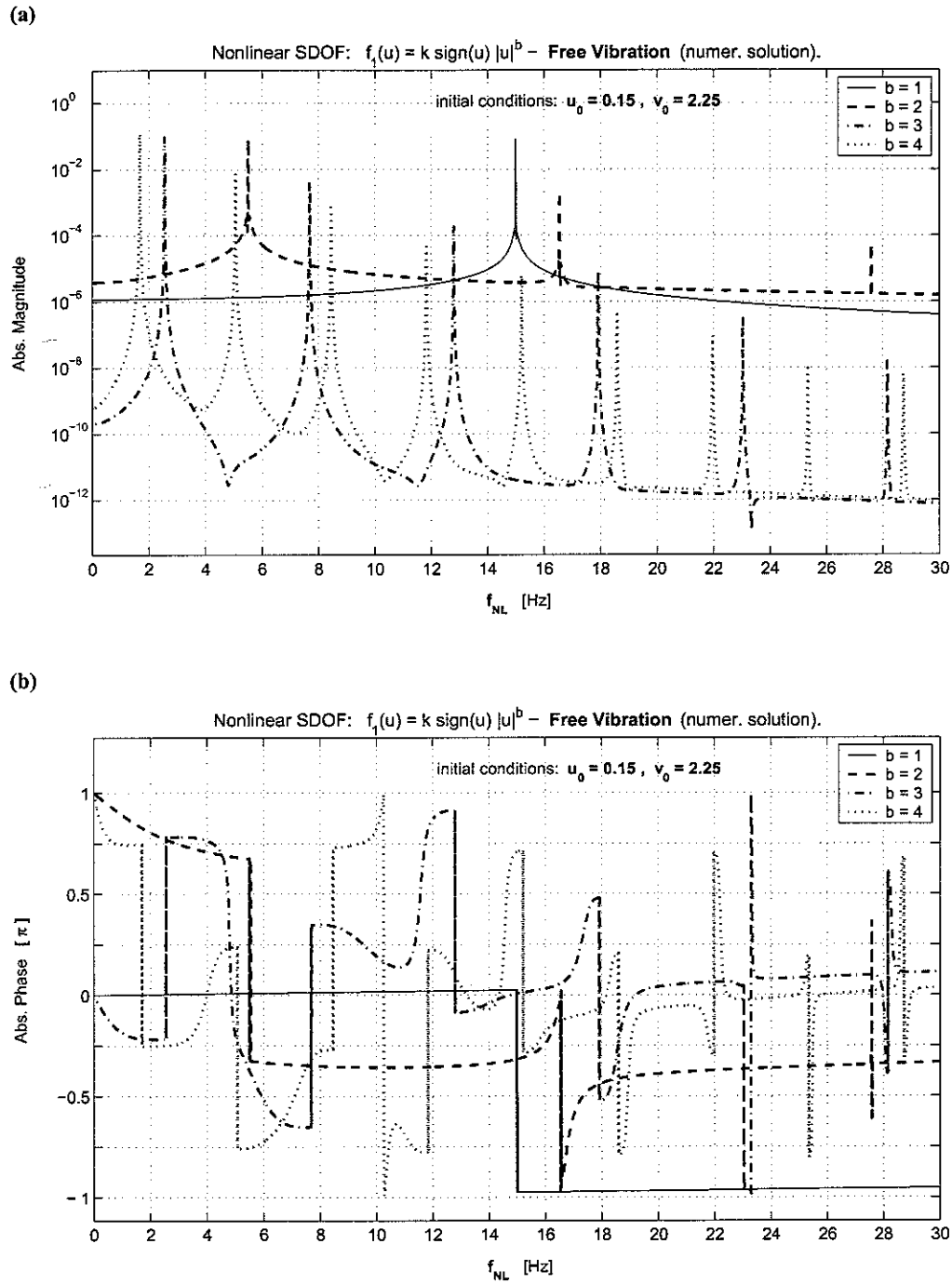

Figure 3.4.22: Nonlinear SDOF oscillator $f_1(u) = k\,\mathrm{sign}(u)\,|u|^b$ - **Free vibration** - *Frequency Domain*: **(a)** Absolute magnitude, **(b)** absolute phase. Maximum values are listed in Table 3.4.2 on page 85. Time-domain data windows: $b = 1,2$ - *Hamming*, $b = 3,4$ - *Hanning*. System properties are: natural frequency $f_n = 15.0\,\mathrm{Hz}$, mass $m = 3.0\,\mathrm{kg}$ $\omega_n = 2\pi f_n\,\mathrm{rad/s}$, stiffness coefficient $k = m\omega_n^2\,\frac{\mathrm{N}}{\mathrm{m}}$. Initial conditions: displacement $u_0 = 0.15\,\mathrm{m}$ and velocity $\dot{u}_0 = 2.25\,\frac{\mathrm{m}}{\mathrm{s}}$.

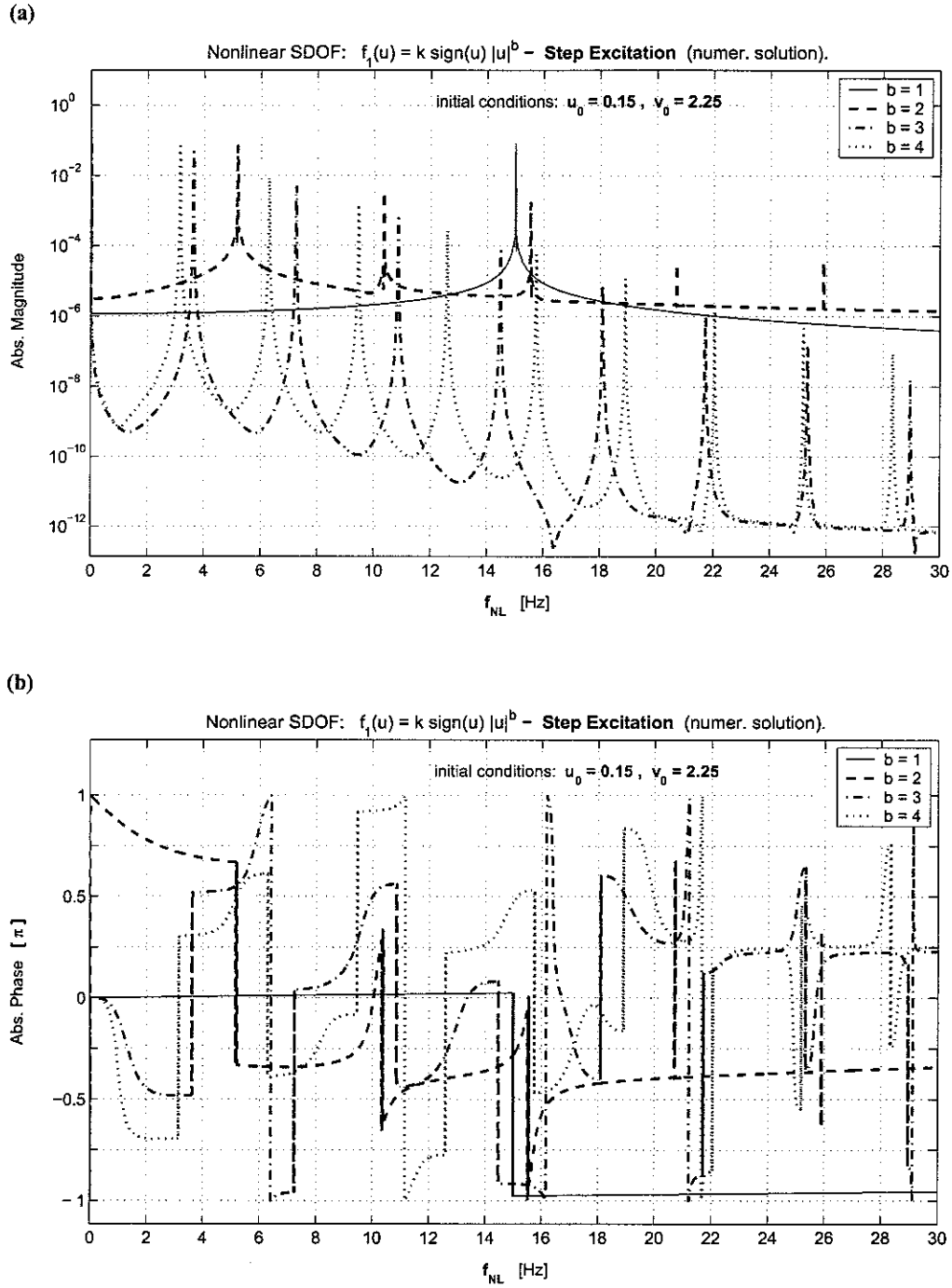

Figure 3.4.23: Nonlinear SDOF system oscillator $f_1(u) = k\,\mathrm{sign}(u)\,|u|^b$ - **Step excitation** - *Frequency Domain*: **(a)** Absolute magnitude, **(b)** absolute phase. The maximum values are listed in table 3.4.2 on page 85. Time-domain data windows: $b = 1,2$ - *Hamming*, $b = 3,4$ - *Hanning*. System properties: natural frequency $f_n = 15.0\,\mathrm{Hz}$, mass $m = 3.0\,\mathrm{kg}$ $\omega_n = 2\pi f_n\,\mathrm{rad/s}$, stiffness coefficient $k = m\omega_n^2\,\frac{\mathrm{N}}{\mathrm{m}}$. Applied load and initial conditions: $p_0 = 100.0\,\mathrm{N}$, $u_0 = 0.15\,\mathrm{m}$ and $\dot{u}_0 = 2.25\,\frac{\mathrm{m}}{\mathrm{s}}$.

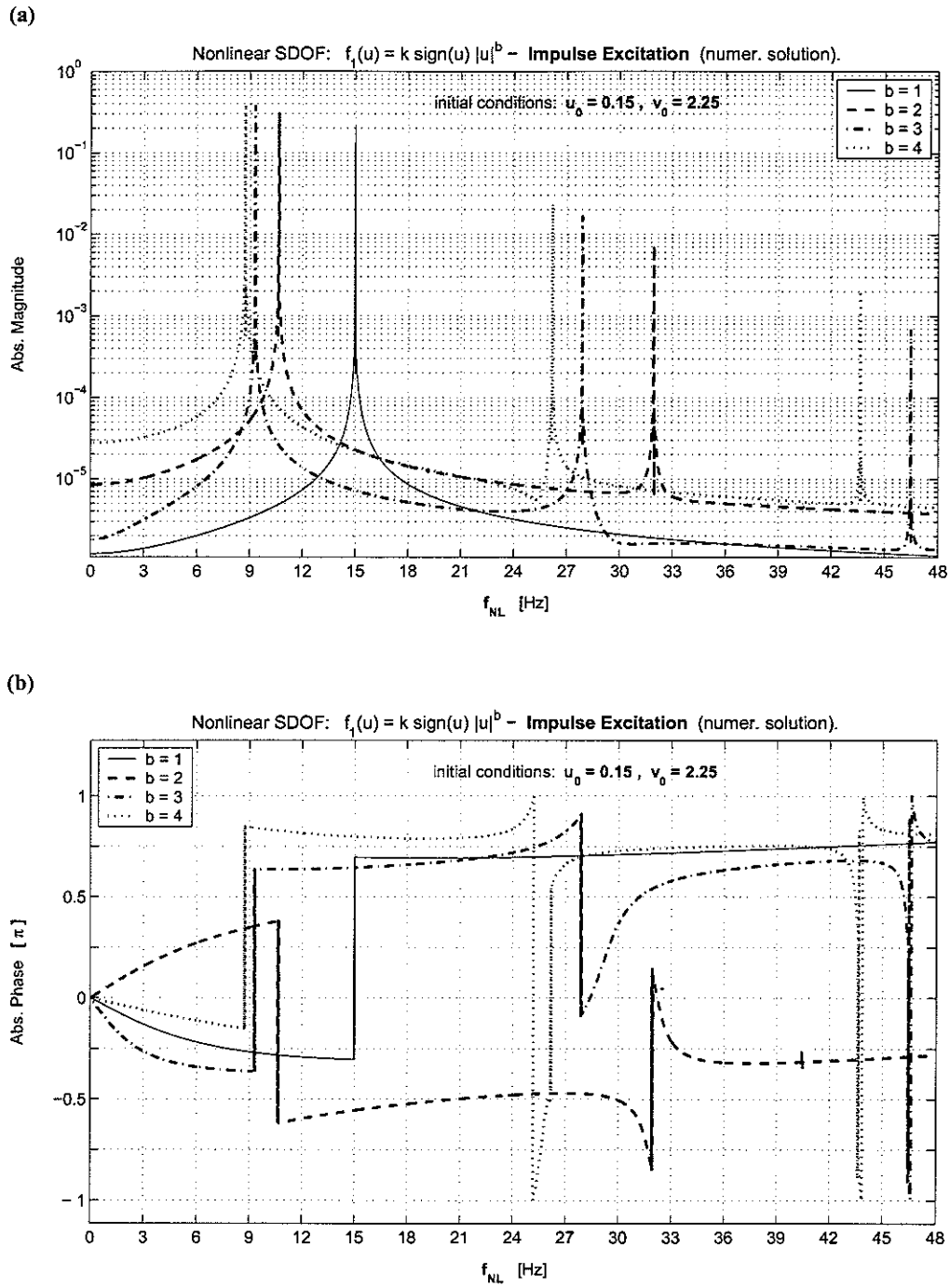

Figure 3.4.24: Nonlinear SDOF system oscillator $f_1(u) = k\,\mathrm{sign}(u)\,|u|^b$ - **Impulse excitation** - *Frequency Domain*: **(a)** Absolute magnitude, **(b)** absolute phase. The maximum values are listed in table 3.4.2 on page 85. Time-domain data windows: $b = 1,\ldots,4$ - *Hamming*. System properties: natural frequency $f_n = 15.0\,\mathrm{Hz}$, mass $m = 3.0\,\mathrm{kg}$, $\omega_n = 2\pi f_n\,\mathrm{rad/s}$, stiffness coefficient $k = m\omega_n^2\,\frac{\mathrm{N}}{\mathrm{m}}$. Applied load and initial conditions: $p_0 = 100.0\,\mathrm{N}$, $u_0 = 0.15\,\mathrm{m}$ and $\dot{u}_0 = 2.25\,\frac{\mathrm{m}}{\mathrm{s}}$.

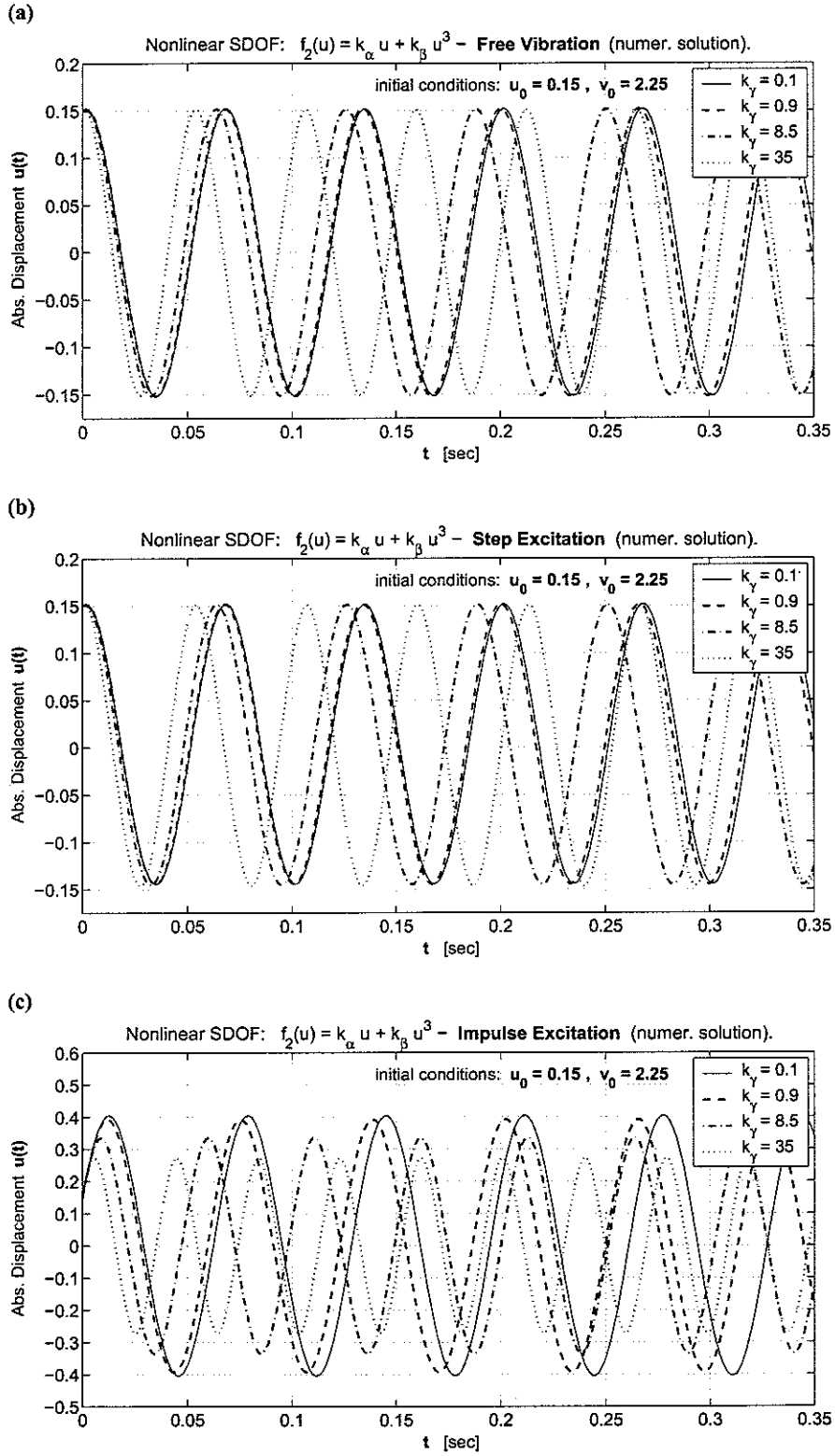

Figure 3.4.25: Nonlinear SDOF system oscillator $f_2(u) = k_\alpha u + k_\beta u^3$ - *Time Domain*: Absolute **displacement** for **(a)** free vibration, **(b)** step excitation, **(c)** impulse excitation. The maximum values are listed in table 3.4.4 on page 88. System properties: natural frequency $f_n = 15.0\,\text{Hz}$, mass $m = 3.0\,\text{kg}$, $\omega_{n,\alpha} = 2\pi f_n\,\text{rad/s}$, stiffness coefficients $k_\alpha = m\omega_{n,\alpha}^2\,\frac{\text{N}}{\text{m}}$, $k_\beta = k_\gamma \times k_\alpha\,\frac{\text{N}}{\text{m}^3}$. Applied load and initial conditions: $p_0 = 100.0\,\text{N}$, $u_0 = 0.15\,\text{m}$ and $\dot{u}_0 = 2.25\,\frac{\text{m}}{\text{s}}$.

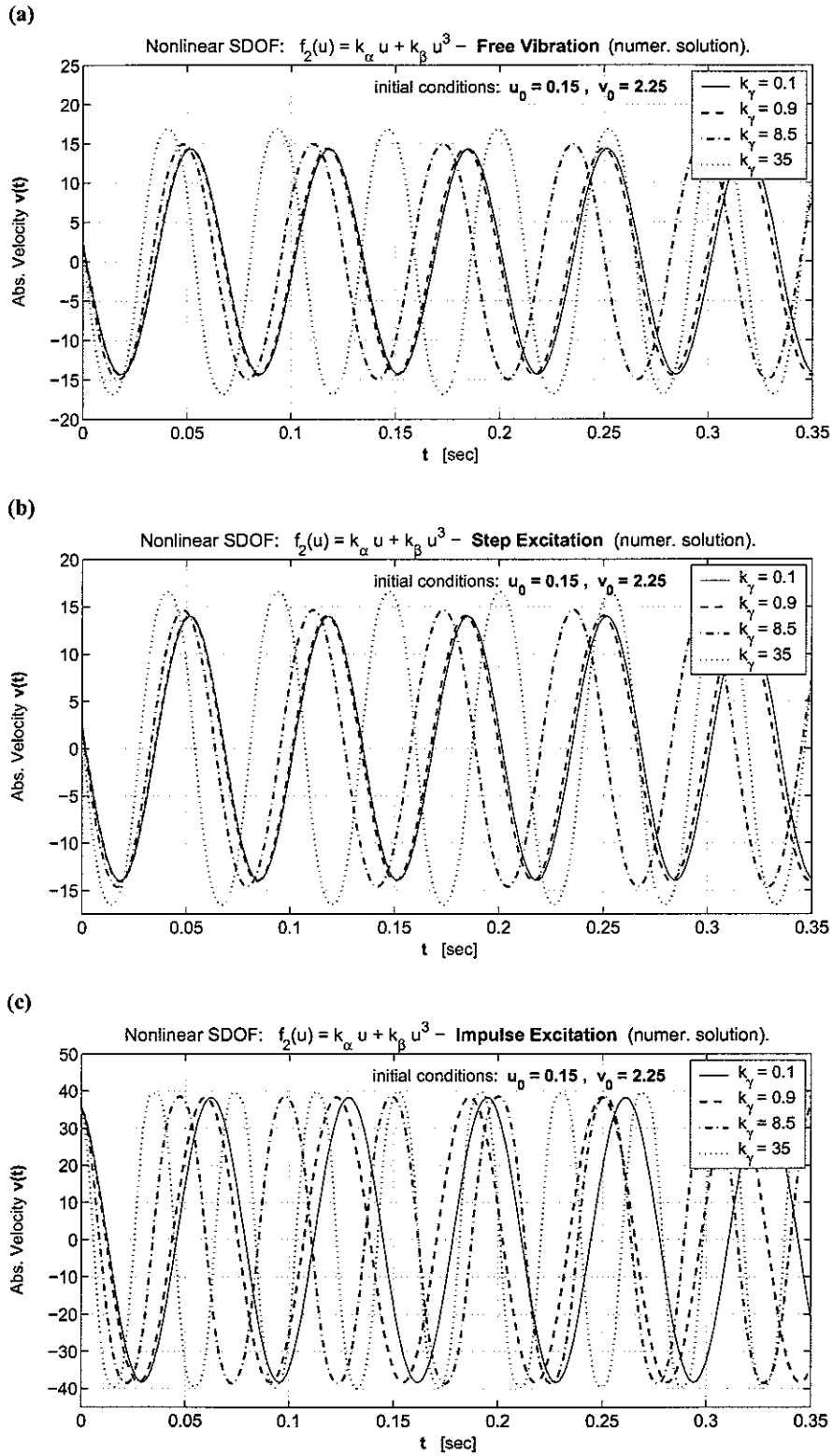

Figure 3.4.26: Nonlinear SDOF system oscillator $f_2(u) = k_\alpha u + k_\beta u^3$ - *Time Domain*: Absolute **velocity** for **(a)** free vibration, **(b)** step excitation, **(c)** impulse excitation. The maximum values are listed in table 3.4.4 on page 88. System properties: natural frequency $f_n = 15.0\,\text{Hz}$, mass $m = 3.0\,\text{kg}$, $\omega_{n,\alpha} = 2\pi f_n\,\text{rad/s}$, stiffness coefficients $k_\alpha = m\,\omega_{n,\alpha}^2\,\frac{\text{N}}{\text{m}}$, $k_\beta = k_\gamma \times k_\alpha\,\frac{\text{N}}{\text{m}^3}$. Applied load and initial conditions: $p_0 = 100.0\,\text{N}$, $u_0 = 0.15\,\text{m}$ and $\dot{u}_0 = 2.25\,\frac{\text{m}}{\text{s}}$.

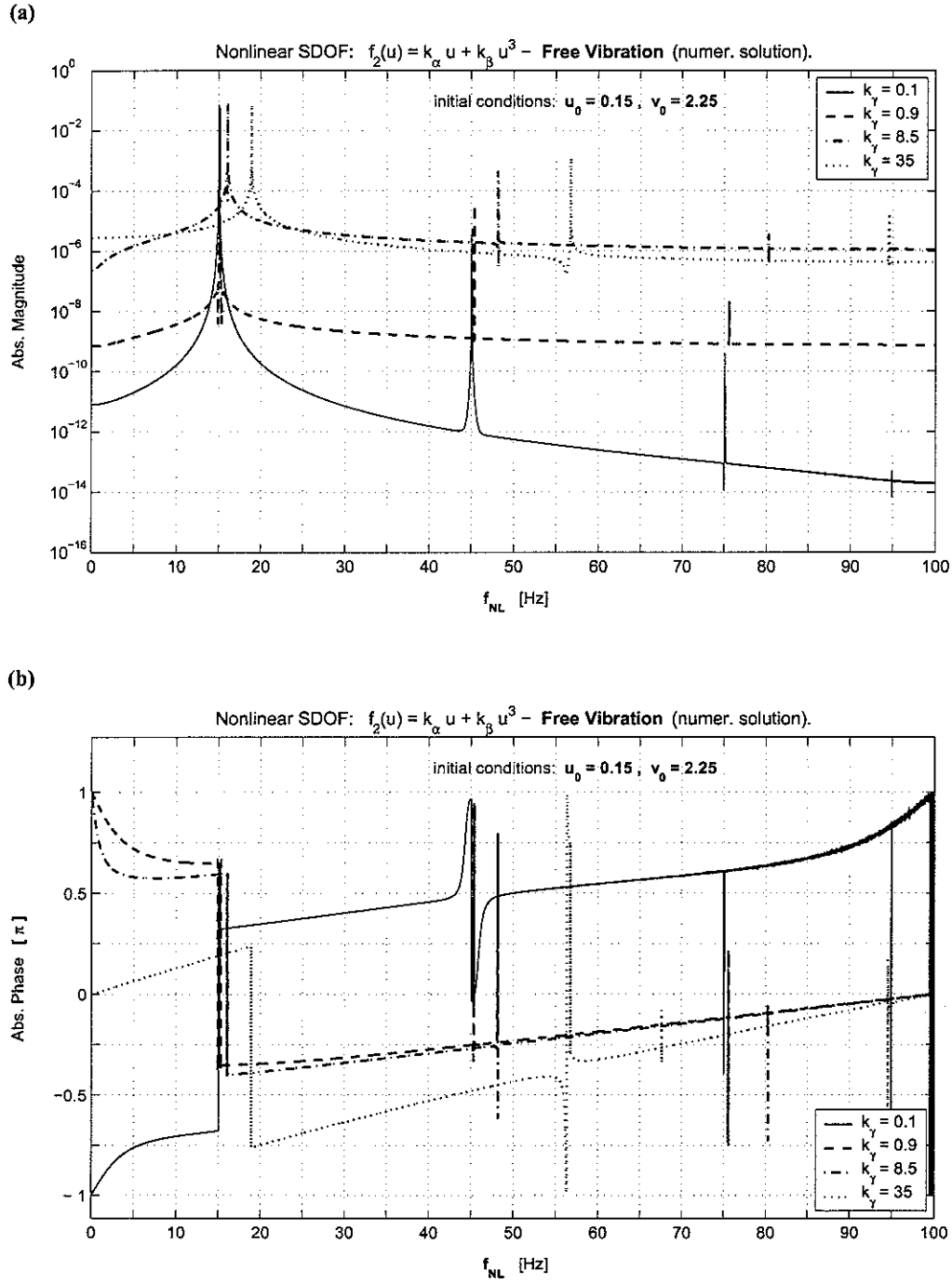

Figure 3.4.27: Nonlinear SDOF system oscillator $f_2(u) = k_\alpha u + k_\beta u^3$ - **Free vibration** - *Frequency Domain*: **(a)** Absolute magnitude, **(b)** absolute phase. The maximum values are listed in table 3.4.4 on page 88. Time-domain data windows: $k_\gamma = 0.1$ - *Hanning*, $k_\gamma = 0.9$ - *Blackman-Harris*, $k_\gamma = 8.5, 35$ - *Hamming*. System properties: natural frequency $f_n = 15.0\,\text{Hz}$, mass $m = 3.0\,\text{kg}$, $\omega_{n,\alpha} = 2\pi f_n = 30\pi\,\text{rad}\cdot\text{s}$, stiffness coefficients $k_\alpha = m\omega_{n,\alpha}^2\,\frac{\text{N}}{\text{m}}$, $k_\beta = k_\gamma \times k_\alpha\,\frac{\text{N}}{\text{m}^3}$. Applied load and initial conditions: $p_0 = 100.0\,\text{N}$, $u_0 = 0.15\,\text{m}$ and $\dot{u}_0 = 2.25\,\frac{\text{m}}{\text{s}}$.

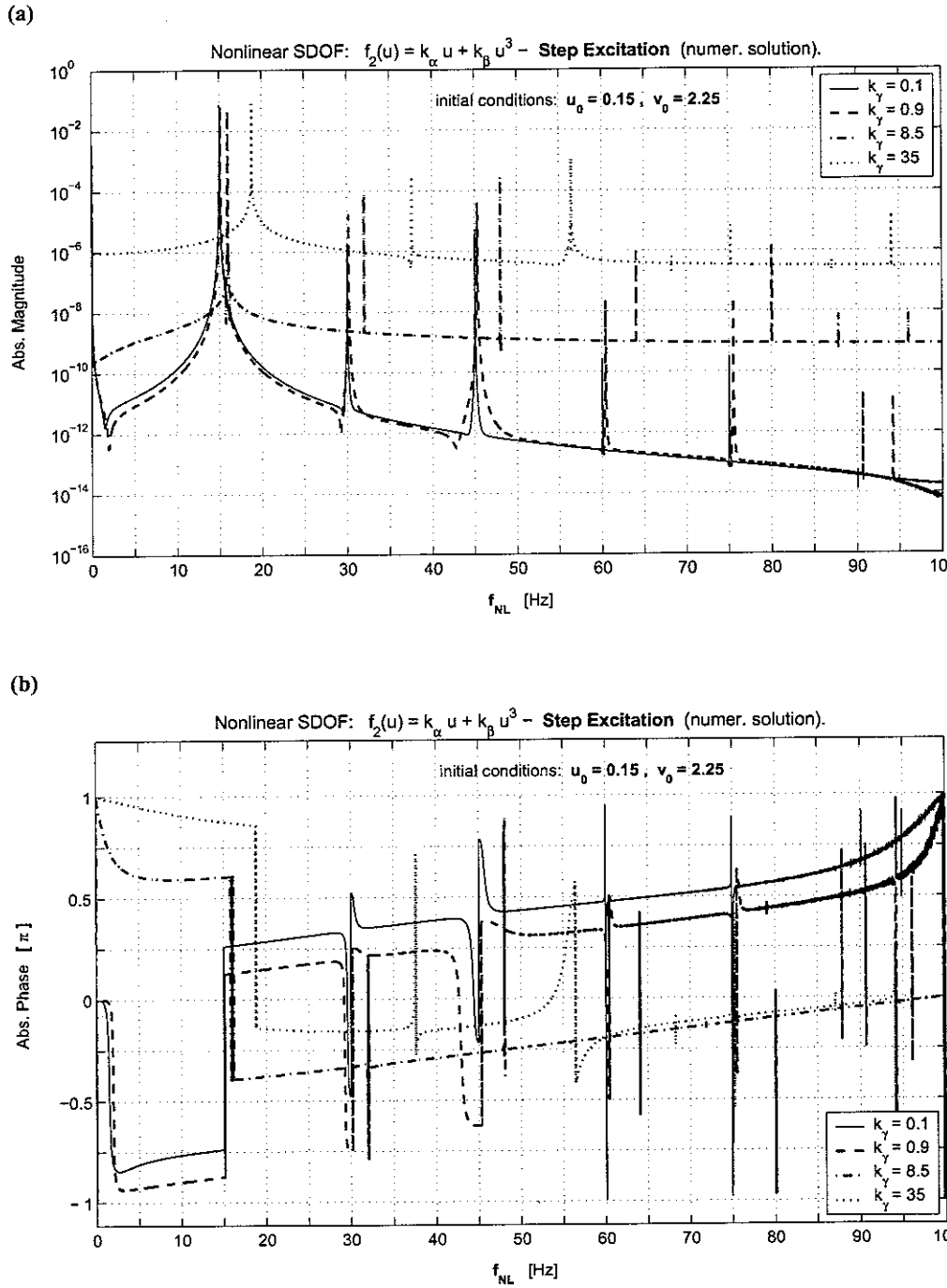

Figure 3.4.28: Nonlinear SDOF system oscillator $f_2(u) = k_\alpha u + k_\beta u^3$ - **Step excitation** - *Frequency Domain*: **(a)** Absolute magnitude, **(b)** absolute phase. The maximum values are listed in table 3.4.4 on page 88. Time-domain data windows: $k_\gamma = 0.1, 0.9$ - *Hanning*, $k_\gamma = 8.5$ - *Blackman-Harris*, $k_\gamma = 35$ - *Hamming*. System properties: natural frequency $f_n = 15.0\,\text{Hz}$, mass $m = 3.0\,\text{kg}$, $\omega_{n,\alpha} = 2\pi f_n\,\text{rad/s}$, stiffness coefficients $k_\alpha = m\,\omega_{n,\alpha}^2\,\frac{\text{N}}{\text{m}}$, $k_\beta = k_\gamma \times k_\alpha\,\frac{\text{N}}{\text{m}^3}$. Applied load and initial conditions: $p_0 = 100.0\,\text{N}$, $u_0 = 0.15\,\text{m}$ and $\dot{u}_0 = 2.25\,\frac{\text{m}}{\text{s}}$.

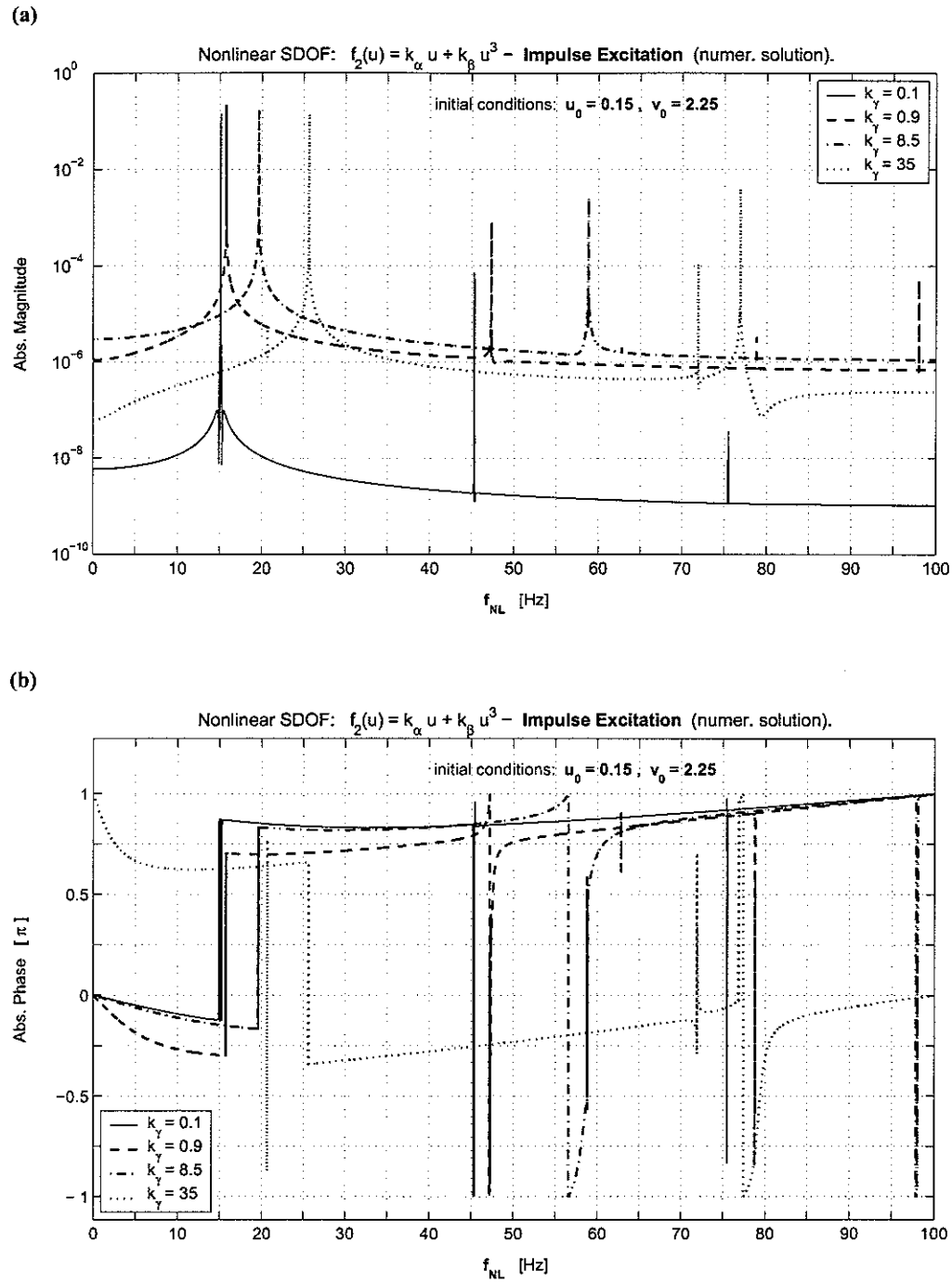

Figure 3.4.29: Nonlinear SDOF system oscillator $f_2(u) = k_\alpha u + k_\beta u^3$ - **Impulse excitation** - *Frequency Domain*: **(a)** Absolute magnitude, **(b)** absolute phase. The maximum values are listed in table 3.4.4 on page 83. Time-domain data windows: $k_\gamma = 0.1$ - *Blackman-Harris*, $k_\gamma = 0.9, 8.5, 35$ - *Hamming*. System properties: natural frequency $f_n = 15.0\,\text{Hz}$, mass $m = 3.0\,\text{kg}$, $\omega_{n,\alpha} = 2\pi f_n\,\text{rad/s}$, stiffness coefficients $k_\alpha = m\omega_{n,\alpha}^2\,\frac{\text{N}}{\text{m}}$, $k_\beta = k_\gamma \times k_\alpha\,\frac{\text{N}}{\text{m}^3}$. Applied load and initial conditions: $p_0 = 100.0\,\text{N}$, $u_0 = 0.15\,\text{m}$ and $\dot{u}_0 = 2.25\,\frac{\text{m}}{\text{s}}$.

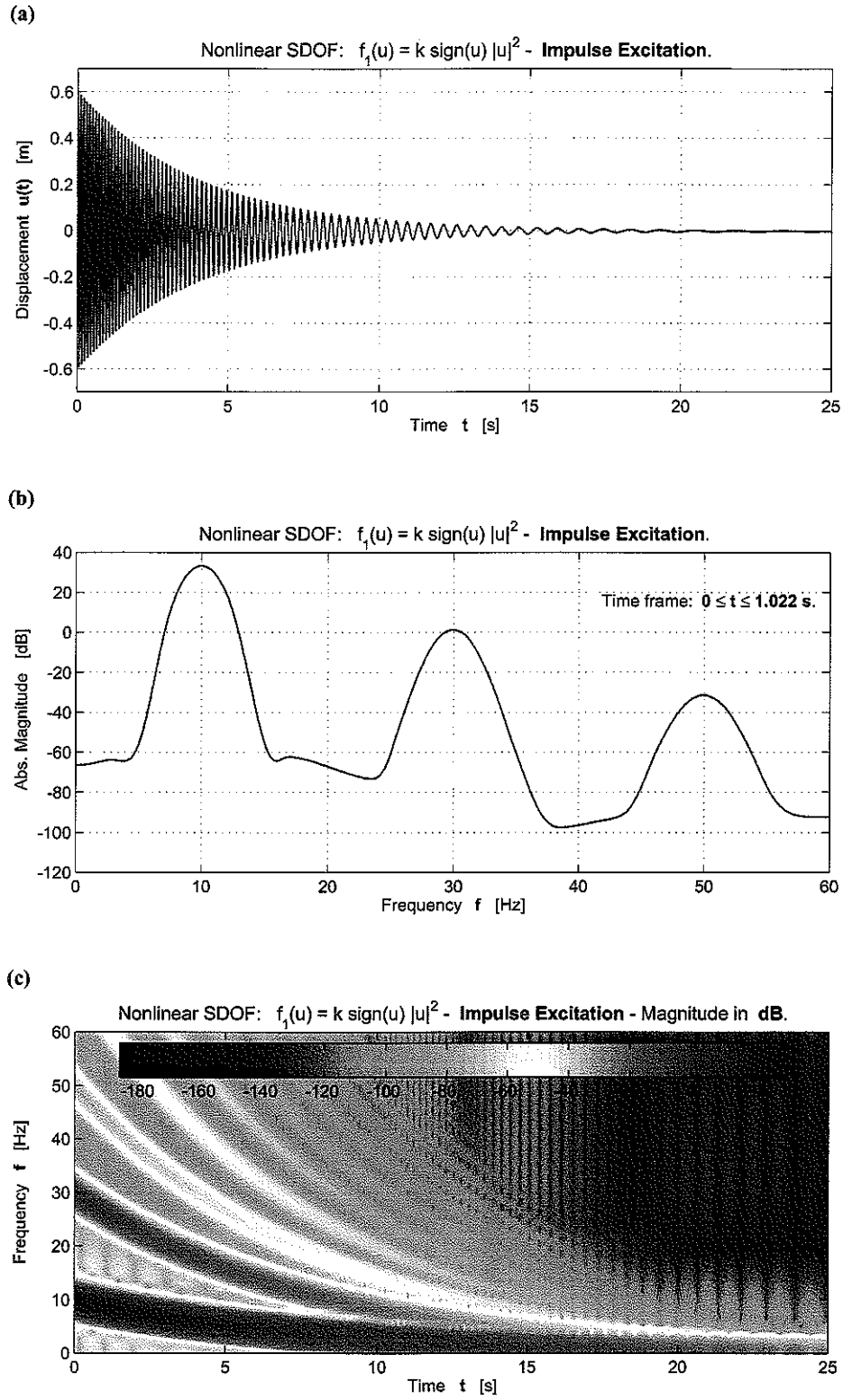

Figure 3.5.1: Nonlinear SDOF system oscillator $f_1(u) = k\,\mathrm{sign}(u)\,|u|^2$ - *Autonomous nonconservative system*: **Impulse excitation. (a)** time-history, **(b)** FFT of first frame, **(c)** response spectra. System properties: natural frequency $f_n = 15.0\,\mathrm{Hz}$, mass $m = 3.0\,\mathrm{kg}$, $\omega_n = 2\pi f_n\,\mathrm{rad/s^2}$, stiffness coefficient $k = m\omega_n^2\,\mathrm{N/m^2}$, viscous damping ratio $\zeta = 0.5\%$, damping coefficient $c = 2m\omega_n\zeta\,\mathrm{Ns/m}$. Applied load and initial conditions: $p_0 = 100.0\,\mathrm{N}$, $u_0 = 0.15\,\mathrm{m}$ and $\dot{u}_0 = 2.25\,\frac{\mathrm{m}}{\mathrm{s}}$ (Blackman-Harris window).

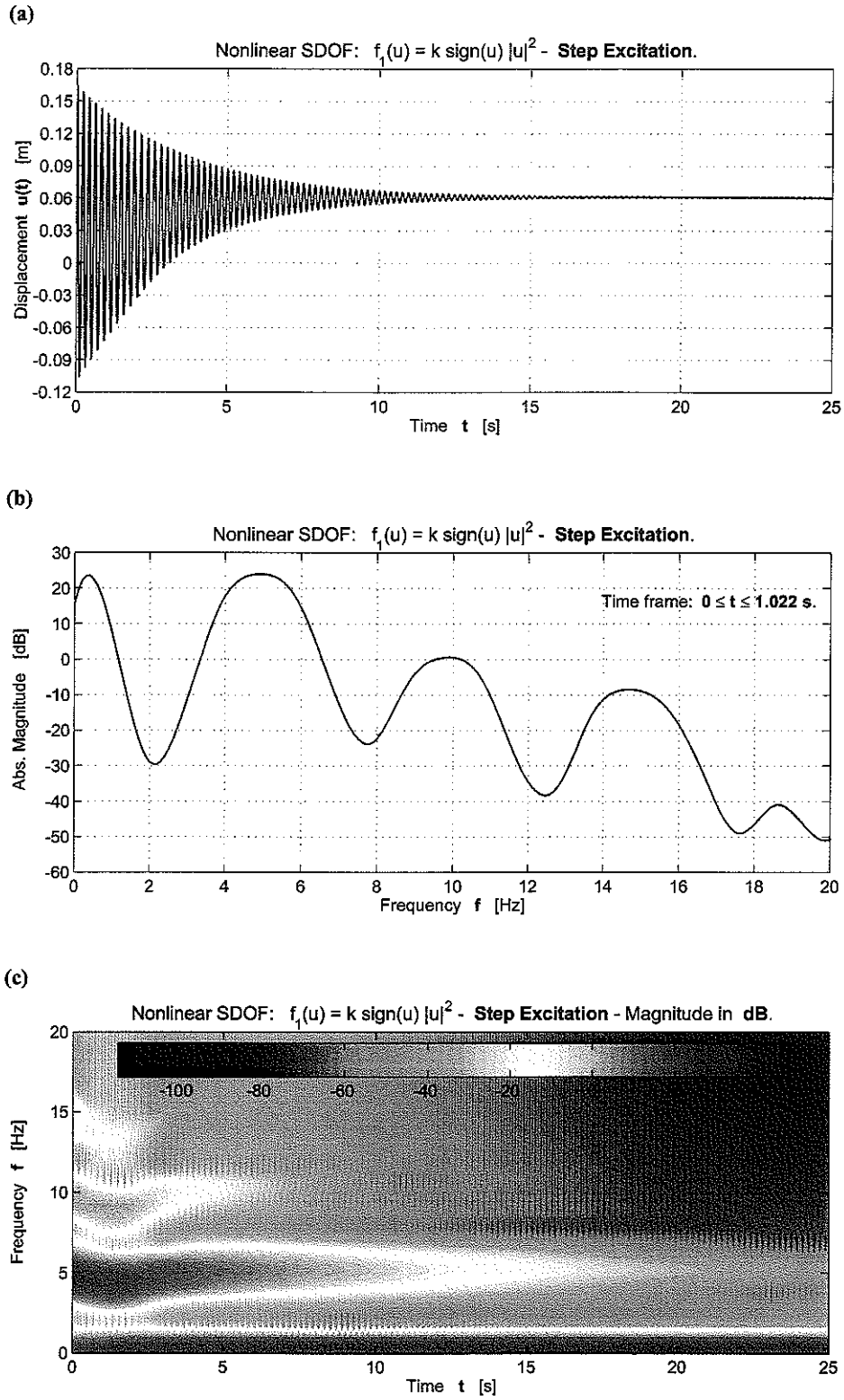

Figure 3.5.2: Nonlinear SDOF system oscillator $f_1(u) = k\,\mathrm{sign}(u)\,|u|^2$ - *Autonomous nonconservative system*: **Step excitation. (a)** time-history, **(b)** FFT of first frame, **(c)** response spectra. System properties: natural frequency $f_n = 15.0\,\mathrm{Hz}$, mass $m = 3.0\,\mathrm{kg}$, $\omega_n = 2\pi f_n\,\mathrm{rad/s^2}$, stiffness coefficient $k = m\omega_n^2\,\mathrm{N/m^2}$, viscous damping ratio $\zeta = 0.5\%$, damping coefficient $c = 2m\omega_n\zeta\,\mathrm{Ns/m}$. Applied load and initial conditions: $p_0 = 100.0\,\mathrm{N}$, $u_0 = 0.15\,\mathrm{m}$ and $\dot{u}_0 = 2.25\,\frac{\mathrm{m}}{\mathrm{s}}$ (Hamming window).

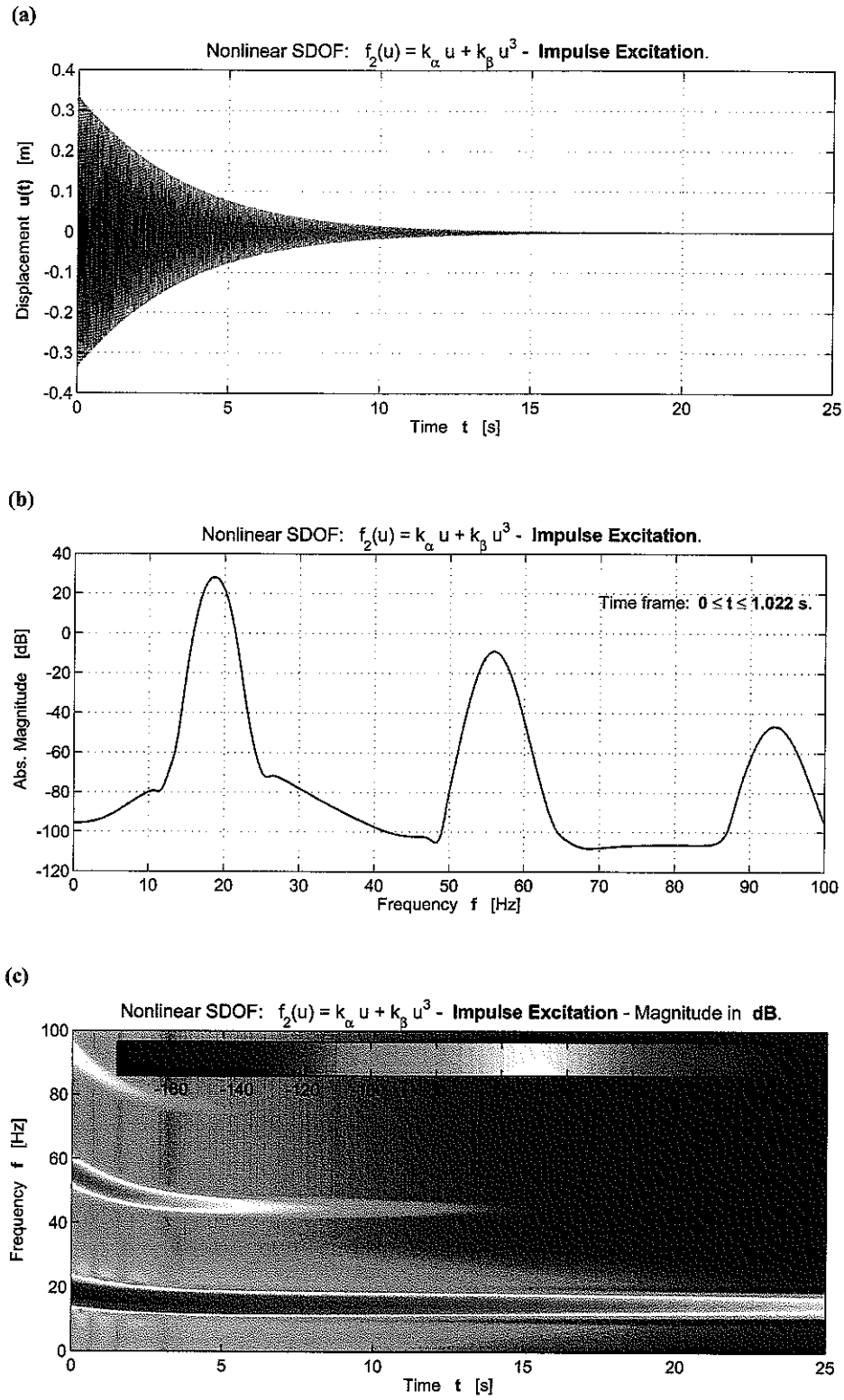

Figure 3.5.3: Nonlinear SDOF system oscillator $f_2(u) = k_\alpha u + k_\beta u^3$ - *Autonomous nonconservative system*: **Impulse excitation. (a)** time-history, **(b)** FFT of first frame, **(c)** response spectra. System properties: natural frequency $f_n = 15.0\,\text{Hz}$, mass $m = 3.0\,\text{kg}$, $\omega_n = 2\pi f_n\,\text{rad/s}$, linear stiffness $k_\alpha = m\omega_n^2\,\text{N/m}$, $k_\beta = 8.5 \times k_\alpha\,\text{N/m}^3$, viscous damping ratio $\zeta = 0.5\%$, damping coefficient $c = 2m\omega_n\zeta\,\text{Ns/m}$. Applied load and initial conditions: $p_0 = 100.0\,\text{N}$, $u_0 = 0.15\,\text{m}$ and $\dot{u}_0 = 2.25\,\frac{\text{m}}{\text{s}}$ (Hanning window).

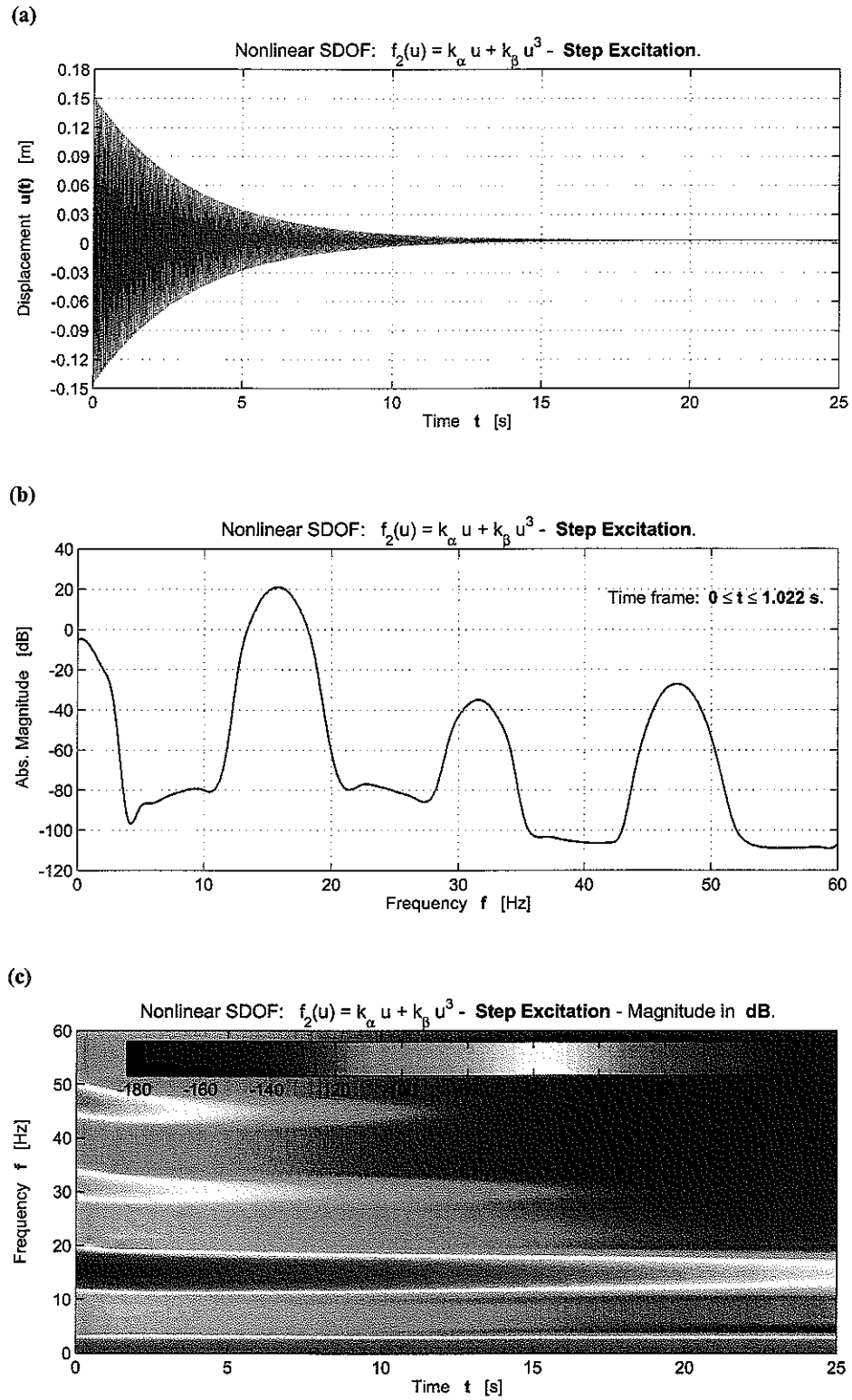

Figure 3.5.4: Nonlinear SDOF system oscillator $f_2(u) = k_\alpha u + k_\beta u^3$ - *Autonomous nonconservative system*: **Step excitation. (a)** time-history, **(b)** FFT of first frame, **(c)** response spectra. System properties: natural frequency $f_n = 15.0\,\text{Hz}$, mass $m = 3.0\,\text{kg}$, $\omega_n = 2\pi f_n\,\text{rad/s}^2$, linear stiffness $k_\alpha = m\omega_n^2\,\text{N/m}$, $k_\beta = 8.5 \times k_\alpha\,\text{N/m}^3$, viscous damping ratio $\zeta = 0.5\%$, damping coefficient $c = 2m\omega_n\zeta\,\text{Ns/m}$. Applied load and initial conditions: $p_0 = 100.0\,\text{N}$, $u_0 = 0.15\,\text{m}$ and $\dot{u}_0 = 2.25\,\frac{\text{m}}{\text{s}}$ (Hamming window).

CHAPTER 4

Non-Autonomous Nonlinear SDOF Systems

4.1 The Equation of Motion

All results presented in the previous chapter 3 are only applicable if the nonlinear system is autonomous. This implies time t does not appear as an independent variable in the equation of motion, i.e. is neither part of the applied external load nor of the internal restoring forces of the oscillator. However, in order to determine the nonlinear system's response due to blast pressure excitation as introduced in chapter 1, the load amplitude has to be a function of t. Using the equation of motion (3.2.1) derived at the very beginning of chapter 3 on page 37 and, apart from $u(t)$ allowing only $P(t)$ to vary explicit with time[1] the nonlinear second order differential equation describing the non-autonomous system's state at all points within $0 \leq t \leq \infty$ is written as

$$m\ddot{u}(t) + f(u(t), \dot{u}(t)) = P(t) \tag{4.1.1}$$

where $P(t)$ on the right-hand site represents any kind of time-varying external loading. In the special cases under consideration in here, $P(t)$ is equal to one of the two characteristic blast wave profiles $p_I(t)$ or $p_{II}(t)$, introduced by Eq.(1.1.1) and (1.1.3) in chapter 1. Two initial conditions necessary to obtain unique solutions from (4.1.1) are given by Eq.(3.2.4) on page 38.

4.2 Response of Conservative Systems to Specific Blast Profile

Assuming that the SDOF system exchanges no energy with its surrounding environment and the restoring force is a function of the displacement $u(t)$ only leads to

$$m\ddot{u}(t) + f[u(t)] = P(t) \tag{4.2.1}$$

as the equation of motion for the non-autonomous conservative oscillator with $f[u(t)]$ being substituted by either $f_1(u)$ or $f_2(u)$ as defined in chapter 3. Due to the transient nature of $P(t)$, conventional

[1] Despite the fact that the restoring force $f(\ldots)$ as a combination of elastic and damping force changes its amplitude with $u(t)$ and $\dot{u}(t)$, and hence with time, it is not regarded as explicitly dependent on t. This would be only the case if the restoring force-displacement or force-velocity diagram exhibits different properties at successive time instances as given for nonlinear material behaviour (creeping, relaxation) or contact problems (sudden changes in stiffness/damping).

analytical approximations such as perturbation methods or the method of harmonic balance [38] are not applicable. Therefore, the following two sections 4.2.1 and 4.2.2 are aimed at comparing results derived for impulse and step excitation in chapter 3 with numerically obtained solutions for non-autonomous systems as given in Eq.(4.2.1). It is important to note that the examples chosen for blast excitation do not represent results given in [18]. They were merely arbitrary selected for illustrating the fact that it is possible to predict SDOF system response due to blast excitation using the Dirac delta function as input. Details of this approximation process will be presented elsewhere[2].

Recalling the transient type-I blast wave excitation as given in chapter 1 by [2]

$$p_I(t) = p_0 \left(1 - \frac{t}{t_d}\right) \mathrm{e}^{-\alpha \frac{t}{t_d}}$$

the total impulse I_{bw_1} can be divided into a positive and a negative part

$$\begin{aligned} I_{bw_1} &= I^+_{bw_1} + I^-_{bw_1} \\ &= \int_0^{t_d} p_I(t)\,\mathrm{d}t + \int_{td}^{\infty} p_I(t)\,\mathrm{d}t \\ &= \frac{t_d}{\alpha} p_0 \left(1 - \frac{1}{\alpha} + \frac{\mathrm{e}^{-\alpha}}{\alpha}\right) - \frac{t_d \mathrm{e}^{-\alpha}}{\alpha^2} p_0 \end{aligned} \tag{4.2.2}$$

referring to the direction in which $p_I(t)$ acts compared to the definition of the displacement $u(t)$. As a first criteria for approximating SDOF blast wave response by Dirac impulse behaviour the positive total impulse of both excitations must be equal

$$I^+_{bw_1} = I_\delta \qquad \text{where} \qquad I_\delta = \int_{-\infty}^{\infty} p_\delta\,\mathrm{d}t = p_\delta \tag{4.2.3}$$

is the amplitude of the Dirac impulse. Second, since I_δ has no negative component, the force in the positive direction of $I^+_{bw_1}$ must be dominating the total impulse I_{bw_1}

$$I^+_{bw_1} >> I^-_{bw_1} \qquad \text{or} \qquad I^+_{bw_1} \approx I_{bw_1}\,. \tag{4.2.4}$$

Both equations above are simple rules for approximating the blast response and they do not hold the potential for obtaining precise and therefore satisfying results compared to the numerical integration. They should rather be seen as two fundamental criteria for a more accurate but also more complex approximation method which bases on the total work done on the structural system by all external forces.

The shortcoming of this simple approximation is demonstrated using the type-I blast profile with three different sets of parameters as given in Table 4.2.1. None of the sets fulfills *both* equations (4.2.3) and (4.2.4) and results are therefore expected to vary considerably from the Dirac impulse response.

4.2.1 Restoring Force $f_1(u) = k\,\mathrm{sign}(u)\,|u|^b$

4.2.1.1 Time Domain

The absolute displacement $u(t)$ and velocity $\dot{u}(t)$ of the type-I excited SDOF system with $f_1(u)$ as nonlinear restoring force are shown in Fig. 4.2.1 to 4.2.4 on pages 137 to 140. Different values of the

[2] At the time of print of this technical memorandum the theory for the blast response approximation using an energy-based method was already outlined. However, the author felt it somewhat inconsistent to include the entire method herein.

Table 4.2.1: Blast wave type-I excitation: Positive $\left(I^{+}_{bw_1}\right)$ and negative $\left(I^{-}_{bw_1}\right)$ part of total impulse input (I_{bw_1}). The blast magnitude p_0 takes either the value 100 N or 10 kN. Dirac-δ impulse (I_δ) is 100 Ns which is equal to $1 \times p_\delta$ Ns.

Blast impulse	$\alpha = 0.9$ $t_d = 0.02\,\mathrm{s}$	$\alpha = 0.9$ $t_d = 0.05\,\mathrm{s}$	$\alpha = 5.4$ $t_d = 0.02\,\mathrm{s}$	Blast magnitude
$I^{+}_{bw_1}$ [Ns]	7.57E-3	1.89E-2	3.02E-3	$\times p_0$
$I^{-}_{bw_1}$ [Ns]	-1.00E-2	-2.51E-2	-3.11E-6	$\times p_0$
I_{bw_1} [Ns]	-2.43E-3	-6.20E-3	3.02E-3	$\times p_0$

excitation force parameters α and t_d are taken into account. For comparison, the response of the oscillator due to a Dirac delta impulse, as introduced in section 3.4.1.3 on page 67, is additionally shown in each figure. The ratios of blast wave to impulse response are given for extreme values of displacement and velocity in Table 4.2.2. The impulse excitation magnitude was kept constant at $p_0 = 100\,\mathrm{N}$ whereas p_0 for the blast was set to 100 N and 10 kN, respectively. For the precise amount of impulse input of the blast profile into the SDOF the values from Table 4.2.1 have to be multiplied by p_0, i.e. 100 N or 10 kN.

Blast, impulse magnitude $\mathbf{p_0 = p_\delta = 100\,N}$. The absolute **displacement** due to blast excitation as given in Fig. 4.2.1(a) for the linear case $b = 1$ is almost 80 $(\alpha = 0.9,\ t_d = 0.05\,\mathrm{s})$ to nearly 350 $(\alpha = 5.4,\ t_d = 0.02\,\mathrm{s})$ times smaller than the response due to impulse, assuming the same force amplitude of $p_0 = 100\,\mathrm{N}$. As b increases and all other parameter remain constant, Fig. 4.2.1(b) to (d), the minimum/maximum displacement due to both blast and impulse force increase at the same time. This weakening in the system's stiffness force $f_1(u)$ is explained by referring to Fig. 3.4.1 on page 46 which shows that for $-1 \leq u(t) \leq 1$ all restoring forces with $b > 1$ are significantly smaller than $f_1(u)$ in the linear case of $b = 1$. However, the first two blocks in Table 4.2.2 allow the conclusion that extreme values of displacement due to blast are faster growing than due to impulse since the ratios ${}_{bw1}u_{\max_{f_1}} / {}_{\delta}u_{\max_{f_1}}$ and ${}_{bw1}u_{\min_{f_1}} / {}_{\delta}u_{\min_{f_1}}$ rise significantly as the nonlinearity of $f_1(u)$, i.e. the value for b, increases.

In contrast, this is not true for the **velocity** where there is no clear pattern observable, neither monotonous rising nor falling. However, for minimum and maximum values some type of asymptotic behaviour exist, at least for two of the three different blast functions relatively close to impulse excitation (column 5 and 7, $\alpha = 0.9$, $t_d = 0.02\,\mathrm{s}$ and $\alpha = 5.4$, $t_d = 0.02\,\mathrm{s}$). Indeed, for the profile in column 7 the velocity ratios due to blast/impulse ${}_{bw1}v_{\max_{f_1}} / {}_{\delta}v_{\max_{f_1}}$ and ${}_{bw1}v_{\min_{f_1}} / {}_{\delta}v_{\min_{f_1}}$ do change very little only, which means, given the fact that the velocity for the impulse excited system ${}_{\delta}v_{\min_{f_1}} = -{}_{\delta}v_{\max_{f_1}} \approx const.$ for all $b = 1 \ldots 4$, the values for extreme velocity ${}_{bw1}v_{\min_{f_1}}$ and ${}_{bw1}v_{\max_{f_1}}$ stay virtually constant.

It is clearly to see, that despite the fact of equal magnitude ($p_0 = 100\,\mathrm{N}$) the responses due to both types of excitation are nowhere near matching, which is not only caused by the differences in time-domain appearance but also due to the total amount of impulse (and therefore energy) input into the system, depending upon the type of excitation. In fact, as with every non-autonomous conservative system, the response is governed by the sum of the force magnitude weighted with respect to the

time instance at which the impulse increment ΔI_{bw_1} acts. Unfortunately, this cannot be expressed by a convolution operation as shown in chapter 2 for linear systems. An energy approach must be chosen, ensuring the total amount of work done by all external forces on the system is equal to the system's internal energy at any given point in time.

Due to the absence of dissipating forces (damping) in the system's equation of motion (4.1.1), and therefore no change in both amplitudes $u_{\min}$ and $u_{\max}$ as $t \to \infty$, the steady-state displacement response $u(t)$ due to blast wave excitation can be described as harmonic for the elastic linear case $b = 1$ and as periodic, i.e. with multiple frequency response, for all other cases $b \neq 1$, which will be examined in greater detail by a separate frequency analysis in what follows.

Blast magnitude $\mathbf{p_0} = 10\,\mathrm{kN}$, impulse magnitude $\mathbf{p_\delta} = 100\,\mathrm{N}$. Increasing the blast wave amplitude p_0 by a factor of 100, but leaving at the same time the amplitude for the unit impulse excitation constant, produced diagrams for both displacement and velocity as shown in Fig. 4.2.3 and 4.2.4. Surprisingly, for the given system with a stiffness coefficient

$$k = \omega_n^2 m = 4\pi^2 f_n^2 m$$

equal to a natural linear frequency f_n of 15 Hz and a mass m of 3 kg, the displacement response ratios ${}_{bw1}u_{\max_{f_1}} / {}_{\delta}u_{\max_{f_1}}$ and ${}_{bw1}u_{\min_{f_1}} / {}_{\delta}u_{\min_{f_1}}$ for the first set of blast parameters ($\alpha = 0.9$, $t_d = 0.02\,\mathrm{s}$) are reasonable close to 1, which indicates extreme values of both displacements are similar in magnitude. This is reinforced by comparing the ratios for the velocity also listed in Table 4.2.2. Unfortunately, as explained earlier, the choice of parameters does not meet the basic requirements as given by both equations (4.2.3) and (4.2.4), and results for the displacement and velocity response ratios for the two remaining sets of blast excitation parameters are rather poor. In conclusion, finding a response ratio close to 1.0 with the assumed SDOF system and blast parameters by increasing the force magnitude by a factor of 100 can be regarded as a mere coincidence.

However, the importance of the above described results lies in the fact that it is possible to approximate the *entire* time history of a Friedlander blast wave excited SDOF system by using it's response behaviour due to a Dirac-impulse. The main difficulty arises from finding the appropriate constraints for all parameter of both, the excitation function as well as the system[3]. This will be presented in a forthcoming second technical memorandum.

4.2.1.2 Frequency Domain

Shock Spectra. The plot of minimum and/or maximum displacement as a function of the systems's stiffness due to a transient excitation force is defined as shock spectra [3]. In chapter 2 section 2.5 the spectra of a linear SDOF oscillator originating from blast wave forcing functions with different parameters α and t_d are shown. For blast excitation forces with similar values for α and t_d, Fig. 4.2.5 on page 141 shows shock spectra for nonlinear systems with $f_1(u)$ as restoring force and equal impulse and blast loading magnitudes of $\mathbf{p_\delta} = \mathbf{p_0} = \mathbf{100}\,\mathrm{N}$. The frequency parameter f_n was chosen as independent variable allowing for the calculation of the stiffness coefficient $k = m\,(2\pi f_n)^2$ and hence $f_1(u)$. For each f_n a displacement-time history $u(t)$ was produced using the Runge-Kutta algorithm

[3] As noted earlier, for nonlinear oscillators, system properties such as normalised oscillation amplitude or frequency are *not* independent of the excitation.

Table 4.2.2: Linear/nonlinear SDOF oscillator $f_1(u) = k\,\mathrm{sign}(u)\,|u|^b$ - *Blast Wave Type-I Excitation*: Comparison of displacement and velocity absolute amplitude ratios of impulse and type-I blast wave profile excitation. System properties and time histories are given in Fig. 4.2.1 and 4.2.2 for impulse and blast $p_0 = 100\,\mathrm{N}$, respectively, and in Fig. 4.2.3 and 4.2.4 for impulse $p_0 = 100\,\mathrm{N}$ and blast wave $p_0 = 10\,\mathrm{kN}$. The non-normalised displacements due to impulse force are 3.537E-01 m, 5.725E-01 m, 7.072E-01 m and 7.926E-01 m for $b = 1,2,3$ and 4, respectively. The values for the velocity stay virtually constant at 3.333E+01 m/s.

b	***Displacement***			***Velocity***		
	$\alpha = 0.9$ $t_d = 0.02\,\mathrm{s}$	$\alpha = 0.9$ $t_d = 0.05\,\mathrm{s}$	$\alpha = 5.4$ $t_d = 0.02\,\mathrm{s}$	$\alpha = 0.9$ $t_d = 0.02\,\mathrm{s}$	$\alpha = 0.9$ $t_d = 0.05\,\mathrm{s}$	$\alpha = 5.4$ $t_d = 0.02\,\mathrm{s}$
	Ratio of maxima: $\dfrac{\text{Blast Wave}}{\text{Impulse}} \longrightarrow \dfrac{{}^{bwl}u_{\max_{f_1}}}{{}_{\delta}u_{\max_{f_1}}}; \dfrac{{}^{bwl}v_{\max_{f_1}}}{{}_{\delta}v_{\max_{f_1}}}$			Impulse, Blast: $\mathbf{p_0 = 100\,N}$		
1	0.0087	0.0124	0.0029	0.0090	0.0104	0.0029
2	0.0280	0.0914	0.0209	0.0076	0.0281	0.0030
3	0.0500	0.1219	0.0549	0.0076	0.0189	0.0030
4	0.0906	0.1397	0.0981	0.0076	0.0189	0.0030
	Ratio of minima: $\dfrac{\text{Blast Wave}}{\text{Impulse}} \longrightarrow \dfrac{{}^{bwl}u_{\min_{f_1}}}{{}_{\delta}u_{\min_{f_1}}}; \dfrac{{}^{bwl}v_{\min_{f_1}}}{{}_{\delta}v_{\min_{f_1}}}$			Impulse, Blast: $\mathbf{p_0 = 100\,N}$		
1	0.0102	0.0119	0.0029	0.0087	0.0112	0.0029
2	0.0280	0.0950	0.0209	0.0047	0.0276	0.0030
3	0.0500	0.1220	0.0549	0.0025	0.0149	0.0030
4	0.0906	0.1397	0.0981	0.0025	0.0073	0.0030
	Ratio of maxima: $\dfrac{\text{Blast Wave}}{\text{Impulse}} \longrightarrow \dfrac{{}^{bwl}u_{\max_{f_1}}}{{}_{\delta}u_{\max_{f_1}}}; \dfrac{{}^{bwl}v_{\max_{f_1}}}{{}_{\delta}v_{\max_{f_1}}}$			Impulse: $\mathbf{p_0 = 100\,N}$ Blast: $\mathbf{p_0 = 10\,kN}$		
1	0.8653	1.2443	0.2961	0.8950	1.0362	0.2926
2	1.0535	1.3189	0.4497	1.1187	1.3861	0.3015
3	1.0502	1.2659	0.5494	1.1372	1.5318	0.3018
4	1.0337	1.2199	0.6193	1.1176	1.5978	0.3018
	Ratio of minima: $\dfrac{\text{Blast Wave}}{\text{Impulse}} \longrightarrow \dfrac{{}^{bwl}u_{\min_{f_1}}}{{}_{\delta}u_{\min_{f_1}}}; \dfrac{{}^{bwl}v_{\min_{f_1}}}{{}_{\delta}v_{\min_{f_1}}}$			Impulse: $\mathbf{p_0 = 100\,N}$ Blast: $\mathbf{p_0 = 10\,kN}$		
1	1.0174	1.1903	0.2926	0.8653	1.1198	0.2926
2	1.1320	1.3551	0.4497	1.0813	1.4618	0.3015
3	1.0955	1.3095	0.5494	1.1031	1.5828	0.3018
4	1.0635	1.2546	0.6193	1.0866	1.6641	0.3018

described in section 3.4.3 and the extreme values of $u(t)$, $u_{\min}$ and $u_{\max}$, respectively, were obtained. In order to allow for comparison with results acquired for the linear SDOF in chapter 2, minimum and maximum displacement were normalised to the static deflection of the equivalent *linear* system $u_{\text{stat,lin}} = p_0/\left(m\omega_n^2\right)$ with $\omega_n = 2\pi f_n$.

Graph (a) of Fig. 4.2.5, showing the response spectra for the linear oscillator, appears very similar to results presented in section 2.5. The blast profile parameters vary only slightly and force amplitude p_0 and system mass m have no influence on the normalised displacement $u_{\text{dyn}}/u_{\text{stat,lin}}$ of the linear SDOF. However, for small linear frequencies f_n the response due to the blast profile with $\alpha = 5.4$ and $t_d = 0.02\,\text{s}$ oscillates somewhat around the zero-displacement equilibrium position.

With the restoring force $f_1(u)$ becoming purely nonlinear as b takes on values greater than 1, the normalised deflection increases significantly by several orders of magnitude. In diagram (b), as $b = 2$, the extreme displacement for the profile $\alpha = 5.4$, $t_d = 0.02\,\text{s}$ starts to oscillate around the equilibrium position with what appears to be random negative and positive values whereas the response for blast profiles one and two, $\alpha = 0.9$, $t_d = 0.02\,\text{s}$ and $\alpha = 0.9$, $t_d = 0.05\,\text{s}$ remain steadily increasing with a jump into positive values at $f_n = 162\,\text{Hz}$ for the latter one. In graph (c) u_{Ex}, due to $\alpha = 0.9$, $t_d = 0.02\,\text{s}$, starts partially oscillating in the same way and in picture (d) of Fig. 4.2.5 both blast profiles produce rapidly changing extreme displacement amplitudes.

For the case of different excitation magnitudes $\mathbf{p_\delta = 100\,N}$ and $\mathbf{p_0 = 10\,kN}$ shock spectra for all four discrete values of $b = 1,\ldots,4$ are shown in Fig. 4.2.6 on page 142. Each graph shows normalised displacement response solutions for three pairs of parameters of blast excitation together with the extreme values of the impulse response. It is evident, the linear system in graph (a) exhibits the same feature as already encountered in chapter 2 and has been added for reasons of comparison only. Graph (b) to (d) illustrate how little the impulse response changes with higher values for b compared to the three blast responses. Despite increasing normalised magnitude the impulse response retains the character of an envelope although two orders of magnitude bigger, which can be explained by the fact that parameters α and t_d have been merely guessed rather than been calculated by stringent approximation criteria. The important fact of Fig. 4.2.6 lies in its quantitative statement: Impulse response functions of geometrically, polynomial-type, nonlinear SDOF systems are suitable for approximating the far more complex response behaviour due to type-I blast waves. Obviously, the closer the excitation function matches with the characteristic of the Dirac delta impulse, the more alike is the expected SDOF response. This is clearly demonstrated by the displacement response curve with parameters $\alpha = 5.4$, $t_d = 0.02\,\text{s}$ in graph (b) to (d) showing very similar oscillatory pattern as the impulse response.

It is important to point out the difference between both figures 4.2.5 and 4.2.6 regarding the apparent random oscillation behaviour of some of the extreme value solutions. Both figures have been obtained using slightly different numerical algorithms for the search of extreme values of displacement. In both cases, time-domain data was calculated using a fifth order embedded Runge-Kutta solution method as explained in section 3.4.3 chapter 3. Omitting any further processing, this data was used to extract minima and maxima values as pictured in Fig. 4.2.5. Naturally, this leads to numerical difficulties and can influence the accuracy of anticipated results. An improved method was chosen for Fig. 4.2.6 which multiplies the time-domain data by the predefined inverse value of the global relative numerical iteration error[4] minus two orders of magnitude, rounds it to the nearest integer value and establishes

[4]According to the MATLAB® implemented solver routines the *relative* error is responsible for the accuracy of min-

than minima and maxima value field indices which refer to the values in the displacement solution array. This ensures shock spectra results are unbiased by numerical errors beyond allowed tolerances. Although the oscillation between minima and maxima displacement values is significantly lower in Fig. 4.2.6, it is still present. For the impulse response this would mean the numerical solutions contradicts the analytical in chapter 3, which clearly states $|u_{\min}| = |u_{\max}|$. A second, different numerical simulation with more stringent error tolerance[5] showed that the numerical results are in line with findings from chapter 3 and upper and lower extreme values of the SDOF impulse response are equal in magnitude but reversed in sign. Therefore, lines interconnecting minima and maxima results for the impulse response should be disregarded.

Contrary, displacement response due to blast excitation retains its marginal oscillatory pattern. These points at distinctive linear equivalent frequencies and hence nonlinear stiffness values are critical for evaluating the work done by the external force on the SDOF system and will be examined in greater detail in a forthcoming memorandum.

Frequency content. A Fourier transformation of the time domain data from section 4.2.1.1 above reveals the individual frequency components participating in the nonlinear oscillation of the SDOF system excited by the different blast profiles. Table 4.2.3 gives frequencies $f_{\mathrm{NL},j}$ where $j = 1,2,3,\ldots,n$ for equal blast and impulse force magnitude $\mathbf{p}_\delta = \mathbf{p_0} = \mathbf{100}\,\mathrm{N}$ and Fig. 4.2.7 on page 143 shows the corresponding graphs for $b = 1,2,3$ and 4. Whereas for $b = 1$ only one single frequency $f_{\mathrm{NL}} = f_n$ governs the SDOF vibration, the system starts to oscillates with odd multiples of the fundamental nonlinear frequency $f_{\mathrm{NL}} = 1/T_{\mathrm{NL}}$

$$f_{\mathrm{NL},j} = (2j-1) \times f_{\mathrm{NL}}\,, \qquad j = 1,2,3,\ldots \tag{4.2.5}$$

for the cases $b = 2,3,4$. Although for all three combinations of t_d and α the nonlinear frequencies $f_{\mathrm{NL},j}$ are considerably smaller than for impulse excitation, the pattern of participating frequencies of odd multiples as seen in chapter 3 is also valid for the non-autonomous blast wave excited SDOF system.

The numerically obtained time domain solution presented in section 4.2.1.1 above suggested that both, impulse response due to magnitude $\mathbf{p}_\delta = \mathbf{100}\,\mathrm{N}$ and blast excitation with $t_d = 0.02\,\mathrm{s}$, $\alpha = 0.9$ and $\mathbf{p_0} = \mathbf{10}\,\mathrm{kN}$ exhibit similar response in displacement and velocity magnitude and oscillation frequency. Figure 4.2.8 on page 144, together with Table 4.2.4, clearly show how reasonable close all nonlinear frequencies $f_{\mathrm{NL},j}$ for both different types of excitation are. Given the fact that the overall power input into the SDOF system for both forces is significantly different, this must be regarded as a mere coincident. Nevertheless, it proves vitally that blast wave response can be expressed by an equivalent Dirac impulse excitation supposed a method is found to establish the impulse's magnitude using the SDOF system parameter and the individual blast wave properties. Some basic aspects of such a proposed method have been briefly touched at the beginning of this chapter but will be presented in full detail in a forthcoming technical memorandum.

ima/maxima values where the *absolute* error influences accuracy for small values close to ± 0, see [34].

[5]For the time history and frequency content shown in Fig. 4.2.1 to 4.2.4, Fig. 4.2.7 and 4.2.8 relative and absolute error for the MATLAB® ode45 solver routine were globally set to $e_R = 1.0\mathrm{E}{-8}$ and $e_A = 1.0\mathrm{E}{-13}$, respectively. In order to ensure reasonable calculation times for the shock spectra in Fig. 4.2.5 and 4.2.6 both limits were increased to $e_R = 1.0\mathrm{E}{-6}$ and $e_A = 1.0\mathrm{E}{-10}$. MATLAB® default values are $e_R = 1.0\mathrm{E}{-3}$, $e_A = 1.0\mathrm{E}{-9}$.

Table 4.2.3: Comparison impulse vs. blast wave type-I excitation for SDOF system $f_1(u) = k\ \mathrm{sign}(u)\ |u|^b$: Nonlinear oscillation frequencies $f_{\mathrm{NL},j}$ in Hz for excitation magnitudes $p_0 = p_\delta = 100\,\mathrm{N}$. Window function: *Blackman-Harris*. The fundamental frequencies $f_{\mathrm{NL},1}$ are **bold**. All values given in the table are pictured in Fig. 4.2.7 on page 143.

b	Impulse	$\alpha = 0.9$ $t_d = 0.02\,\mathrm{s}$	$\alpha = 0.9$ $t_d = 0.05\,\mathrm{s}$	$\alpha = 5.4$ $t_d = 0.02\,\mathrm{s}$	Factor
1	**15.00**	**15.00**	**15.00**	**15.00**	-
2	**10.35** 31.05 51.75 ...	**1.75** 5.25 8.75 ...	**3.15** 9.45 15.75 ...	**1.51** 4.53 7.55 ...	3, 5, 7,...
3	**8.97** 26.92 44.85 ...	**0.45** 1.35 2.25 ...	**1.08** 3.24 5.41 ...	**0.49** 1.49 2.48 ...	3, 5, 7,...
4	**8.41** 25.23 42.05 ...	**0.23** 0.69 1.16 ...	**0.26** 0.79 1.31 ...	**0.43** 1.30 2.14 ...	3, 5, 7,...

It should be noted here that for both cases $p_0 = p_\delta = 100\,\mathrm{N}$ and $p_0 = 10\,\mathrm{kN}$, $p_\delta = 100\,\mathrm{N}$ the nonlinear oscillation frequency changes with time as can easily be seen in Fig. 4.2.1 to 4.2.4. However, a time-dependent Fourier analysis (spectrogram) as produced in chapter 3 for autonomous nonconservative systems revealed no significant difference since the absolute non-steady state (transient) oscillation time in all graphs due to blast loading is rather short compared to the individual oscillation cycles. Since nonlinear oscillation frequency is, amongst other parameters, a function of displacement response amplitude u_{Ex}, this results mainly from the fact that extreme values of displacement response for both states (transient and steady state) differ not significantly.

4.2.2 Restoring force $f_2(u) = k_\alpha u + k_\beta u^3$

The above mentioned forthcoming second part of this report will deal more extensively with SDOF systems having $f_2(u)$ as internal stiffness force, including experimental data analysis. Therefore, investigations presented in the following section will be less exhaustive than in 4.2.1.

4.2.2.1 Time Domain

For a SDOF system with $f_2(u)$ as restoring force figures 4.2.9 and 4.2.10 on pages 145 and 146 show time histories of displacement and velocity response of both, impulse and blast wave type-I excitation. The system under consideration has an assumed linear equivalent oscillation frequency of $f_n = 15\,\mathrm{Hz}$ which establish together with a mass of $m = 3.0\,\mathrm{kg}$ a linear stiffness coefficient of

$$k_\alpha = m\,(2\pi f_n)^2 = m\,\omega_{n,\alpha}^2 .$$

Table 4.2.4: Comparison impulse vs. blast wave type-I excitation for SDOF system $f_1(u) = k\,\mathrm{sign}(u)\,|u|^b$: Nonlinear oscillation frequencies $f_{\mathrm{NL},j}$ in Hz for excitation magnitudes $p_\delta = 100\,\mathrm{N}$ and $p_0 = 10\,\mathrm{kN}$. Window function: *none*. The fundamental frequencies $f_{\mathrm{NL},1}$ are **bold**. All values given in the table are pictured in Fig. 4.2.8 on page 144.

b	Impulse	$\alpha = 0.9$ $t_d = 0.02\,\mathrm{s}$	$\alpha = 0.9$ $t_d = 0.05\,\mathrm{s}$	$\alpha = 5.4$ $t_d = 0.02\,\mathrm{s}$	Factor
1	**15.00**	**15.00**	**15.00**	**15.00**	-
2	**10.35** 31.05 51.75 ...	**10.66** 31.95 53.32 ...	**11.45** 34.35 57.31 ...	**6.95** 20.89 34.81 ...	3, 5, 7,...
3	**8.97** 26.92 44.85 ...	**9.43** 28.31 47.19 ...	**10.81** 32.43 54.09 ...	**4.93** 14.81 24.65 ...	3, 5, 7,...
4	**8.41** 25.23 42.05 ...	**8.61** 25.84 43.07 ...	**10.58** 31.74 52.91 ...	**4.12** 12.36 20.65 ...	3, 5, 7,...

Fixed values for the ratio $k_\gamma = k_\beta / k_\alpha$ define the nonlinear stiffness coefficient $k_\beta = k_\alpha \times k_\gamma$. The shock wave profile parameter α and t_d are identical to the one in the preceding section 4.2.1.

Blast, impulse magnitude $\mathbf{p_0 = p_\delta = 100\,N}$. In Fig. 4.2.9 and 4.2.10 both impulse and blast excitation have identical amplitudes of $p_0 = p_\delta = 100\,\mathrm{N}$. With an increasing nonlinear stiffness ratio $k_\gamma = k_\beta / k_\alpha$ from $0.1\,\mathrm{m}^{-2}$ to $35\,\mathrm{m}^{-2}$ the autonomous system (impulse excitation) shows only small changes in its displacement u_{Ex} and velocity $\dot{u}_{\mathrm{Ex}}$ response amplitudes, which is partially due to the fact that even at $k_\gamma = 35\,\mathrm{m}^{-2}$ the nonlinear stiffness term is not entirely predominant. However, in both figures it is easy to see that $|u_{\mathrm{Ex}}|$ decreases as k_γ increases and the time history of $\dot{u}(t) = v(t)$ takes on a rather different shape[6] compared to $k_\gamma = 0.1\,\mathrm{m}^{-2}$. This clearly indicates that with increasing nonlinearity multi-frequency response becomes prominent and oscillation frequency rises, which is in perfect agreement with the results obtained from the analytical approach in chapter 3 section 3.4.2.

It is worth pointing out that the rather minor changes in the oscillators response in Fig. 4.2.9 and 4.2.10 originate from the narrow range of defined nonlinear ratios $0.1\,\mathrm{m}^{-2} \leq k_\gamma \leq 35\,\mathrm{m}^{-2}$ as well as the small blast and impulse amplitudes of 100 N.

Blast magnitude $\mathbf{p_0 = 10\,kN}$, impulse magnitude $\mathbf{p_0 = 100\,N}$. Leaving the oscillatory SDOF system unaltered and changing only the force magnitude of the blast excitation from $p_0 = 100\,\mathrm{N}$ to $p_0 = 10\,\mathrm{kN}$, hence approximately equalising the total positive force[7] of blast profiles with the pa-

[6]The change of the characteristic sinusoidal, hence harmonic appearance of $v(t)$ into a periodic curve has already been witnessed in section 4.2.1 Fig. 4.2.2 and 4.2.4.

[7]The term 'positive force' of the blast wave profile refers to the force applied to the structure during the interval of positive dynamic overpressure, e.g. $0 \leq t \leq t_d$.

rameter $t_d = 0.02\,\mathrm{s}$ to the force of the scaled Dirac impulse as demonstrated in section 4.2.1, leads to the diagrams presented in Fig. 4.2.11 and 4.2.12. As expected, for stiffness ratios of $k_\gamma = 0.1$ and 0.9, i.e. quasi linear systems, the change in amplitude of u_{Ex} and $\dot{u}_{\mathrm{Ex}}$ is almost exactly the same as for the force magnitude p_0, e.g. an increase of p_0 by a factor of one hundred gives the same magnification of minimum/maximum displacement and velocity compared to extreme values shown in Fig. 4.2.9 and 4.2.10. A minor difference between graphs (a) and (b) of 4.2.11 and 4.2.12 compared to Fig. 4.2.9 and 4.2.10 lies in the slightly lower oscillation frequency f_{NL} for the latter, especially for pictures of case (b) with $k_\gamma = 0.9$, which corresponds to results given in Fig. 3.4.19 section 3.4.2.3 on page 81.

As k_γ increases further the non-normalised displacement and velocity amplitudes become smaller whereas f_{NL} increases further, shown in both graphs (c) and (d) of Fig. 4.2.11 and 4.2.12.

4.2.2.2 Frequency Domain

Shock Spectra. For equal excitation magnitudes $\mathbf{p_\delta = p_0 = 100\,N}$ and loading parameters as given above, Fig. 4.2.13 on page 149 shows shock spectra of the Duffing-type nonlinear SDOF system. Without any doubt, all four plots look similar, which can be mainly ascribed to the small ratio of $k_\gamma = k_\beta / k_\alpha$ and a rather low excitation amplitude p_0. However, a rather striking effect can be observed for the autonomous impulse response, which seems to rise almost linear as f_n increases. A series expansion for ${}_\delta u_{\mathrm{max}_{f_2}} / u_{\mathrm{stat,lin}}$ produces a satisfying approximation for both minima and maxima straight lines shown in Fig. 4.2.13 indicating quasi-linear behaviour for the chosen set of parameters.

As done in the previous section, the system's response is obtained by keeping the impulse amplitude constant at $\mathbf{p_\delta = 100\,N}$ but multiplying the blast profile peak by 100 giving $\mathbf{p_0 = 10\,kN}$. Results for the blast response look familiar to normalised spectra for the linear SDOF in chapter 2 with the negative minimum value in the lower frequency range and the asymptotic approach of the value 2 for the ratio ${}_\delta u_{\mathrm{max}_{f_2}} / u_{\mathrm{stat,lin}}$ as $f_n \to \infty$. Clearly, the chosen impulse response appears far less suitable for modelling the blast behaviour of the Duffing-type characteristic SDOF as this was the case for the $f_1(u)$-type system in Fig. 4.2.5 and 4.2.5 in section 4.2.1.

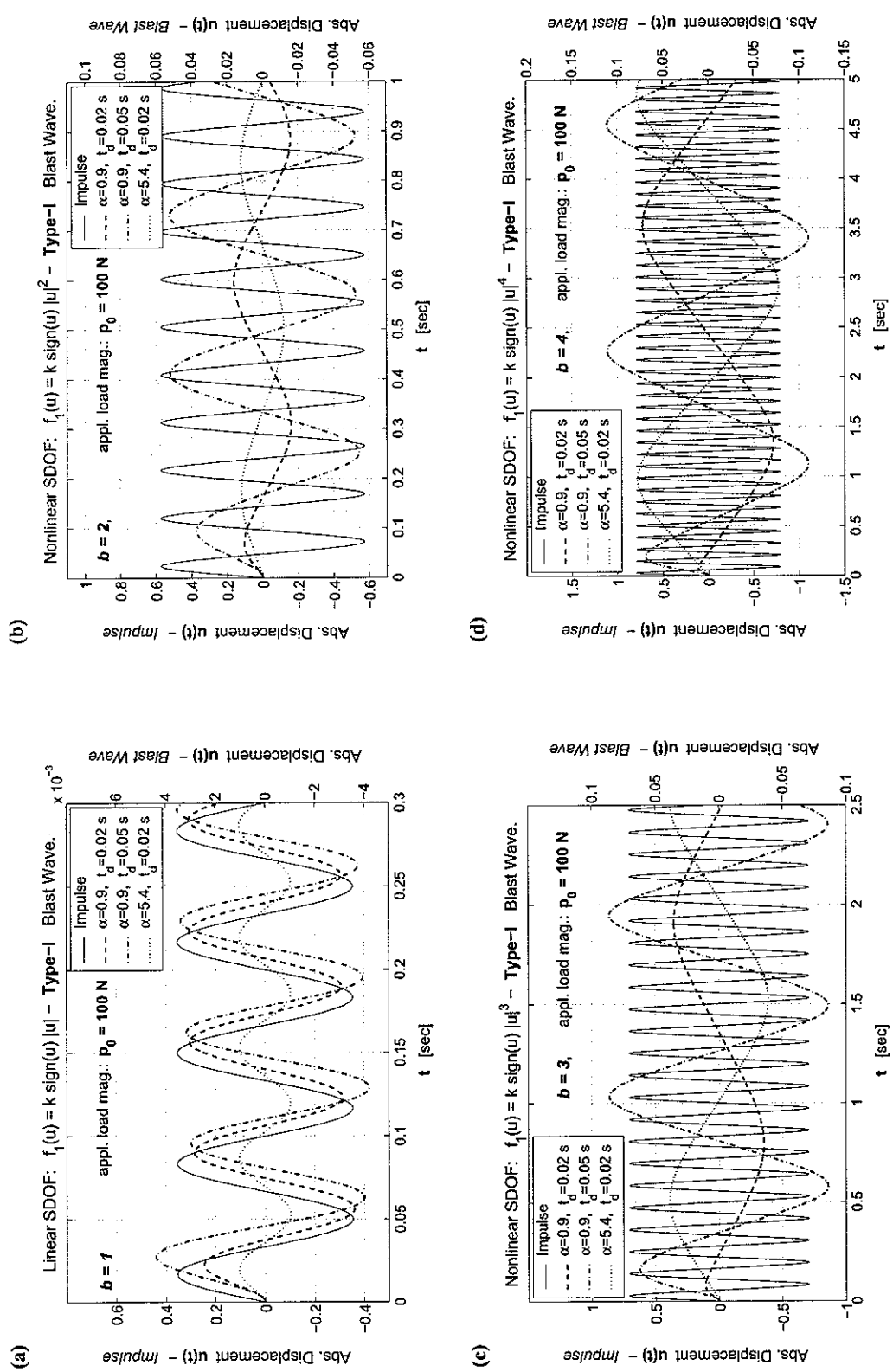

Figure 4.2.1: Nonlinear SDOF oscillator $f_1(u) = k\,\mathrm{sign}(u)\,|u|^b$ - *Blast Wave Type-I Excitation*: Maximum **absolute displacement** for different values of α and t_d (right y-scale) in comparison with Dirac impulse response (left y-scale). All values are given in metres (m). System properties: natural frequency $f_n = 15.0\,\mathrm{Hz}$, mass $m = 3.0\,\mathrm{kg}$, $\omega_n = 2\pi f_n = 30\pi\,\mathrm{rad/s}$, stiffness coefficient $k = m\omega_n^2\,\frac{\mathrm{N}}{\mathrm{m}^b}$. Applied load and initial conditions: $p_0 = 100.0\,\mathrm{N}$, $u_0 = 0.0\,\mathrm{m}$ and $\dot{u}_0 = 0.0\,\frac{\mathrm{m}}{\mathrm{s}}$.

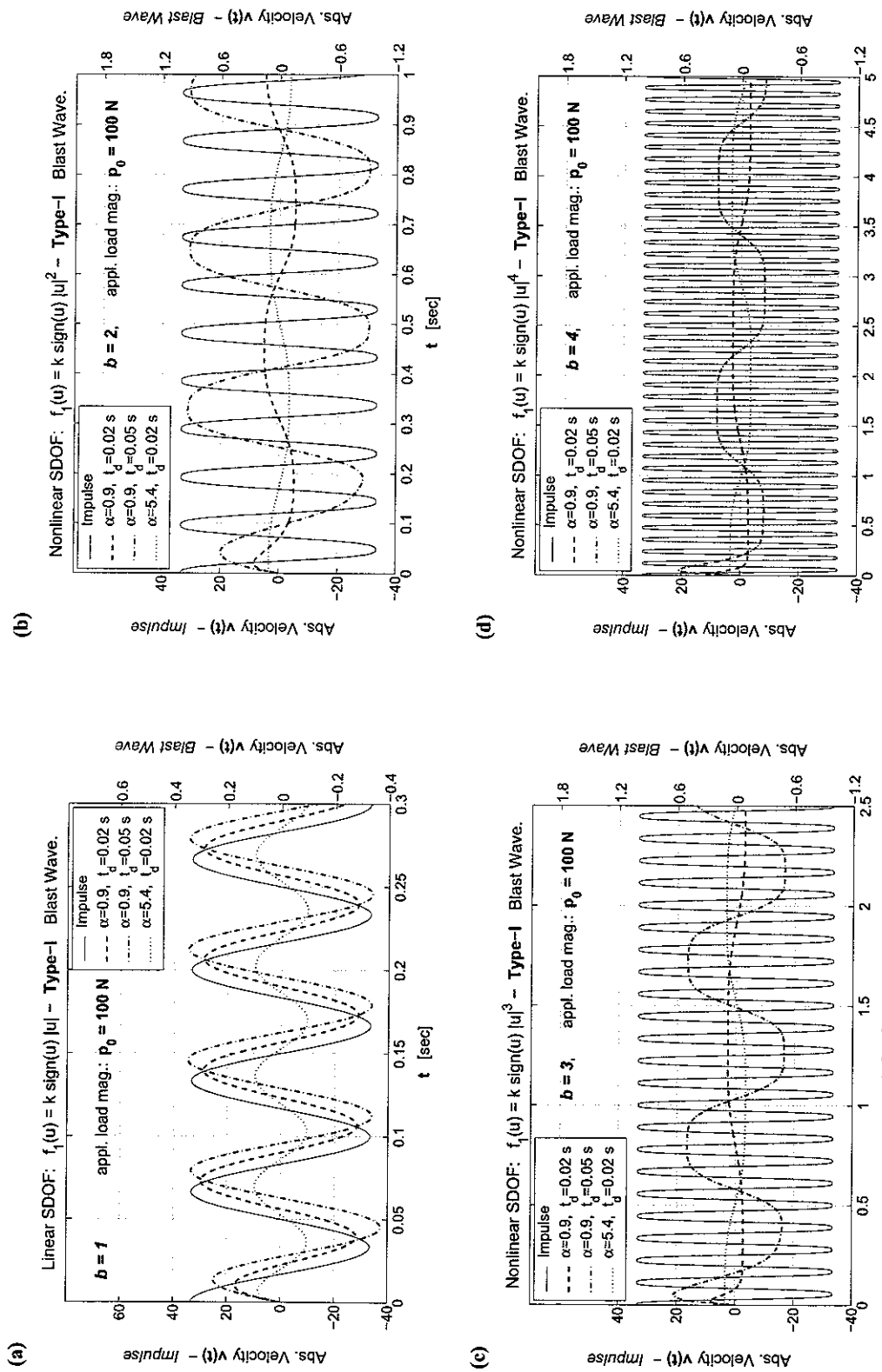

Figure 4.2.2: Nonlinear SDOF system oscillator $f_1(u) = k\,\mathrm{sign}(u)\,|u|^b$ - *Blast Wave Type-I Excitation*: Maximum **absolute velocity** for different values of α and t_d (right y-scale) in comparison with Dirac impulse response (left y-scale). All values are given in meter/second ($\frac{\mathrm{m}}{\mathrm{s}}$). System properties: natural frequency $f_n = 15.0\,\mathrm{Hz}$, mass $m = 3.0\,\mathrm{kg}$, $\omega_n = 2\pi f_n = 30\pi\,\mathrm{rad/s}$, stiffness coefficient $k = m\,\omega_n^2\,\frac{\mathrm{N}}{\mathrm{m}^b}$. Applied load and initial conditions: $p_0 = 100.0\,\mathrm{N}$, $u_0 = 0.0\,\mathrm{m}$ and $\dot{u}_0 = 0.0\,\frac{\mathrm{m}}{\mathrm{s}}$.

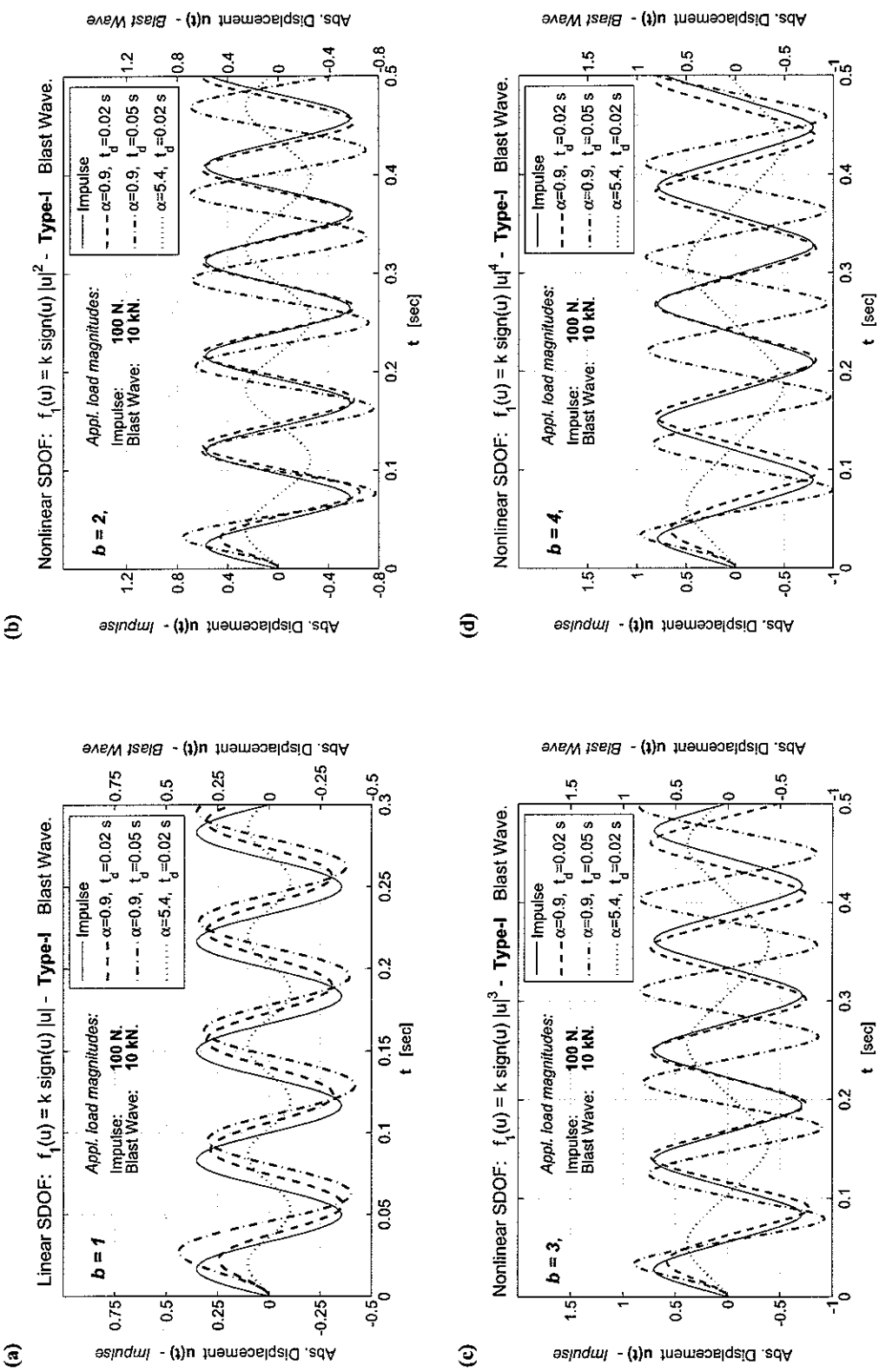

Figure 4.2.3: Nonlinear SDOF oscillator $f_1(u) = k\,\mathrm{sign}(u)\,|u|^b$ - *Blast Wave Type-I Excitation*: Maximum **absolute displacement** for different values of α and t_d (right y-scale) in comparison with Dirac impulse response (left y-scale). All values are given in metres (m). System properties: natural frequency $f_n = 15.0\,\mathrm{Hz}$, mass $m = 3.0\,\mathrm{kg}$, $\omega_n = 2\pi f_n = 30\pi\,\mathrm{rad/s}$, stiffness coefficient $k = m\omega_n^2\,\frac{\mathrm{N}}{\mathrm{m}^b}$. Applied load and initial conditions: $p_0 = 100\,\mathrm{N}$ (impulse), $p_0 = 10\,\mathrm{kN}$ (blast wave), $u_0 = 0.0\,\mathrm{m}$ and $\dot{u}_0 = 0.0\,\frac{\mathrm{m}}{\mathrm{s}}$.

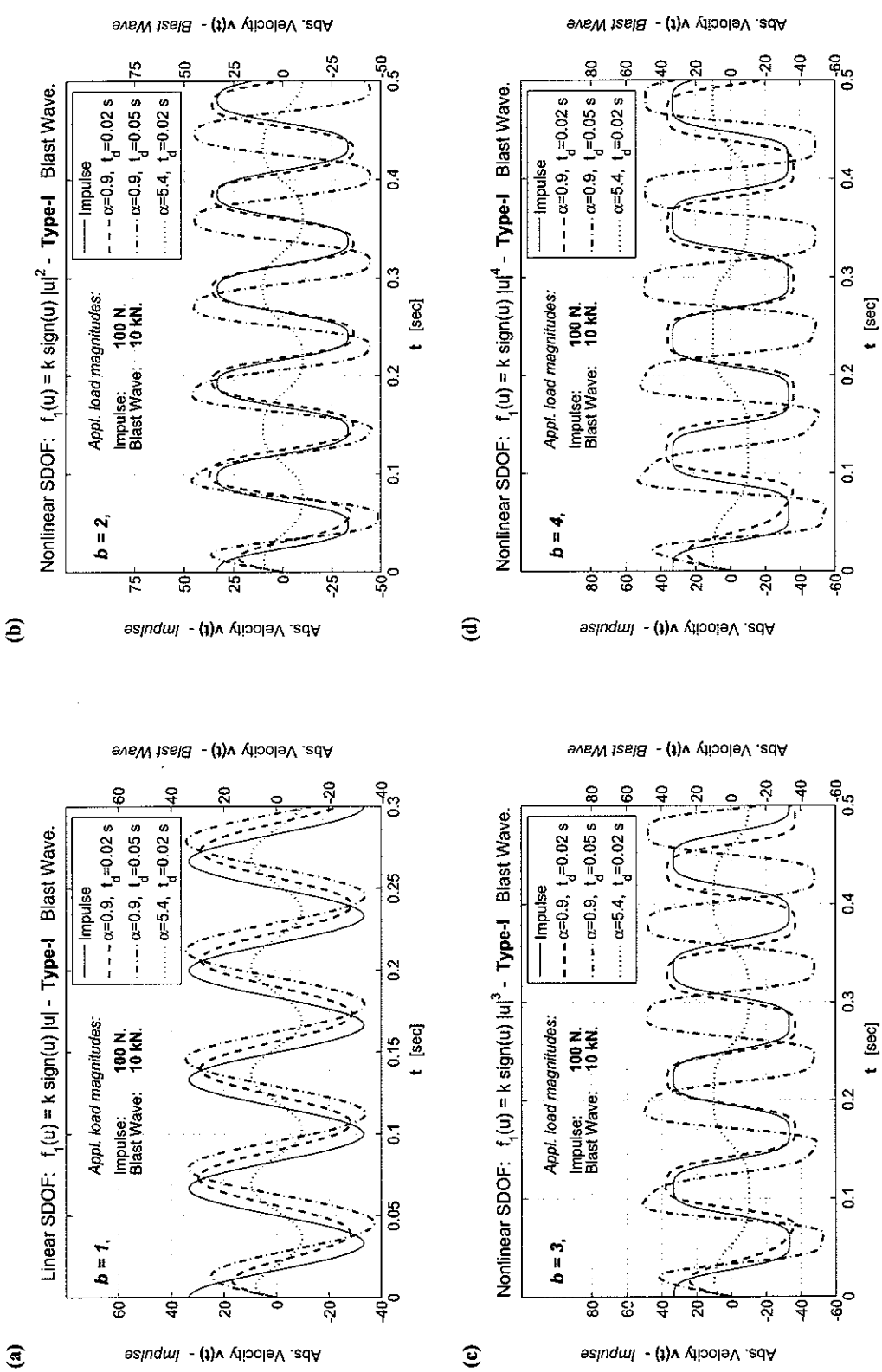

Figure 4.2.4: Nonlinear SDOF system oscillator $f_1(u) = k\,\mathrm{sign}\,(u)\,|u|^b$ - *Blast Wave Type-I Excitation*: Maximum **absolute velocity** for different values of α and t_d (right y-scale) in comparison with Dirac impulse response (left y-scale). All values are given in meter/second ($\frac{\mathrm{m}}{\mathrm{s}}$). System properties: natural frequency $f_n = 15.0\,\mathrm{Hz}$, mass $m = 3.0\,\mathrm{kg}$, $\omega_n = 2\pi f_n = 30\pi\,\mathrm{rad/s}$, stiffness coefficient $k = m\,\omega_n^2\,\frac{\mathrm{N}}{\mathrm{m}^b}$. Applied load and initial conditions: $p_0 = 100\,\mathrm{N}$, $p_0 = 10\,\mathrm{kN}$ (blast wave), $u_0 = 0.0\,\mathrm{m}$ and $\dot{u}_0 = 0.0\,\frac{\mathrm{m}}{\mathrm{s}}$.

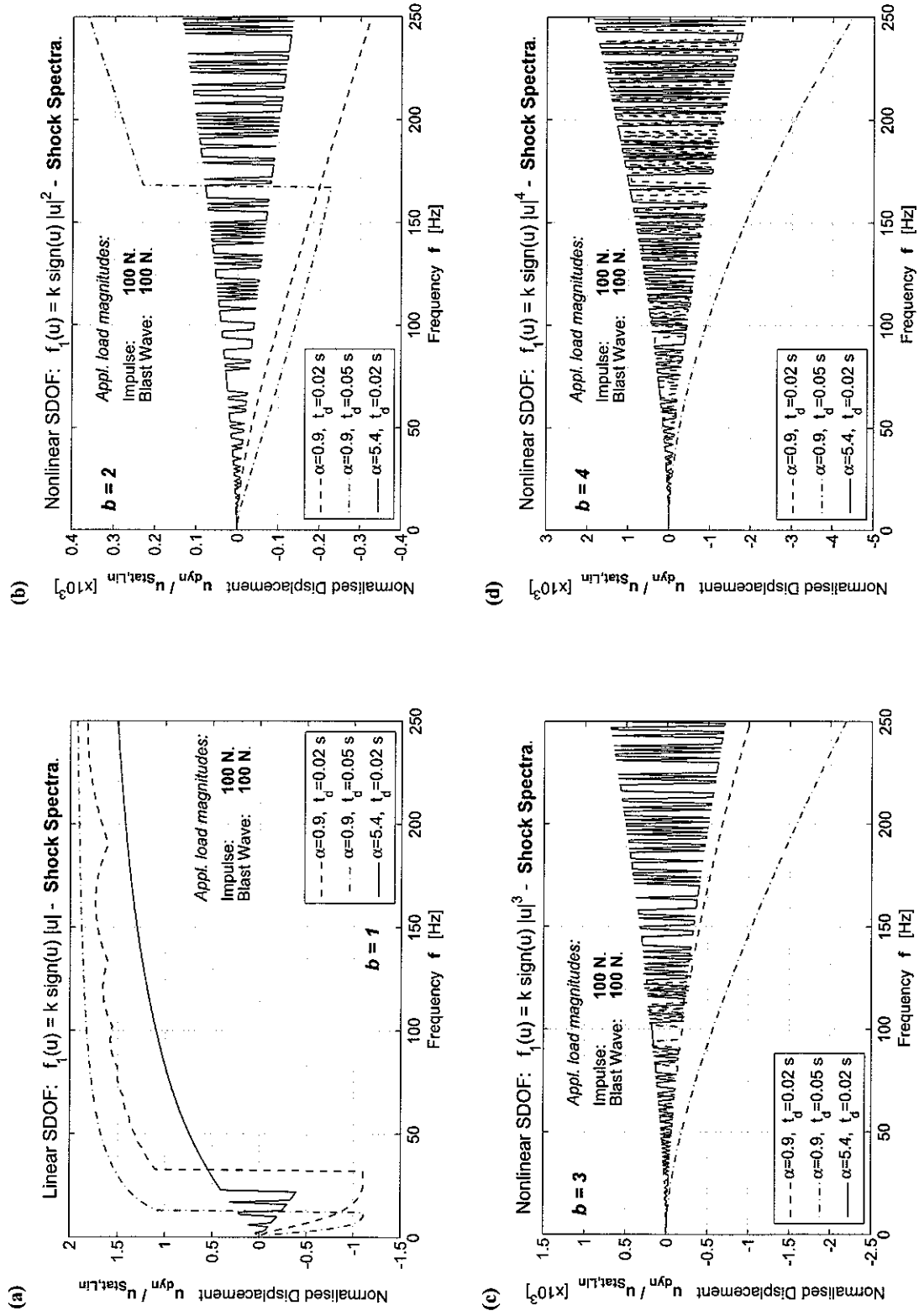

Figure 4.2.5: Nonlinear SDOF system oscillator $f_1(u) = k\,\mathrm{sign}(u)\,|u|^b$ - *Blast Wave Type-I Excitation:* **Shock spectra** for different values of α and t_d normalised to linear static displacement. System properties: natural frequency $0 \leq f_n \leq 250\,\mathrm{Hz}$, mass $m = 3.0\,\mathrm{kg}$, $\omega_n = 2\pi f_n$, stiffness coefficient $k = m\,\omega_n^2\,\frac{\mathrm{N}}{\mathrm{m}^b}$. Applied load and initial conditions: $p_0 = 100\,\mathrm{N}$, $u_0 = 0.0\,\mathrm{m}$ and $\dot{u}_0 = 0.0\,\frac{\mathrm{m}}{\mathrm{s}}$.

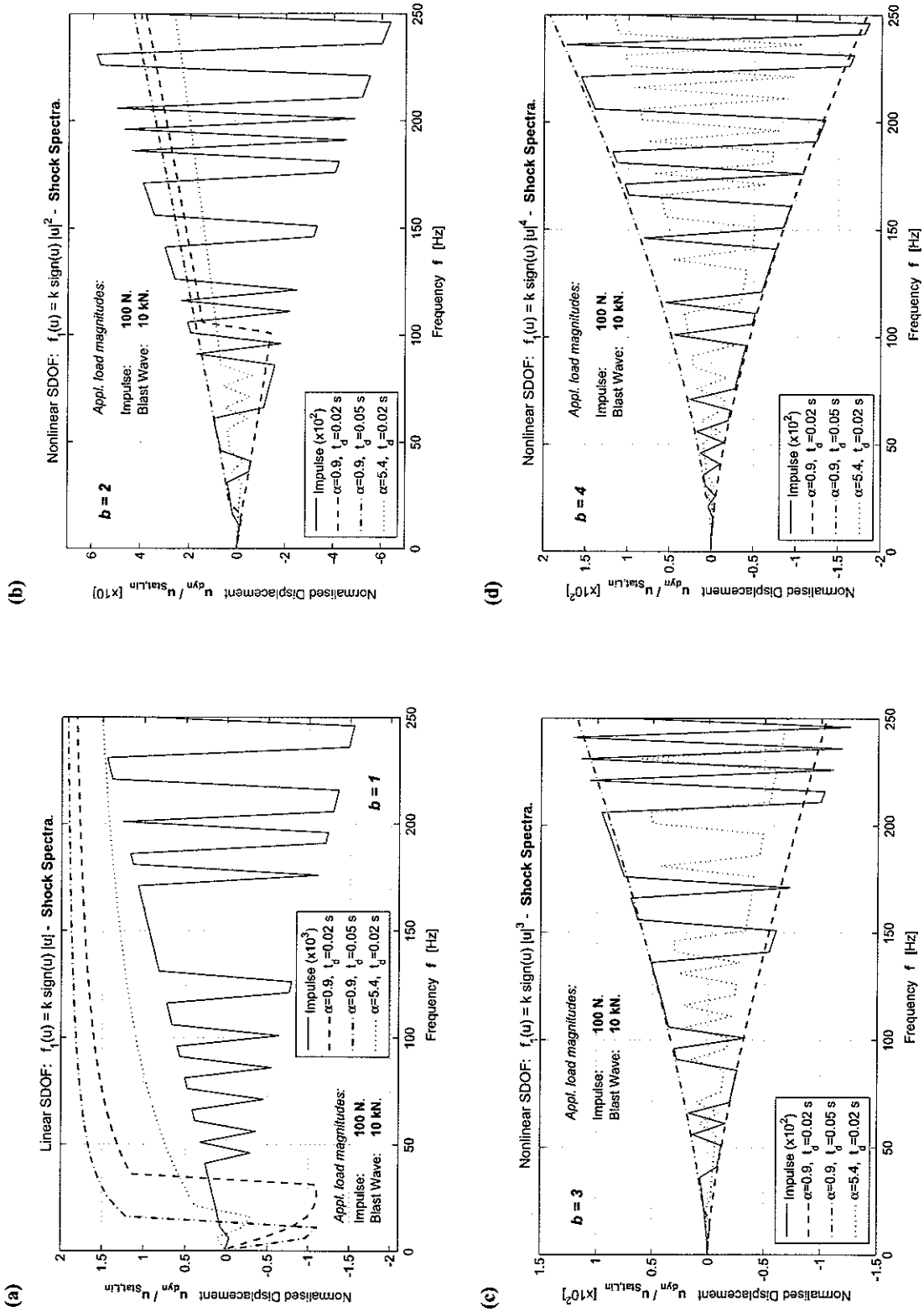

Figure 4.2.6: Nonlinear SDOF system oscillator $f_1(u) = k\,\mathrm{sign}\,(u)\,|u|^b$ - *Blast Wave Type-I Excitation*: **Shock spectra** for different values of α and t_d normalised to linear static displacement. System properties: natural frequency $0 \leq f_n \leq 250\,\mathrm{Hz}$, mass $m = 3.0\,\mathrm{kg}$, $\omega_n = 2\pi f_n$, stiffness coefficient $k = m\,\omega_n^2\,\frac{\mathrm{N}}{\mathrm{m}^b}$. Applied load and initial conditions: $p_0 = 10\,\mathrm{kN}$, $p_\delta = 100\,\mathrm{N}$, $u_0 = 0.0\,\mathrm{m}$ and $\dot{u}_0 = 0.0\,\frac{\mathrm{m}}{\mathrm{s}}$.

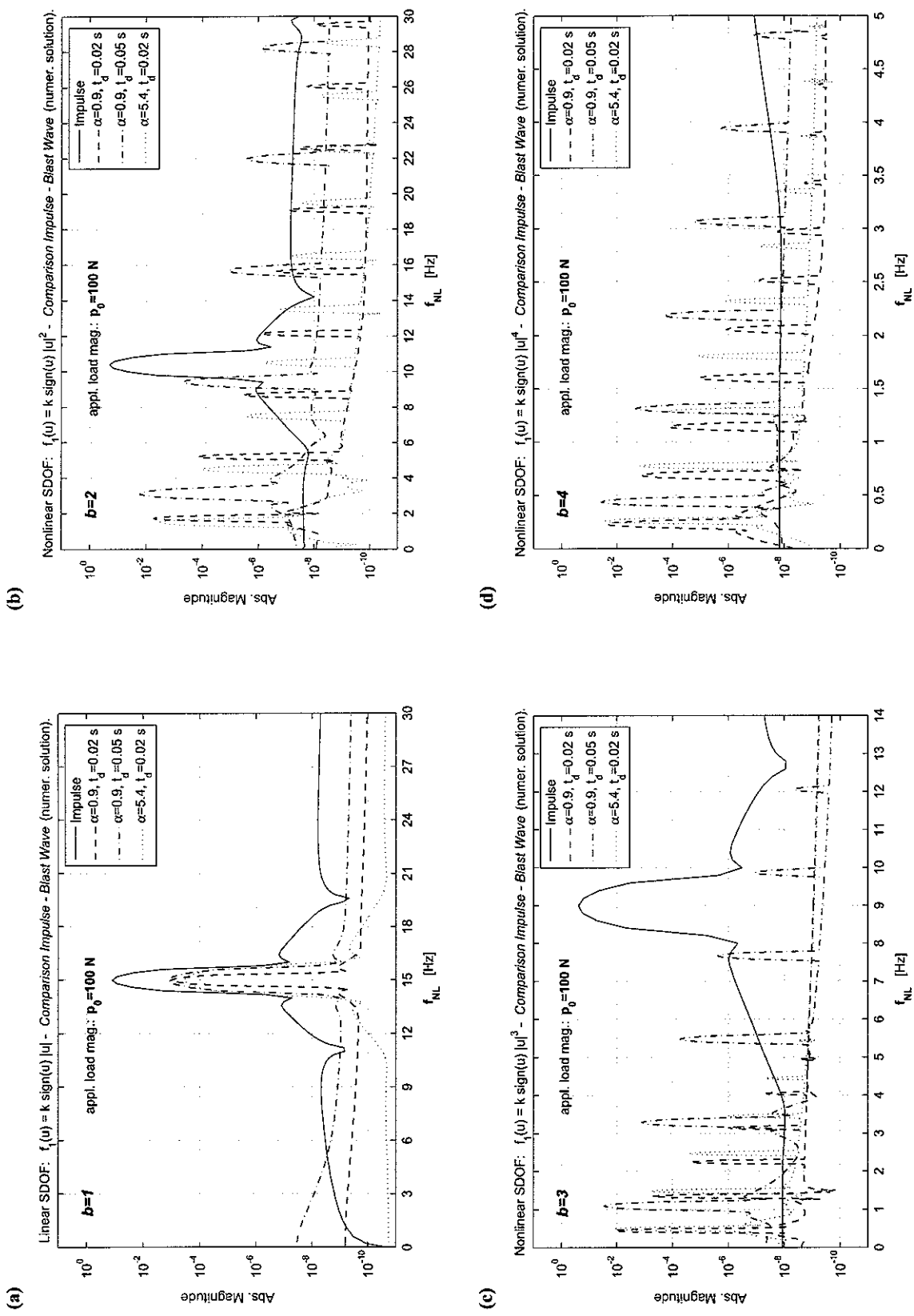

Figure 4.2.7: Nonlinear SDOF system oscillator $f_1(u) = k\,\mathrm{sign}(u)\,|u|^b$ - *Blast Wave Type-I Excitation*: **Frequency content** for different values of α and t_d. Window function: *Blackman-Harris*. System properties: equivalent linear natural frequency $f_n = 15\,\mathrm{Hz}$, mass $m = 3.0\,\mathrm{kg}$, $\omega_n = 2\pi f_n$, stiffness coefficient $k = m\,\omega_n^2\,\frac{\mathrm{N}}{\mathrm{m}^b}$. Applied load and initial conditions: $p_0 = p_\delta = 100\,\mathrm{N}$, $u_0 = 0.0\,\mathrm{m}$ and $\dot{u}_0 = 0.0\,\frac{\mathrm{m}}{\mathrm{s}}$.

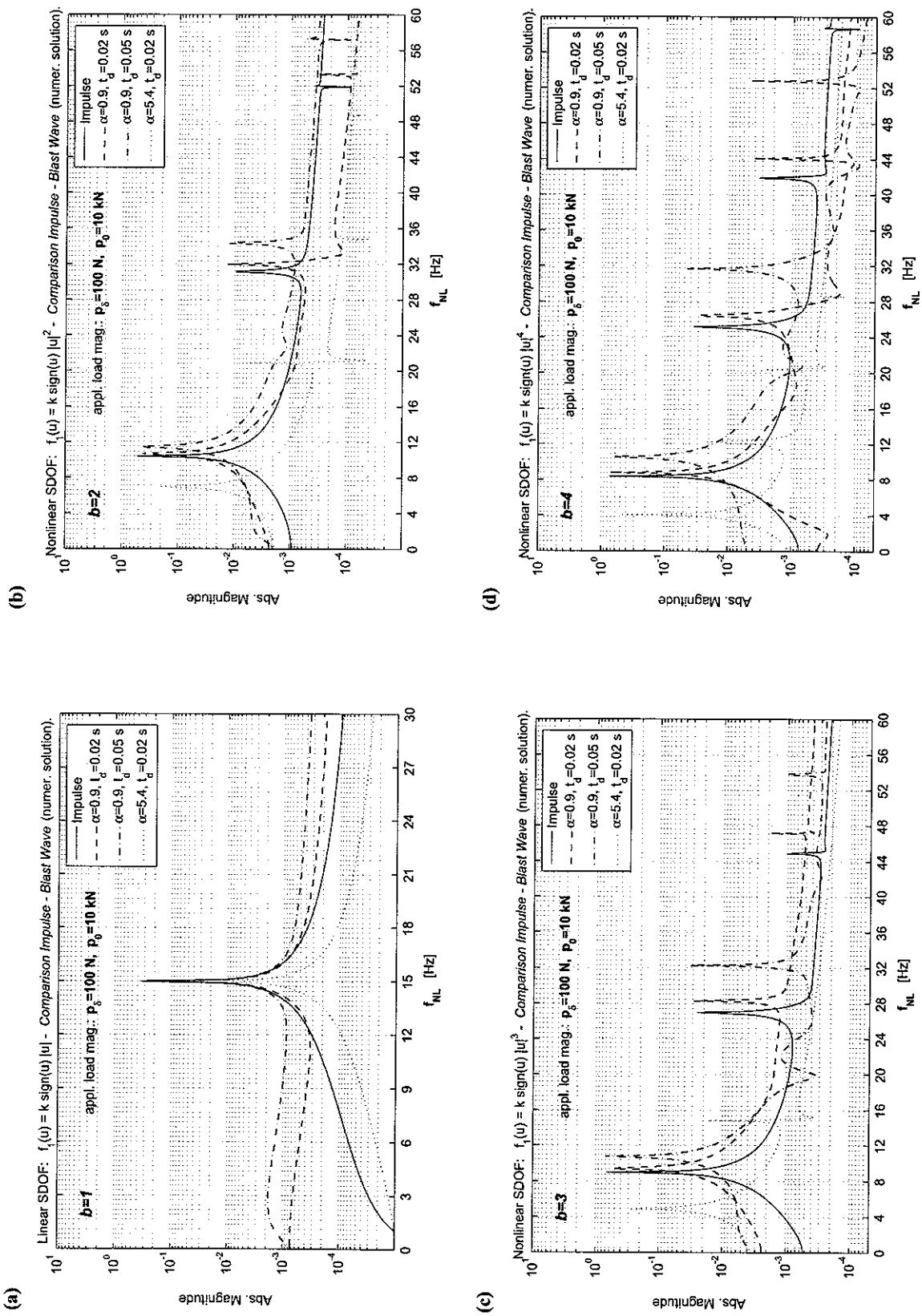

Figure 4.2.8: Nonlinear SDOF system oscillator $f_1(u) = k\,\mathrm{sign}(u)\,|u|^b$ - *Blast Wave Type-I Excitation*: **Frequency content** for different values of α and t_d. Window function: *none*. System properties: equivalent linear natural frequency $f_n = 15\,\mathrm{Hz}$, mass $m = 3.0\,\mathrm{kg}$, $\omega_n = 2\pi f_n$, stiffness coefficient $k = m\,\omega_n^2\,\frac{\mathrm{N}}{\mathrm{m}^b}$. Applied load and initial conditions: $p_0 = 10\,\mathrm{kN}$, $p_\delta = 100\,\mathrm{N}$, $u_0 = 0.0\,\mathrm{m}$ and $\dot{u}_0 = 0.0\,\frac{\mathrm{m}}{\mathrm{s}}$.

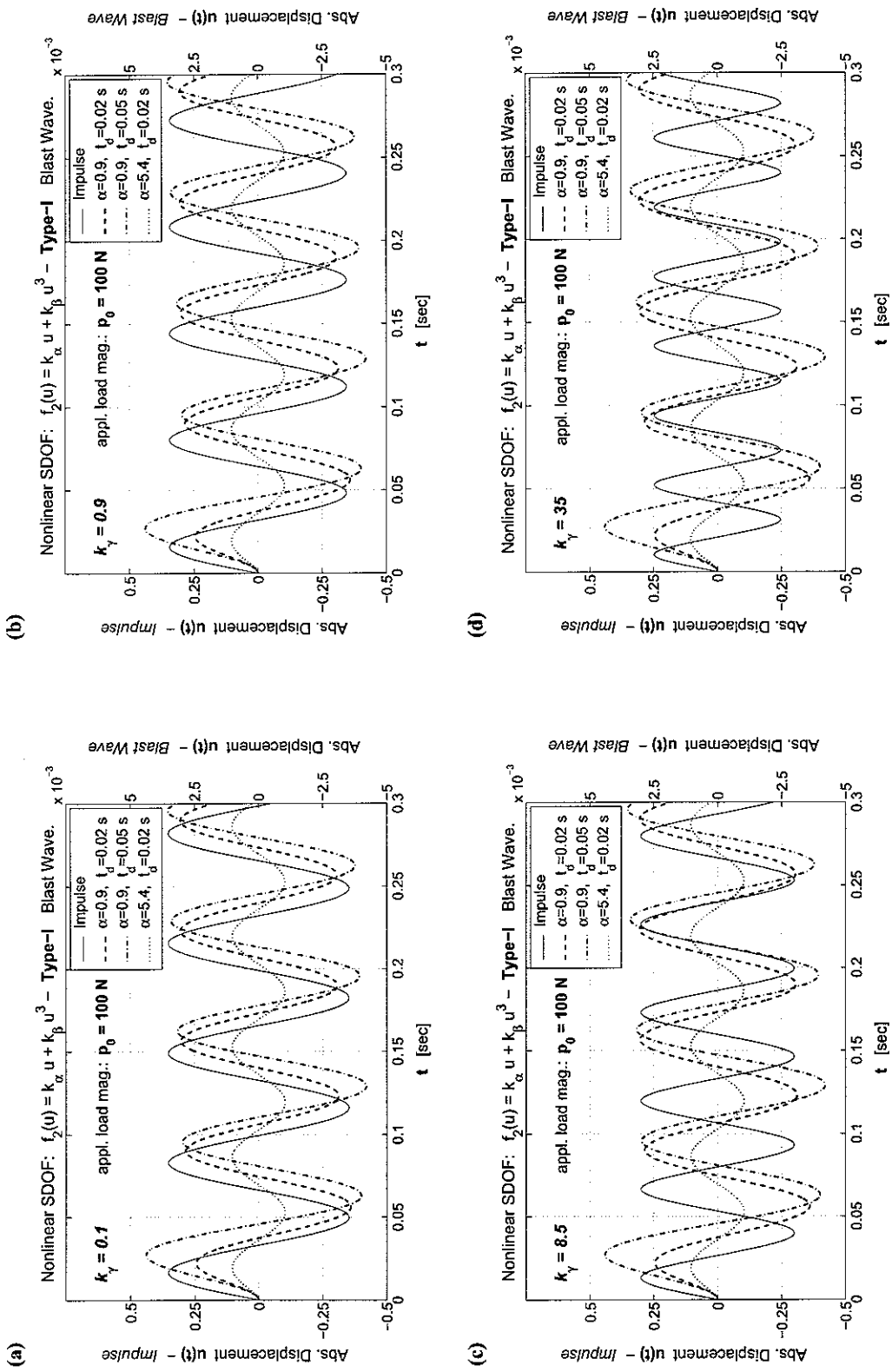

Figure 4.2.9: Nonlinear SDOF system oscillator $f_2(u) = k_\alpha u + k_\beta u^3$ - *Blast Wave Type-I Excitation*: Maximum **absolute displacement** for different values of α and t_d (right y-scale) in comparison with Dirac impulse response (left y-scale). All values are given in metres (m). System properties: natural frequency $f_n = 15.0\,\text{Hz}$, mass $m = 3.0\,\text{kg}$, $\omega_{n,\alpha} = 2\pi f_n = 30\pi\,\text{rad/s}$, stiffness $k_\alpha = m\,\omega_{n,\alpha}^2\,\frac{\text{N}}{\text{m}}$, $k_\beta = k_\gamma \times k_\alpha\,\frac{\text{N}}{\text{m}^3}$. Applied load and initial conditions: $p_0 = 100.0\,\text{N}$, $u_0 = 0.0\,\text{m}$ and $\dot{u}_0 = 0.0\,\frac{\text{m}}{\text{s}}$.

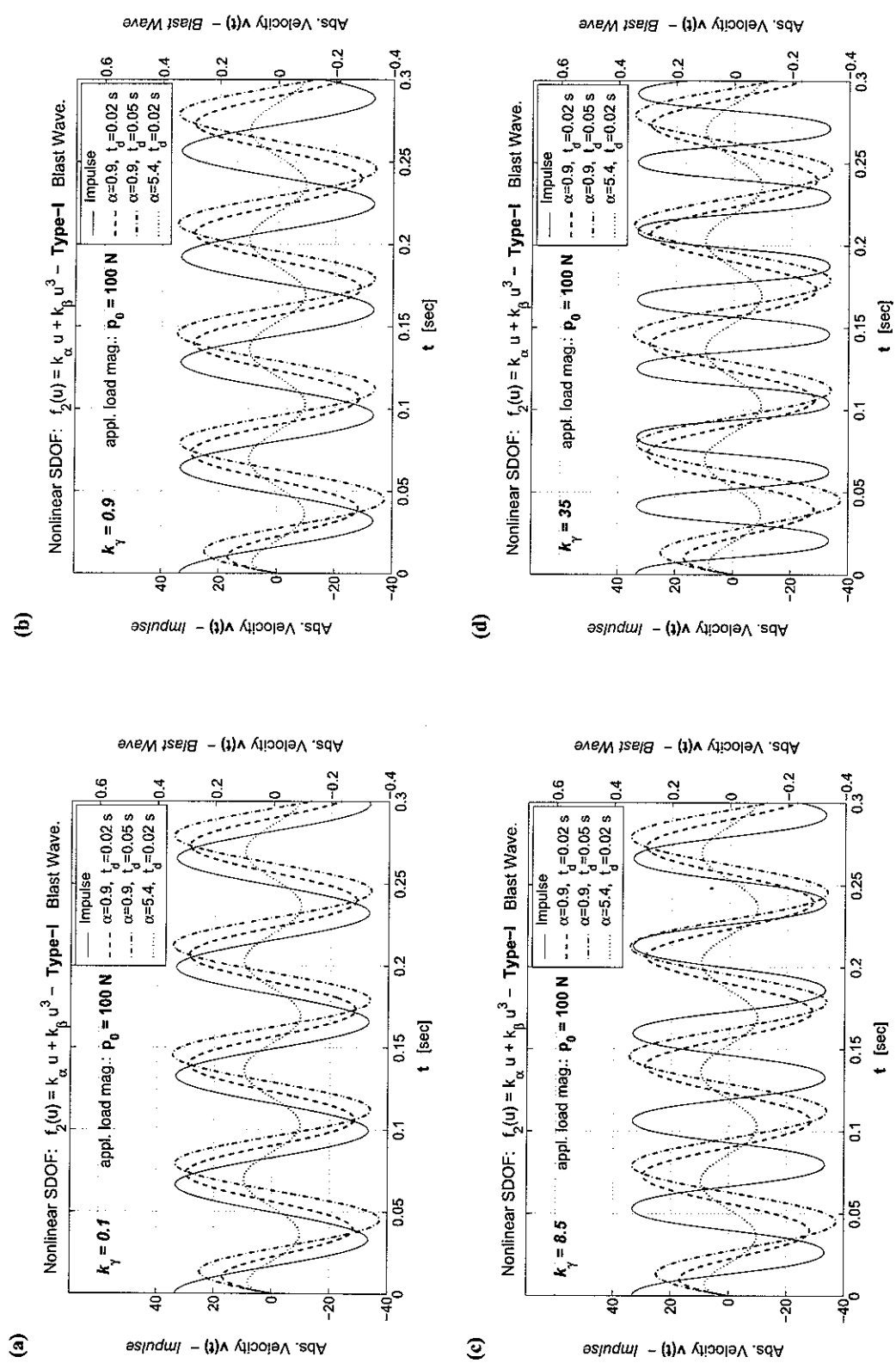

Figure 4.2.10: Nonlinear SDOF system oscillator $f_2(u) = k_\alpha u + k_\beta u^3$ - *Blast Wave Type-I Excitation*: Maximum **absolute velocity** for different values of α and t_d (right y-scale) in comparison with Dirac impulse response (left y-scale). All values are given in meter/second ($\frac{\text{m}}{\text{s}}$). System properties: natural frequency $f_n = 15.0\,\text{Hz}$, mass $m = 3.0\,\text{kg}$, $\omega_{n,\alpha} = 2\pi f_n = 30\pi\,\text{rad/s}$, stiffness $k_\alpha = m\,\omega_{n,\alpha}^2\,\frac{\text{N}}{\text{m}}$, $k_\beta = k_\gamma \times k_\alpha\,\frac{\text{N}}{\text{m}^3}$. Applied load and initial conditions: $p_0 = 100.0\,\text{N}$, $u_0 = 0.0\,\text{m}$ and $\dot{u}_0 = 0.0\,\frac{\text{m}}{\text{s}}$.

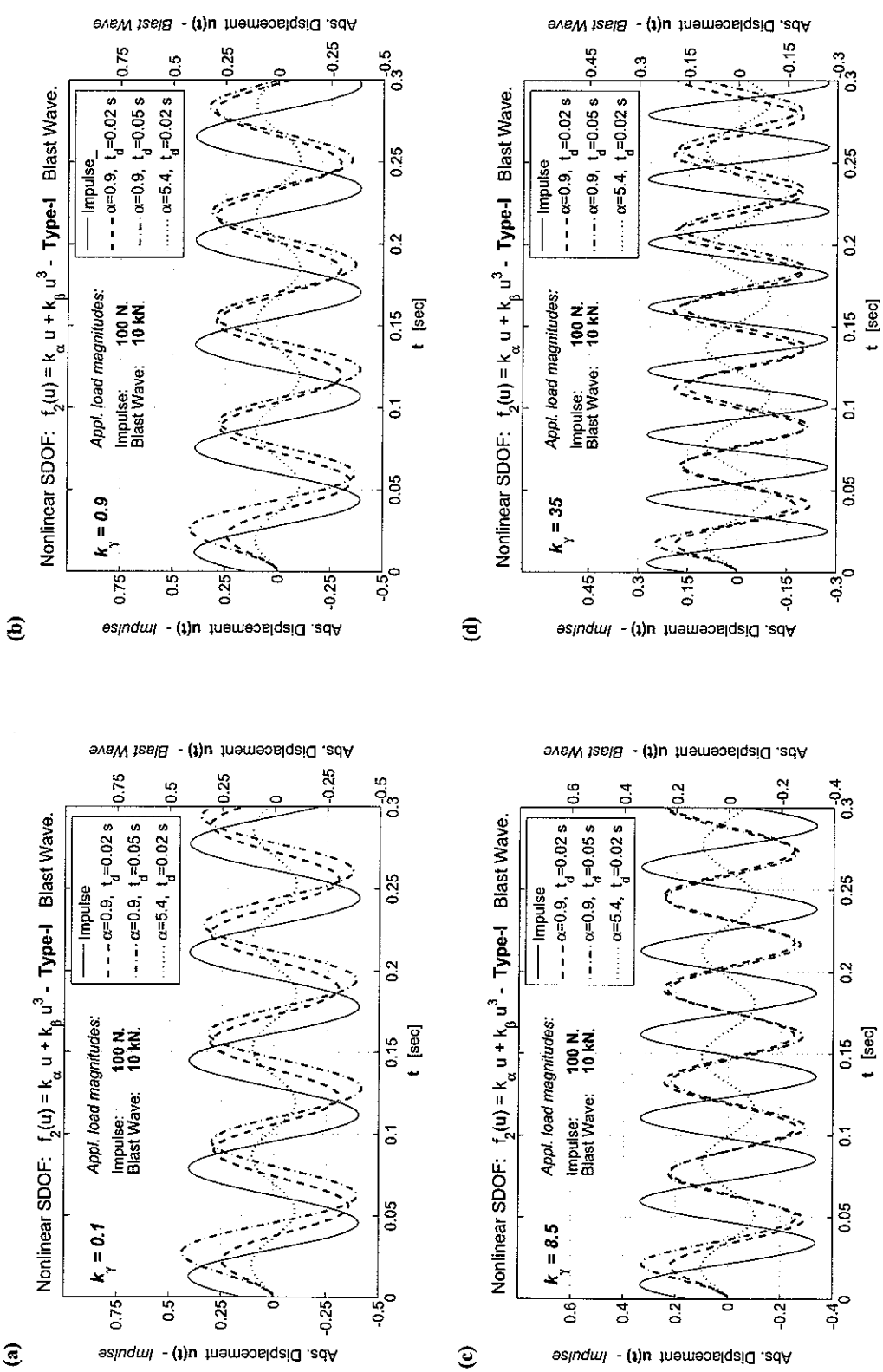

Figure 4.2.11: Nonlinear SDOF system oscillator $f_2(u) = k_\alpha u + k_\beta u^3$ - *Blast Wave Type-I Excitation*: Maximum **absolute displacement** for different values of α and t_d (right y-scale) in comparison with Dirac impulse response (left y-scale). All values are given in metres (m). System properties: natural frequency $f_n = 15.0\,\text{Hz}$, mass $m = 3.0\,\text{kg}$, $\omega_{n,\alpha} = 2\pi f_n = 30\pi\,\text{rad/s}$, stiffness $k_\alpha = m\,\omega_{n,\alpha}^2\,\frac{\text{N}}{\text{m}}$, $k_\beta = k_\gamma \times k_\alpha\,\frac{\text{N}}{\text{m}^3}$. Applied load and initial conditions: $p_0 = 100.0\,\text{N}$ (impulse), $p_0 = 10\,\text{kN}$ (blast wave), $u_0 = 0.0\,\text{m}$ and $\dot{u}_0 = 0.0\,\frac{\text{m}}{\text{s}}$.

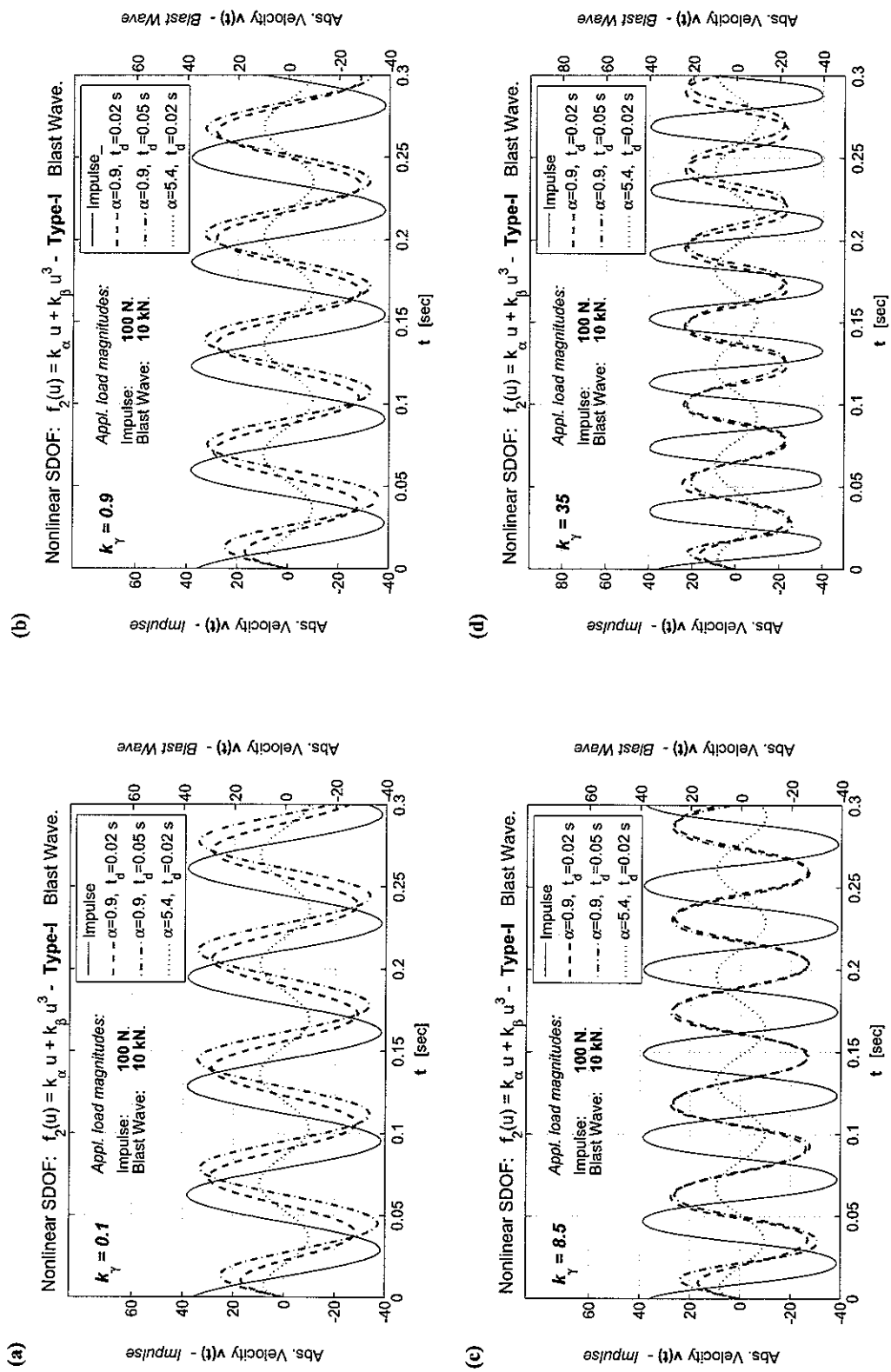

Figure 4.2.12: Nonlinear SDOF system oscillator $f_2(u) = k_\alpha u + k_\beta u^3$ - *Blast Wave Type-I Excitation:* Maximum **absolute velocity** for different values of α and t_d (right y-scale) in comparison with Dirac impulse response (left y-scale). All values are given in meter/second ($\frac{m}{s}$). System properties: natural frequency $f_n = 15.0\,\text{Hz}$, mass $m = 3.0\,\text{kg}$, $\omega_{n,\alpha} = 2\pi f_n = 30\pi\,\text{rad/s}$, stiffness $k_\alpha = m\,\omega_{n,\alpha}^2\,\frac{N}{m}$, $k_\beta = k_\gamma \times k_\alpha\,\frac{N}{m^3}$. Applied load and initial conditions: $p_0 = 100.0\,\text{N}$ (impulse), $p_0 = 10\,\text{kN}$ (blast wave), $u_0 = 0.0\,\text{m}$ and $\dot{u}_0 = 0.0\,\frac{m}{s}$.

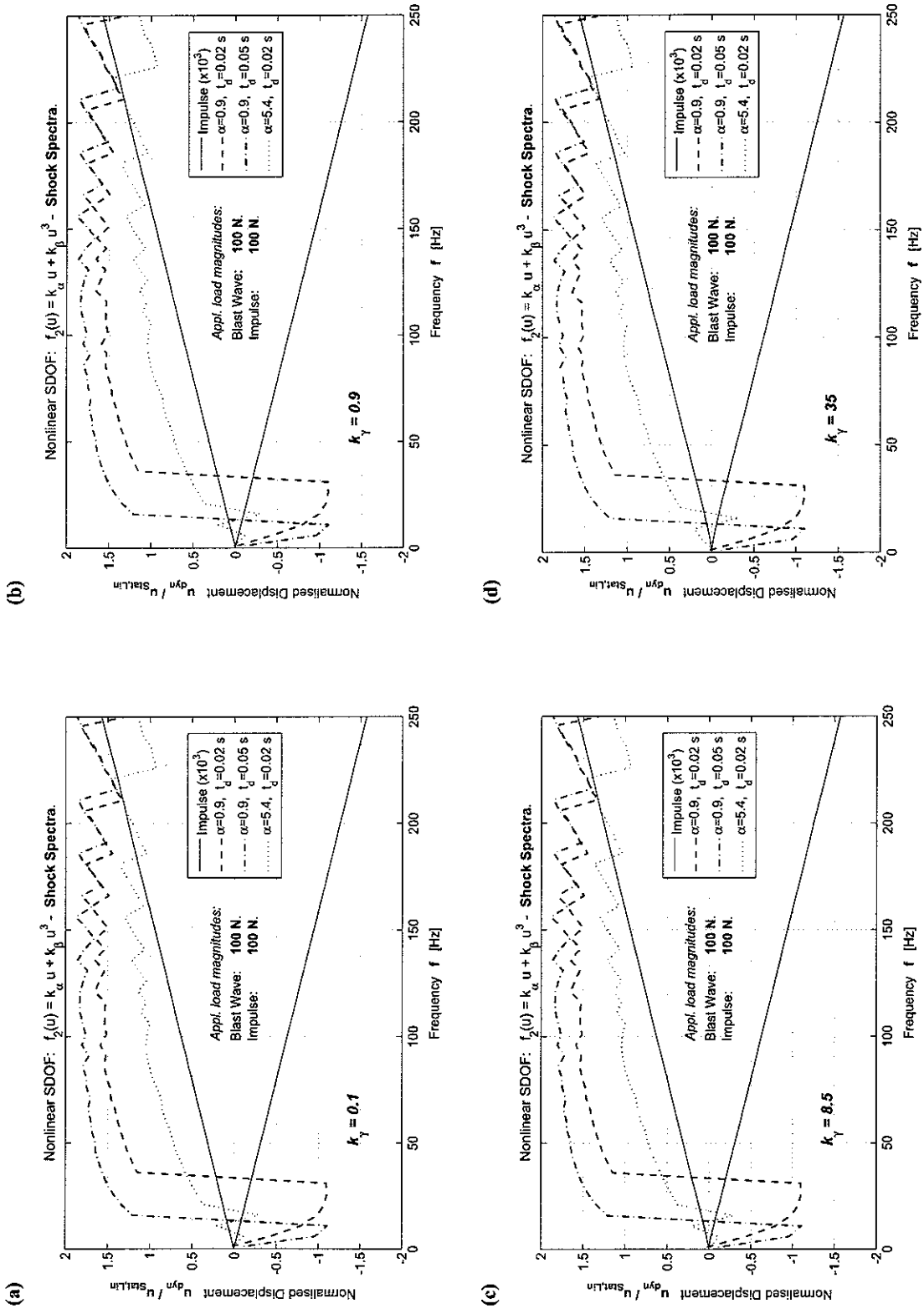

Figure 4.2.13: Nonlinear SDOF system oscillator $f_2(u) = k_\alpha\, u + k_\beta\, u^3$ - *Blast Wave Type-I Excitation*: **Shock spectra** for different values of α and t_d normalised to linear static displacement. System properties: natural frequency $0 \leq f_n \leq 250\,\mathrm{Hz}$, mass $m = 3.0\,\mathrm{kg}$, $\omega_n = 2\pi f_n$, stiffness coefficients $k_\alpha = m\,\omega_n^2\,\mathrm{N/m}$, $k_\beta = k_\alpha \times k_\gamma\,\mathrm{N/m^3}$. Applied load and initial conditions: $p_0 = p_\delta = 100\,\mathrm{N}$, $u_0 = 0.0\,\mathrm{m}$ and $\dot{u}_0 = 0.0\,\mathrm{m/s}$.

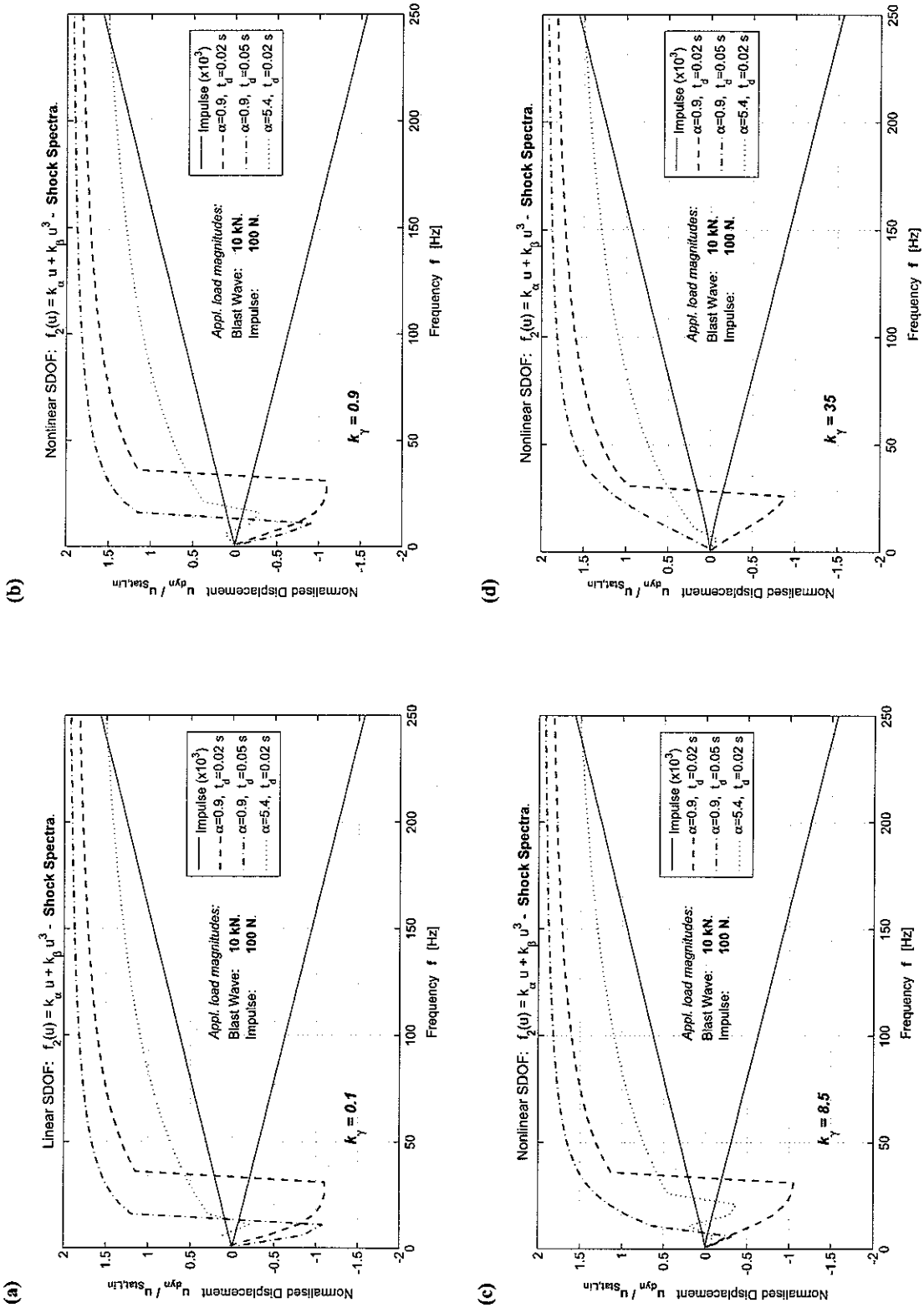

Figure 4.2.14: Nonlinear SDOF system oscillator $f_2(u) = k_\alpha u + k_\beta u^3$ - *Blast Wave Type-I Excitation*: **Shock spectra** for different values of α and t_d normalised to linear static displacement. System properties: natural frequency $0 \leq f_n \leq 250\,\text{Hz}$, mass $m = 3.0\,\text{kg}$, $\omega_n = 2\pi f_n$, stiffness coefficients $k_\alpha = m\,\omega_n^2\,\frac{\text{N}}{\text{m}}$, $k_\beta = k_\alpha \times k_\gamma\,\text{N/m}^3$. Applied load and initial conditions: $p_0 = 10\,\text{kN}$, $p_\delta = 100\,\text{N}$, $u_0 = 0.0\,\text{m}$ and $\dot{u}_0 = 0.0\,\text{m/s}$.

CHAPTER 5

Summary and Discussion

This work has been aimed to help understanding the rather complex dynamic processes involved in describing the geometrical nonlinear response of structural single-degree-of-freedom (SDOF) systems to specific types of transient excitation, in particular shock waves originating from blasts.

The well established empirical blast profile has been extended taking the small but finite rising time of the positive dynamic overpressure into account. However, for most linear or nonlinear structural systems with low natural frequencies up to 250 Hz this proved not to be of major significance.

For linear SDOF oscillator closed form solutions for both types of blast profiles were established describing the system's displacement response in both time and frequency domain. No analytical solution could be retrieved in order to rewrite minimum and maximum displacement due to blast excitation as a function of the linear system's natural frequency. Nevertheless, a piecewise linearisation of the excitation force function lead to an analytical approximation method, which proved to be reliable and much faster than time domain numerical methods.

Reformulating and extending an established energy conservation approach for autonomous non-dissipative SDOF systems made it possible to find closed form solutions for oscillators with elastic but geometrical nonlinear restoring forces which give extreme values of displacement and velocity as well as the nonlinear oscillation frequencies. The newly derived expressions were applied to two commonly known polynomial-type nonlinear restoring forces and verified using well-established numerical procedures. Comparison between both methods revealed very good agreement.

Using numerical algorithms, since analytical expressions do not exist, data for autonomous non-conservative systems with different levels of viscous damping was produced. It has been found that for a broad range of structural systems under consideration having light to moderate damping the results obtained for the conservative system using the analytical solution methods are still very useful.

Finding specific combinations of nonlinear SDOF oscillators and blast wave profiles which can be described in terms of extreme values of displacement and velocity by using the analytical results for impulse excitation functions can be regarded as successful, at least for the $f_1(u)$-type restoring force. Although the method employed is merely a first-order approximation, time and frequency domain results obtained for autonomous systems exhibit similar characteristics compared to the behaviour of the actual blast response of the SDOF. The obvious disagreement of results for the Duffing-type

system can mainly be ascribed to the crude approximation of the simplified method. This will be improved considerably as the approximation method will be developed further and a forthcoming report containing a more elaborated and detailed description is already in progress.

Furthermore, this second part will not only contain experimental data supporting all theoretical results presented in this work, it also aimed at reproducing entire time-histories of nonlinear autonomous SDOF systems.

Bibliography

[1] Schaedlich, M. and Ferguson, N., "Blast Induced Shock Waves in Structures - 12 Month Progress Report." ISVR PhD progress report 2, Institute of Sound and Vibration Research, University of Southampton, December 2003.

[2] Kinney, G. and Graham, K., *Explosive Shocks in Air*, Springer-Verlag, New York, 1985.

[3] Harris, C., *Shock and Vibration Handbook*, McGraw-Hill, New York, 3rd ed., 1988.

[4] Newmark, N., "A method of computation for structural dynamics," *ASCE Journal of the Engineering Mechanics Division*, Vol. 85, No. EM3, 1959, pp. 67–94.

[5] Runge, C., "Ueber die numerische Aufloesung von Differentialgleichungen," *Mathematische Annalen*, Vol. 3, No. 46, 1895, pp. 167–178.

[6] Bapat, V. and Srinivasan, P., "Response spectrum of nonlinear spring mass system subjected to transient disturbance," *Journal of Sound and Vibration*, Vol. 8, No. 3, 1968, pp. 482–487.

[7] Bapat, V. and Srinivasan, P., "Response of undamped non-linear spring mass systems subjected to constant force excitation," *Journal of Sound and Vibration*, Vol. 9, No. 1, 1969, pp. 53–58.

[8] Bapat, V. and Srinivasan, P., "Response of undamped non-linear spring mass systems subjected to constant force excitation," *Journal of Sound and Vibration*, Vol. 9, No. 3, 1969, pp. 438–446.

[9] "The Prediction of the Pressure Loading on Structures Resulting from an Explosion." Offshore Technology Information OTI 92 594, British Gas Research and Technology (MRS), The Steel Construction Institute, Silwood Park, Ascot, Berkshire, SL5 7NQ, 1992.

[10] "Explicit Analytical Methods for determining Structural Response," Offshore Technology Information OTI 92600, British Gas Research and Technology (MRS), The Steel Construction Institute, Silwood Park, Ascot, Berkshire, SL5 7NQ, 1992.

[11] Glasstone, S. and Dolan, P., *The Effects of Nuclear Weapons*, Castle House Publications Ltd., 3rd ed., 1980.

[12] Baker, W., *Explosion Hazards Evaluation*, Elsevier Scientific Publishing Co., 1983.

[13] Biggs, J., *Introduction to Structural Dynamics*, McGraw-Hill, New York, 1964.

[14] Warburton, G., *The Dynamical Behaviour of Structures*, Structures and Solid Body Mechanics, Pergamon Press, Oxford, 2nd ed., 1976.

[15] Bronstein, I. and Semendjajew, K., *Taschenbuch der Mathematik (Handbook of mathematical Formulas)*, Verlag Nauka, Moscow; B.G.Teubner Verlagsgesellschaft Stuttgart, 26th ed., 1992.

[16] Meirovitch, L., *Elements of Vibration Analysis*, McGraw-Hill Book Company, New York, 2nd ed., 1986.

[17] Jeffrey, A., *Table of Integrals, Series, and Products*, Academic Press, London, Corrected and Enlarged ed., 1980.

[18] Dyne, S., "The Prediction of the Response and Damage Potential of Structures under Shock Loading," Contract Report Ref.: D/ER1/9/4/2040/394-SAL 1053, Institute of Sound and Vibration, University of Southampton, 1985.

[19] Timoshenko, S., Young, D., and Weaver, W., *Vibration Problems in Engineering*, John Wiley & Sons, New York, 4th ed., 1974.

[20] Wolfram, S., *The Mathematica Book*, Wolfram Research, Inc., Urbana-Champaign, Il., USA; www.wolfram.com, 4th ed., 1998.

[21] Abramowitz, M. and Stegun, I., *Handbook of mathematical functions*, Dover, New York, 1968.

[22] Byrd, P. and Friedman, M., *Handbook of Elliptic Integrals for Engineers and Physicists*, Vol. LXVII of *Die Grundlehren der Mathematischen Wissenschaften*, Springer-Verlag, Berlin, Heidelberg, 1954.

[23] Groebner, W. and Hofreiter, N., *Integraltafeln - Erster Teil: Unbestimmte Integrale*, Vol. 1, Springer-Verlag, Wien and Innsbruck, 2nd ed., 1957.

[24] Hancock, H., *Elliptic Integrals*, Dover Publications, New York, 1958.

[25] Kutta, W., "Beitrag zur naeherungsweisen Integration totaler Differentialgleichungen," *Zeitschrift fuer Mathematik und Physik*, Vol. 46, 1901, pp. 435–453.

[26] Bathe, K. and Wilson, E., "Stability and accuracy analysis of direct integration methods," *Earthquake Engineering and Structural Dynamics*, Vol. 1, 1973, pp. 283–291.

[27] Bert, C. and Stricklin, J., "Comparative evaluation of six different numerical integration methods for nonlinear dynamic systems," *Journal of Sound and Vibration*, Vol. 127, No. 2, 1988, pp. 221–229.

[28] Xie, Y., "An assessment of time integration schemes for nonlinear dynamic equations," *Journal of Sound and Vibration*, Vol. 192, No. 1, 1996, pp. 321–331.

[29] Press, W., Teukolsky, S., Vetterling, W., and Flannery, B., *Numerical Recipes in C*, Cambridge University Press, New York, 1992.

[30] Cash, J. and Karp, A., "A Variable Order Runge-Kutta Method for Initial Value Problems with Rapidly Varying Right-Hand Sides," *ACM Transactions on Mathematical Software*, Vol. 16, No. 3, 1990, pp. 201–222.

[31] Dorman, J. and Prince, J., "A family of embedded Runge-Kutta formulae," *Journal of Computational Applied Mathematics*, Vol. 6, 1980, pp. 19–26.

[32] Dorman, J. and Prince, J., "High order embedded Runge-Kutta formulae," *Journal of Computational Applied Mathematics*, Vol. 7, 1981, pp. 67–75.

[33] Grimshaw, R., *Nonlinear Ordinary Diffential Equations*, Applied Mathematics and Engineering Science Texts, Blackwell Scientific Publications, Oxford, 1990.

[34] *Matlab Reference*, The MathWorks, Inc., 3 Apple Hill Drive, Natick, MA 01760-2098, vers. 6/7 ed., 2000.

[35] Ergin, E., "Transient response of a nonlinear system," *Journal of Applied Mechanics*, Vol. 23, 1956, pp. 635–644.

[36] Thomson, W., "Shock spectra of nonlinear systems," *Journal of Applied Mechanics*, Vol. 27, 1960, pp. 635–643.

[37] Paz, M., *Structural Dynamics - Theory and Computation*, Van Nostrand Reinhold Company, New York, 2nd ed., 1985.

[38] Hagedorn, P., *Non-linear Oscillations*, Clarendon Press, Oxford, 1981.

[39] Ruge, P., *Baudynamik - Umdruck zur Vorlesung*, Vol. 1 of *Lecture Notes in Structural Dynamics*, Dresden University of Technology, Faculty of Civil Engineering, Institute for Mechanics and Computer Science, Dresden, Germany, 8th ed., 2002, p. 198.

APPENDIX A

Response Behaviour of a Linear SDOF Oscillator

A.1 Linear Non-Autonomous - Blast Wave Excitation

A.1.1 Exact Solution

The response of a linear single-degree-of-freedom (SDOF) system to the two different types of blast wave excitations is given in chapter 2, Eq.(2.4.1) in terms of mathematic symbolic notation. The explicit expressions for $u_I(t)$ and $u_{II}(t)$ are partially obtained using the computer based mathematical formula manipulation program MATHEMATICA® [20]. For the response due to $p_I(t)$ Eq.(2.4.1) gives together with (2.3.10)

$$u_I(t) = p_0 \mathfrak{L}^{-1}\left\{\bar{p}_I(\omega)\bar{h}(\omega)\right\} + \mathfrak{L}^{-1}\left\{\bar{q}_0(\omega)\bar{h}(\omega)\right\} \tag{A.1.1}$$

leading to

$$u_I(t) = \frac{-p_0 t_d \, e^{\frac{-t\left(\alpha + t_d\omega_n\left(\zeta+\sqrt{\zeta^2-1}\right)\right)}{t_d}}}{2m\sqrt{\zeta^2-1}\,\omega_n\left(\alpha^2 - 2\alpha\zeta t_d\omega_n + t_d^2\omega_n^2\right)^2}\Bigg[- e^{\frac{\alpha}{t_d}t}\left(-1 + e^{2t\sqrt{\zeta^2-1}\omega_n}\right)\left\{\alpha^2(\alpha-1) - \right.$$

$$\left. -\alpha(3\alpha-2)\zeta t_d\omega_n + \left(1+\alpha+2(\alpha-1)\zeta^2\right)t_d^2\omega_n^2 - \zeta t_d^3\omega_n^3\right\} +$$

$$+\sqrt{\zeta^2-1}\left\{2\omega_n e^{t\omega_n\left(\zeta+\sqrt{\zeta^2-1}\right)}\left[\alpha(t\alpha-(\alpha-2)t_d) - 2\zeta t_d\omega_n(\alpha t + t_d - \alpha t_d) + \right.\right.$$

$$\left. + (t-t_d)t_d^2\omega_n^2\right] + t_d\omega_n e^{\frac{\alpha}{t_d}t}\left(1 + e^{2t\omega_n\sqrt{\zeta^2-t}}\right)\left[\alpha^2 + t_d\omega_n(2\zeta + t_d\omega_n) - \right.$$

$$\left.\left. - 2\alpha(1+\zeta t_d\omega_n)\right]\right\}\Bigg] \tag{A.1.2}$$

where $\omega_n = \sqrt{k/m} = 2\pi f_n$ is the system's linear angular natural frequency, k and m are the stiffness and mass of the SDOF, respectively, and ζ is viscous damping ratio as defined in Eq.(2.3.3). The variables α and t_d describe properties of the blast wave profile as shown in Fig. 1.1.1.

For the pressure-time history as defined by the type-II blast profile $p_{II}(t)$, Eq.(2.4.1) yields

$$u_{II}(t) = p_0 \mathfrak{L}^{-1}\left\{\bar{p}_{II}(\omega)\bar{h}(\omega)\right\} + \mathfrak{L}^{-1}\left\{\bar{q}_0(\omega)\bar{h}(\omega)\right\} \quad \text{with} \quad i\omega \to s \tag{A.1.3}$$

as the response of the damped linear system. Solving (A.1.3) is rather difficult and laborious. However, using the symbolic mathematic manipulation package MATHEMATICA® still involves a considerably amount of work but results are far less prone to errors. The next 17 pages derive the explicit expression for Eq.(A.1.3) obtained in two slightly different ways. The standard approach of splitting the complex-valued Laplace transform of the sought solution $u_{II}(t)$

$$\bar{u}_{II}(s) = \frac{e^{-st_a}\left(s^2 t_a t_d(-1+st_d+\alpha)+(-1+e^{st_a}-st_a)(st_d+\alpha)^2\right)}{ms^2 t_a (st_d+\alpha)^2 (s^2+2s\zeta\omega_n+\omega_n^2)} \tag{A.1.4}$$

into partial fractions and transforming each of them individually into the time domain is given in the first section of the print-out. However, due to the capabilities of the used software it is possible to transform the entire expression as given in Eq.(A.1.4) at once. Although the obtained result is extreme complex and needs carefully selected substitutions and simplification, it has been include for the purpose of comparison with the solution given by the partial fraction approach.

The MATHEMATICA® file is thoroughly commented and self-contained using the same variables as in the preceding chapters of this report. It starts with the input of Eq.(A.1.4) and all used simplifications and abbreviations are explained. The two results obtained at the end of each section give the response of the viscously damped, linear SDOF oscillator to a transient load input as given by Eq.(1.1.2) in chapter 1. For comparison of analytical and numerical results see section 2.4.

Time Domain Response of Inverse Laplace Transform using Partial Fractions

SDOF Response in Complex Laplace Domain

Type-II blast response in the complex domain:

(StarDust-V) In[35]:=

$$uC = \frac{e^{-s\,t_a}\,(s^2\,t_a\,t_d\,(-1+s\,t_d+\alpha)+(-1+e^{s\,t_a}-s\,t_a)\,(s\,t_d+\alpha)^2)}{m\,s^2\,t_a\,(s\,t_d+\alpha)^2\,(s^2+2\,s\,\zeta\,\omega_n+\omega_n^2)};$$

Defining the mathematical domain of the variables:

(StarDust-V) In[36]:=

```
s ∈ Complexes &&
  {t, t_a, t_d, α, ω_n, ζ, m} ∈ Reals && {t, t_a, t_d, α, ω_n, ζ, m} ≥ 0;
```

■ Splitting uC into two parts:

(StarDust-V) In[37]:=

$$uC1 = \text{Expand}\left[\frac{e^{-s\,t_a}\,(s^2\,t_a\,t_d\,(-1+s\,t_d+\alpha))}{m\,s^2\,t_a\,(s\,t_d+\alpha)^2\,(s^2+2\,s\,\zeta\,\omega_n+\omega_n^2)}\right]$$

(StarDust-V) Out[37]=

$$-\frac{e^{-s\,t_a}\,t_d}{m\,(\alpha+s\,t_d)^2\,(s^2+2\,s\,\zeta\,\omega_n+\omega_n^2)}+\frac{e^{-s\,t_a}\,\alpha\,t_d}{m\,(\alpha+s\,t_d)^2\,(s^2+2\,s\,\zeta\,\omega_n+\omega_n^2)}+\frac{e^{-s\,t_a}\,s\,t_d^2}{m\,(\alpha+s\,t_d)^2\,(s^2+2\,s\,\zeta\,\omega_n+\omega_n^2)}$$

(StarDust-V) In[38]:=

$$uC2 = \text{Apart}\left[\frac{e^{-s\,t_a}\,((-1+e^{s\,t_a}-s\,t_a)\,(s\,t_d+\alpha)^2)}{m\,s^2\,t_a\,(s\,t_d+\alpha)^2\,(s^2+2\,s\,\zeta\,\omega_n+\omega_n^2)}\right]$$

(StarDust-V) Out[38]=

$$\frac{1}{m\,s^2\,t_a\,(s^2+2\,s\,\zeta\,\omega_n+\omega_n^2)}-\frac{e^{-s\,t_a}\,(1+s\,t_a)}{m\,s^2\,t_a\,(s^2+2\,s\,\zeta\,\omega_n+\omega_n^2)}$$

Test if uC1 and uC2 are equal uC:

(StarDust-V) In[39]:=

```
Simplify[uC == (uC1 + uC2)]
```

(StarDust-V) Out[39]=

```
True
```

Partial Fractions

■ Splitting up uC1 from above:

(StarDust-V) In[49]:=

$$uC1A = -\frac{e^{-s\,t_a}\,t_d}{m\,(\alpha + s\,t_d)^2\,(s^2 + 2\,s\,\zeta\,\omega_n + \omega_n^2)};$$

$$uC1B = \frac{e^{-s\,t_a}\,\alpha\,t_d}{m\,(\alpha + s\,t_d)^2\,(s^2 + 2\,s\,\zeta\,\omega_n + \omega_n^2)};$$

$$uC1C = \frac{e^{-s\,t_a}\,s\,t_d^2}{m\,(\alpha + s\,t_d)^2\,(s^2 + 2\,s\,\zeta\,\omega_n + \omega_n^2)};$$

Testing if uC1 == uC1A + uC1B + uC1C :

(StarDust-V) In[52]:=

```
Simplify[uC1 == uC1A + uC1B + uC1C]
```

(StarDust-V) Out[52]=

```
True
```

■ Splitting up uC2 from above:

(StarDust-V) In[53]:=

$$uC2A = \frac{1}{m\,s^2\,t_a\,(s^2 + 2\,s\,\zeta\,\omega_n + \omega_n^2)};$$

$$uC2B = -\frac{e^{-s\,t_a}\,(1 + s\,t_a)}{m\,s^2\,t_a\,(s^2 + 2\,s\,\zeta\,\omega_n + \omega_n^2)};$$

Testing if uC2 == uC2A + uC2B :

(StarDust-V) In[55]:=

```
Simplify[uC2 == uC2A + uC2B]
```

(StarDust-V) Out[55]=

```
True
```

Inverse Laplace Transformation of Partial Fractions

■ All parts of uC1 :

uC1A :

(StarDust-V) In[83]:=

```
ut1A = Evaluate[InverseLaplaceTransform[uC1A, s, t]]
```

(StarDust-V) Out[83]=

$$-\frac{1}{m}\left(t_d\left(-\frac{2\,e^{-\frac{\alpha\,(t-t_a)}{t_d}}\,t_d\,(-\alpha+\zeta\,t_d\,\omega_n)}{(\alpha^2-2\,\alpha\,\zeta\,t_d\,\omega_n+t_d^2\,\omega_n^2)^2}+\frac{e^{-\frac{\alpha\,(t-t_a)}{t_d}}\,(t-t_a)}{\alpha^2-2\,\alpha\,\zeta\,t_d\,\omega_n+t_d^2\,\omega_n^2}+\right.\right.$$
$$\left(-e^{(t-t_a)\,(-\zeta\,\omega_n-\sqrt{-\omega_n^2+\zeta^2\,\omega_n^2})}\,\alpha^2+e^{(t-t_a)\,(-\zeta\,\omega_n+\sqrt{-\omega_n^2+\zeta^2\,\omega_n^2})}\,\alpha^2+\right.$$
$$2\,e^{(t-t_a)\,(-\zeta\,\omega_n-\sqrt{-\omega_n^2+\zeta^2\,\omega_n^2})}\,\alpha\,\zeta\,t_d\,\omega_n-2\,e^{(t-t_a)\,(-\zeta\,\omega_n+\sqrt{-\omega_n^2+\zeta^2\,\omega_n^2})}\,\alpha\,\zeta\,t_d\,\omega_n+$$
$$e^{(t-t_a)\,(-\zeta\,\omega_n-\sqrt{-\omega_n^2+\zeta^2\,\omega_n^2})}\,t_d^2\,\omega_n^2-e^{(t-t_a)\,(-\zeta\,\omega_n+\sqrt{-\omega_n^2+\zeta^2\,\omega_n^2})}\,t_d^2\,\omega_n^2-$$
$$2\,e^{(t-t_a)\,(-\zeta\,\omega_n-\sqrt{-\omega_n^2+\zeta^2\,\omega_n^2})}\,\zeta^2\,t_d^2\,\omega_n^2+2\,e^{(t-t_a)\,(-\zeta\,\omega_n+\sqrt{-\omega_n^2+\zeta^2\,\omega_n^2})}\,\zeta^2\,t_d^2\,\omega_n^2-$$
$$2\,e^{(t-t_a)\,(-\zeta\,\omega_n-\sqrt{-\omega_n^2+\zeta^2\,\omega_n^2})}\,\alpha\,t_d\,\sqrt{-\omega_n^2+\zeta^2\,\omega_n^2}-2\,e^{(t-t_a)\,(-\zeta\,\omega_n+\sqrt{-\omega_n^2+\zeta^2\,\omega_n^2})}$$
$$\alpha\,t_d\,\sqrt{-\omega_n^2+\zeta^2\,\omega_n^2}+2\,e^{(t-t_a)\,(-\zeta\,\omega_n-\sqrt{-\omega_n^2+\zeta^2\,\omega_n^2})}\,\zeta\,t_d^2\,\omega_n\,\sqrt{-\omega_n^2+\zeta^2\,\omega_n^2}+$$
$$\left.\left.2\,e^{(t-t_a)\,(-\zeta\,\omega_n+\sqrt{-\omega_n^2+\zeta^2\,\omega_n^2})}\,\zeta\,t_d^2\,\omega_n\,\sqrt{-\omega_n^2+\zeta^2\,\omega_n^2}\right)\Big/\right.$$
$$\left.\left.\left(2\,\sqrt{-\omega_n^2+\zeta^2\,\omega_n^2}\,(\alpha^2-2\,\alpha\,\zeta\,t_d\,\omega_n+t_d^2\,\omega_n^2)^2\right)\right)\,\text{UnitStep}[t-t_a]\right)$$

(StarDust-V) In[104]:=

```
ut1ARep = ReplaceRepeated[ut1A,
  {Sqrt[(-1 + ζ^2) ω_n^2] → A, Sqrt[-ω_n^2 + ζ^2 ω_n^2] → A, 1/Sqrt[(-1 + ζ^2) ω_n^2] → 1/A,
   (t - t_a) → Δ_a, (-t + t_a) → -Δ_a, t_a ω_n → τ_a, t_d ω_n → τ_n, t_d^2 ω_n^2 → τ_n^2}]
```

(StarDust-V) Out[104]=

$$-\frac{1}{m}$$
$$\left(t_d\left(-\frac{2\,e^{-\frac{\alpha\,\Delta_a}{t_d}}\,t_d\,(-\alpha+\zeta\,\tau_n)}{(\alpha^2-2\,\alpha\,\zeta\,\tau_n+\tau_n^2)^2}+\frac{e^{-\frac{\alpha\,\Delta_a}{t_d}}\,\Delta_a}{\alpha^2-2\,\alpha\,\zeta\,\tau_n+\tau_n^2}+(-e^{\Delta_a\,(-A-\zeta\,\omega_n)}\,\alpha^2+e^{\Delta_a\,(A-\zeta\,\omega_n)}\right.\right.$$
$$\alpha^2-2\,A\,e^{\Delta_a\,(-A-\zeta\,\omega_n)}\,\alpha\,t_d-2\,A\,e^{\Delta_a\,(A-\zeta\,\omega_n)}\,\alpha\,t_d+2\,e^{\Delta_a\,(-A-\zeta\,\omega_n)}\,\alpha\,\zeta\,\tau_n-$$
$$2\,e^{\Delta_a\,(A-\zeta\,\omega_n)}\,\alpha\,\zeta\,\tau_n+e^{\Delta_a\,(-A-\zeta\,\omega_n)}\,\tau_n^2-e^{\Delta_a\,(A-\zeta\,\omega_n)}\,\tau_n^2-2\,e^{\Delta_a\,(-A-\zeta\,\omega_n)}\,\zeta^2\,\tau_n^2+$$
$$\left.\left.2\,e^{\Delta_a\,(A-\zeta\,\omega_n)}\,\zeta^2\,\tau_n^2+2\,A\,e^{\Delta_a\,(-A-\zeta\,\omega_n)}\,\zeta\,t_d^2\,\omega_n+2\,A\,e^{\Delta_a\,(A-\zeta\,\omega_n)}\,\zeta\,t_d^2\,\omega_n\right)\Big/\right.$$
$$\left.\left.\left(2\,(\alpha^2-2\,\alpha\,\zeta\,\tau_n+\tau_n^2)^2\,\sqrt{-\omega_n^2+\zeta^2\,\omega_n^2}\right)\right)\,\text{UnitStep}[\Delta_a]\right)$$

Output in traditional mathematical notation:

(StarDust-V) In[105]:=

```
TraditionalForm[utlARep]
```

(StarDust-V) Out[105]//TraditionalForm=

$$-\frac{1}{m}\left(t_d\left(\frac{e^{-\frac{\alpha\,\Delta_a}{t_d}}\,\Delta_a}{\alpha^2-2\,\zeta\,\tau_n\,\alpha+\tau_n^2}+\right.\right.$$
$$(-e^{\Delta_a\,(-A-\zeta\,\omega_n)}\,\alpha^2+e^{\Delta_a\,(A-\zeta\,\omega_n)}\,\alpha^2-2\,A\,e^{\Delta_a\,(-A-\zeta\,\omega_n)}\,t_d\,\alpha-$$
$$2\,A\,e^{\Delta_a\,(A-\zeta\,\omega_n)}\,t_d\,\alpha+2\,e^{\Delta_a\,(-A-\zeta\,\omega_n)}\,\zeta\,\tau_n\,\alpha-$$
$$2\,e^{\Delta_a\,(A-\zeta\,\omega_n)}\,\zeta\,\tau_n\,\alpha+e^{\Delta_a\,(-A-\zeta\,\omega_n)}\,\tau_n^2-e^{\Delta_a\,(A-\zeta\,\omega_n)}\,\tau_n^2-$$
$$2\,e^{\Delta_a\,(-A-\zeta\,\omega_n)}\,\zeta^2\,\tau_n^2+2\,e^{\Delta_a\,(A-\zeta\,\omega_n)}\,\zeta^2\,\tau_n^2+$$
$$2\,A\,e^{\Delta_a\,(-A-\zeta\,\omega_n)}\,\zeta\,t_d^2\,\omega_n+2\,A\,e^{\Delta_a\,(A-\zeta\,\omega_n)}\,\zeta\,t_d^2\,\omega_n)\Big/$$
$$\left(2\,(\alpha^2-2\,\zeta\,\tau_n\,\alpha+\tau_n^2)^2\,\sqrt{\zeta^2\,\omega_n^2-\omega_n^2}\right)-$$
$$\left.\left.\frac{2\,e^{-\frac{\alpha\,\Delta_a}{t_d}}\,t_d\,(\zeta\,\tau_n-\alpha)}{(\alpha^2-2\,\zeta\,\tau_n\,\alpha+\tau_n^2)^2}\right)\theta(\Delta_a)\right)$$

uC1B :

(StarDust-V) In[86]:=

```
ut1B = Evaluate[InverseLaplaceTransform[uC1B, s, t]]
```

(StarDust-V) Out[86]=

$$\frac{1}{m}\left(\alpha\,t_d\left(-\frac{2\,e^{-\frac{\alpha\,(t-t_a)}{t_d}}\,t_d\,(-\alpha+\zeta\,t_d\,\omega_n)}{(\alpha^2-2\,\alpha\,\zeta\,t_d\,\omega_n+t_d^2\,\omega_n^2)^2}+\frac{e^{-\frac{\alpha\,(t-t_a)}{t_d}}\,(t-t_a)}{\alpha^2-2\,\alpha\,\zeta\,t_d\,\omega_n+t_d^2\,\omega_n^2}+\right.\right.$$
$$\left(-e^{(t-t_a)\,(-\zeta\,\omega_n-\sqrt{-\omega_n^2+\zeta^2\,\omega_n^2})}\,\alpha^2+e^{(t-t_a)\,(-\zeta\,\omega_n+\sqrt{-\omega_n^2+\zeta^2\,\omega_n^2})}\,\alpha^2+\right.$$
$$2\,e^{(t-t_a)\,(-\zeta\,\omega_n-\sqrt{-\omega_n^2+\zeta^2\,\omega_n^2})}\,\alpha\,\zeta\,t_d\,\omega_n-2\,e^{(t-t_a)\,(-\zeta\,\omega_n+\sqrt{-\omega_n^2+\zeta^2\,\omega_n^2})}\,\alpha\,\zeta\,t_d\,\omega_n+$$
$$e^{(t-t_a)\,(-\zeta\,\omega_n-\sqrt{-\omega_n^2+\zeta^2\,\omega_n^2})}\,t_d^2\,\omega_n^2-e^{(t-t_a)\,(-\zeta\,\omega_n+\sqrt{-\omega_n^2+\zeta^2\,\omega_n^2})}\,t_d^2\,\omega_n^2-$$
$$2\,e^{(t-t_a)\,(-\zeta\,\omega_n-\sqrt{-\omega_n^2+\zeta^2\,\omega_n^2})}\,\zeta^2\,t_d^2\,\omega_n^2+2\,e^{(t-t_a)\,(-\zeta\,\omega_n+\sqrt{-\omega_n^2+\zeta^2\,\omega_n^2})}\,\zeta^2\,t_d^2\,\omega_n^2-$$
$$2\,e^{(t-t_a)\,(-\zeta\,\omega_n-\sqrt{-\omega_n^2+\zeta^2\,\omega_n^2})}\,\alpha\,t_d\,\sqrt{-\omega_n^2+\zeta^2\,\omega_n^2}-2\,e^{(t-t_a)\,(-\zeta\,\omega_n+\sqrt{-\omega_n^2+\zeta^2\,\omega_n^2})}$$
$$\alpha\,t_d\,\sqrt{-\omega_n^2+\zeta^2\,\omega_n^2}+2\,e^{(t-t_a)\,(-\zeta\,\omega_n-\sqrt{-\omega_n^2+\zeta^2\,\omega_n^2})}\,\zeta\,t_d^2\,\omega_n\,\sqrt{-\omega_n^2+\zeta^2\,\omega_n^2}+$$
$$\left.2\,e^{(t-t_a)\,(-\zeta\,\omega_n+\sqrt{-\omega_n^2+\zeta^2\,\omega_n^2})}\,\zeta\,t_d^2\,\omega_n\,\sqrt{-\omega_n^2+\zeta^2\,\omega_n^2}\right)\Big/$$
$$\left.\left.\left(2\,\sqrt{-\omega_n^2+\zeta^2\,\omega_n^2}\;(\alpha^2-2\,\alpha\,\zeta\,t_d\,\omega_n+t_d^2\,\omega_n^2)^2\right)\right)\,\text{UnitStep}[t-t_a]\right)$$

(StarDust-V) In[107]:=

```
ut1BRep = ReplaceRepeated[ut1B,
  {Sqrt[(-1 + ζ^2) ω_n^2] → A, Sqrt[-ω_n^2 + ζ^2 ω_n^2] → A, 1/Sqrt[(-1 + ζ^2) ω_n^2] → 1/A,
   (t - t_a) → Δ_a, (-t + t_a) → -Δ_a, t_a ω_n → τ_a, t_d ω_n → τ_n, t_d^2 ω_n^2 → τ_n^2}]
```

(StarDust-V) Out[107]=

$$\frac{1}{m}\left(\alpha\, t_d \left(-\frac{2\, e^{-\frac{\alpha \Delta_a}{t_d}}\, t_d\, (-\alpha + \zeta\, \tau_n)}{(\alpha^2 - 2\,\alpha\,\zeta\,\tau_n + \tau_n^2)^2} + \frac{e^{-\frac{\alpha \Delta_a}{t_d}}\, \Delta_a}{\alpha^2 - 2\,\alpha\,\zeta\,\tau_n + \tau_n^2} + \left(-e^{\Delta_a\,(-A-\zeta\,\omega_n)}\,\alpha^2 + e^{\Delta_a\,(A-\zeta\,\omega_n)}\,\alpha^2 - 2\,A\,e^{\Delta_a\,(-A-\zeta\,\omega_n)}\,\alpha\, t_d - 2\,A\,e^{\Delta_a\,(A-\zeta\,\omega_n)}\,\alpha\, t_d + 2\,e^{\Delta_a\,(-A-\zeta\,\omega_n)}\,\alpha\,\zeta\,\tau_n - 2\,e^{\Delta_a\,(A-\zeta\,\omega_n)}\,\alpha\,\zeta\,\tau_n + e^{\Delta_a\,(-A-\zeta\,\omega_n)}\,\tau_n^2 - e^{\Delta_a\,(A-\zeta\,\omega_n)}\,\tau_n^2 - 2\,e^{\Delta_a\,(-A-\zeta\,\omega_n)}\,\zeta^2\,\tau_n^2 + 2\,e^{\Delta_a\,(A-\zeta\,\omega_n)}\,\zeta^2\,\tau_n^2 + 2\,A\,e^{\Delta_a\,(-A-\zeta\,\omega_n)}\,\zeta\, t_d^2\,\omega_n + 2\,A\,e^{\Delta_a\,(A-\zeta\,\omega_n)}\,\zeta\, t_d^2\,\omega_n\right) \Big/ \left(2\,(\alpha^2 - 2\,\alpha\,\zeta\,\tau_n + \tau_n^2)^2 \sqrt{-\omega_n^2 + \zeta^2\,\omega_n^2}\right)\right)\, \text{UnitStep}[\Delta_a]\right)$$

Output in traditional mathematical notation:

(StarDust-V) In[108]:=

```
TraditionalForm[ut1BRep]
```

(StarDust-V) Out[108]//TraditionalForm=

$$\frac{1}{m}\left(\alpha\, t_d \left(\frac{e^{-\frac{\alpha \Delta_a}{t_d}}\, \Delta_a}{\alpha^2 - 2\,\zeta\,\tau_n\,\alpha + \tau_n^2} + \left(-e^{\Delta_a\,(-A-\zeta\,\omega_n)}\,\alpha^2 + e^{\Delta_a\,(A-\zeta\,\omega_n)}\,\alpha^2 - 2\,A\,e^{\Delta_a\,(-A-\zeta\,\omega_n)}\,t_d\,\alpha - 2\,A\,e^{\Delta_a\,(A-\zeta\,\omega_n)}\,t_d\,\alpha + 2\,e^{\Delta_a\,(-A-\zeta\,\omega_n)}\,\zeta\,\tau_n\,\alpha - 2\,e^{\Delta_a\,(A-\zeta\,\omega_n)}\,\zeta\,\tau_n\,\alpha + e^{\Delta_a\,(-A-\zeta\,\omega_n)}\,\tau_n^2 - e^{\Delta_a\,(A-\zeta\,\omega_n)}\,\tau_n^2 - 2\,e^{\Delta_a\,(-A-\zeta\,\omega_n)}\,\zeta^2\,\tau_n^2 + 2\,e^{\Delta_a\,(A-\zeta\,\omega_n)}\,\zeta^2\,\tau_n^2 + 2\,A\,e^{\Delta_a\,(-A-\zeta\,\omega_n)}\,\zeta\,t_d^2\,\omega_n + 2\,A\,e^{\Delta_a\,(A-\zeta\,\omega_n)}\,\zeta\,t_d^2\,\omega_n\right) \Big/ \left(2\,(\alpha^2 - 2\,\zeta\,\tau_n\,\alpha + \tau_n^2)^2 \sqrt{\zeta^2\,\omega_n^2 - \omega_n^2}\right) - \frac{2\,e^{-\frac{\alpha \Delta_a}{t_d}}\, t_d\,(\zeta\,\tau_n - \alpha)}{(\alpha^2 - 2\,\zeta\,\tau_n\,\alpha + \tau_n^2)^2}\right)\theta(\Delta_a)\right)$$

uC1C :

(StarDust-V) In[89]:=

```
ut1C = Evaluate[InverseLaplaceTransform[uC1C, s, t]]
```

(StarDust-V) Out[89]=

$$\frac{1}{m}\left(t_d^2\left(\frac{e^{-\frac{\alpha\,(t-t_a)}{t_d}}\,(-\alpha^2+t_d^2\,\omega_n^2)}{(\alpha^2-2\,\alpha\,\zeta\,t_d\,\omega_n+t_d^2\,\omega_n^2)^2}-\frac{e^{-\frac{\alpha\,(t-t_a)}{t_d}}\,\alpha\,(t-t_a)}{t_d\,(\alpha^2-2\,\alpha\,\zeta\,t_d\,\omega_n+t_d^2\,\omega_n^2)}-\right.\right.$$
$$\left(e^{-(t-t_a)\,(\zeta\,\omega_n+\sqrt{(-1+\zeta^2)\,\omega_n^2})}\left(\left(-1+e^{2\,(t-t_a)\,\sqrt{(-1+\zeta^2)\,\omega_n^2}}\right)\alpha^2\,\zeta\,\omega_n+\right.\right.$$
$$\left(-1+e^{2\,(t-t_a)\,\sqrt{(-1+\zeta^2)\,\omega_n^2}}\right)\zeta\,t_d^2\,\omega_n^3-\left(1+e^{2\,(t-t_a)\,\sqrt{(-1+\zeta^2)\,\omega_n^2}}\right)$$
$$\alpha^2\sqrt{(-1+\zeta^2)\,\omega_n^2}+t_d\,\omega_n^2\left(-2\left(-1+e^{2\,(t-t_a)\,\sqrt{(-1+\zeta^2)\,\omega_n^2}}\right)\alpha+\right.$$
$$\left.\left.\left.\left(1+e^{2\,(t-t_a)\,\sqrt{(-1+\zeta^2)\,\omega_n^2}}\right)t_d\sqrt{(-1+\zeta^2)\,\omega_n^2}\right)\right)\right)\Big/$$
$$\left.\left.\left(2\sqrt{(-1+\zeta^2)\,\omega_n^2}\;(\alpha^2-2\,\alpha\,\zeta\,t_d\,\omega_n+t_d^2\,\omega_n^2)^2\right)\right)\text{UnitStep}[t-t_a]\right)$$

(StarDust-V) In[109]:=

```
ut1CRep =
 ReplaceRepeated[ut1C, {Sqrt[(-1 + ζ^2) ω_n^2] → A, 1/Sqrt[(-1 + ζ^2) ω_n^2] → 1/A,
  (t - t_a) → Δ_a, (-t + t_a) → -Δ_a, t_a ω_n → τ_a, t_d ω_n → τ_n, t_d^2 ω_n^2 → τ_n^2}]
```

(StarDust-V) Out[109]=

$$\frac{1}{m}\left(t_d^2\left(\frac{e^{-\frac{\alpha\,\Delta_a}{t_d}}\,(-\alpha^2+\tau_n^2)}{(\alpha^2-2\,\alpha\,\zeta\,\tau_n+\tau_n^2)^2}-\frac{e^{-\frac{\alpha\,\Delta_a}{t_d}}\,\alpha\,\Delta_a}{t_d\,(\alpha^2-2\,\alpha\,\zeta\,\tau_n+\tau_n^2)}-\right.\right.$$
$$\frac{1}{2\,A\,(\alpha^2-2\,\alpha\,\zeta\,\tau_n+\tau_n^2)^2}\left(e^{-\Delta_a\,(A+\zeta\,\omega_n)}\,(-A\,(1+e^{2\,A\,\Delta_a})\,\alpha^2+\right.$$
$$(-1+e^{2\,A\,\Delta_a})\,\alpha^2\,\zeta\,\omega_n+t_d\,(-2\,(-1+e^{2\,A\,\Delta_a})\,\alpha+A\,(1+e^{2\,A\,\Delta_a})\,t_d)\,\omega_n^2+$$
$$\left.\left.(-1+e^{2\,A\,\Delta_a})\,\zeta\,t_d^2\,\omega_n^3)\right)\text{UnitStep}[\Delta_a]\right)$$

Output in traditional mathematical notation:

(StarDust-V) In[110]:=

```
TraditionalForm[ut1CRep]
```

(StarDust-V) Out[110]//TraditionalForm=

$$\frac{1}{m}\left(t_d^2\left(-\frac{e^{-\frac{\alpha\,\Delta_a}{t_d}}\,\alpha\,\Delta_a}{t_d\,(\alpha^2-2\,\zeta\,\tau_n\,\alpha+\tau_n^2)}-\right.\right.$$
$$\frac{1}{2\,A\,(\alpha^2-2\,\zeta\,\tau_n\,\alpha+\tau_n^2)^2}\left(e^{-\Delta_a\,(A+\zeta\,\omega_n)}\left((-1+e^{2\,A\,\Delta_a})\,\zeta\,t_d^2\,\omega_n^3+\right.\right.$$
$$t_d\,(A\,(1+e^{2\,A\,\Delta_a})\,t_d-2\,(-1+e^{2\,A\,\Delta_a})\,\alpha)\,\omega_n^2+$$
$$\left.\left.(-1+e^{2\,A\,\Delta_a})\,\alpha^2\,\zeta\,\omega_n-A\,(1+e^{2\,A\,\Delta_a})\,\alpha^2\right)\right)+$$
$$\left.\left.\frac{e^{-\frac{\alpha\,\Delta_a}{t_d}}\,(\tau_n^2-\alpha^2)}{(\alpha^2-2\,\zeta\,\tau_n\,\alpha+\tau_n^2)^2}\right)\theta(\Delta_a)\right)$$

ut1 = ut1A + ut1B + ut1C :

(StarDust-V) In[113]:=

```
ut1Rep = ReplaceRepeated[
  Simplify[ut1ARep + ut1BRep + ut1CRep], Sqrt[(-1 + ζ^2) ω_n^2] → A]
```

(StarDust-V) Out[113]=

$$\left(e^{-\frac{\Delta_a\,(\alpha+t_d\,(A+\zeta\,\omega_n))}{t_d}}\,t_d\,\left(A\,\left(\alpha^2\,\left(e^{\frac{\alpha\,\Delta_a}{t_d}}\,\left(-1+e^{2\,A\,\Delta_a}\right)\,(-1+\alpha)-2\,A\,e^{\Delta_a\,(A+\zeta\,\omega_n)}\,\Delta_a\right)-\right.\right.\right.$$
$$2\,\alpha\,\zeta\,\left(e^{\frac{\alpha\,\Delta_a}{t_d}}\,\left(-1+e^{2\,A\,\Delta_a}\right)\,(-1+\alpha)-2\,A\,e^{\Delta_a\,(A+\zeta\,\omega_n)}\,\Delta_a\right)\,\tau_n+$$
$$\left.\left(e^{\frac{\alpha\,\Delta_a}{t_d}}\,\left(-1+e^{2\,A\,\Delta_a}\right)\,(-1+\alpha)\,\left(-1+2\,\zeta^2\right)-2\,A\,e^{\Delta_a\,(A+\zeta\,\omega_n)}\,\Delta_a\right)\,\tau_n^2\right)+$$
$$2\,e^{\frac{\alpha\,\Delta_a}{t_d}}\,t_d^2\,\omega_n\,\left(A^2\,\left(1+e^{2\,A\,\Delta_a}\right)\,(-1+\alpha)\,\zeta+A\,\left(-1+e^{2\,A\,\Delta_a}\right)\,\alpha\,\omega_n\right)-$$
$$A\,e^{\frac{\alpha\,\Delta_a}{t_d}}\,t_d^3\,\omega_n^2\,\left(A\,\left(1+e^{2\,A\,\Delta_a}\right)+\left(-1+e^{2\,A\,\Delta_a}\right)\,\zeta\,\omega_n\right)+$$
$$t_d\,\left(-4\,A^2\,e^{\Delta_a\,(A+\zeta\,\omega_n)}\,(-1+\alpha)\,\zeta\,\tau_n+2\,A^2\,e^{\Delta_a\,(A+\zeta\,\omega_n)}\,\tau_n^2-\right.$$
$$\alpha\,\left(-A\,\left(-2\,A\,e^{\frac{\alpha\,\Delta_a}{t_d}}\,\left(1+e^{2\,A\,\Delta_a}\right)\,(-1+\alpha)+A\,\left(2\,e^{\Delta_a\,(A+\zeta\,\omega_n)}\,(-2+\alpha)+\right.\right.\right.$$
$$\left.\left.\left.\left.e^{\left(2\,A+\frac{\alpha}{t_d}\right)\,\Delta_a}\,\alpha+e^{\frac{\alpha\,\Delta_a}{t_d}}\,\alpha\right)\right)+A\,e^{\frac{\alpha\,\Delta_a}{t_d}}\,\left(-1+e^{2\,A\,\Delta_a}\right)\,\alpha\,\zeta\,\omega_n\right)\right)\Big)$$
$$\text{UnitStep}[\Delta_a]\Big)\Big/\left(2\,A\,m\,\left(\alpha^2-2\,\alpha\,\zeta\,\tau_n+\tau_n^2\right)^2\,\sqrt{\left(-1+\zeta^2\right)\,\omega_n^2}\right)$$

Output in traditional mathematical notation:

(StarDust-V) In[114]:=

```
TraditionalForm[ut1Rep]
```

(StarDust-V) Out[114]//TraditionalForm=

$$\left(e^{-\frac{\Delta_a\,(\alpha+t_d\,(A+\zeta\,\omega_n))}{t_d}}\,t_d\right.$$
$$\left(-A\,e^{\frac{\alpha\,\Delta_a}{t_d}}\,\omega_n^2\,(A\,(1+e^{2\,A\,\Delta_a})+(-1+e^{2\,A\,\Delta_a})\,\zeta\,\omega_n)\,t_d^3+2\,e^{\frac{\alpha\,\Delta_a}{t_d}}\,\omega_n\right.$$
$$((1+e^{2\,A\,\Delta_a})\,(\alpha-1)\,\zeta\,A^2+(-1+e^{2\,A\,\Delta_a})\,\alpha\,\omega_n\,A)\,t_d^2+$$
$$\left(2\,e^{\Delta_a\,(A+\zeta\,\omega_n)}\,\tau_n^2\,A^2-4\,e^{\Delta_a\,(A+\zeta\,\omega_n)}\,(\alpha-1)\,\zeta\,\tau_n\,A^2-\right.$$
$$\alpha\,\left(A\,e^{\frac{\alpha\,\Delta_a}{t_d}}\,(-1+e^{2\,A\,\Delta_a})\,\alpha\,\zeta\,\omega_n-\right.$$
$$A\,\left(A\,\left(2\,e^{\Delta_a\,(A+\zeta\,\omega_n)}\,(\alpha-2)+e^{\left(2\,A+\frac{\alpha}{t_d}\right)\,\Delta_a}\,\alpha+e^{\frac{\alpha\,\Delta_a}{t_d}}\right.\right.$$
$$\left.\left.\left.\left.\alpha\right)-2\,A\,e^{\frac{\alpha\,\Delta_a}{t_d}}\,(1+e^{2\,A\,\Delta_a})\,(\alpha-1)\right)\right)\right)$$
$$t_d+A\,\left(\left(e^{\frac{\alpha\,\Delta_a}{t_d}}\,(-1+e^{2\,A\,\Delta_a})\,(\alpha-1)-2\,A\,e^{\Delta_a\,(A+\zeta\,\omega_n)}\,\Delta_a\right)\,\alpha^2-\right.$$
$$2\,\zeta\,\left(e^{\frac{\alpha\,\Delta_a}{t_d}}\,(-1+e^{2\,A\,\Delta_a})\,(\alpha-1)-2\,A\,e^{\Delta_a\,(A+\zeta\,\omega_n)}\,\Delta_a\right)$$
$$\tau_n\,\alpha+\left(e^{\frac{\alpha\,\Delta_a}{t_d}}\,(-1+e^{2\,A\,\Delta_a})\,(\alpha-1)\,(2\,\zeta^2-1)-\right.$$
$$\left.\left.2\,A\,e^{\Delta_a\,(A+\zeta\,\omega_n)}\,\Delta_a\right)\,\tau_n^2\right)\Big)$$
$$\theta(\Delta_a)\Big)\Big/\left(2\,A\,m\,(\alpha^2-2\,\zeta\,\tau_n\,\alpha+\tau_n^2)^2\right.$$
$$\left.\sqrt{(\zeta^2-1)\,\omega_n^2}\right)$$

■ All parts of uC2 :

uC2A :

(StarDust-V) In[115]:=

```
ut2A = Evaluate[InverseLaplaceTransform[uC2A, s, t]]
```

(StarDust-V) Out[115]=

$$\frac{1}{2\,m\,t_a\,\omega_n^3}\left(-4\,\zeta+2\,t\,\omega_n+\frac{1}{\sqrt{(-1+\zeta^2)\,\omega_n^2}}\left(e^{-t\,(\zeta\,\omega_n+\sqrt{(-1+\zeta^2)\,\omega_n^2})}\left(\left(-1+e^{2\,t\,\sqrt{(-1+\zeta^2)\,\omega_n^2}}\right)\,(-1+2\,\zeta^2)\,\omega_n+2\left(1+e^{2\,t\,\sqrt{(-1+\zeta^2)\,\omega_n^2}}\right)\,\zeta\,\sqrt{(-1+\zeta^2)\,\omega_n^2}\right)\right)\right)$$

(StarDust-V) In[116]:=

```
ut2ARep =
 ReplaceRepeated[ut2A, {Sqrt[(-1 + ζ^2) ω_n^2] → A, 1/Sqrt[(-1 + ζ^2) ω_n^2] → 1/A,
   (t - t_a) → Δ_a, (-t + t_a) → -Δ_a, t_a ω_n → τ_a, t_d ω_n → τ_n, t_d^2 ω_n^2 → τ_n^2}]
```

(StarDust-V) Out[116]=

$$\frac{-4\,\zeta+2\,t\,\omega_n+\frac{e^{-t\,(A+\zeta\,\omega_n)}\,(2\,A\,(1+e^{2\,A\,t})\,\zeta+(-1+e^{2\,A\,t})\,(-1+2\,\zeta^2)\,\omega_n)}{A}}{2\,m\,t_a\,\omega_n^3}$$

Output in traditional mathematical notation:

(StarDust-V) In[117]:=

```
TraditionalForm[Factor[ut2ARep]]
```

(StarDust-V) Out[117]//TraditionalForm=

$$\frac{1}{2\,A\,m\,t_a\,\omega_n^3}\left(e^{-t\,(A+\zeta\,\omega_n)}\left(2\,e^{2\,A\,t}\,\omega_n\,\zeta^2-2\,\omega_n\,\zeta^2+2\,A\,e^{2\,A\,t}\,\zeta-4\,A\,e^{t\,(A+\zeta\,\omega_n)}\,\zeta+2\,A\,\zeta-e^{2\,A\,t}\,\omega_n+2\,A\,e^{t\,(A+\zeta\,\omega_n)}\,t\,\omega_n+\omega_n\right)\right)$$

uC2B :

(StarDust-V) In[118]:=

```
ut2B = Evaluate[InverseLaplaceTransform[uC2B, s, t]]
```

(StarDust-V) Out[118]=

$$-\frac{1}{2\,m\,t_a\,\omega_n^3}\left(\left(-4\,\zeta+2\,(t-t_a)\,\omega_n+\frac{1}{\sqrt{(-1+\zeta^2)\,\omega_n^2}}\right.\right.$$
$$\left(e^{-(t-t_a)\,(\zeta\,\omega_n+\sqrt{(-1+\zeta^2)\,\omega_n^2})}\left(\left(-1+e^{2\,(t-t_a)\,\sqrt{(-1+\zeta^2)\,\omega_n^2}}\right)\,(-1+2\,\zeta^2)\,\omega_n+\right.\right.$$
$$\left.\left.2\left(1+e^{2\,(t-t_a)\,\sqrt{(-1+\zeta^2)\,\omega_n^2}}\right)\,\zeta\,\sqrt{(-1+\zeta^2)\,\omega_n^2}\right)\right)+$$
$$t_a\,\omega_n\left(2-\frac{1}{\sqrt{(-1+\zeta^2)\,\omega_n^2}}\left(e^{-(t-t_a)\,(\zeta\,\omega_n+\sqrt{(-1+\zeta^2)\,\omega_n^2})}\right.\right.$$
$$\left(\left(-1+e^{2\,(t-t_a)\,\sqrt{(-1+\zeta^2)\,\omega_n^2}}\right)\,\zeta\,\omega_n+\right.$$
$$\left.\left.\left.\left.\left(1+e^{2\,(t-t_a)\,\sqrt{(-1+\zeta^2)\,\omega_n^2}}\right)\,\sqrt{(-1+\zeta^2)\,\omega_n^2}\right)\right)\right)\,\text{UnitStep}[t-t_a]\right)$$

(StarDust-V) In[119]:=

```
ut2BRep = Simplify[ReplaceRepeated[Factor[ut2B],
    {Sqrt[(-1 + ζ^2) ωn^2] → A, 1/Sqrt[(-1 + ζ^2) ωn^2] → 1/A, (t - ta) → Δa,
     (-t + ta) → -Δa, ta ωn → τa, td ωn → τn, td^2 ωn^2 → τn^2}]]
```

(StarDust-V) Out[119]=

$$-\frac{1}{2\,A\,m\,t_a\,\omega_n^3}\left(e^{-\Delta_a\,(A+\zeta\,\omega_n)}\,\left(2\,A\,\left(1+e^{2\,A\,\Delta_a}-2\,e^{\Delta_a\,(A+\zeta\,\omega_n)}\right)\,\zeta-\right.\right.$$
$$A\,\left(1+e^{2\,A\,\Delta_a}\right)\,\tau_a+\left(1+2\,A\,e^{\Delta_a\,(A+\zeta\,\omega_n)}\,t-2\,\zeta^2+e^{2\,A\,\Delta_a}\,(-1+2\,\zeta^2)\right)\,\omega_n-$$
$$\left.\left.\left(-1+e^{2\,A\,\Delta_a}\right)\,\zeta\,t_a\,\omega_n^2\right)\,\text{UnitStep}[\Delta_a]\right)$$

Output in mathematical traditional format:

(StarDust-V) In[120]:=

```
TraditionalForm[ut2BRep]
```

(StarDust-V) Out[120]//TraditionalForm=

$$-\frac{1}{2\,A\,m\,t_a\,\omega_n^3}\left(e^{-\Delta_a\,(A+\zeta\,\omega_n)}\,\left(-\left(-1+e^{2\,A\,\Delta_a}\right)\,\zeta\,t_a\,\omega_n^2+\right.\right.$$
$$\left(-2\,\zeta^2+2\,A\,e^{\Delta_a\,(A+\zeta\,\omega_n)}\,t+e^{2\,A\,\Delta_a}\,(2\,\zeta^2-1)+1\right)\,\omega_n+$$
$$\left.\left.2\,A\,\left(1+e^{2\,A\,\Delta_a}-2\,e^{\Delta_a\,(A+\zeta\,\omega_n)}\right)\,\zeta-A\,\left(1+e^{2\,A\,\Delta_a}\right)\,\tau_a\right)\,\theta(\Delta_a)\right)$$

ut2 = ut2A + ut2B :

(StarDust-V) In[121]:=

```
ut2Rep = Simplify[ut2ARep + ut2BRep]
```

(StarDust-V) Out[121]=

$$\frac{1}{2\,m\,t_a\,\omega_n^3}\left(-4\,\zeta+2\,t\,\omega_n+\frac{e^{-t\,(A+\zeta\,\omega_n)}\,(2\,A\,(1+e^{2\,A\,t})\,\zeta+(-1+e^{2\,A\,t})\,(-1+2\,\zeta^2)\,\omega_n)}{A}+\right.$$
$$\frac{1}{A}\left(e^{-\Delta_a\,(A+\zeta\,\omega_n)}\,(-2\,A\,(1+e^{2\,A\,\Delta_a}-2\,e^{\Delta_a\,(A+\zeta\,\omega_n)})\,\zeta+A\,(1+e^{2\,A\,\Delta_a})\,\tau_a+\right.$$
$$(-1-2\,A\,e^{\Delta_a\,(A+\zeta\,\omega_n)}\,t+2\,\zeta^2+e^{2\,A\,\Delta_a}\,(1-2\,\zeta^2))\,\omega_n+$$
$$\left.\left.(-1+e^{2\,A\,\Delta_a})\,\zeta\,t_a\,\omega_n^2)\,\text{UnitStep}[\Delta_a]\right)\right)$$

Output in mathematical traditional format:

(StarDust-V) In[122]:=

```
TraditionalForm[ut2Rep]
```

(StarDust-V) Out[122]//TraditionalForm=

$$\frac{1}{2\,m\,t_a\,\omega_n^3}\left(-4\,\zeta+2\,t\,\omega_n+\right.$$
$$\frac{e^{-t\,(A+\zeta\,\omega_n)}\,(2\,A\,(1+e^{2\,A\,t})\,\zeta+(-1+e^{2\,A\,t})\,(2\,\zeta^2-1)\,\omega_n)}{A}+$$
$$\frac{1}{A}\left(e^{-\Delta_a\,(A+\zeta\,\omega_n)}\,((-1+e^{2\,A\,\Delta_a})\,\zeta\,t_a\,\omega_n^2+\right.$$
$$(2\,\zeta^2-2\,A\,e^{\Delta_a\,(A+\zeta\,\omega_n)}\,t+e^{2\,A\,\Delta_a}\,(1-2\,\zeta^2)-1)\,\omega_n-$$
$$\left.\left.2\,A\,(1+e^{2\,A\,\Delta_a}-2\,e^{\Delta_a\,(A+\zeta\,\omega_n)})\,\zeta+A\,(1+e^{2\,A\,\Delta_a})\,\tau_a)\,\theta(\Delta_a)\right)\right)$$

Complete Solution in Time Domain

Adding "ut1Rep" and "ut2Rep" from above, replacing long expressions by abbreviations and assigning attributes to newly introduced expressions:

(StarDust-V) In[159]:=

```
utPF1 = Simplify[ut1Rep + ut2Rep]
```

Introducing further abbreviations, simplifying expressions:

(StarDust-V) In[168]:=

```
utPF2 = ReplaceRepeated[utPF1,
  {e^(α Δa / td) → e1, e^(2 A t) → e2, e^(2 A Δa) → e3, e^(Δa (A+ζ ωn)) → e4, e^(-Δa (A+ζ ωn)) → e5,
   e^((2 A + α/td) Δa) → e6, e^(-Δa (α+td (A+ζ ωn))/td) → e7, e^(-t (A+ζ ωn)) → e8,
   1/(α^2 - 2 α ζ τn + τn^2)^2 → 1/B1, 1/Sqrt[(-1 + ζ^2) ωn^2] → 1/A,
   (1 + e3) → C1, (-1 + e3) → C2}]
```

(StarDust-V) Out[168]=

$$\frac{1}{2\,m}\left(\frac{1}{A\,B_1}\left(e_7\,t_d\,\left(\alpha^2\,\left((-1+\alpha)\,C_2\,e_1-2\,A\,e_4\,\Delta_a\right)-2\,\alpha\,\zeta\,\left((-1+\alpha)\,C_2\,e_1-2\,A\,e_4\,\Delta_a\right)\,\tau_n+\right.\right.\right.$$
$$\left((-1+\alpha)\,\left(-1+2\,\zeta^2\right)\,C_2\,e_1-2\,A\,e_4\,\Delta_a\right)\,\tau_n^2+$$
$$2\,e_1\,t_d^2\,\omega_n\,\left(A\,(-1+\alpha)\,\zeta\,C_1+\alpha\,C_2\,\omega_n\right)-$$
$$e_1\,t_d^3\,\omega_n^2\,\left(A\,C_1+\zeta\,C_2\,\omega_n\right)+t_d\,\left(-4\,A\,(-1+\alpha)\,\zeta\,e_4\,\tau_n+2\,A\,e_4\,\tau_n^2-\right.$$
$$\left.\left.\alpha\,\left(A\,(-2+\alpha)\,\left(e_1-2\,e_4+e_6\right)+\alpha\,\zeta\,C_2\,e_1\,\omega_n\right)\right)\right)\,\text{UnitStep}[\Delta_a]\Big)+$$
$$\frac{1}{t_a\,\omega_n^3}\left(-4\,\zeta+2\,t\,\omega_n+\frac{e_8\,\left(2\,A\,\zeta\,\left(1+e_2\right)+\left(-1+2\,\zeta^2\right)\,\left(-1+e_2\right)\,\omega_n\right)}{A}+\right.$$
$$\frac{1}{A}\left(e_5\,\left(-2\,A\,\zeta\,\left(C_1-2\,e_4\right)+A\,C_1\,\tau_a+\right.\right.$$
$$\left.\left.\left.\left(-1+2\,\zeta^2+\left(1-2\,\zeta^2\right)\,e_3-2\,A\,t\,e_4\right)\,\omega_n+\zeta\,C_2\,t_a\,\omega_n^2\right)\,\text{UnitStep}[\Delta_a]\right)\right)\Big)$$

(StarDust-V) In[169]:=

```
utPF3 = Simplify[utPF2]
```

(StarDust-V) Out[169]=

$$\frac{1}{2\,m}\left(-\frac{1}{A\,B_1}\left(e_7\,t_d\,\left(C_2\,e_1\,\left(\alpha^2-\alpha^3+2\,(-1+\alpha)\,\alpha\,\zeta\,\tau_n-(-1+\alpha)\,\left(-1+2\,\zeta^2\right)\,\tau_n^2+\alpha^2\,\zeta\right.\right.\right.\right.$$
$$\left.t_d\,\omega_n-2\,\alpha\,t_d^2\,\omega_n^2+\zeta\,t_d^3\,\omega_n^3\right)+A\,\left((-2+\alpha)\,\alpha\,e_6\,t_d-$$
$$2\,e_4\,\left(t_d\,\left((-2+\alpha)\,\alpha-2\,(-1+\alpha)\,\zeta\,\tau_n+\tau_n^2\right)-\Delta_a\,\left(\alpha^2-2\,\alpha\,\zeta\,\tau_n+\tau_n^2\right)\right)+$$
$$\left.\left.\left.e_1\,t_d\,\left((-2+\alpha)\,\alpha+C_1\,t_d\,\omega_n\,\left(2\,\zeta-2\,\alpha\,\zeta+t_d\,\omega_n\right)\right)\right)\right)\,\text{UnitStep}[\Delta_a]\Big)+$$
$$\frac{1}{t_a\,\omega_n^3}\left(-4\,\zeta+2\,t\,\omega_n+\frac{e_8\,\left(2\,A\,\zeta\,\left(1+e_2\right)+\left(-1+2\,\zeta^2\right)\,\left(-1+e_2\right)\,\omega_n\right)}{A}+\right.$$
$$\frac{1}{A}\left(e_5\,\left(A\,C_1\,\left(-2\,\zeta+\tau_a\right)+e_4\,\left(4\,A\,\zeta-2\,A\,t\,\omega_n\right)+\right.\right.$$
$$\left.\left.\left.\omega_n\,\left(-1+2\,\zeta^2+e_3-2\,\zeta^2\,e_3+\zeta\,C_2\,t_a\,\omega_n\right)\right)\,\text{UnitStep}[\Delta_a]\right)\right)\Big)$$

(StarDust-V) In[171]:=

```
utPF4 = ReplaceRepeated[utPF3,
  {td ωn → τn, td^2 ωn^2 → τn^2, td^3 ωn^3 → τn^3, (α^2 - 2 α ζ τn + τn^2) → √B1}]
```

(StarDust-V) Out[171]=

$$\frac{1}{2\,m}\left(-\frac{1}{A\,B_1}\left(e_7\,t_d\left(C_2\,e_1\,(\alpha^2-\alpha^3+2\,(-1+\alpha)\,\alpha\,\zeta\,\tau_n+\alpha^2\,\zeta\,\tau_n-2\,\alpha\,\tau_n^2-(-1+\alpha)\,(-1+2\,\zeta^2)\,\tau_n^2+\zeta\,\tau_n^3)+A\left((-2+\alpha)\,\alpha\,e_6\,t_d+e_1\,t_d\,((-2+\alpha)\,\alpha+C_1\,\tau_n\,(2\,\zeta-2\,\alpha\,\zeta+\tau_n))-2\,e_4\left(-\sqrt{B_1}\,\Delta_a+t_d\,((-2+\alpha)\,\alpha-2\,(-1+\alpha)\,\zeta\,\tau_n+\tau_n^2)\right)\right)\right)\right.\right.$$
$$\left.\left.\text{UnitStep}[\Delta_a]\right)+\frac{1}{t_a\,\omega_n^3}\left(-4\,\zeta+2\,t\,\omega_n+\frac{e_8\,(2\,A\,\zeta\,(1+e_2)+(-1+2\,\zeta^2)\,(-1+e_2)\,\omega_n)}{A}+\frac{1}{A}\left(e_5\,(A\,C_1\,(-2\,\zeta+\tau_a)+e_4\,(4\,A\,\zeta-2\,A\,t\,\omega_n)+\omega_n\,(-1+2\,\zeta^2+e_3-2\,\zeta^2\,e_3+\zeta\,C_2\,t_a\,\omega_n))\,\text{UnitStep}[\Delta_a]\right)\right)\right)$$

Splitting time domain solution into two terms - one without and one with Heaviside step function (UnitStep[Δ_a]):

(StarDust-V) In[179]:=

```
utPF5 = Collect[utPF4, {UnitStep[Δa]}]
```

(StarDust-V) Out[179]=

$$\frac{-\frac{4\,\zeta}{t_a\,\omega_n^3}+\frac{2\,t}{t_a\,\omega_n^2}+\frac{e_8\,(2\,A\,\zeta\,(1+e_2)+(-1+2\,\zeta^2)\,(-1+e_2)\,\omega_n)}{A\,t_a\,\omega_n^3}}{2\,m}+\frac{1}{2\,m}\left(\left(-\frac{1}{A\,B_1}\left(e_7\,t_d\left(C_2\,e_1\,(\alpha^2-\alpha^3+2\,(-1+\alpha)\,\alpha\,\zeta\,\tau_n+\alpha^2\,\zeta\,\tau_n-2\,\alpha\,\tau_n^2-(-1+\alpha)\,(-1+2\,\zeta^2)\,\tau_n^2+\zeta\,\tau_n^3)+A\left((-2+\alpha)\,\alpha\,e_6\,t_d+e_1\,t_d\,((-2+\alpha)\,\alpha+C_1\,\tau_n\,(2\,\zeta-2\,\alpha\,\zeta+\tau_n))-2\,e_4\left(-\sqrt{B_1}\,\Delta_a+t_d\,((-2+\alpha)\,\alpha-2\,(-1+\alpha)\,\zeta\,\tau_n+\tau_n^2)\right)\right)\right)\right)+\frac{1}{A\,t_a\,\omega_n^3}\left(e_5\,(A\,C_1\,(-2\,\zeta+\tau_a)+e_4\,(4\,A\,\zeta-2\,A\,t\,\omega_n)+\omega_n\,(-1+2\,\zeta^2+e_3-2\,\zeta^2\,e_3+\zeta\,C_2\,t_a\,\omega_n))\right)\text{UnitStep}[\Delta_a]\right)$$

Output in traditional mathematical notation:

(StarDust-V) In[180]:=

```
TraditionalForm[utPF5]
```

(StarDust-V) Out[180]//TraditionalForm=

$$\frac{\frac{2t}{t_a\,\omega_n^2}+\frac{e_8\,(2A\zeta\,(e_2+1)+(2\zeta^2-1)\,(e_2-1)\,\omega_n)}{A\,t_a\,\omega_n^3}-\frac{4\zeta}{t_a\,\omega_n^3}}{2m}+\frac{1}{2m}$$

$$\left(\left(\frac{1}{A\,t_a\,\omega_n^3}\left(e_5\,(A\,C_1\,(\tau_a-2\zeta)+e_4\,(4A\zeta-2A\,t\,\omega_n)+\right.\right.\right.$$

$$\left.\left.\left.\omega_n\,(-2\,e_3\,\zeta^2+2\zeta^2+C_2\,t_a\,\omega_n\,\zeta+e_3-1)\right)\right)-\frac{1}{A\,B_1}$$

$$\left(e_7\,t_d\left(C_2\,e_1\,(-\alpha^3+\zeta\,\tau_n\,\alpha^2+\alpha^2-2\,\tau_n^2\,\alpha+2\,(\alpha-1)\,\zeta\,\tau_n\,\alpha+\right.\right.$$

$$\zeta\,\tau_n^3-(\alpha-1)\,(2\zeta^2-1)\,\tau_n^2)+A\left((\alpha-2)\,\alpha\,e_6\,t_d+\right.$$

$$e_1\,((\alpha-2)\,\alpha+C_1\,\tau_n\,(-2\,\alpha\,\zeta+2\zeta+\tau_n))\,t_d-$$

$$2\,e_4\left(t_d\,(\tau_n^2-2\,(\alpha-1)\,\zeta\,\tau_n+(\alpha-2)\,\alpha)-\right.$$

$$\left.\left.\left.\left.\sqrt{B_1}\,\Delta_a)\right)\right)\right)\theta(\Delta_a)\right)$$

The above expression gives the Type-II blast wave response of a linear, viscously damped SDOF system as an analytical solution in the time-domain. It has been derived by inverse Laplace transformation of the partial fractions of the complex domain solution shown at the start of this print-out.

(StarDust-V) In[57]:=

```
Remove["Global`*"]
```

(Deleting all introduced variables and freeing memory.)

Time Domain Response of Inverse Laplace Transform using Complete Solution

Complete Time Domain Solution -- Closed Form

Type-II blast response in the complex domain:

(StarDust-V) In[1]:=

$$uC = \frac{e^{-s\,t_a}\left(s^2\,t_a\,t_d\,(-1+s\,t_d+\alpha)+(-1+e^{s\,t_a}-s\,t_a)\,(s\,t_d+\alpha)^2\right)}{m\,s^2\,t_a\,(s\,t_d+\alpha)^2\,(s^2+2\,s\,\zeta\,\omega_n+\omega_n^2)};$$

(StarDust-V) In[2]:=

```
s ∈ Complexes &&
  {t, t_a, t_d, α, ω_n, ζ, m} ∈ Reals && {t, t_a, t_d, α, ω_n, ζ, m} ≥ 0;
```

(StarDust-V) In[3]:=

```
utCF0 = Evaluate[InverseLaplaceTransform[uC, s, t]]
```

(Result has been omitted - too long for printing.)

Expanding numerator and denominator:

(StarDust-V) In[4]:=

```
utCF2 = Expand[utCF0]
```

(Result has been omitted - too long for printing.)

Introducing abbreviations:

(StarDust-V) In[5]:=

```
Depth[utCF2]
```

(StarDust-V) Out[5]=

```
12
```

(StarDust-V) In[15]:=

```
utCF3 = ReplaceRepeated[utCF2, {
  (t - ta) → Δa, (-t + ta) → -Δa,
  e^(t (-ζ ωn+√(-ωn^2+ζ^2 ωn^2))) → e1, e^(t (-ζ ωn-√(-ωn^2+ζ^2 ωn^2))) → e2,
  e^(Δa (-ζ ωn+√(-ωn^2+ζ^2 ωn^2))) → e3, e^(Δa (-ζ ωn-√(-ωn^2+ζ^2 ωn^2))) → e4, e^(-α Δa/td) → e5,
  e^(-Δa (ζ ωn+√((-1+ζ^2) ωn^2))) → e6, e^(2 Δa √((-1+ζ^2) ωn^2) - Δa (ζ ωn+√((-1+ζ^2) ωn^2))) → e7,
  e^(2 A2 Δa - Δa (A2+ζ ωn)) → e8, e^(-Δa (A2+ζ ωn)) → e9,
  1/(α^2 - 2 α ζ td ωn + td^2 ωn^2)^2 → 1/A1, 1/(α^2 - 2 α ζ td ωn + td^2 ωn^2) → 1/√A1,
  (α^2 - 2 α ζ td ωn + td^2 ωn^2)^2 → A1, (α^2 - 2 α ζ td ωn + td^2 ωn^2) → √A1,
  1/√(-ωn^2 + ζ^2 ωn^2) → 1/A2, √((-1 + ζ^2) ωn^2) → A2}]
```

(Result has been omitted - too long for printing.)

Collecting terms:

(StarDust-V) In[16]:=

```
utCF4 = Collect[utCF3, {UnitStep[Δa], 1/(A1 A2), 1/A1, 1/m, 1/ta, A2, 1/ωn}]
```

Simplifying:

(StarDust-V) In[17]:=

```
utCF5 = Simplify[utCF4]
```

(StarDust-V) Out[17]=

$$\frac{1}{2\,m\,A_1\,A_2\,t_a\,\omega_n^3}\Big(2\,A_1\,A_2\,(2\,\zeta - t\,\omega_n)\,(-1 + \text{UnitStep}[\Delta_a]) + 2\sqrt{A_1}\,A_2\,e_5\,t_a\,(-t + t_a)\,t_d\,\omega_n^3\,\text{UnitStep}[\Delta_a] + \omega_n\Big((-1 + 2\,\zeta^2)\,e_1\,(\alpha^2 - 2\,\alpha\,\zeta\,t_d\,\omega_n + t_d^2\,\omega_n^2)^2 - (-1 + 2\,\zeta^2)\,e_2\,(\alpha^2 - 2\,\alpha\,\zeta\,t_d\,\omega_n + t_d^2\,\omega_n^2)^2 - (e_3 - e_4)\Big((-1 + 2\,\zeta^2)\,(\alpha^2 - 2\,\alpha\,\zeta\,t_d\,\omega_n + t_d^2\,\omega_n^2)^2 - t_a\,\omega_n\,(\alpha^4\,\zeta + \alpha^2\,(-1 + \alpha - 4\,\alpha\,\zeta^2)\,t_d\,\omega_n + \alpha\,\zeta\,(2 + \alpha\,(-1 + 4\,\zeta^2))\,t_d^2\,\omega_n^2 - (1 + \alpha)\,(-1 + 2\,\zeta^2)\,t_d^3\,\omega_n^3)\Big)\,\text{UnitStep}[\Delta_a]\Big) + A_2\Big(2\,\zeta\,e_1\,(\alpha^2 - 2\,\alpha\,\zeta\,t_d\,\omega_n + t_d^2\,\omega_n^2)^2 + 2\,\zeta\,e_2\,(\alpha^2 - 2\,\alpha\,\zeta\,t_d\,\omega_n + t_d^2\,\omega_n^2)^2 + \Big(2\,e_5\,t_a\,t_d^2\,\omega_n^3\,((-2 + \alpha)\,\alpha - 2\,(-1 + \alpha)\,\zeta\,t_d\,\omega_n + t_d^2\,\omega_n^2) + e_3\Big(-2\,\zeta\,(\alpha^2 - 2\,\alpha\,\zeta\,t_d\,\omega_n + t_d^2\,\omega_n^2)^2 + t_a\,\omega_n\,(\alpha^4 - 4\,\alpha^3\,\zeta\,t_d\,\omega_n + \alpha\,(2 + \alpha + 4\,\alpha\,\zeta^2)\,t_d^2\,\omega_n^2 - 2\,(1 + \alpha)\,\zeta\,t_d^3\,\omega_n^3)\Big) + e_4\Big(-2\,\zeta\,(\alpha^2 - 2\,\alpha\,\zeta\,t_d\,\omega_n + t_d^2\,\omega_n^2)^2 + t_a\,\omega_n\,(\alpha^4 - 4\,\alpha^3\,\zeta\,t_d\,\omega_n + \alpha\,(2 + \alpha + 4\,\alpha\,\zeta^2)\,t_d^2\,\omega_n^2 - 2\,(1 + \alpha)\,\zeta\,t_d^3\,\omega_n^3)\Big)\Big)\,\text{UnitStep}[\Delta_a]\Big)\Big)$$

Further abbreviations:

(StarDust-V) In[18]:=

```
utCF6 = ReplaceRepeated[utCF5, {t_a ω_n → τ_a, t_a^2 ω_n^2 → τ_a^2, t_a^3 ω_n^3 → τ_a^3,
    t_d ω_n → τ_d, t_d^2 ω_n^2 → τ_d^2, t_d^3 ω_n^3 → τ_d^3, (α^2 - 2 α ζ τ_d + τ_d^2) → √A_1,
    (t - t_a) → Δ_a, τ_a (-α^4 + 4 ζ τ_d α^3 + (-4 α ζ^2 + α - 2) τ_d^2 α + 2 ζ τ_d^3) → B_1,
    B_1 + 2 α (ζ α^3 - 4 ζ^2 τ_d α^2 + 2 ζ (2 ζ^2 + 1) τ_d^2 α + (1 - 4 ζ^2) τ_d^3) → B_2,
    (2 ζ^2 - 1) → B_4, (-2 ζ^2 + 1) → -B_4,
    1/(A_1 A_2) → 1/C_1, A_1 A_2 → C_1}]
```

(StarDust-V) Out[18]=

$$\frac{1}{2\,m\,C_1\,t_a\,\omega_n^3}\Big(2\,C_1\,(2\,\zeta - t\,\omega_n)\,(-1 + \text{UnitStep}[\Delta_a]) + 2\,\sqrt{A_1}\,A_2\,e_5\,t_a\,(-t + t_a)\,t_d\,\omega_n^3\,\text{UnitStep}[\Delta_a] + \omega_n\,(A_1\,B_4\,e_1 - A_1\,B_4\,e_2 - (e_3 - e_4)\,(A_1\,B_4 - \tau_a\,(\alpha^4\,\zeta + \alpha^2\,(-1 + \alpha - 4\,\alpha\,\zeta^2)\,\tau_d + \alpha\,\zeta\,(2 + \alpha\,(-1 + 4\,\zeta^2))\,\tau_d^2 - (1 + \alpha)\,B_4\,\tau_d^3))\,\text{UnitStep}[\Delta_a]) + A_2\,(2\,\zeta\,A_1\,e_1 + 2\,\zeta\,A_1\,e_2 + (e_3\,(-2\,\zeta\,A_1 + \tau_a\,(\alpha^4 - 4\,\alpha^3\,\zeta\,\tau_d + \alpha\,(2 + \alpha + 4\,\alpha\,\zeta^2)\,\tau_d^2 - 2\,(1 + \alpha)\,\zeta\,\tau_d^3)) + e_4\,(-2\,\zeta\,A_1 + \tau_a\,(\alpha^4 - 4\,\alpha^3\,\zeta\,\tau_d + \alpha\,(2 + \alpha + 4\,\alpha\,\zeta^2)\,\tau_d^2 - 2\,(1 + \alpha)\,\zeta\,\tau_d^3)) + 2\,e_5\,t_a\,t_d^2\,((-2 + \alpha)\,\alpha - 2\,(-1 + \alpha)\,\zeta\,\tau_d + \tau_d^2)\,\omega_n^3)\,\text{UnitStep}[\Delta_a])\Big)$$

Collecting, simplifying and abbreviating:

(StarDust-V) In[24]:=

```
utCF7 = ReplaceRepeated[Simplify[Collect[utCF6, UnitStep[Δ_a]]],
  {(-t + t_a) → -Δ_a, A_1 A_2 → C_1, A_1 B_4 → C_2,
   (-2 ζ A_1 + τ_a (α^4 - 4 α^3 ζ τ_d + α (2 + α + 4 α ζ^2) τ_d^2 - 2 (1 + α) ζ τ_d^3)) → B_5,
   (2 ζ - t ω_n) → B_6}]
```

(StarDust-V) Out[24]=

$$\frac{1}{2\,m\,C_1\,t_a\,\omega_n^3}\Big(-2\,B_6\,C_1 + 2\,\zeta\,C_1\,e_1 + 2\,\zeta\,C_1\,e_2 + C_2\,e_1\,\omega_n - C_2\,e_2\,\omega_n + \big(2\,B_6\,C_1 + (-e_3 + e_4)\,(C_2 + \tau_a\,(-\alpha^4\,\zeta + \alpha^2\,(1 - \alpha + 4\,\alpha\,\zeta^2)\,\tau_d + \alpha\,\zeta\,(-2 + \alpha - 4\,\alpha\,\zeta^2)\,\tau_d^2 + (1 + \alpha)\,B_4\,\tau_d^3))\,\omega_n - 2\,\sqrt{A_1}\,A_2\,e_5\,t_a\,t_d\,\Delta_a\,\omega_n^3 + A_2\,(B_5\,e_3 + B_5\,e_4 + 2\,e_5\,t_a\,t_d^2\,((-2 + \alpha)\,\alpha - 2\,(-1 + \alpha)\,\zeta\,\tau_d + \tau_d^2)\,\omega_n^3)\big)\,\text{UnitStep}[\Delta_a]\Big)$$

Output in traditional mathematical notation:

(StarDust-V) In[25]:=

```
TraditionalForm[utCF7]
```

(StarDust-V) Out[25]//TraditionalForm=

$$\frac{1}{2\,m\,C_1\,t_a\,\omega_n^3}\Big(-2\,B_6\,C_1+2\,\zeta\,e_1\,C_1+2\,\zeta\,e_2\,C_1+C_2\,e_1\,\omega_n-C_2\,e_2\,\omega_n+\Big(-2\,\sqrt{A_1}\,A_2\,e_5\,t_a\,t_d\,\Delta_a\,\omega_n^3+(e_4-e_3)\,(C_2+\tau_a\,(-\zeta\,\alpha^4+(4\,\alpha\,\zeta^2-\alpha+1)\,\tau_d\,\alpha^2+\zeta\,(-4\,\alpha\,\zeta^2+\alpha-2)\,\tau_d^2\,\alpha+(\alpha+1)\,B_4\,\tau_d^3))\,\omega_n+2\,B_6\,C_1+A_2\,(2\,e_5\,t_a\,t_d^2\,(\tau_d^2-2\,(\alpha-1)\,\zeta\,\tau_d+(\alpha-2)\,\alpha)\,\omega_n^3+B_5\,e_3+B_5\,e_4)\Big)\,\theta(\Delta_a)\Big)$$

The above expression gives the Type-II blast wave response of a linear, viscously damped SDOF system as an analytical solution in the time-domain. It has been derived by inverse Laplace transformation of entire complex domain solution shown at the start of this print-out.

A.1.2 Piecewise Linear Approximation

This section gives the analytical solutions for displacement $u_r(t)$, velocity $v_r(t)$, extreme displacement time points t_{Ex} and the minimum/maximum displacement $u_{r,Ex}$ itself for each time segment r in Fig. 2.5.1 on page 29 with $r = 1,\ldots,4$ as introduced in section 2.5.2 on page 20.

Segment 1: $0 \leq t \leq t_d$

Referring to picture 2.5.1 on page 29 the force $p_1(t)$ for the interval $(0;t_d)$ is given by Eq.(2.5.5a) which leads together with the three equations (2.5.6) - (2.5.8) to the following expression for SDOF displacement and velocity response

$$u_1(t) = \frac{p_0\Delta}{m t_d \omega_n^2}\left(t + t_d[1-\cos(t\,\omega_n)] + \frac{1}{\omega_n}\sin(t\,\omega_n)\right) \tag{A.1.5a}$$

$$v_1(t) = \frac{p_0\Delta}{m t_d \omega_n^2}\left(\cos(t\,\omega_n) + t_d\,\omega_n \sin(t\,\omega_n)\right). \tag{A.1.5b}$$

The condition $v_1(t) = 0$ together with two substitutions

$$\sin(t\,\omega_n) = \sqrt{1-\cos^2(t\,\omega_n)} \qquad \text{and} \qquad \cos(t\,\omega_n) = y \tag{A.1.6}$$

makes it possible to rewrite equation (A.1.5b)

$$A_1\sqrt{1-y^2} + B_1 y - B_1 = 0 \tag{A.1.7a}$$

where

$$A_1 = \frac{p_0\Delta}{m\,\omega_n} \qquad \text{and} \qquad B_1 = \frac{p_0\Delta}{m t_d \omega_n^2}. \tag{A.1.7b}$$

Solutions for y are easily obtained as

$$y_1 = 1 \qquad \text{and} \qquad y_2 = \frac{1-(t_d\,\omega_n)^2}{1+(t_d\,\omega_n)^2}. \tag{A.1.8}$$

Both solutions y_1 and y_2 are in principal feasible since for the physically correct definition of $t_d\,\omega_n \geq 0$ both *always* give valid solutions for t with $t = \frac{1}{\omega_n}\arccos(y)$ where the trigonometric function $\arccos(.)$ is defined in the interval $(-1;1)$. Therefore,

$$t_{1,1} = \frac{1}{\omega_n}\arccos(1) = 0,$$

$$t_{1,2} = \frac{1}{\omega_n}\arccos\left(\frac{1-(t_d\,\omega_n)^2}{1+(t_d\,\omega_n)^2}\right), \qquad 1 \leq t_d\,\omega_n. \tag{A.1.9}$$

Multiple solutions of t_1 are obtained by

$$t_{1,1j} = 2j\frac{\pi}{\omega_n}, \qquad t_{1,2j} = 2j\frac{\pi}{\omega_n} + t_{1,2} \quad \text{with} \quad (j = 1,2,3,\ldots). \tag{A.1.10}$$

Making use of the second derivative of Eq.(A.1.5a), namely the SDOF acceleration,

$$a_1(t) = \frac{p_0\Delta}{m t_d \omega_n^2}\left(t_d\,\omega_n^2\cos(t\,\omega_n) - \omega_n\sin(t\,\omega_n)\right) \tag{A.1.11}$$

reveals the type of solution for the extreme displacement at time points $t_{1,1j}$ and $t_{1,2j}$. It is easy to see that

$$a_1(t_{1,1j}) > 0 \qquad \text{and} \qquad a_1(t_{1,2j}) < 0 \quad \text{but only if} \quad 1 \leq t_d\,\omega_n \tag{A.1.12}$$

which states that at time points $t_{1,1j}$ the displacement function $u(t)$, Eq.(A.1.5a) has local minima and at $t_{1,2j}$ local maxima if $1 \leq t_d\,\omega_n$. Hence, minima displacements of the approximated blast wave excited SDOF system occur at regular time intervals spaced apart exactly at the inverse of the oscillators natural frequency f_n. In contrast, displacement maxima values appear to have an additional shift of $t_{1,2}$ as obtained from Eq.(A.1.9).

It is important to note here, that for the fixed value of $y_1 = 1$ there will always be at least *one* local minima within the interval $(0; t_d)$, i.e. at $t_{1,1} = 0$. In contrast, for values of the product $t_d\,\omega_n$ smaller 1 the displacement function (A.1.5a) has *no* local maxima within $0 \leq t \leq t_d$.

Substitution of Eq.(A.1.10) into (A.1.5a) gives the respective local minimum and maximum values of $u_{r;\max}$ $(r = 1)$. However, those values do not necessarily present global extreme solutions. Results obtained have to be compared against extreme values of displacement $u_{r;\mathrm{Ex}}$ from other time sections $r = 2, 3, 4$. This will be shown in what follows.

Segment 2: $\mathbf{t_d \leq t \leq t_{A2}}$

Introducing the initial conditions for the second segment in Fig. 2.5.1 as

$$u_{0,2} = u_1(t = t_d)\,, \quad \dot{u}_{0,2} = v_1(t = t_d)$$

and using the definition given by Eq.(2.5.6) on page 21 the time domain response of the system between

$$t_d \leq t \leq t_{\mathrm{A2}} \tag{A.1.13}$$

is obtained from the integral expression

$$u_2(t) = \frac{1}{m\,\omega_n} \int_{t_d}^{t} p_2(t-\hat{t}) \sin\left[\omega_n(\hat{t}-t_d)\right] \mathrm{d}\hat{t} + u_{0,2} \cos\left[\omega_n\,(t-t_d)\right] + \frac{\dot{u}_{0,2}}{\omega_n} \sin\left[\omega_n\,(t-t_d)\right] \tag{A.1.14a}$$

and equates to

$$\begin{aligned} u_2(t) = \frac{1}{m\,(t_{\mathrm{A2}}-t_d)\,\omega_n^3} \Big\{ & p_{1\Delta}\,(t-2t_d)\,\omega_n + \ldots \\ & \omega_n \left(p_{1\Delta}\,t_d + m\,(t_{\mathrm{A2}}-t_d)\,u_{20}\,\omega_n^2\right) \cos\left[\omega_n\,(t-t_d)\right] + \ldots \\ & - \left(p_{1\Delta} + m\,(t_d - t_{\mathrm{A2}})\,v_{20}\,\omega_n^2\right) \sin\left[\omega_n\,(t-t_d)\right] \Big\}. \end{aligned} \tag{A.1.14b}$$

This gives for the velocity as the first derivative with respect to time

$$\begin{aligned} v_2(t) = \frac{1}{m\,(t_{\mathrm{A2}}-t_d)\,\omega_n^2} \Big\{ & p_{1\Delta} - \left(p_{1\Delta} + m\,(t_d - t_{\mathrm{A2}})\,v_{20}\,\omega_n^2\right) \cos\left[\omega_n\,(t-t_d)\right] + \ldots \\ & - \omega_n \left(p_{1\Delta}\,t_d + m\,(t_{\mathrm{A2}}-t_d)\,u_{20}\,\omega_n^2\right) \sin\left[\omega_n\,(t-t_d)\right] \Big\}. \end{aligned} \tag{A.1.14c}$$

Similarly, the acceleration is given by

$$a_2(t) = \frac{1}{m\,(t_{A2} - t_d)\,\omega_n}\Big\{-\omega_n\left(p_{1\Delta}\,t_d + m\,(t_{A2} - t_d)\,u_{20}\,\omega_n^2\right)\cos\Big[\omega_n\,(t - t_d)\Big] + \ldots$$
$$\left(p_{1\Delta} + m\,(t_d - t_{A2})\,v_{20}\,\omega_n^2\right)\sin\Big[\omega_n\,(t - t_d)\Big]\Big\}. \quad \text{(A.1.14d)}$$

Again, setting $v_2(t) = 0$ and making use of Eq.(A.1.6) leads to a quadratic-type equation

$$A_2\sqrt{1 - y^2} + B_2 y + p_{1\Delta} = 0 \quad \text{(A.1.15a)}$$

where

$$A_2 = -\omega_n\left(p_{1\Delta}\,t_d + m\,(t_{A2} - t_d)\,u_{20}\,\omega_n^2\right)\cos\left(t_d\,\omega_n\right) - \left(p_{1\Delta} + m\,(t_d - t_{A2})\,v_{20}\,\omega_n^2\right)\sin\left(t_d\,\omega_n\right)$$
$$B_2 = -\left(p_{1\Delta} + m\,(t_d + t_{A2})\,v_{20}\,\omega_n^2\right)\cos\left(t_d\,\omega_n\right) + \omega_n\left(p_{1\Delta}\,t_d + m\,(t_{A2} - t_d)\,u_{20}\omega_n^2\right)\sin\left(t_d\,\omega_n\right) \quad \text{(A.1.15b)}$$

and solutions for y are

$$y_{1/2} = \frac{p_{1\Delta}\,B_2}{A_2^2 + B_2^2} \pm \sqrt{\left(\frac{p_{1\Delta}\,B_2}{A_2^2 + B_2^2}\right)^2 - \frac{p_{1\Delta}^2 - A_2^2}{A_2^2 + B_2^2}}\,. \quad \text{(A.1.16)}$$

Fundamental time points t_2 of extreme displacement are obtained using the inverse function of equation (A.1.6)

$$t_{2,1/2} = \arccos\left(y_{1/2}\right). \quad \text{(A.1.17)}$$

In the special case of $y_1 > 0$ and $y_2 < 0$ equation (A.1.14b) has at least one minimum and maximum, respectively, within the interval $t_d \le t \le t_{A2}$. Inserting $y_{1/2}$ into a transformed version of Eq.(A.1.14d) by using the rules given in Eq.(A.1.6), i.e. $a_2 = a_2(y)$, reveals the nature of the two solutions of (A.1.16). Positive values of y give local displacement minima and negative values for y local displacement maxima. However, it should be noted that actual solutions for t at which Eq.(A.1.14b) has extreme values *do not* necessarily correspond to the basic solution obtained by Eq.(A.1.17). They are calculated in a similar way as shown for t_1 in Eq.(A.1.10),

$$y > 0: \qquad t_{2,1j} = \frac{2j\pi}{\omega_n} - t_{2,1} \qquad \text{local minima} \qquad \text{(A.1.18a)}$$

$$y < 0: \qquad t_{2,2j} = \frac{2j\pi}{\omega_n} + t_{2,2} \qquad \text{local maxima} \qquad (j = 1,2,3,\ldots) \qquad \text{(A.1.18b)}$$

whereas Eq.(A.1.17) gives usually solutions $t_{2,1/2} < t_d$ if Eq.(A.1.14b) exhibits at least two extreme solutions, i.e. one minima and one maxima. However, depending on the configuration of parameters $(f_n, p_{1\Delta}, \alpha, td, \ldots)$ the fundamental or basic solution given by Eq.(A.1.17) can be identical to a first time point of extreme displacement within the interval (A.1.13).

In the second case of one extreme solution *only*, either minima or maxima, $t_{2,1/2}$ is obtained using Eq.(A.1.17) and (A.1.18) bearing in mind the solution has to be within the interval given by Eq.(A.1.13).

Finally, if Eq.(A.1.14b) has no local extremal values within $(t_d; t_{A2})$ none of the solutions obtained by (A.1.17) or (A.1.18) will fulfil condition (A.1.13).

Segment 3: $\mathbf{t_{A2} \leq t \leq t_E}$

The SDOF displacement oscillation in this region of the time axis starts with the initial conditions $u_{0,3} = u_2\,(t = t_{A2})$ and $v_{0,3} = v_2\,(t = t_{A2})$ inherited from section 2, see Fig. 2.5.1 on page 29. Using a convolution expression similar to Eq.(A.1.14a)

$$u_3(t) = \frac{1}{m\,\omega_n} \int_{t_{A2}}^{t} p_3(t-\hat{t}) \sin\left[\omega_n\,(\hat{t}-t_{A2})\right] \mathrm{d}\hat{t} + u_{0,2} \cos\left[\omega_n\,(t-t_{A2})\right] + \frac{\dot{u}_{0,2}}{\omega_n} \sin\left[\omega_n\,(t-t_{A2})\right] \tag{A.1.19a}$$

gives the displacement as a function of time for the interval $t_{A2} \leq t \leq t_E$

$$u_3(t) = \frac{1}{m\,(t_{A2}-t_E)\,\omega_n^3} \Big\{ p_{1\Delta}\,(t-t_{A2}-t_E)\,\omega_n + \ldots \\ \omega_n \left(p_{1\Delta}\,t_E + m\,(t_{A2}-t_E)\,u_{0,3}\,\omega_n^2\right) \cos\left[\omega_n\,(t-t_{A2})\right] + \ldots \\ - \left(p_{1\Delta} + m\,(t_E-t_{A2})\,v_{0,2}\,\omega_n^2\right) \sin\left[\omega_n\,(t-t_{A2})\right] \Big\} \tag{A.1.19b}$$

as well as the corresponding velocity

$$v_3(t) = \frac{1}{m\,(t_{A2}-t_E)\,\omega_n^2} \Big\{ p_{1\Delta} - \left(p_{1\Delta} + m\,(t_E-t_{A2})\,v_{0,3}\,\omega_n^2\right) \cos\left[\omega_n\,(t-t_{A2})\right] + \ldots \\ - \omega_n \left(p_{1\Delta}\,t_E + m\,(t_{A2}-t_E)\,u_{0,3}\,\omega_n^2\right) \sin\left[\omega_n\,(t-t_{A2})\right] \Big\} \tag{A.1.19c}$$

and acceleration

$$a_3(t) = \frac{1}{m\,(t_{A2}-t_E)\,\omega_n} \Big\{ -\omega_n \left(p_{1\Delta}\,t_E + m\,(t_{A2}-t_E)\,u_{0,3}\,\omega_n^2\right) \cos\left[\omega_n\,(t-t_{A2})\right] + \ldots \\ \left(p_{1\Delta} + m\,(t_E-t_{A2})\,v_{0,3}\,\omega_n^2\right) \sin\left[\omega_n\,(t-t_{A2})\right] \Big\}. \tag{A.1.19d}$$

With $v_3(t) = 0$ and Eq.(A.1.6) the solutions for extreme displacement $u_{3,Ex}$ are obtained from an equation completely identical to (A.1.15a), but now with the different constants

$$A_3 = -\omega_n \left(p_{1\Delta}\,t_E + m\,(t_{A2}-t_E)\,u_{0,3}\,\omega_n^2\right) \cos\left(t_{A2}\,\omega_n\right) + \ldots \\ - \left(p_{1\Delta} + m\,(t_E-t_{A2})\,v_{0,3}\,\omega_n^2\right) \sin\left(t_{A2}\,\omega_n\right)$$

and

$$B_3 = -\left(p_{0\Delta} + m\,(t_E-t_{A2})\,v_{0,3}\,\omega_n^2\right) \cos\left(t_{A2}\,\omega_n\right) + \ldots \\ + \omega_n \left(p_{0\Delta}\,t_E + m\,(t_{A2}-t_E)\,u_{0,3}\,\omega_n^2\right) \sin\left(t_{A2}\,\omega_n\right) \tag{A.1.20}$$

but the same solution procedure as shown above in Eq.(A.1.16) to (A.1.18).

Segment 4: $\mathbf{t_E \leq t}$

For all time instances greater than t_E the forcing function is zero and the SDOF system undergoes free vibration with the initial conditions $u_{0,4} = u_3\,(t = t_E)$ and $v_{0,4} = v_3\,(t = t_E)$. Hence, displacement,

velocity and acceleration are given by the well-known expressions

$$u_4(t) = u_{0,4}\cos\left[(t-t_E)\,\omega_n\right] + \frac{v_{0,4}}{\omega_n}\sin\left[(t-t_E)\,\omega_n\right], \tag{A.1.21a}$$

$$v_4(t) = -u_{0,4}\,\omega_n \sin\left[(t-t_E)\,\omega_n\right] + v_{0,4}\cos\left[(t-t_E)\,\omega_n\right] \tag{A.1.21b}$$

and

$$a_4(t) = -u_{0,4}\,\omega_n^2 \cos\left[(t-t_E)\,\omega_n\right] - v_{0,4}\,\omega_n \sin\left[(t-t_E)\,\omega_n\right], \tag{A.1.21c}$$

respectively. Utilising Eq.(A.1.6), after setting $v_4(t) = 0$, leads to

$$A_4\sqrt{1-y^2} + B_4 y = 0 \tag{A.1.22}$$

with the two solutions

$$y_{1/2} = \pm\sqrt{\frac{A_4^2}{A_4^2+B_4^2}}. \tag{A.1.23}$$

and the constants

$$\begin{aligned} A_4 &= -u_{0,4}\,\omega_n\cos(t_E\,\omega_n) + v_{0,4}\sin(t_E\,\omega_n) \\ B_4 &= u_{0,4}\,\omega_n\,\omega_n\sin(t_E\,\omega_n) + v_{0,4}\cos(t_E\,\omega_n)\,. \end{aligned} \tag{A.1.24}$$

The symmetry of solution (A.1.23) as argument for the inverse cosine function $t = \frac{1}{\omega_n}\arccos(y)$ reflects the typical behaviour of freely vibrating undamped linear system with equal minimum and maximum amplitudes and no static offset of the equilibrium position. Equation (A.1.23) guaranties furthermore the existence of both extremal solutions, since $y_1 > 0$ and $y_2 < 0$ for all A_4 and B_4, as a logical consequence of the fact $\zeta = 0$ and $t \to \infty$.

A.2 Linear Autonomous - Step and Impulse Excitation

A.2.1 Free Vibration

The solution to the linear second order differential equation of motion of the undamped single-degree-of-freedom system

$$\ddot{u}(t) + \omega_n^2 u(t) = p(t) \tag{A.2.1a}$$

can be found in various textbooks, see [37] for example. In case of $p(t) = 0\ \forall\, t$ the system undergoes free vibration subjected to the initial conditions

$$u(t=0) = u_0 \qquad \text{and} \qquad \dot{u}(t=0) = \dot{u}_0\,. \tag{A.2.1b}$$

A solution for the equation of motion is obtained substituting [39]

$$u(t) = \Re\left\{\tilde{u}_m\, e^{\mathrm{i}\omega_n t}\right\}, \qquad \tilde{u}_m = u_{m,\Re} + \mathrm{i}\,u_{m,\Im} \tag{A.2.2}$$

into (A.2.1a) and applying the initial conditions which leads to

$$u(t) = u_0\cos(\omega_n t) + \frac{\dot{u}_0}{\omega_n}\sin(\omega_n t)\,. \tag{A.2.3}$$

Although no explicit expression for the maximum response $u_{\max}$ could be found in literature, its derivation is straight forward. To start with, the first derivative of Eq.(A.2.3) is set to zero and the equation is solved for the time point $t_{\max}$ at which the maximum deflection occurs

$$\frac{\mathrm{d}u(t)}{\mathrm{d}t} \stackrel{!}{=} 0 = -u_0\omega_n \sin(\omega_n t_{\max}) + \dot{u}_0 \cos(\omega_n t_{\max}) \tag{A.2.4a}$$

$$\omega_n t_{\max} = \arctan(A_0) \qquad \text{with} \qquad A_0 = \frac{\dot{u}_0}{u_0\omega_n}. \tag{A.2.4b}$$

By inserting (A.2.4b) into (A.2.3) and making use of the relations [15]

$$\cos[\arctan(A_0)] = \frac{1}{\sqrt{1+A_0^2}} \qquad \text{and} \qquad \sin[\arctan(A_0)] = \frac{A_0}{\sqrt{1+A_0^2}} \tag{A.2.5}$$

an explicit expression for $u_{\max}$ is derived

$$\begin{aligned} u_{\max}^2\left(1+A_0^2\right) &= \left(u_0 + \frac{\dot{u}_0}{\omega_n}A_0\right)^2 \\ &= \left(1+A_0^2\right)\left(u_0^2 + \frac{\dot{u}_0^2}{\omega_n^2}\right) \\ u_{\max} &= \sqrt{u_0^2 + \frac{\dot{u}_0^2}{\omega_n^2}}. \end{aligned} \tag{A.2.6}$$

The proof of (A.2.6) giving a global maximum at $t_{\max}$ for $u(t)$ is given as follows

$$0 \stackrel{!}{>} \frac{\mathrm{d}^2u(t)}{\mathrm{d}t^2} = -u_0\omega_n^2 \cos(\omega_n t_{\max}) - \dot{u}_0\omega_n \sin(\omega_n t_{\max}) \tag{A.2.7}$$

which holds true for the first half of the oscillation period. i.e. $0 \leq t_{\max} \leq \frac{\pi}{\omega_n}$, where $u_{\max}$ is assumed to occur.

A.2.2 Step Excitation

In the case of $p(t) = \mathbb{H}(t)p_0$ in Eq.(A.2.1a) the solution is derived using the convolution integral [37]

$$u(t) = u_0 \cos(\omega_n t) + \frac{\dot{u}_0}{\omega_n}\sin(\omega_n t) + \frac{1}{m\omega_n}\int_0^t p_0 \sin(\omega_n[t-\tau])\,dt \tag{A.2.8a}$$

where the last term in (A.2.8a) equates to

$$\frac{p_0}{k}\left(1 - \cos(\omega_n t)\right). \tag{A.2.8b}$$

Using the same approach as in section A.2.1 the first derivative of (A.2.8a) is set to zero

$$\frac{\mathrm{d}u(t)}{\mathrm{d}t} \stackrel{!}{=} 0 = -u_0\omega_n \sin(\omega_n t_{\max}) + \dot{u}_0 \cos(\omega_n t_{\max}) + \frac{p_0}{k}\omega_n^2 \cos(\omega_n t_{\max}) \tag{A.2.9a}$$

and solved for $t_{\max}$

$$t_{\max} = \frac{1}{\omega_n}\arctan\left(\frac{\dot{u}}{\omega_n\left(u_0 - \frac{p_0}{k}\right)}\right) = \frac{1}{\omega_n}\arctan(A_1). \tag{A.2.9b}$$

Substitution into (A.2.8a) together with (A.2.5) leads to

$$u_{\max}\sqrt{1+A_1^2} = u_0 + \frac{\dot{u}_0}{\omega_n}A_1 + \frac{p_0}{k}\left(\sqrt{1+A_1^2}-1\right)$$
$$u_{\max}\sqrt{1+A_1^2} - \frac{p_0}{k}\sqrt{1+A_1^2} = u_0 + \frac{\dot{u}_0}{\omega_n}A_1 - \frac{p_0}{k}$$

squaring both sides and dividing by $\left(1+A_1^2\right)$ gives

$$u_{\max}^2 - 2\frac{p_0}{k}u_{\max} + \left(\frac{p_0}{k}\right)^2 = \frac{1}{\left(1+A_1^2\right)}\left(u_0 + \frac{\dot{u}_0}{\omega_n}A_1 - \frac{p_0}{k}\right)^2$$
$$= \left(\frac{\dot{u}_0}{\omega_n}\right)^2 + \left(\frac{p_0}{k}\right)^2 - 2\frac{p_0}{k}u_0 + \dot{u}_0^2$$
$$u_{\max}^2 - 2\frac{p_0}{k}u_{\max} - u_0^2 + 2\frac{p_0}{k}u_0 - \frac{\dot{u}_0^2}{\omega_n^2} = 0 \qquad \text{(A.2.10)}$$

a quadratic algebraic equation with the two solutions [15]

$$u_{\mathrm{Ex},1/2} = \frac{p_0}{k} \pm \sqrt{\left(\frac{p_0}{k}\right)^2 + u_0^2 - 2\frac{p_0}{k}u_0 + \frac{\dot{u}_0^2}{\omega_n^2}} = \frac{p_0}{k} \pm \sqrt{\left(u_0 - \frac{p_0}{k}\right)^2 + \frac{\dot{u}_0^2}{\omega_n^2}} \qquad \text{(A.2.11)}$$

which in case of $p_0 = 0$ simplifies to Eq.(A.2.6) and for zero initial conditions to

$$u_{\mathrm{min/max}} = \frac{p_0}{k} \mp \frac{p_0}{k}. \qquad \text{(A.2.12)}$$

A.2.3 Impulse Excitation

The time-displacement solution for a linear impulse excited SDOF system is given by [39]

$$u(t) = u_0\cos(\omega_n t) + \left(\frac{p_0}{m\omega_n} + \frac{\dot{u}_0}{\omega_n}\right)\sin(\omega_n t) \qquad \text{(A.2.13)}$$

where p_0 is the area under a scaled unit impulse function. The first derivative of (A.2.13) is similar to (A.2.4a)

$$\frac{\mathrm{d}u(t)}{\mathrm{d}t} \stackrel{!}{=} 0 = -u_0\omega_n\sin(\omega_n t) + \left(\frac{p_0}{m} + \dot{u}_0\right)\cos(\omega_n t) \qquad \text{(A.2.14)}$$

and can be rearranged to give an explicit expression for the time t_{Ex} at which the minimum/maximum response u_{Ex} occurs

$$\omega_n t_{\mathrm{Ex}} = \arctan(A_2) \qquad \text{with} \qquad A_2 = \frac{1}{u_0\,\omega_n}\left(\frac{p_0}{m} + \dot{u}_0\right). \qquad \text{(A.2.15)}$$

Inserting Eq.(A.2.15) into (A.2.14) and making use of Eq.(A.2.5) gives

$$u_{\mathrm{Ex}} = u_0\frac{1}{\sqrt{1+A_2}} + \frac{1}{\omega_n}\left(\frac{p_0}{m} + \dot{u}_0\right)\frac{A_2}{\sqrt{1+A_2^2}} \qquad \text{(A.2.16a)}$$

equating to

$$u_{\mathsf{Ex}}^2\left(1+A_2^2\right) = \left[u_0+\left(\frac{p_0}{\omega_n m}+\frac{\dot{u}_0}{\omega_n}\right)A_2^2\right]^2 = \left[u_0+\frac{1}{u_0}\left(\frac{p_0}{\omega_n m}+\frac{\dot{u}_0}{\omega_n}\right)^2\right]^2 \tag{A.2.16b}$$

$$= u_0^2+2\left(\frac{p_0}{\omega_n m}+\frac{\dot{u}_0}{\omega_n}\right)^2+\frac{1}{u_0^2}\left(\frac{p_0}{\omega_n m}+\frac{\dot{u}_0}{\omega_n}\right)^4$$

$$= \left(1+\frac{1}{u_0^2}\left(\frac{p_0}{\omega_n m}+\frac{\dot{u}_0}{\omega_n}\right)^2\right)\left(u_0^2+\left(\frac{p_0}{\omega_n m}+\frac{\dot{u}_0}{\omega_n}\right)^2\right)$$

$$= \left(1+A_2^2\right)\left(u_0^2+\left(\frac{p_0}{\omega_n m}+\frac{\dot{u}_0}{\omega_n}\right)^2\right) \tag{A.2.16c}$$

which gives finally the result for minimum and maximum displacement, respectively

$$u_{\mathsf{min/max}} = \mp\sqrt{u_0^2+\frac{1}{\omega_n^2}\left(\frac{p_0}{m}+\dot{u}_0\right)^2}. \tag{A.2.17}$$

The second derivative of Eq.(A.2.13) must be smaller or greater then zero if (A.2.17) is a global maximum or minimum, respectively

$$\frac{\mathrm{d}^2u(t)}{\mathrm{d}t^2} = -u_0\omega_n^2\cos\left(\omega_n t\right)-\omega_n\left(\frac{p_0}{m}+\dot{u}_0\right)\sin\left(\omega_n t\right) = \begin{cases} <0 & \text{for } 0\le t\le\frac{\pi}{2}, \\ >0 & \text{for } \frac{3}{2}\pi\le t\le 2\pi \end{cases}. \tag{A.2.18}$$

APPENDIX B

Nonlinear SDOF Systems

B.1 Hypergeometric and Gamma Functions

The Gauss' hypergeometric function ${}_2\mathcal{F}_1$ has a series expansion of the form [15]

$$ {}_2\mathcal{F}_1(a,b;c;x) = \sum_{k=0}^{\infty} \frac{a_k b_k}{c_k k!} x^k \tag{B.1.1} $$

and is a special case of the generalised hypergeometric series

$$ {}_v\mathcal{F}_w(a_1,a_2,\ldots,a_v;c_1,\ldots,c_w;x) = \sum_{m=0}^{\infty} \frac{(a_1)_m \ldots (a_v)_m}{m!\,(c_1)_m \ldots (c_w)_m} x^m . \tag{B.1.2} $$

Equation (B.1.1) satisfies the differential equation

$$ x(1-x)y''(x) + [c-(a+b+1)x]y'(x) = aby(x) \tag{B.1.3} $$

and terminates if a or b is equal to a negative integer or to zero. For the case

$$ \Re\{a+b-c\} < 0 \tag{B.1.4} $$

(B.1.1) converges absolutely throughout the entire unit circle [17], i.e. a solution to the specific problem exists. ${}_2\mathcal{F}_1$ can be written in terms of an integral representation [20] as

$$ {}_2\mathcal{F}_1(a,b;c;x) = \frac{\Gamma(c)}{\Gamma(b)\Gamma(c-b)} \int_0^1 \xi^{b-1}(1-\xi)^{c-b-1}(1-\xi x)^{-a}\, d\xi , \quad (c > a > 0) \tag{B.1.5} $$

where $\Gamma(\ldots)$ is the Gamma function defined as [15]

$$ \Gamma(x) \stackrel{def}{=} \lim_{n\to\infty} \frac{n!\,n^{x-1}}{x(x+1)(x+2)\ldots(x+n)} , \qquad \begin{array}{l} x \in \mathbb{R}, \\ x \notin \{0,-1,-2,-3,\ldots\} . \end{array} \tag{B.1.6} $$

In the special case of $x > 0$ this simplifies to

$$ \Gamma(x) \stackrel{def}{=} \int_0^{\infty} \mathrm{e}^{-\vartheta}\vartheta^{x-1}\, d\vartheta . \tag{B.1.7} $$

For a certain range of specific values of a, b and c the hypergeometric function in Eq.(B.1.5) can be represented in terms of elementary functions [17], e.g.

$$ {}_2\mathcal{F}_1\left(\frac{1}{2},\frac{1}{2};\frac{3}{2};\frac{x^2}{a}\right)=\frac{\sqrt{a}}{x}\arcsin(x)\,. \tag{B.1.8} $$

B.2 Elliptic Integrals

The integral [15]

$$ \mathbf{I}=\int R\left[x,\left(a_0x^4+a_1x^3+a_2x^2+a_3x+a_4\right)^{\frac{1}{2}}\right] \tag{B.2.1} $$

is called an elliptic integral[1] if the equation

$$ a_0x^4+a_1x^3+a_2x^2+a_3x+a_4=0\,,\qquad (a_0\,,a_1\neq 0) \tag{B.2.2} $$

has no multiple roots and if R is a rational function of x and the square root

$$ \sqrt{a_0x^4+a_1x^3+a_2x^2+a_3x+a_4}\,. \tag{B.2.3} $$

Using various different methods of substitution it is always possible to express a very few types of equation (B.2.1) in terms of elementary functions[2] but certainly all variants of (B.2.1) in terms of three fundamental integrals [22], the so-called uncomplete (or normal) elliptic integrals of first $\mathcal{F}(\phi,k)$, second $\mathcal{E}(\phi,k)$ and third $\Pi(\phi,n,k)$ kind in Legendre's canonical form [15]. The inversion of the first kind of elliptic integrals leads to the elliptic functions of Abel, Jacobi and Weierstrass [22].

Because of the various definitions and incompatible conversions for the integrals the three forms of $\mathcal{F}(\phi,k)$, $\mathcal{E}(\phi,k)$ and $\Pi(\phi,n,k)$ used in this work are given below. They represent the most commonly used forms found in numerous standard reference books such as [15], [21] and [22] for example.

$$ \mathcal{F}(\phi,k)=\int_0^y\frac{dx}{(1-x^2)(1-k^2x^2)}=\int_0^\varphi\frac{d\vartheta}{\sqrt{1-k^2\sin^2(\vartheta)}} \tag{B.2.4} $$

$$ \mathcal{E}(\phi,k)=\int_0^y\frac{(1-k^2x^2)\,dx}{\sqrt{(1-x^2)(1-k^2x^2)}}=\int_0^\varphi\sqrt{1-k^2\sin^2(\vartheta)}\,d\vartheta \tag{B.2.5} $$

$$ \Pi(\phi,n,k)=\int_0^y\frac{dx}{(1+nx^2)\sqrt{(1-x^2)(1-k^2x^2)}}=\int_0^\varphi\frac{d\vartheta}{\left(1+n\sin^2(\vartheta)\right)\sqrt{1-k^2\sin^2(\vartheta)}} \tag{B.2.6} $$

with $0<k<1$. The transition from the form with x to $\sin\varphi$ in Eq.(B.2.4) to (B.2.6) is done by a simple substitution [15]

$$ x=\sin\varphi\,,\qquad \left(0<\varphi<\frac{\pi}{2}\right). \tag{B.2.7} $$

[1] The name originates from a special example where an integral of this type occurs in the rectification of the arc of an ellipse, see [22].

[2] Elementary functions are algebraic, trigonometric, inverse trigonometric, logarithmic and exponential functions.

Table B.3.1: Nature of possible solutions for y depending upon the sign of D as given inEq.(B.3.1d); see [15]).

	$x \in \mathbb{R}$	$x \in \mathbb{C}$
$D > 0$	one real	one real, two conjugate complex
$D < 0$	three real	three real
$D = 0$	one real, two double real, or triple real (if $p = q = 0$)	one real, two double real, or triple real (if $p = q = 0$)

B.3 Third-order Polynomials

There are only a few analytical procedures for solving a cubic algebraic equation. A very robust and straightforward one is Cardan's method as described in [15]. A very brief outline of the method is given in what follows.

Using the substitution

$$y = x + \frac{r}{3} \tag{B.3.1a}$$

the general third-order equation

$$x^3 + rx^2 + sx + t = 0 \tag{B.3.1b}$$

is rewritten in its reduced form

$$y^3 + py + q = 0 \tag{B.3.1c}$$

where

$$p = \frac{3s - r^2}{3}, \quad q = \frac{2r^3}{27} - \frac{rs}{3} + t \quad \text{and} \quad D = \left(\frac{p}{3}\right)^3 + \left(\frac{q}{2}\right)^2 \tag{B.3.1d}$$

with the sign of D and the nature of x (real or imaginary) determining the number of solutions of (B.3.1b) as shown in Table B.3.1. Since the displacement is $u_{\max} \in \mathbb{R}$, Eq.(B.3.1c) has always one real solution determined by [15]

$$y_1 = w + v \tag{B.3.2a}$$

with

$$w = \sqrt[3]{\frac{-q}{2} + \sqrt{D}} \qquad \text{and} \qquad v = -\frac{p}{3w}. \tag{B.3.2b}$$

The two other solutions, which will be of complex nature in the case $D > 0$, are given by

$$\begin{aligned} y_2 &= -\frac{w+v}{2} + \frac{w-v}{2}\,\mathrm{i}\sqrt{3} \\ y_3 &= -\frac{w+v}{2} - \frac{w-v}{2}\,\mathrm{i}\sqrt{3}. \end{aligned} \tag{B.3.2c}$$

It is important to note here that for $D < 0$ Eq.(B.3.2b) seems to contradict Table B.3.1 since w becomes complex. This might be seen as an integral part of the solution process and can be circumvented by introducing [15]

$$\rho_p = \sqrt{-\frac{p}{27}} \qquad \text{and} \qquad \cos\varphi_p = -\frac{q}{2\rho_p} \tag{B.3.3a}$$

which leads to three real solutions for (B.3.1c) in the case $D < 0$

$$y_k = 2\sqrt[3]{\rho_p}\cos\left[\frac{1}{3}\left(\varphi_p + 2\pi(k-1)\right)\right], \qquad (k = 1,2,3). \tag{B.3.3b}$$

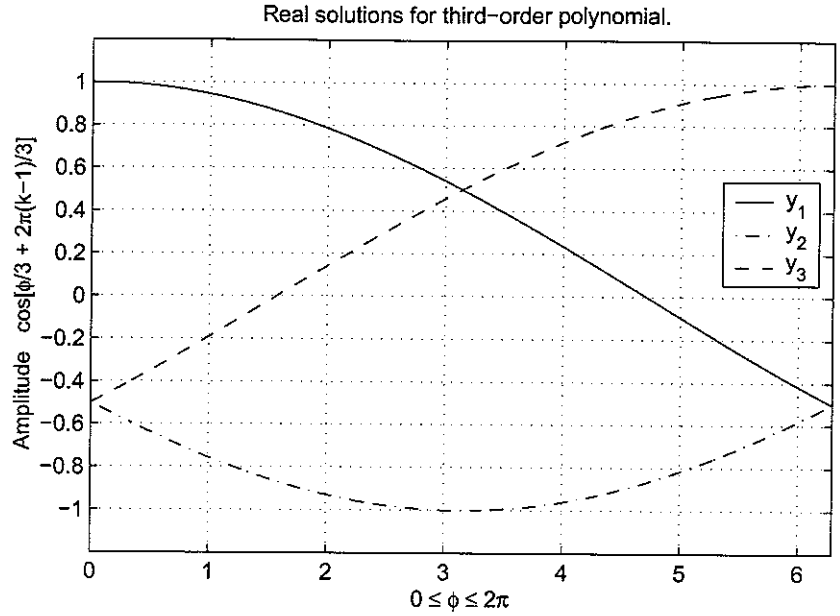

Figure B.3.1: Oscillation of the solutions for y_k with $0 \leq \varphi_p \leq 2\pi$.

The variation of y_k for $0 \leq \varphi_p \leq 2\pi$ is shown in Fig. B.3.1 and documents that the amplitude of any solution y_k is very much dependent upon φ_p, i.e. the ratio of q to p and is not ordered by absolute size in any way with either increasing or decreasing index k.

Finally, rearranging the substitution made at the beginning in Eq.(B.3.1a) the solutions for the original problem (B.3.1b) are obtained as

$$x_j = y_j - \frac{r}{3}, \qquad (j = 1,2,3). \tag{B.3.4}$$

B.4 Fourth-order Polynomials

A nonlinear fourth-order algebraic equation

$$ax^4 + bx^3 + cx^2 + dx + e = 0, \qquad a,b,c,d,e \in \mathbb{R};\ a \neq 0 \tag{B.4.1a}$$

can be rewritten in a reduced form

$$y^4 + py^2 + qy + r = 0 \tag{B.4.1b}$$

using the substitution [15]

$$y = x + \frac{b}{4a}. \tag{B.4.1c}$$

The nature of solution of (B.4.1b) depends upon the solution behaviour of the equivalent *cubic resolving term*, [15]

$$z^3 + 2py^2 + (p^2 - 4r)y - q^2 = 0 \tag{B.4.2}$$

Table B.4.1: Nature of possible solutions for y depending upon the solution of the cubic resolving term; see [15].

cubic resolving term	**fourth-order equation**
all roots real and positive[a]	four real roots
all roots real, one positive, two negative	two pairs of conjugate complex roots
one root real, two conjugate complex	two real, two conjugate complex roots

[a] According to Vieta's theorem the product of $z_1 z_2 z_3 = q^2$ of the roots z_1, z_2, z_3 must be positive, see [15] for example.

which can be solved using Eq.(B.3.1c) to (B.3.4). The solutions to (B.4.1b) can than be obtained using

$$
\begin{aligned}
y_1 &= \frac{1}{2}\left(\sqrt{z_1}+\sqrt{z_2}-\sqrt{z_3}\right), \\
y_2 &= \frac{1}{2}\left(\sqrt{z_1}-\sqrt{z_2}+\sqrt{z_3}\right), \\
y_3 &= \frac{1}{2}\left(-\sqrt{z_1}+\sqrt{z_2}+\sqrt{z_3}\right), \\
y_4 &= \frac{1}{2}\left(-\sqrt{z_1}-\sqrt{z_2}-\sqrt{z_3}\right).
\end{aligned}
\tag{B.4.3}
$$

It should be noted here that in addition to the signs given in (B.4.3) all roots $\sqrt{z_i}$ have to be chosen in a manner to comply with Vieta's Lemma [15]

$$
z_1 z_2 z_3 = q^2 . \tag{B.4.4}
$$